IMPORTANCE OF ELECTROSTATICALLY DRIVEN NON-COVALENT INTERACTIONS IN ASYMMETRIC CATALYSIS

A Dissertation

by

RAJAT MAJI

Submitted to the Office of Graduate and Professional Studies of
Texas A&M University
in partial fulfillment of the requirements for the degree of

DOCTOR OF PHILOSOPHY

Chair of Committee,	Steven E. Wheeler
Co-Chair of Committee,	Daniel A Singleton
Committee Members,	David C Powers
	Lei Fang
Head of Department,	Simon W. North

August 2018

Major Subject: Chemistry

ABSTRACT

Computational chemistry has become a powerful tool for understanding the principles of physical organic chemistry and rationalizing and even predicting the outcome of catalytic and non-catalytic organic reactions. Non-covalent interactions are prevalent in organic systems and accurately capturing their impact is vital for the reliable description of myriad chemical phenomena. These interactions impact everything from molecular conformations and stability to the outcome of stereoselective organic reactions and the function of biological macromolecules. Driven by the emergence of density functional theory (DFT) methods that can account for dispersion-driven noncovalent interactions, there has been a renaissance in terms of computational chemistry shaping modern organic chemistry. DFT Studies of the origins of stereoselectivity in asymmetric organocatalytic reactions can not only provide key information on the mode of asymmetric induction, but can also guide future rational catalyst design.

We start with an overview of weak intermolecular interactions and aromatic interactions. Special emphasis is given to the methods that one can use to study these ephemeral interactions. We next provide a brief account how computational chemistry has aided our understanding of chiral phosphoric acid (CPA) catalyzed reactions. Thereafter, three case studies showcasing the importance of non-covalent interactions in chiral NHC catalysis, CPA catalysis, and chiral nucleophilic catalysis has been elaborated. Each of these studies highlights the importance of electrostatically-driven non-covalent interactions in controlling reactivity and selectivity. Moreover,

unprecedented activation modes are identified and new predictive selectivity models developed that can be used to rationalize the outcome of future reactions.

Studying these reactions using state of art DFT methods, we aimed not only to contribute to the understanding of their selectivity and the importance of noncovalent interactions in catalysis, but also to bring a sound understanding that will enable the design of new reactions and better catalysts. Overall, this dissertation highlights the underappreciated role of electrostatic interactions in controlling reactivity and selectivity in asymmetric catalysis.

DEDICATION

To my parents, family, teachers, friends!

ACKNOWLEDGEMENTS

I would like to take this opportunity to thank everyone who had left a memorable mark in my journey. First and foremost, I would like to thank my advisor, Prof. Steven Wheeler, for giving me the opportunity to work in his group. He knew I had no formal exposure to computational chemistry and was still kind enough to welcome me in his group when I decided to switch in my 3rd year of grad school. In retrospect, I can proudly say that this was certainly the best decision I have taken to date. Steven spent an enormous amount of time working with me, teaching me how to run calculations. There are far too many things to enumerate in this page, for which I owe him this gratitude. His attention to promote students' scientific and career development via custom-tailored research topics contributes a lot to creating a well-rounded experience and preparing for life after graduation. He was more than a research advisor to me. Not only he is an excellent guide and a nice and approachable person whom I really I enjoyed working with but also he has provided me a terrific role model of what an advisor should be. If you are reading this, Boss, I hope you know how grateful I am to you. Although I am sad to be leaving, I am looking forward to see exciting science from our lab in future. I also want to thank his wife Margaret for her friendly presence and discussions during my time in the Wheeler group.

I owe a great debt to Prof. Daniel A Singleton, who is also my co-supervisor. DAS is a stalwart in this area and it has been a privilege to have him in my committee. I am extremely grateful for the time and effort he has put into scrutinizing my work with a fine-toothed comb for the last four years! I have also thoroughly enjoyed countless

stimulating conversation with him and his insightful comments have been useful over the years in helping me develop my intuition as a chemist. Most of all, I value his highly interactive teaching style and the philosophical discussions that he promotes!

Although Prof. Powers and Prof. Fang are new to my committee, I have already gotten to know them quite well, thanks to several departmental events and some close friends. They agreed to serve on my committee within a very short notice and I really appreciate them devoting valuable time. Special thanks to my previous committee members Prof. David Bergbeiter and Prof. W. Liu for all their help.

The Wheeler group members, past and present, made every day of research in the lab a happy and exciting experience. It was a pleasure to be a part of a dynamic, supportive and friendly research group. I would like to thank Yi, Trevor, Yanfei, Sharath, Andrea, Drew, Bryan, Stephen, Victoria, Aarya, and Juni for being awesome lab mates…you guys are amazing and I wish you all the best in your respective career. I will treasure the moments that I spent with you all during my time in the Wheeler group. A special shout out goes to Stephen for providing me shelter during my visits to Athens, which meant a lot to me. Thank you! I have to single out Sharath for a second. Not only because he is the only person in the group with whom I have been working in multiple projects but also his excitement about chemistry and eagerness to learn is what I admire the most. This research would not have been possible without a number of other very enthusiastic collaborators like Pier Alexander Champagne and Heena Ugale. I also consider myself lucky to have had a chance to closely work with Prof. Ken Houk's group at UCLA.

I was fortunate to have supportive departmental staff during my tenure as a grad student at Texas A & M. I am extremely grateful to Sandy Manning and Julie Zercher in particular for their constant support. I am also thankful to Dr. Amber Schafer for her numerous advice related to teaching.

I would like to thank my teachers without whose influence I could have been anything except a chemist. I am grateful to late Dr. Arunava Sen for squandering life-long dream of my parents' to send their only child in medical school. I can't thank him ever enough for all his teaching, motivation and of course ruining my parents plans! I also must thank Dr. Chandan Saha and Dr. Atanu Bhattacharya for their passionate teaching in organic chemistry that left an indelible impression in my mind. My roots as a researcher come from working in the labs of Prof. Tanmaya Pathak and Prof. Saumen Hajra at IIT Kharagpur. They not only taught me different synthetic chemistry skills but also the importance of rigorous work in a lab that helped me in my perseverance and consistency in grad school.

Life in College Station would not have been nearly as enjoyable as it was without all of my friends. Every time when I found myself lost in the trenches of grad school, their inspiration and support kept me going. I am fortunate to have several great friends in the department whom I had the pleasure of working with in different student organizations: Trang, Courtney, Tan, Peerada, Ryan, Zhengyang to name a few. Brateen and Bibaswan deserve special mention for hosting me when I first arrived in College Station. Yindrila will remain forever one of the most influential people in my life. She was truly a great mentor and this journey would have been a little less interesting if I had

missed out those opportunities to bully her! Her friendship and compassion is something that I will cherish forever. Shyamalendu was a fantastic roommate over the years in grad school and I really enjoyed discussing politics, making travel plans, and engaging in wild gossip mostly after 3 AM when we finally got a chance to see each other! Arghya, Srobona, Deepika and Vangmayee were great batch mates and we had a lot of fun in our first year. “Parar Maye” Isita epitomizes the art of culinary skills in College Station and fed us numerous times. It was wonderful to have people like Sanjoy, Asim, Anuvab, Indra da who are always willing to engage in scientific discussions and offer some great insights. I am thankful to my surrogate family here at College Station: Sayan Saha, Bacha Sayan, Anushree, Nandini, Nairita, Sagnika, Raka, Sajal, Sougata and the list goes on. I am also fortunate to have several great friends outside chemistry courtesy to Riad, Shahina, Piyali, Farida for their warm friendship. Thank you all for accepting me with open arms and making College Station a home away from home. I could not more proud to have someone like Bakwas in my life. She stood by my side firmly during my darkest time and believed in me. Her patience, love, trust and support means the world to me. I am looking forward to have many more travels, flights and disagreements in rest of our life!

Finally, I am eternally thankful to my family and close relatives for their constant love and support and that’s why this work is dedicated to them. Despite numerous obstacles they remain always supportive to me in helping to reach my goals. Although I may not visibly demonstrate my appreciation all the time, I hope that they can recognize how much their support has meant to me.

CONTRIBUTORS AND FUNDING SOURCES

Contributors

This work was supervised by a dissertation committee consisting of Professor Steven E. Wheeler (advisor and committee chair) and Professors Daniel Singleton (Co-chair). Invaluable guidance of Prof. David C Powers and Prof. Lei Fang of the Department of Chemistry are also acknowledged.

Experimental data in Chapters V, VI and VII were published previously by research groups of K.Yamada, M. Kozlowski, Y.Zhou, J.Sun and M.P.Sibi respectively.

All other work in the dissertation was conducted independently by the student under the supervision of Steven E. Wheeler.

Funding Sources

The work in this dissertation was supported by The Welch Foundation (Grant A-1775) and the National Science Foundation (Grants CHE-1266022 and CHE-1665407).

TABLE OF CONTENTS

Page

LIST OF FIGURES

Page

LIST OF TABLES

Page

LIST OF SCHEMES

Page

CHAPTER I

INTRODUCTION

Chirality is a fundamental property which is immensely important to life-sustaining biological and molecular recognition processes. The infamous story of thalidomide serves as a shocking reminder of how even a simple enantiomeric pair can produce catastrophic side effects under biological conditions.[1] The contemporary importance of enantio-pure compounds can be readily appreciated by the fact that more than half of today's marketed drugs are chiral. While Nature's ability to generate single enantiomers with minute precision continues to inspire chemists and serves as a motivation to discover new stereoselective synthetic methodologies, modern computational chemistry should also be acknowledged for providing key insights into such transformations. Therefore, a synergy between computation and experiment is highly desirable in order to increase the efficiency of existing catalytic protocols as well as to design new and better catalysts.

Kinetic resolutions (KR) and desymmetrizations are two of the most important strategies of generating chiral compounds. In KR, two enantiomers from a racemic mixture react at different rates in the presence of a chiral catalyst, reagent, or environment, resulting in an enantioenrichment of the less reactive isomer. This enantiomeric excess (*ee*) of the unreacted starting material continually rises as more product is formed, reaching 100% just before full completion of the reaction.[2] A fundamental limitation of traditional KR is that conversion is limited to 50%, as there is no interconversion between the starting materials.[3] However, this shortcoming can be

circumvented by a variation of KR known as dynamic kinetic resolution (DKR), (see Figure I-I). In DKR, the rate of interconversion between two enantiomers is faster than the corresponding reaction rates, and hence maximum conversion can go up to 100%.[4] One can often take advantages of these techniques to prepare chiral compounds using inexpensive racemic starting materials. Desymmetrization is a popular method to convert prochiral symmetric substrates into chiral products.[5] This strategy is particularly important for preparing quaternary carbon stereocenters. Similar to DKR, enantioselective desymmetrizations have the advantage in terms of reaction yield that can reach 100%. In view of their widespread use and applications in the pharmaceutical industry, materials science, and academic settings, a molecular level understanding of these processes is highly desirable.

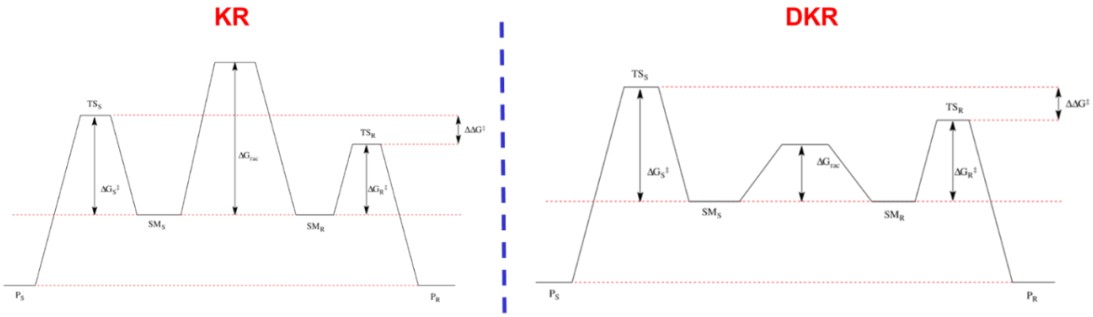

Figure I-1**.** Reaction energy profiles for kinetic resolutions and dynamic kinetic resolutions.

The last two decades have witnessed monumental progress in the area of asymmetric organocatalysis, which makes use of small organic molecules to carry out enantioselective transformations.[6-8] A few notable advantages of organocatalysis over traditional metal-based approaches are lower cost, higher availability, and greater

environmental friendliness. Among different types of organocatalysts, chiral *N*-heterocyclic carbenes (NHCs), axially-chiral phosphoric acids (CPA), and chiral dimethylamino pyridines (DMAP) remain (see Figure I-2) at the forefront for synthetic methodology development.[9-11] One intriguing aspect of these catalysts is their ability to engage with substrates via different activation modes, giving rise to multifaceted reactivity patterns. Moreover, in recent times these catalysts have also promise to act cooperatively with other catalysts to impart unprecedented reactivity and selectivity. Studying these reactions using state-of-the art computational tools will provide additional mechanistic clarity that will further propel future reaction development.

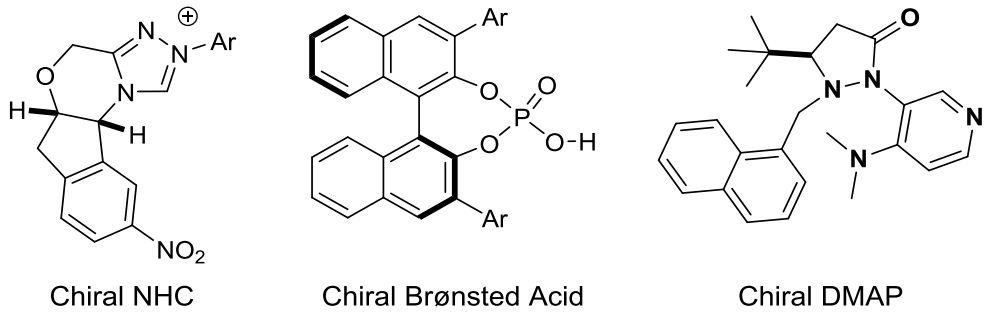

Figure I-2**.** Three representative examples of different classes of organocatalysts.

One prevailing trend in the current literature is the development of transition state (TS) models based on greater steric repulsion between the substrate and catalyst in the transition state leading to the minor stereoisomeric product. However, there has been a gradual shift in appreciation of the potentially vital role of ephemeral non-covalent interactions in many of these processes. Non-covalent interactions are weak, long range attractive interactions often governed by dispersion effects. Among the most notable examples of this type of interactions are stacking interactions involving aromatic rings

(See Figure I-3 for typical examples of such interactions). However, other non-covalent interactions can have significant electrostatic components, such as classical OH···O and non-classical XH···O hydrogen bonds.[12]

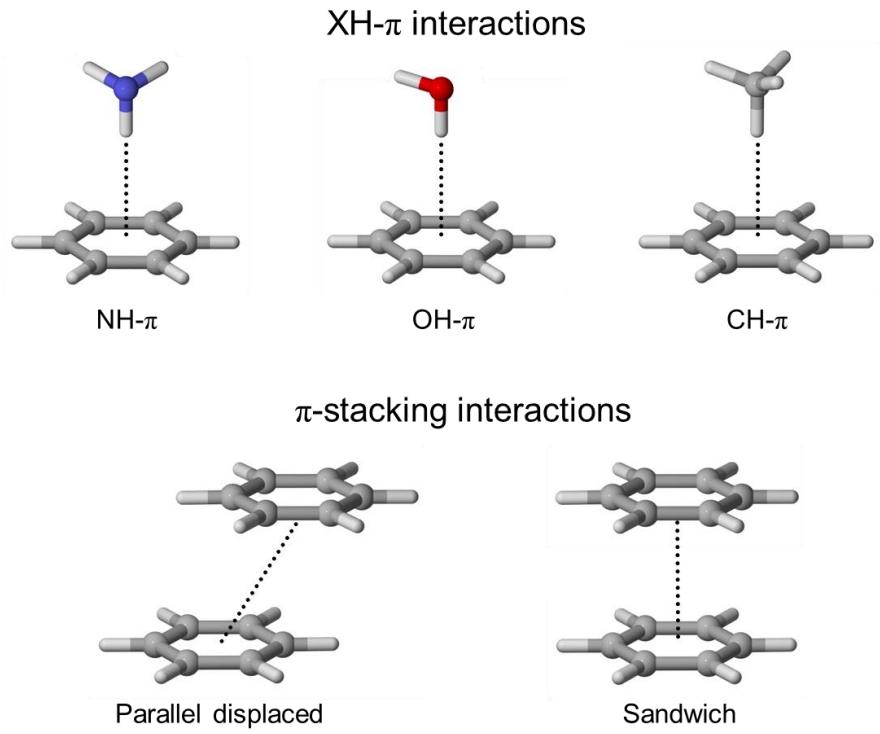

Figure I-3**.** Prototypical non-covalent interactions involving aromatic rings.

The central theme of this dissertation is to understand and quantify the underappreciated role of such weak interactions in controlling reactivity and selectivity in asymmetric reactions.[13-14] The work described in this dissertation involves theoretical investigations of several examples of asymmetric organocatalytic reactions using density functional theory (DFT) computations.[15] These computations can offer an in-depth understanding of the mode of asymmetric induction by modelling the competing TS structures leading to the different stereochemical outcomes.

Despite the many advances in DFT methods over the last two decades, the inability of many of these methods to adequately describe dispersion-driven interactions is well documented,[16-18] and a subject of ongoing development. Driven by the emergence of DFT functionals that account for dispersion driven non-covalent interactions, there has been a renaissance in terms of computational techniques in reshaping modern mechanistic organic chemistry. Perhaps the most notable addition in this area is the DFT-D methods of Grimme[19] which append an energy correction based on a sum of pairwise terms depending on the atom type and interatomic distance to account for dispersion interactions:

$$E_{disp} = -\sum_{i=1}^{N-1}\sum_{j=i+1}^{N}\frac{C_6^{ij}}{R_{ij}^6}f_{damp}(R_{ij}).$$

In this expression, f_{damp} is a damping function that smoothly reduces the dispersion correction to zero at close interatomic distances, and the C_6 coefficients are predefined for each atom type based on fitting to high accuracy data. This dispersion expression incurs negligible computational cost and is simply added onto the DFT energy,

$$E_{DFT-D} = E_{DFT} + E_{disp}.$$

When implemented in conjunction with standard DFT methods (B97 and wB97X), the newly obtained functionals (for e.g. the B97-D[19] and wB97X-D respectively) have been shown to reproduce interaction energies of non-covalently bound complexes with remarable accuracy.[19-20] The subsequently modified method DFT-D3 allows further improvements (including three body corrections and a term depending on R^8), providing are some of the most accurate and cost-effective approaches to modeling non-covalent

interactions developed to date.[21-22] For instance, comparisons of DFT-D3 data with benchmark interaction energies, conformational energies, and reaction energies shown an improvement by at least 1 kcal/mol over methods excluding –D3 correactions. We have employed the above-mentioned functionals to compute TS geometries. Although not explicitly designed for dispersion interactions, the M06-2X functional[23] also performs particularly well with regard to non-covalent interactions[24-25] as well as for overall reaction energetics and barrier heights. This is usually attributed to the large number of parameters in this functional. In view of its efficacy and superior performance, we heavily relied on this functional to compute single point energies for our systems. Finally, our geometry optimization and energy computations employed continuum solvent models including PCM, CPCM, and SMD to account the effect of solvation.

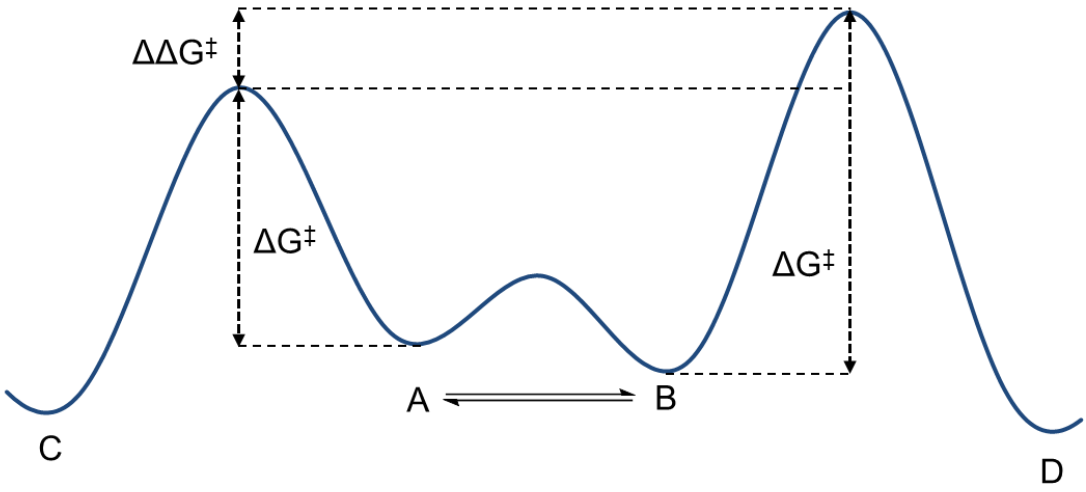

Figure I-4**.** Curtin-Hammett scenario. If A and B are in rapid equilibrium, the distribution of C and D only depends on the difference in free energy of the transition states leading to each product, $\Delta\Delta G^{\ddagger}$.

We have assumed that the reactions studied in this dissertation are under Curtin-Hammett control.[26] According to the Curtin-Hammett principle (See Figure I-4 for typical energy diagram in Curtin-Hammett scenario), the distribution of products does not depend on the population of possible reactant configurations (*e.g.* different non-bonded pre-reaction complexes) but rather the difference in free energies of the transition states leading to the those products, $\Delta\Delta G^{\ddagger}$. This is due to the rapid interconversion of pre-reaction complexes. Given the Curtin-Hammett scenario, the enantiomeric ratio (*er*) of a particular transformation can be computed based on the difference in free energy of the transition states using classical transition state theory (TST),[27] as

$$er = e^{\frac{\Delta\Delta G^{\ddagger}}{RT}},$$

where *R* is the ideal gas constant and *T* is the temperature. When applicable, we also considered Boltzmann distributions over all accessible TS structures to compute selectivity (Figure I-5)

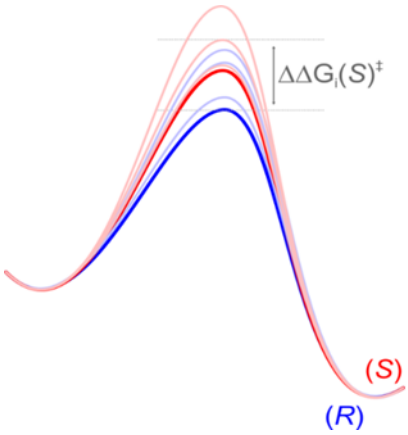

$$ee = \frac{\sum e^{-\Delta\Delta G_i\,(R)^{\ddagger}/RT} - \sum e^{-\Delta\Delta G_i(S)^{\ddagger}/RT}}{\sum e^{-\Delta\Delta G_i(R)^{\ddagger}/RT} + \sum e^{-\Delta\Delta G_i(S)^{\ddagger}/RT}}$$

Figure I-5. Selectivity based on a Boltzmann distribution over multiple thermodynamically accessible TS structures.

For conformationally flexible systems, finding the lowest energy TS structures out of potentially several hundreds of possibilities can be a daunting task. In order to perform a thorough conformational search, we made use of some automatic conformation search methods (e.g. by the MacroModel program[28]). We also performed extensive manual conformational searches. Once TS structures have been identified, analyses of the origin of stereoselectivity have been performed using Non-Covalent Interaction plots (NCI plots),[29] Atoms in Molecules (AIM)[30] and Natural Bond Orbital (NBO) analysis, and distortion-interaction analyses.[31-32] A detailed description of the above methods has been provided in the subsequent chapters with illustrative examples.

In Chapters II and III, we provide an overview of different noncovalent interactions operative in organic systems along with specific examples that serve as a foundation of our later studies. In the following chapter (Chapter IV), we review the use of computational chemistry to explain the activity and selectivity of chiral phosphoric acid catalysis, emphasizing importance of non-covalent interactions. Thereafter, in Chapters V-VII, we elaborate three case studies encompassing three different organocatalysts (NHC, CPA and chiral DMAP) mediated KR and desymmetrization reactions, where we show that non-covalent interactions play various important roles. These studies not only offer molecular level insight into selectivity but also identify unprecedented activation modes and refined views of activity. During these studies, we have unveiled the crucial role of different electrostatically-guided non-covalent interactions in controlling selectivity and conformations. This dissertation concludes with an outlook which represents a marked departure from the still-dominant steric-

based view of stereoinduction, highlighting the ability of non-covalent interactions to dictate the outcome of reactions and the many parallels between small molecular organocatalysis and enzyme-catalyzed processes.

CHAPTER II

ROLE OF AROMATIC INTERACTIONS IN DIRECTING ORGANIC REACTIONS*

2.1. Introduction

Non-covalent interactions involving aromatic rings (π-stacking interactions, CH/π interactions, *etc*.; see Figure II-1) abound in organic systems, and the last decade has witnessed a surge in interest in organic reactions directed by these aromatic interactions. This interest has accompanied a general shift in emphasis from a predominantly steric view of organic reactions to a more nuanced view in which the fate of a reaction hinges on the interplay of both attractive and repulsive non-covalent interactions. For instance, asymmetric reactions were long thought to result primarily from the destabilization of the disfavored pathway through repulsive steric interactions (*e.g.* the steric shielding of one face of a pro-chiral molecule to favor direct attack of the less hindered face).[33] More modern views, however, highlight the potential role of both stabilizing and destabilizing non-covalent interactions in determining the relative free energy of stereocontrolling transition states.[13, 34-35] There have been a number of excellent recent reviews of non-covalent interactions in the context of organic reactions. For instance, Krenske and Houk[36] provided an overview of aromatic interactions as control elements in stereoselective organic reactions. More recently, Wagner and Schreiner[37] reviewed the role of dispersion effects, which are the drivers of many

---

* Adapted with permission from "Role of Aromatic Interactions in Directing Organic Reactions" by R.Maji and S. E. Wheeler, 2016. *Aromatic Interactions: Frontiers in Knowledge and Applications RSC*, 18. Copyright 2016 Royal Chemical Society.

aromatic interactions, in everything from the structure and stability of organic molecules to reactivity, catalysis, and spectroscopy. Similarly, Matile and co-workers have very recently published a perspective on the intriguing world of anion-π catalyzed reactions.[38]

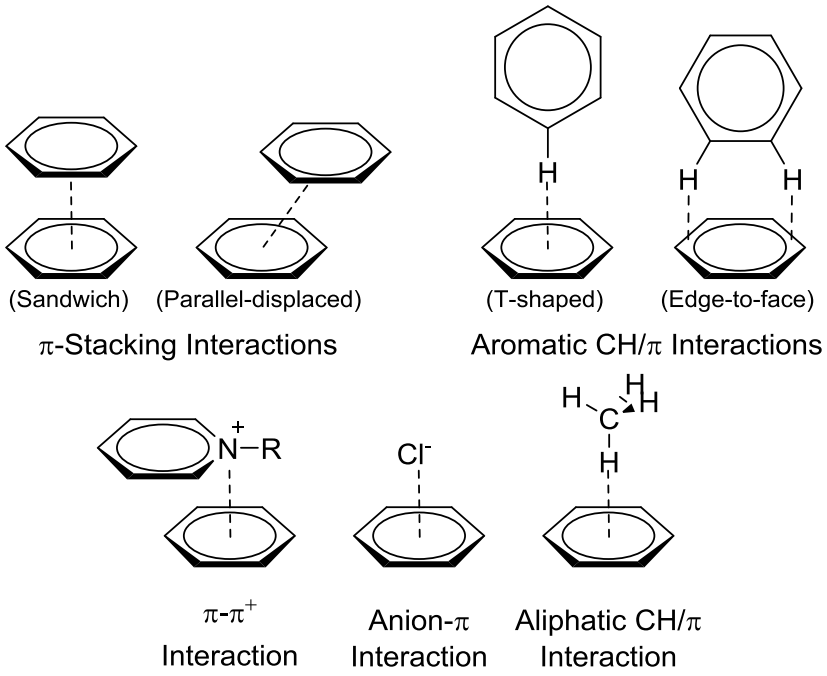

Figure II-1. Prototypical non-covalent interactions involving aromatic rings.[39]

In order to harness the power of non-covalent interactions to control organic reactions, one needs to first understand both the nature of these non-covalent interactions and their role in existing organic transformations. Our understanding of aromatic interactions has seen tremendous advances in the last few years,[40] and continues to evolve. Concurrent with these changes in our understanding of aromatic interactions is a growing body of examples of organic reactions in which these non-covalent interactions appear to play key roles.

Herein, we proceed by first providing a brief overview of aromatic interactions, followed by selected examples of both catalytic and non-catalytic reactions in which these interactions play important roles. The aim is not to provide a comprehensive review of aromatic interactions in organic reactions, but instead to convey the breadth of systems in which non-covalent interactions appear to be operative. Our hope is that this overview will inspire other, novel uses of aromatic interactions in directing organic reactions, leveraging the power of supramolecular chemistry to advance the field of organic synthesis.

2.2. Aromatic Interactions of Relevance to Organic Reactions

There are a number of non-covalent interactions involving aromatic rings that play vital roles in many organic reactions, including π-stacking interactions, CH/π interactions, anion-π interactions, and π-π^+ interactions, among others (see Figure II-1). Below, we summarize these main classes of interactions and direct the reader to recent reviews for more detailed discussions of their origin and nature.[40-45]

π-stacking interactions, which are generally defined as attractive interactions between aromatic rings, have long been known;[46] however, their origin and nature continues to be debated.[47-61] Indeed, even the utility of the term "π-stacking" has recently come into question.[43] The simplest system exhibiting π-stacking interactions is the benzene dimer, which is typically considered in four prototypical arrangements (see Figure II-1). Among these, we consider the sandwich and parallel displaced configurations to be 'π-stacked', whereas the interaction present in the T-shaped and edge-to-face dimers are examples of aromatic CH/π interactions (*vide infra*). This

differentiation between the sandwich and parallel displaced configurations, on one hand, and the T-shaped and edge-to-face dimers on the other, is justifiable on both geometric grounds and physical grounds. For instance, while the interactions in the T-shaped and edge-to-face dimers are primarily electrostatic in nature, the π-stacking interactions in the sandwich and parallel displaced benzene dimers are due mostly to dispersion interactions.[62] For non-substituted arenes, the parallel-displaced configuration is strongly favored over sandwich-like stacking; the sandwich configuration, while still favorable relative to separated benzenes, is a saddle point on the potential energy surface.[62]

Although dispersion interactions are the primary drivers of π-stacking interactions, the ability of heteroatoms and substituents to tune the strength and geometry of these interactions is largely attributed to electrostatic effects. Traditionally, the impact of substituents on π-stacking interactions was explained in terms of resonance-based changes in the aryl π-electron density induced by the substituents.[47, 49-50, 63-67] That is, electron-withdrawing substituents (*e.g.* CN, NO_2, *etc*.) deplete the electron density of the substituted ring, rendering it "electron-deficient." This electron-deficient ring then interacts more favorably with the "electron-rich" π-electron cloud of the other ring. However, mounting computational data[57, 60, 68] suggests that, at least in the gas phase, the dominant effect of substituents in π-stacking interactions arises from local, direct interactions of the substituents on one ring with the nearby C-H bonds of the other ring. More recently, Raju, *et al*.[58] have shown that substituent effects in sandwich dimers of diverse aromatic rings can be explained by the interaction of the local dipole moment associated with the substituents and the electric field of the other ring. One

special case of substituent effects in π-stacking interactions concerns so-called arene-perfluoroarene interactions.[41-42] These interactions, typified by the sandwich-like dimer of benzene and hexafluorobenzene, are generally more favorable than aryl-aryl interactions between rings of comparable size. Moreover, perfluoroarene-arene interactions tend to favor sandwich-like stacking configurations, rather than the parallel-displaced stacking most often exhibited by non-fluorinated arenes.

Aliphatic CH/π interactions,[69] in which a CH bond is directed toward the face of an arene, are also largely driven by dispersion interactions.[70-71] However, the relative contribution of dispersion and electrostatic effects varies with the hybridization of the carbon atom involved, with the importance of electrostatics decreasing with the increasing p-character of the carbon. For instance, Tsuzuki *et al*. showed[72-73] that *sp*-hybridized CH/π interactions (*i.e.* an acetylenic CH group directed toward the face of an arene) are largely electrostatic in nature, whereas the complex between methane and benzene is almost entirely dispersion-driven. Similarly, aromatic CH/π interactions are mostly electrostatic in origin. With regard to substituent effects, Bloom, *et al*.[74] showed that for sp^3-hybridized CH/π interactions, substituent effects are driven primarily by dispersion effects. Consequently, the polarizability of the substituent is the primary predictor of the strength of interaction in model complexes of methane with substituted benzenes. On the other hand, the electronic character of the substituent will determine the strength of *sp*- and sp^2-hybridized CH/π interactions, including aromatic CH/π interactions. In these cases, substitution of the arene accepting the CH…π interaction with electron donating groups leads to more favorable interactions.

Anion-π interactions are typically defined as attractive interactions between atomic or polyatomic anions and the face of an electron-deficient ring. These interactions, often viewed as analogous to the more well-known cation-π interactions,[75-79] were proposed by theorists a dozen years ago and have rapidly shifted the supramolecular landscape.[80] As seen below, anion-π interactions have emerged as a potentially powerful means of both accelerating and steering organic reactions. Finally, π-π^+ interactions are attractive interactions between a cationic arene (*e.g.* pyridnium) and a neutral arene. While quite distinct from π-stacking and cation-π interactions, π-π^+ interactions combine some features of both of these more well-known interactions.[81-82] Pioneering work by Tsuzuki *et al*.[82] have shown that, in contrast to π-stacking interactions, π-π^+ interactions arise primarily from electrostatic interactions and induction.

Since many of these non-covalent interactions depend strongly on dispersion interactions, their computational description has long been a challenge. Correlated *ab initio* methods (*e.g*. MP2, CCSD, *etc*.) are able to capture dispersion interactions but at considerable computational cost; moreover, MP2 tends to overestimate the impact of dispersion interactions.

Traditional density functional theory (DFT) methods (*e.g*. B3LYP), on the other hand, fail to capture any substantial dispersion-like interactions. However, the last decade has witnessed tremendous advances in DFT-based methods to capture dispersion-like interactions, which has opened the door to robust computational studies of these interactions in the context of organic reactions. The most common methods

used to capture dispersion-driven non-covalent interactions in organic systems are the empirical dispersion correction of Grimme (the so-called –D, –D2, and -D3 methods)[19, 83-84] and the M05 and M06 families of functionals from Truhlar and co-workers.[85-87] Notably, the venerable B3LYP functional, which for many years was the workhorse of computational organic chemistry, fails to capture dispersion interactions, and results from this functional applied to systems in which dispersion interactions play key roles should be viewed with some skepticism.

2.3. Aromatic Interactions in Non-Catalytic Reactions

Aromatic interactions play key roles in many organic reactions, including non-catalytic processes, such as cycloadditions and macocyclizations. Cycloadditions have long been a staple of physical organic chemistry, and the impact of stereoelectronic effects on their regiochemistry and reactivity is a common topic in the undergraduate and graduate organic chemistry curricula. However, in some cases, aromatic interactions provide an additional means of steering these reactions. For example, in 2006, McNeil, Swager, and co-workers[88] introduced a remarkably stereoselective and high-yielding Diels-Alder cycloaddition of anthracene with a substituted maleic anhydride in their synthesis of conjugated polymers incorporating π-stacking interactions along the polymer backbone (Figure II-2). In unpublished work, McNeil *et al*. found that substituents (X) modulated the stereoselectivity of this reaction, which was tentatively attributed to differences in π-stacking interactions in the transition states for the two possible cycloadditions. Building on this work, Wheeler, McNeil, *et al*.[89] sought to quantify the role of π-stacking interactions in the stereoselectivity of these reactions,

and, ultimately, to use these reactions as an experimental probe of substituent effects in π-stacking interactions. Unlike π-stacking interactions in most unconstrained systems, which tend to adopt parallel-displaced arrangements, the nature of these Diels-Alder transition state structures places two phenyl rings in almost idealized stacked sandwich dimer configurations (see Figure II-2b). Thus, these reactions provided a unique opportunity to probe the impact of substituent effects on model sandwich benzene dimers.

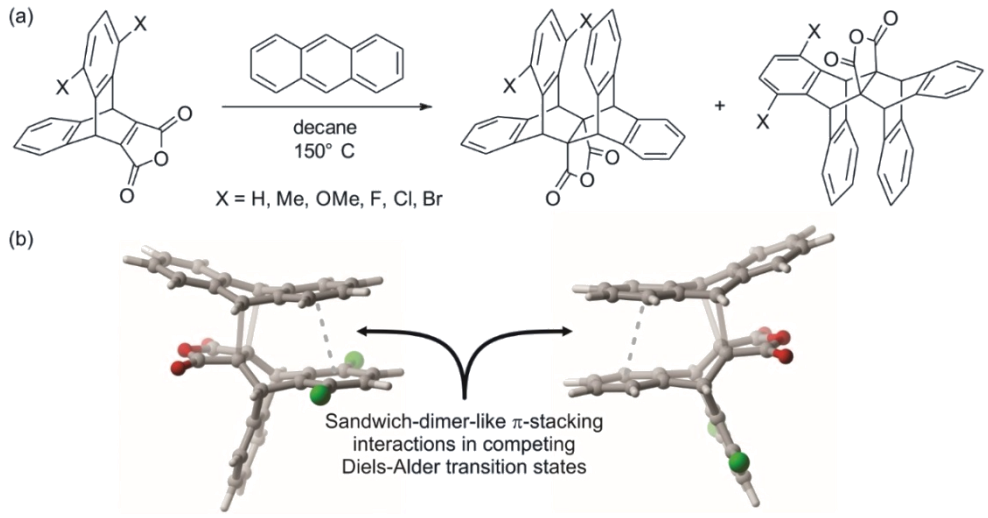

Figure II-2**.** (a) Stereoselective Diels-Alder cycloaddition studied by Wheeler, McNeil, *et al*. in which π-stacking interactions in competing transition states modulate the stereoselectivity. (b) Computed TS structures from Ref. [89]. Reprinted from American Chemical Society.

Experimental and computational data confirmed that substituent effects in π-stacking interactions could be used to control the stereoselectivity of this reaction,[89] guiding the addition of anthracene to one or the other face of the maleic anhydride. Ultimately, these data provided experimental confirmation of the importance of direct

interactions in substituent effects in π-stacking interactions.[57, 60, 68] Moreover, this work provided one of the first confirmations of the utility of M05-2X as a suitable means of studying organic reactions in which π-stacking interactions play key roles.

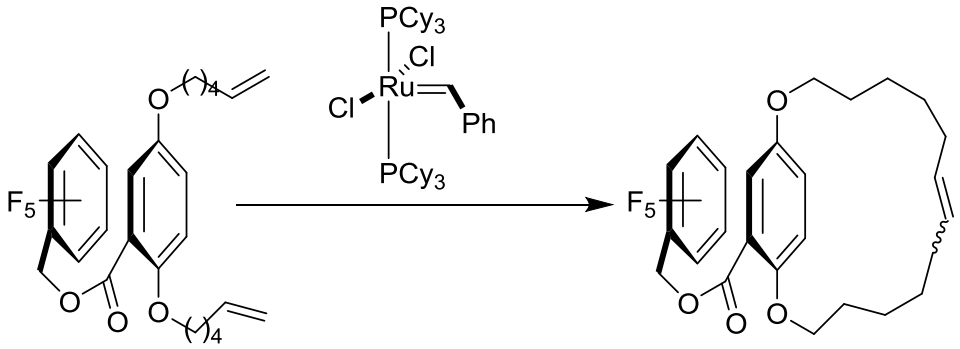

Figure II-3**.** Macrocyclization scheme of Collins and co-workers.[90]

In 2006, Collins and coworkers[90] exploited attractive aromatic interactions to promote macrocyclizations via ring closing metathesis (Figure II-3). During preliminary studies, they noted that they could reduce the conformational flexibility of their acyclic diene precursor through stabilizing π-stacking interactions that favored a closed conformation, thereby increasing the probability of macrocyclization. This was supported by semi-empirical (AM1) and *ab initio* (MP2) computations that showed a clear preference for closed conformations featuring stacked aromatic rings over open conformations. Moreover, this conformational preference was strongly impacted by the use of a perfluorophenyl group, which lead to even more favorable stacking interactions through perfluoroarene-arene interactions. Subsequently, Collins *et al*.[91] observed that replacing the pentafluorophenyl ring with a 3,5-(trifloromethyl)phenyl ring provided even better yields for macrocyclizations via an ene-yne metathesis reaction. This can be

attributed to the enhanced π-stacking afforded by the two CF_3 groups, in addition to possible lone-pair/π interactions in the low-lying conformers. In 2008, Collins *et al*.[92] found that replacing the ester linkage by an amide resulted in even greater macrocyclization yields (up to 27%), which was rationalized based on further enhanced π-stacking interactions based on computational studies. Finally, in 2010, Collins *et al*.[93] extended this concept to an intermolecular version where a quinolinium salt additive acts as a conformation controlling element through cation π-π^+ interactions.

2.4. Aromatic Interactions in Transition-Metal Catalyzed Reactions

Transition-metal catalyzed processes have long dominated the field of homogeneous catalysis, and are often impacted by aromatic interactions.[4] A seminal example of CH/π interactions in transition-metal catalyzed reactions was provided by Noyori and co-workers[94-97] during their study of the transfer hydrogenation of aromatic carbonyl compounds using chiral Ru^{III} complexes.[94-97] Intriguingly, Noyori *et al*. found that there was preferential formation of the (*S*)-isomer, despite the expected greater steric repulsion in the corresponding transition state. This was explained, based on computations at the MP2 level of theory, by the presence of favorable aromatic CH/π interactions (edge-to-face interactions) between the benzene complexed with the Ru and the pendant aryl group of the reacting ketone that preferentially stabilized the more sterically crowded (*S*)-transition state. This same trend persisted even after replacing the phenyl ring on Ru with a hexamethylphenyl ring. In this case, a favorable aliphatic CH/π interaction between one of the methyl groups of the hexamethylbenzene and the aryl

group of the ketone still managed to outweigh the increasing unfavorable steric interactions in the TS leading to (*S*)-isomer.

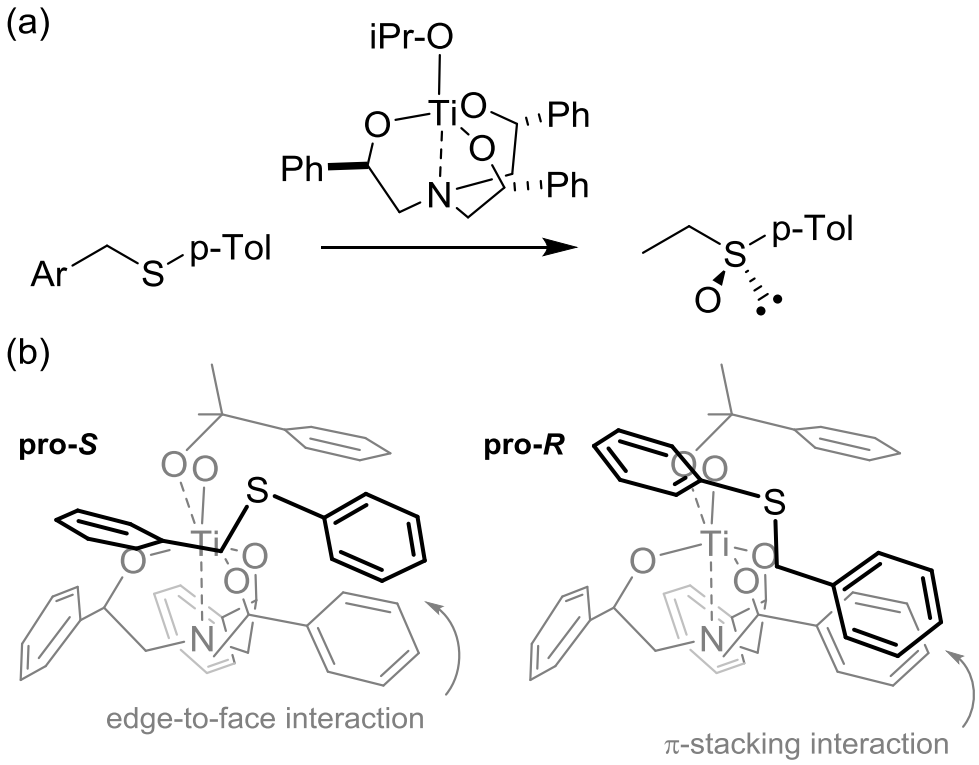

Figure II-4**.** (a) Ti^{IV} mediated enantioselective sulfoxidation reaction of Santoni *et al.*,[98] along with their TS model (b), in which the stereoselectivity depends on the competition between edge-to-face and stacked aryl-aryl interactions.

During their study of C_3-symmetric Ti^{IV} amino trialkolate mediated enantioselective sulfoxidation reaction (Figure II-4a), Santoni *et al.*[99] observed enhanced selectivity with catalysts containing aromatic rings. They used B3LYP to study the intermediate alkyl peroxo Ti^{IV} complex to unravel the origin of the selectivity for (*S*)-sulfoxides in this reaction.. They identified two possible approaches of the substrate (see Figure II-4b), which lead to formation of the two enantiomeric sulfoxides. In these competing reaction pathways, the pro-*S* configuration features an edge-to-face

interaction between phenyl rings on the substrate and catalyst; the pro-*R* configuration instead features π-stacking interactions between two rings. Santoni *et al*.[99] postulated that the former interaction is more favorable, explaining the preferential formation of the (*S*)-sulfoxide. This was corroborated by the fact that replacing one of the phenyl rings with either a perfluorophenyl ring or *p*-nitrobenzene, both of which should enhance the π-stacking interaction in the pro-*R* configuration, resulted in a drop in the observed stereoselectivity.

2.5. Aromatic Interactions in Organocatalysis

Aromatic interactions also play vital roles in myriad organocatalytic reactions, which often rely on subtle non-covalent interactions for both catalytic activity and stereoselectivity. For instance, proline catalyzed aldol reactions form the foundation of modern organocatalysis, and there has been a long line of TS models explaining the stereoselectivity of these reactions in terms of various non-covalent interactions.[100] Intriguingly, even 13 years after the initial publication of the Houk-List model of proline-catalyzed intramolecular aldol reactions, computational studies continue to unveil additional subtleties regarding the non-covalent interactions responsible for the stereoselectivity of these transformations.[101-102]

In related work on substituent effects in proline catalyzed aldol condensations in water (Figure II-5), Houk *et al*.[103] identified π-stacking interactions as a key determinant of the catalytic activity of **1a**. In particular, catalyst **1a** was 43.5 times more reactive in water than **1f**, while these catalysts have similar rates in non-polar solvents (*e.g*. toluene). M06-2X computed activation energies were in general agreement. For instance,

the energy difference between the rate-limiting transition states in vacuum was very small (0.2 kcal/mol). Accounting for solvent led to a 2.6 kcal/mol difference in the predicted activation energies for catalysis by **1f** vs **1a** in water. Ultimately, this difference in catalytic activity was attributed to a stabilizing edge-to-face interaction between the benzyl group of catalyst **1a** and the phenyl ring of the acceptor aldehyde (see Figure II-5). Clearly, this stabilizing interaction is not possible in the analogous transition state with **1f**.

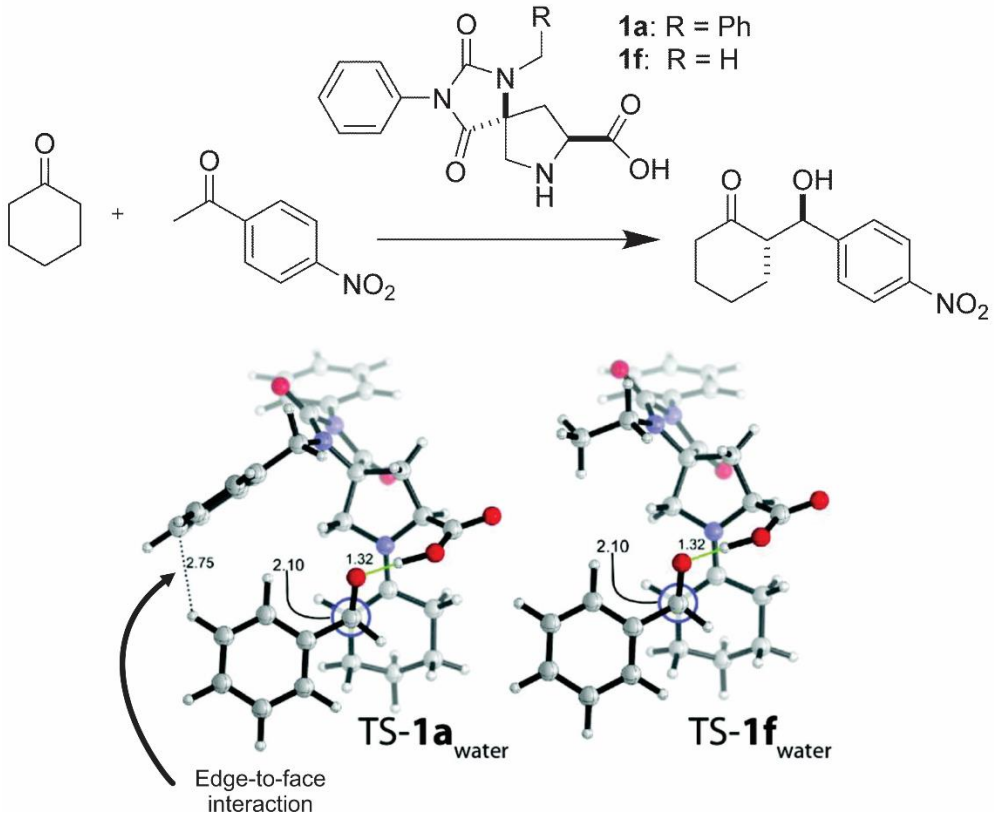

Figure II-5**.** . Proline-catalyzed aldol reaction of Houk *et al*. in water, along with their computed TS structures for the rate-limiting TS for catalysts **1a** and **1f**. Reprinted from American Chemical Society.

Asymmetric Diels-Alder reactions of α,β-unsaturated aldehydes in the presence of chiral imidazolidinones constitute another class of reactions in which aromatic interactions can play key roles. Pioneering work by Houk *et al.*,[104-105] as well as studies from Platts *et al*.[106] and Singleton *et al*.,[107] showed that stereoselectivity in these reactions is governed by the formation of a reactive iminium species for which the lowest energy conformer is stabilized by a CH/π interaction. More recently, Krenske *et al*.[108] offered insight into a similar enantioselective Diels-Alder reaction based on two camphor-derived catalysts developed by Ogilvie.[109-111] These reactions displayed markedly different stereoselectivities depending on the substituent R (see Figure II-6). A detailed conformational search followed by TS optimization revealed a stabilizing CH/π interaction between hydrogens from the cyclopentadiene and the benzyl group in the case of catalyst **2a**. A fragment based decomposition scheme was used to quantify the impact of this interaction on the stereoselectivity. Ultimately, it was shown that the (*R*)-transition state enjoys an additional 1.3 kcal/mol stabilization compared the (*S*)-transition state, which accounts for almost two thirds of the overall enantioselectivity.

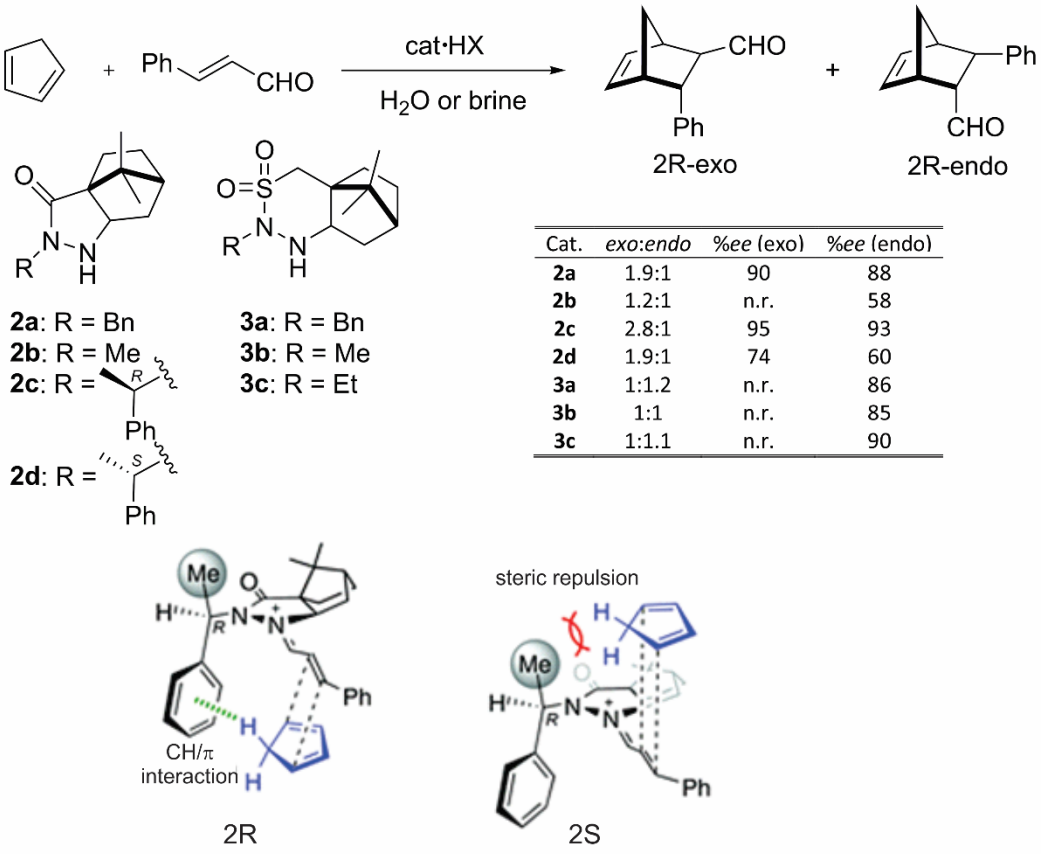

Figure II-6**.** Enantioselective Diels-Alder cycloaddition studied by Krenske *et al*., in which CH/π interactions help stabilize the TS structure leading to the favored stereoisomer.[108] Reprinted from American Chemical Society.

Further examples of the central role of non-covalent interactions in iminium catalysis have been presented by Gilmour *et al*.,[112] who showed that the electronic modulation of the pendant aryl group controls the conformation and reactivity of α,β–unsaturated Macmillian type iminium salts. Similarly, Phiko and coworkers[113] ascribed the enantioselectivity of an iminium catalyzed Mukaiyama-Michael reaction to attractive CH/π interactions, rather than steric hindrance as initially conceived. However, we note that Mück-Lichtenfeld and coworkers[114] recently presented a different

view regarding the positioning of the aryl side chain in iminium-catalyzed conjugated additions to α,β unsaturated aldehydes and ketones. In particular, computational and crystallographic data indicate that the benzyl group in 2-benzyl-imidazolidinone iminium ions is freely rotating at ambient temperature due to the small rotational barriers between conformers. This free rotation effectively shields one particular face of the iminium-π system through an effect they termed the "windshield-wiper effect," leading to the observed stereoselectivities.

N-heterocyclic carbene (NHC) catalyzed cross-benzoin reactions have also been shown to involve stabilizing aromatic interactions. For instance, Legault and Gravel[115] disclosed a strong π-stacking interaction in alkyl-aryl cross benzoin and aryl-aryl homo benzoin reactions. The enantioselectivity of these reactions was traced to π-stacking interactions between the triazole of the catalyst and the aromatic moiety of the aldehyde, which preferentially stabilized one particular transition state relative to its diastereomers.

In 2012, Kozlowski *et al*.[116] studied the highly stereoselective γ,δ-unsaturated δ lactone formation by a NHC catalyzed [4+2] cycloaddition between an enolate derived from the α,β-unsaturated ketone and an enone (Figure II-7). They found that a CH/π interaction between the terminal CH_2 of the enolate and the mesitylene ring was a key stabilizing feature of the TS leading to the major isomer. This view was supported by the observation that replacing the mesitylene ring with a perfluorophenyl ring, which is not expected to engage in as strong of CH/π interactions, resulted in a significant drop in *ee* both experimentally and computationally.

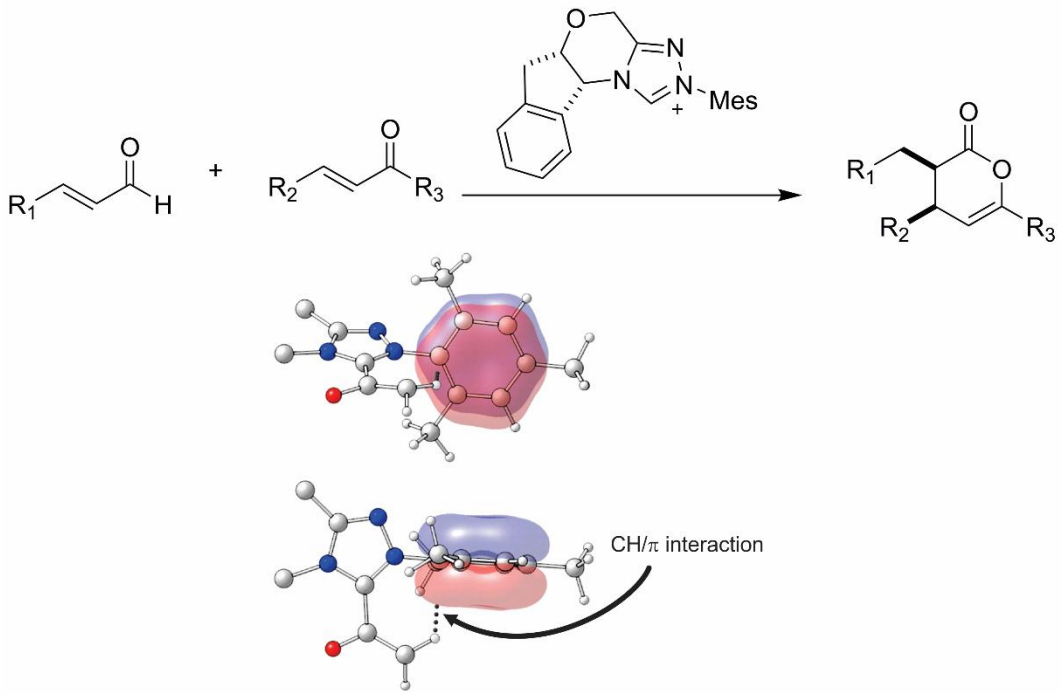

Figure II-7. NHC-catalyzed [4+2] cycloaddition of Kozlowski and co-workers, along with a depiction of a key CH/π interaction in one of the transition states (the enone and indane ring were removed for clarity).[116] Adapted with permission from *J. Am. Chem. Soc.* **2012,** *134*, 12098-12103. Copyright 2012 American Chemical Society.

Phosphoric acids derived from chiral diols have emerged as a powerful platform for organocatalyst development,[117] and many chiral phosphoric acid catalyzed reactions benefit from stabilizing non-covalent interactions between the substrates and aryl substituents of these catalysts. For example, Ess, Kürti, and coworkers[112] identified CH/π and π-stacking interactions as key determinants of stereoselectivity in their synthesis of axially chiral biaryls through a chiral phosphoric acid catalyzed atroposelective [3,3] rearrangement (Figure II-8). Computations corroborated the experimental finding of reduced stereoselectivity upon replacement of aryl CF_3

substituents by CH_3, supporting the involvement of π-stacking interactions in the stereocontrolling TS.

Seguin *et al.*[118] also recently presented a study of the first catalytic asymmetric Fischer indole reaction, from List and co-workers.[119] Computations revealed that the stereoselectivity of this reaction hinged on the competition between π-stacking interactions, which preferentially stabilize the transition state leading to the (*R*)-isomer of product, and CH/π interactions, which provide greater stabilization of the TS leading to the (*S*)-product. Ultimately, the CH/π interactions prevailed, and, when combined with hydrogen bonding interactions that also favor TS(*S*), the (*S*)-product was formed preferentially.

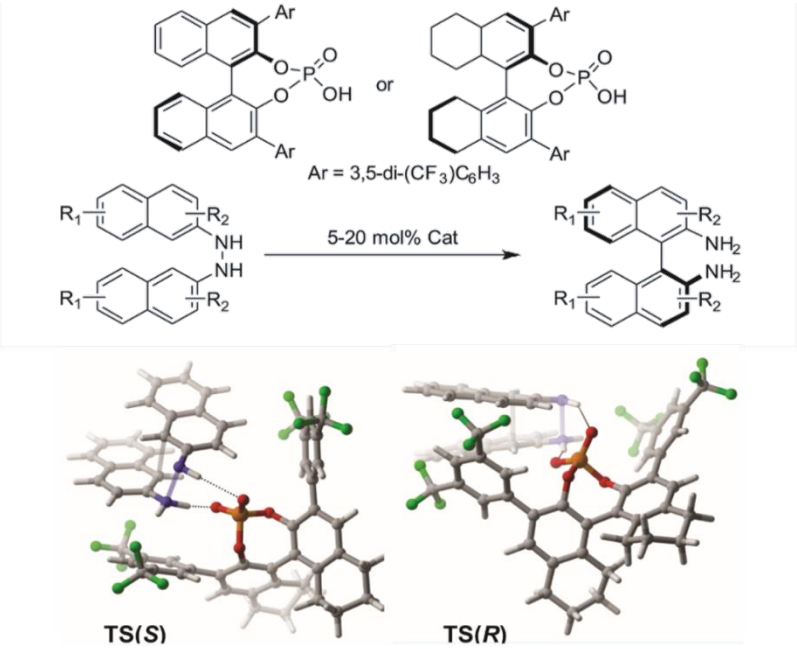

Figure II-8. Chiral phosphoric acid catalyzed [3,3] sigmatropic rearrangement of Ess, Kürti, *et al.*,[120] along with their computed TS structures.[120] Reprinted from American Chemical Society.

CH/π interactions have also proved pivotal in the realm of phase-transfer catalysis. In an elegant study of the phase-transfer catalyzed 5-*endo-trig* cyclization in the stereoselective synthesis of indanes, Paton, Smith, and co-workers[121] observed the importance of CH/π interactions in determining enantioselectivity (Figure II-9). M06-2X computations revealed that the transition state leading to the major stereoisomer is preferentially stabilized by CH/π interactions in conjunction with an array of non-classical CH···O interactions.

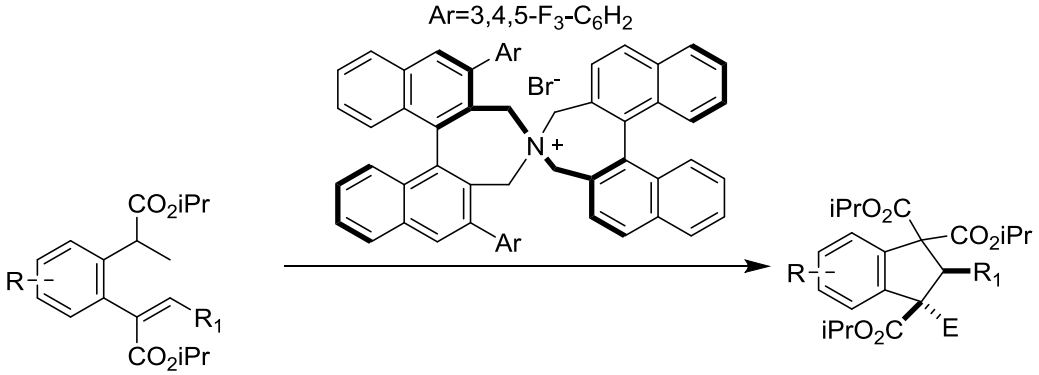

Figure II-9. Enantioselective synthesis of indanes via a cation-directed 5-*endo-trig* cyclization.[121]

During their investigation of TADDOL catalyzed hetero-Diels-Alder reaction of benzaldehyde with 1-dimethylamino-3-tert-butyldimethylsiloxy butadiene, Houk *et al*.[122] identified CH/π interactions to be the key factor for stereoselectivity (Figure II-10). A Monte-Carlo conformational search followed by mixed QM/QM calculations [ONIOM(B3LYP/6-31(d): AM1)] were employed to find the low lying TS. It was observed the lowest energy TS corresponding to *si*-facial *endo* addition (with respect to the aldehyde) is stabilized by a CH/π interaction between the aldehyde CH and the

pseudoequatorial naphthyl group of the TADDOL catalyst. Computations predicted that this TS is 1.5 kcal/mol more stable than the TS for *re*-facial attack, in reasonable agreement with the experimental *ee*. Notably, the TS for *re*-face attack lacks the CH/π interactions present in the competing TS, but instead features a π-stacking interaction. Thus, like the case of the phosphoric acid catalyzed Fischer indole reaction studied by Seguin *et al.*,[118] this TADDOL catalyzed hetero-Diels-Alder reaction is an additional case in which CH/π interactions overwhelm the competing effects of π-stacking interactions in controlling stereoselectivity.

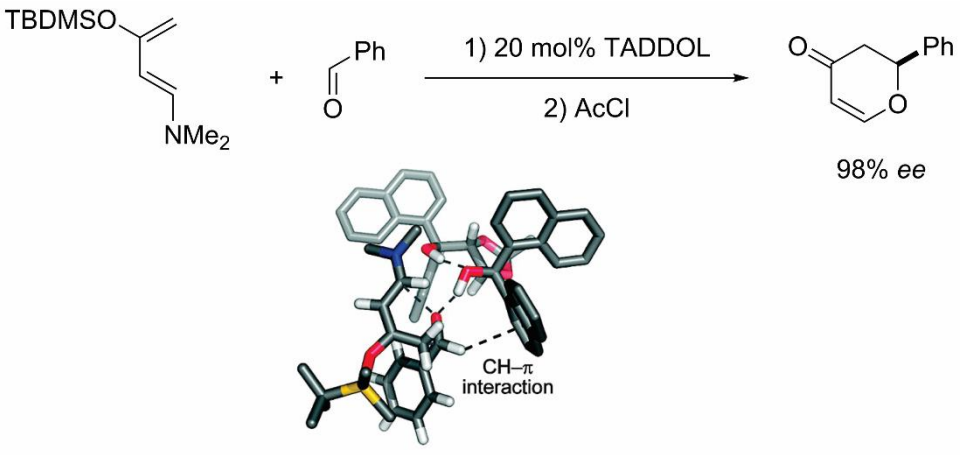

Figure II-10. TADDOL-catalyzed hetero-Diels-Alder reaction of Houk *et al.*,[122] along with a key transition state stabilized by CH/π interactions.[122] Reprinted from American Chemical Society.

Finally, we highlight a case where understanding the nature of π-stacking interactions enabled the design of a more effective metal-free catalyst for asymmetric borane reductions. In particular, the oxazaborolidine from Quallich and Woodall[123] (Figure II-11) has been shown to catalyze the borane reduction of ketones with a high degree of enantioselectivity. Quallich and Woodall[123] attributed this to the steric

shielding of one face of the oxazaborolidine by the two stacked phenyl rings, which controls the coordination of BH_3 to the nitrogen. Sakai and coworkers[124] exploited the tendency of perfluoroarene-arene interactions to adopt more sandwich-like configurations, compared to arene-arene stacking interactions, to design a more rigid chiral oxazaborolidine that provided an even more hindered approach of BH_3 to one face. The more sandwich-like configuration of these stacked rings was confirmed by both *ab initio* computations and a ^1H NMR study.

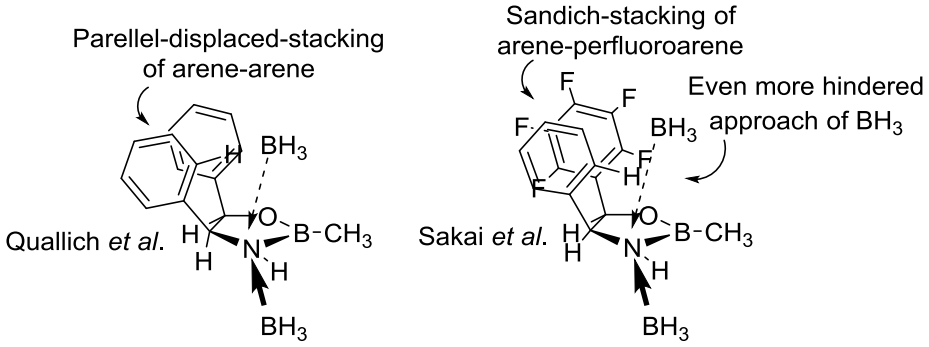

Figure II-11. Chiral oxazaborolidines from Quallich *et al*.[123] and Sakai *et al*.[124] for asymmetric borane reductions of ketones In the latter case, arene-perfluoroarene interactions are exploited to provide greater steric shielding of one face of the oxazaborolidine from complexation with BH_3.

2.6. Aromatic Interactions in Cooperative Catalysis

There have been tremendous advances in our understanding of cooperative catalysis in recent years, and non-covalent interactions have been documented in many of these reactions. This topic was recently reviewed by Sunoj *et al*.;[125] here we present two representative example in which aromatic interactions play key roles. The importance of non-covalent CH/π interactions in cooperative catalysis was highlighted by Xiao and coworkers[126] in the context of the enantioselective hydrogenation of imines

using an achiral Ir-complex and a chiral phosphoric acid. Based on results from an extensive NMR study, they concluded that a ternary complex formed involving the achiral Ir-complex, phosphate anion, and iminium cation is responsible for stereocontrol. Comprehensive NOE, DFT, and semiempirical studies showed that the lowest-lying TS structure, which leads to the major product, is stabilized by multiple CH/π interactions.

Another key example of asymmetric cooperative catalysis in which non-covalent interactions play a central role was reported by Jacobsen and coworkers[127] during their study of an enantioselective Povarov reaction by the cooperative catalysis of a chiral bifunctional sulfamido urea with *o*-nitrobenzenesulfonic acid (Figure II-12). Computational studies using both DFT and *ab initio* methods predicted that the lowest-lying TS, leading to the observed major product, is stabilized by both hydrogen-bonding and π-stacking interactions between the cationic aniline moiety of the substrate and the $(CF_3)_2$-C_6H_3N component of the catalyst. Notably, this stacking interaction is absent in the TS structures leading to the minor enantiomers, suggesting that it is important for the observed stereoselectivity.

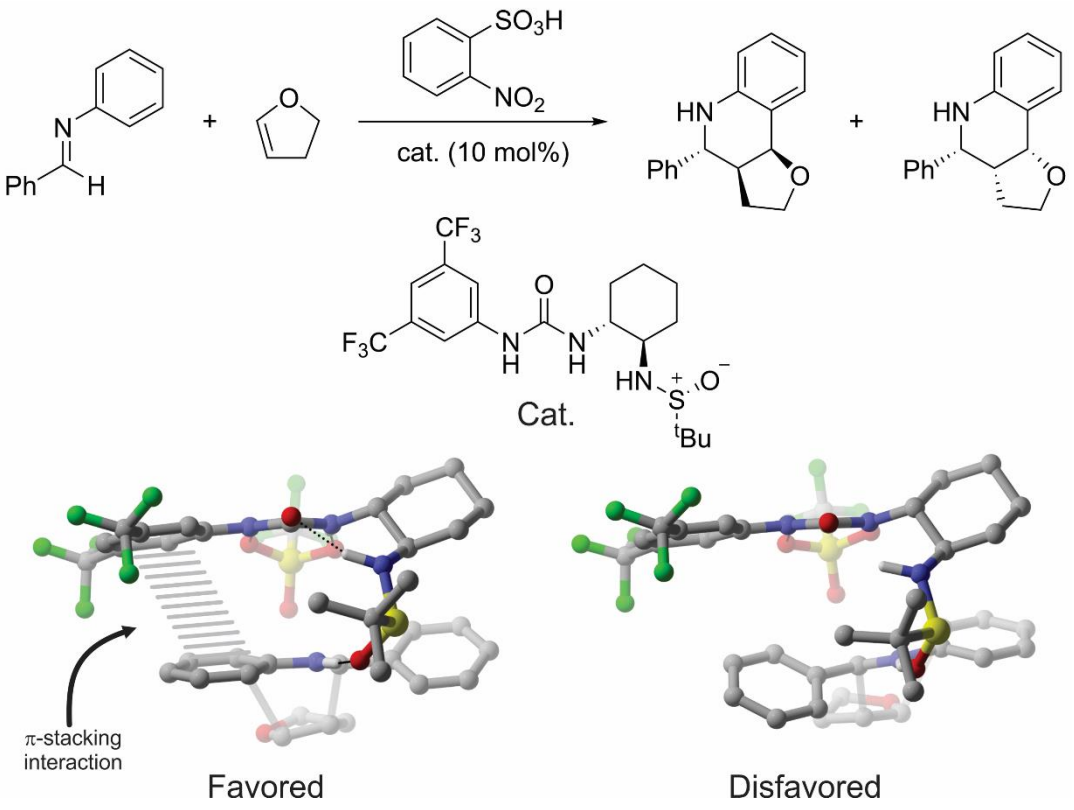

Figure II-12. (a) Enantiodetermining Povarov reaction studied by Jacobsen and co-workers along with the favored TS structure and one of the disfavored TS structures.[127] Non-polar hydrogens omitted for clarity.

2.7. Aromatic Interactions in Anion- π catalysis

Matile and co-workers recently introduced the potentially transformative concept of anion-π catalysis—the acceleration of reactions through favorable anion-π interactions.[128-129] During their initial study of the Kemp elimination of 5-nitrobenzisoxazole, Matile *et al*. synthesized two naphthalene diimide (NDI) based catalysts (**2** and **3**, Figure II-13) with pendant carboxylates designed to stabilize the forming oxyanion in the rate-limited deprotonation of this base-catalyzed reaction. Matile *et al*.[128-129] observed marked rate-accelerations using these NDI-based catalysts,

which are expected to interact favorably with anions, whereas pyrene butyrate (**4**, which is not expected to stabilize anions) showed no catalytic activity. Further demonstrations of the concept of anion-π catalysis came in later work, in which they studied the deprotonation of a malonic acid covalently linked to an NDI, compared to free dimethyl malonic acid.[130-131] Overall, they observed a two unit shift in pKa for the acid linked to the NDI, providing direct experimental evidence of the stabilization of an enolate through anion-π interactions.

Lu and Wheeler attempted to quantify the impact of anion-π interaction in Matile's anion-π catalyzed Kemp elimination reaction.[132] Computations results revealed that even though anion-π interactions were indeed stabilizing the rate-limiting transition state, they were stabilizing the catalyst-substrate complex to a greater extent. The result was that the *net effect* of anion-π interactions was to increase the overall reaction barrier. The problem was that with **2** and **3**, the negatively charged catalytic carboxylate is stabilized to a greater extent than the partially anionic transition state. This is shown in Figure II-13 for catalyst **2**. In this case, the electrostatic interactions of the substrate with the NDI are enhanced by 0.7 kcal/mol going from CS to TS. However, this is overshadowed by the 1.3 kcal/mol loss of stabilization of the carboxylate going from CS to TS. To remedy this, Lu and Wheeler devised modified versions of Matile's NDI-based catalysts in which the catalytic carboxylate was prevented from engaging in stabilizing anion-π interactions through the introduction of a rigid ethynyl linker (catalysts **4**-**6** in Figure II-13). With these newly designed catalysts, the net effect of anion-π interactions was shown to significantly reduce the overall reaction barrier.

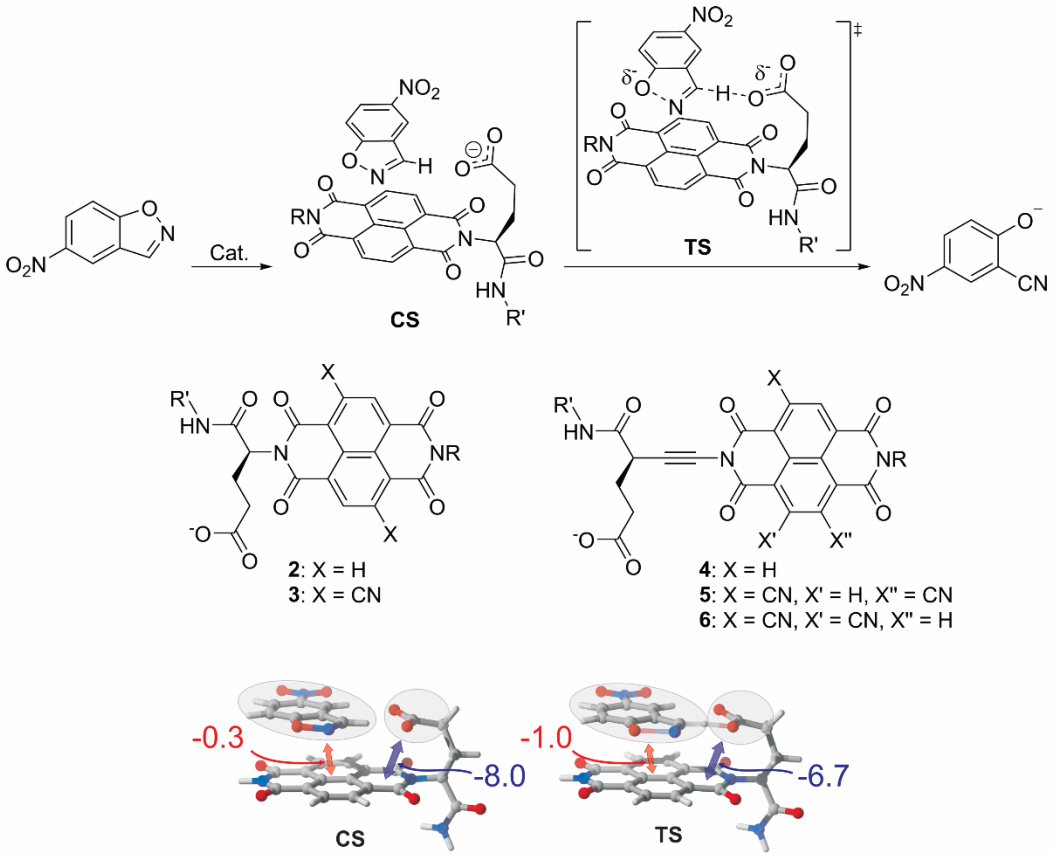

Figure II-13. Kemp elimination of 5-nitrobenzisoxazole studied by Matile and co-workers,[38] along with an analysis of the electrostatic interactions occurring in the catalyst-substrate complex (CS) and transition state (TS) for this reaction from Lu and Wheeler.[132]

More recently, Matile and co-workers have showcased additional examples of anion-π catalysis. For instance, they exploited this strategy to selectively promote the conjugate addition of β-keto thioesters to nitroolefines over a more favorable decarboxylation reaction.[133] They observed that the extent to which these anion-π catalysts could accelerate the conjugate addition while suppressing the decarboxylation depended only on the π-acidity of the catalyst, not other external parameters. This further underscored the central role of anion-π interactions. In a similar vein, Matile *et al.*[134] also

achieved stereoselective enamine addition to nitroolefins using a new NDI-based trifunctional organocatalyst. Ultimately, they concluded that while the enantioselectivity of this reaction is dependent on the π-acidity of the catalyst, the diastereoselectivity is determined primarily by the geometric matching of catalyst and substrate.

2.8. Aromatic Interactions in π-π^+ catalysis

Yamada and coworkers[135] have published extensively on the role of intramolecular non-covalent π-π^+ interactions involving pyridinium ions as conformational control elements in stereoselective reactions. In particular, based on NMR, CD, and analyses of crystal structures, they showed that these attractive π-π^+ interactions are able to conformationally lock fluxional systems into a single conformer that dictates the outcome of a number of enantioselective cyclopropanations,[136-137] kinetic resolutions,[138-140] and desymmetrizations.[141]

Intermolecular π-π^+ interactions, in which a cationic arene stacks with a neutral arene, are also prevalent in the literature. One of the most popular examples involves DMAP mediated nucleophilic catalysis. For instance, Zipse and coworkers[142] showed that π-π^+ interactions serve as guiding elements in various acyl transfer catalyzed reactions. In a similar vein, Birman, Houk, *et al*.[143] reported stabilizing π-π^+ attractions between phenyl and pyridinium rings in a parallel-displaced geometry as the key factor in CF_3-PIP-catalyzed linetic resolution of alcohols and enatioselective *N*-acylation of lactams and thiolactams.[144] π-π^+ interactions have also been identified as enantiocontrolling elements in recent work from Jacobsen *et al*, including the enantioselective acylation of silyl ketene acetals through fluoride anion binding

catalysis,[145] the enantioselective addition of indoles to pyrenes,[146] and enantioselective oxidopyrylium based cycloadditions.[147]

2.9. Conclusions

Aromatic interactions are potentially powerful control elements in organic reactions. Our ability to exploit these interactions has grown with our increased understanding of the factors that impact the strength and geometry of these non-covalent interactions. Above, we tried to survey a wide range of organic transformations in which aromatic interactions play key roles, demonstrating the breadth of systems for which such interactions have been identified to be pivotal for either reactivity of selectivity. Ultimately, the combination of experimental data and computation studies has proved invaluable in elucidating the role of these interactions, and will help drive the development of more efficient and selective organic reactions moving forward.

CHAPTER III

WEAK INTERMOLECULAR INTERACTIONS*

3.1. Introduction

The Weak non-covalent interactions are prevalent in organic systems and accurately capturing their impact is vital for the reliable description of myriad chemical phenomena. These interactions impact everything from molecular conformations and stability to the outcome of stereoselective organic reactions and the function of biological macromolecules. These non-covalent interactions have long posed a challenge to popular quantum chemical methods, hampering efforts to provide reliable computational predictions for many problems in organic chemistry.[148] However, recent years have witnessed tremendous advances in efficient computational methods suitable for the description of these non-covalent interactions, which is enabling reliable computational studies of many problems in organic chemistry that would not have been feasible a decade ago.

There have been a number of excellent reviews in recent years covering non-covalent interactions relevant to organic systems. For instance, Diederich *et al.*[149] have provided general reviews of non-covalent interactions involving aromatic rings, while recent reviews of Nishio *et al.*[150-151] have focused on weak hydrogen bonds and CH/π interactions. There have also been more focused reviews on non-covalent interactions in the context of organic chemistry, including the reviews by Krenske and Houk[108] on non-

*Adapted with permission from "Weak Intermolecular Interaction" by R.Maji and S. E. Wheeler, 2018. *Applied Theoretical Organic Chemistry*. 289. Copyright 2018 Edited by Dean Tantillo.

covalent interactions as control elements in chemical reactions, Johnston and Cheong[152] on non-classical CH···O interactions, Singh and Das[153] on lone-pair/π interactions, Matile and co-workers[38] on anion-π interactions, and Jacobsen et al. on cation-π interactions.[154] Herein, we proceed by first discussing the general classes of non-covalent interactions and their physical nature, followed by discussions of the many challenges and pitfalls associated with capturing weak non-covalent interactions computationally. This is followed by representative examples of non-covalent drawn from across the spectrum of organic systems.

3.2. Nature of Non-Covalent Interactions

The Weak Favorable non-covalent interactions can occur between diverse functional groups, and there is a plethora of 'named' non-covalent interactions in the literature. However, all of these interactions arise from some combination of the same fundamental physical interactions. Non-covalent interactions can be classified based on the relative importance of different physical effects, including electrostatic interactions (*i.e*. Coulombic interactions between fixed partial charges), induction or polarization effects (*i.e*. interactions arising from the polarization of one molecule due to its proximity to another), dispersion interactions (*i.e*. interaction of an instantaneous dipole in one molecule with the induced dipole in another), and exchange repulsion or Pauli repulsion (interaction due to overlapping electron distributions). Among these, dispersion interactions and induction/polarization interactions are always stabilizing, while exchange repulsions are always unfavorable.

Electrostatic interactions can be either repulsive or attractive, and are often discussed in terms of charge-charge, charge-dipole, dipole-dipole, charge-quadrupole, *etc*. interactions. Often, the first non-zero term of such multipole expansions dominates, and the contribution of the higher-order contributions is generally small. For instance, the interaction of two neutral, dipolar molecules can often be understood in terms of the leading dipole-dipole term based on the favorable orientation of the two molecular dipoles. However, for complexes of larger molecular systems the use of such multipole expansions is often on shaky physical ground. The multipole expansion of an electrostatic interaction is always convergent for large intermolecular distances. That is, the interaction of two molecules at large separation (*i.e.* where the distance between molecules is much larger than the dimension of either molecule) can be written exactly as a sum of multipolar interaction terms. As molecules move closer together, this expansion becomes more protracted. Ultimately, when the distance between molecular centers is smaller than the radius of either molecule, the multipole expansion of the electrostatic interaction diverges! While the leading term in such divergent multipole expansions can still be qualitatively correct, one must be cognizant of the fact that this is the first term in a divergent mathematical expression. Thus, while simple concepts such as the favorable alignment of molecular dipole moments can often serve as a qualitative guide to intermolecular interactions, such simple pictures become more unreliable as the sizes of the interacting systems grow larger.

As noted above, interactions between molecules can also be classified based on the identity of the interacting groups, and tremendous efforts have been expended in

recent years to understand the origin of these different named interactions. Many of the key classes of interactions are discussed below, with a particular emphasis on those involving aromatic rings. These interactions include π-stacking interactions, ion-π interactions, and XH/π interactions, among others.[44, 155-156]

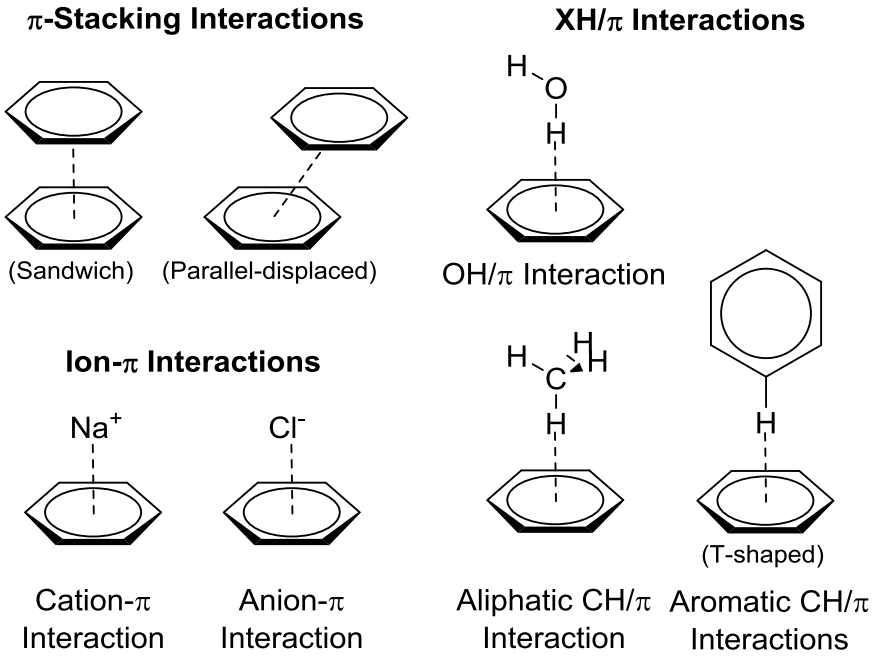

Figure III-1. Prototypical non-covalent interactions involving aromatic rings.

π-stacking interactions are generally defined as attractive interactions between aromatic rings. However, there has been some recent debate regarding the role of aromaticity in these interactions and even the utility of the name "π-stacking interaction" itself.[43, 56, 61] For instance, Grimme[61] showed that for aromatic systems smaller than anthracene there does not appear to be anything special about π-stacking interactions involving aromatic systems. That is, saturated cyclic systems (*e.g.* cyclohexane) interact just as strongly as their comparably sized aromatic counterparts. Bloom and Wheeler[56]

examined the impacts of aromaticity more directly, showing that the π-electron delocalization associated with aromaticity actually hinders π-stacking interactions! That is, non-aromatic cyclic conjugated species can actually engage in stronger π-stacking interactions than their aromatic counterparts. Finally, Martinez and Iverson[43] reviewed both experimental and computational literature on diverse π-stacking interactions, coming to the conclusion that the name itself is highly misleading, since the attractive nature of these interactions is unrelated to the π-electron systems. Following Grimme,[61] we elect to use the term π-stacking purely as a geometric descriptor. That is, we consider two π-systems to be "stacked" if they are in a roughly parallel arrangement with significant overlap.

For the simplest system the exhibits π-stacking interactions, the benzene dimer, one generally considers three prototypical configurations: sandwich, parallel-displaced, and T-shaped (see Figure III-1). Among these, the sandwich dimer is a saddle point on the potential energy surface, and lies about 1 kcal/mol higher in energy than the parallel-displaced and T-shaped configurations. Among these, we consider the sandwich and parallel displaced configurations to be stacked; the T-shaped dimer is an example of an aromatic CH/π interaction (*vide infra*). This distinction between the sandwich and parallel displaced interactions on the one hand and the T-shaped configuration on the other is justified not only on geometric grounds but also on physical grounds; whereas the first two configurations are driven primarily by dispersion interactions in the gas phase, the T-shaped interaction is primarily electrostatic in origin.[157] The strength of π-stacking interactions can vary considerably across systems, and depends strongly on the

incorporation of substituents and heteroatoms as well as the size of the interacting rings. Generally, π-stacking interactions increase with increasing size of the arenes. For instance, the π-stacking interaction of two stacked naphthalenes is much stronger than two stacked benzenes.[61]

There has been considerable effort aimed at understanding the impact of substituents on the strength of π-stacking interactions, which can be substantial.[54, 155-156, 158-172] Since the early 1990s, the prevailing model of substituent effects in π-stacking interactions was that championed by Hunter and co-workers.[167-170] In this electrostatic model, π-stacking interactions are maximized when the two interacting arenes have complementary electrostatic character. That is, strong stacking interactions arise when an 'electron-rich' ring interacts with an 'electron-poor' ring. This view was based on the underlying idea that substituents modulate the strength of π-stacking interactions by altering the π-electron density of the rings. However, computational work over the last decades, as well as mounting experimental examples of strong π-stacking interactions between electron-poor rings, has upended this widely entrenched view.[54, 158-163] Wheeler *et al*.[155-156, 171-172] have introduced an alternative view, dubbed the local, direct interaction model of substituent effects in π-stacking interactions. In this conceptual model, the impact of substituents is primarily a result of direct, through space electrostatic interactions between the substituents on one ring and the electric field of the other ring. The practical ramification is that the overall electronic character of the interacting arenes is unimportant; instead, the relative strength of π-stacking interactions

depends on the presence of favorable or unfavorable local interactions around the periphery of the interactions rings.[155-156, 171-172]

Ion-π interactions include cation-π and anion-π interactions, in which an atomic or polyatomic ion interactions with the face of an aromatic ring. The former interaction has been known for decades, popularized in large part by Dougherty and co-workers[77-78, 173-174] in the mid-1990s. Cation-π interactions are predominantly electrostatic in origin, although cation-induced polarization of the arene by the cation also contributes to binding.[175] Anion-π interactions are also largely electrostatic, although dispersion and induction effects are more important to binding in these systems than in cation-π interactions. For instance, Kim *et al*.[176] demonstrated that favorable anion-π interactions can arise even in systems in which the electrostatic component of the interaction is slightly repulsive.

Both anion-π and cation-π interactions are widely discussed in terms of charge-quadrupole interactions, which will be the leading term in the multipolar expansion of the electrostatic interaction between an ion and a symmetric (non-dipolar) arene. However, the interaction distances in these complexes is often smaller than the radius of the arene, rendering such multipole expansions divergent. Regardless, the strength of these interactions across similar arenes is generally well-correlated with the Q_{zz} component of the arene quadrupole moment; potential pitfalls arise when considering particularly large arenes, in which case the charge-quadrupole model becomes notably worse. Electrostatic potentials (ESPs), which implicitly account for all order multipoles of the arene, provide a more reliable predictor of the strength of both cation-π and anion-

π interactions.[177-179] For instance, Dougherty and co-workers demonstrated the predictive power of ESP plots in the context of cation-π interactions two decades ago.[177] More recently, Wheeler and Houk[178-179] reported very strong correlations between computed ESP values at the position of the ion and the interaction energy in model anion-π and cation-π interactions (see Figure III-2). This correlation can break down, however, when arenes with drastically different polarizabilities are considered. In such cases, variations in the contribution of induction effects interfere with the correlation of the total interaction energies with the electrostatic component predicted by the ESP. In general, the addition of electron-withdrawing substituents to an arene enhances anion-π interaction and hinders cation-π interactions; the incorporation of nitrogens into the arene has similar impact.

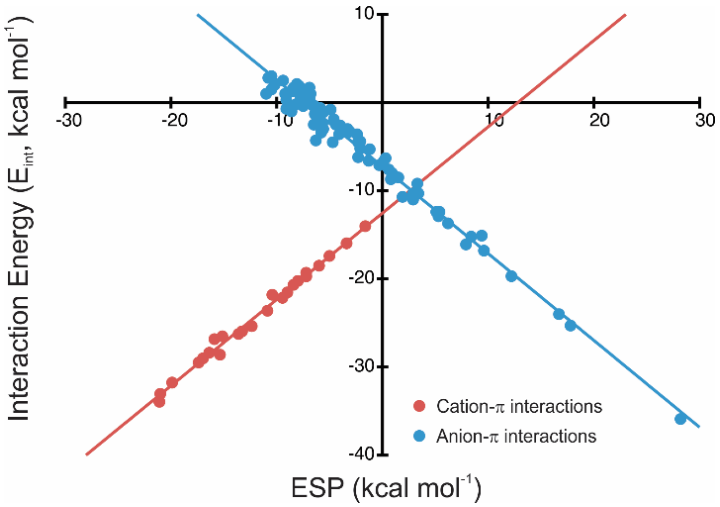

Figure III-2. Interaction energies (kcal/mol) of model cation-π and anion-π interactions vs the electrostatic potential (ESP) at the position of ion above the center of substituted benzenes. Data are adapted from Refs [178] and [179] and were computed at the M05-2X/6-31+G(d) and M06-2X/6-31+G(d) levels of theory for the cation-π and anion-π interactions, respectively.

XH/π interactions can describe any interaction between any X-H bond and the face of an arene. Common examples include CH/π and OH/π interactions, although Cremer *et al*. recently reported the first examples of BH/π interactions.[180] The nature of these interactions depends largely on the nature of the X-atom. For instance, Bloom *et al*.[74] showed that as one progresses from BH/π to FH/π interactions, there is a shift from largely dispersion-driven interactions (in BH/π and CH/π interactions) to almost entirely electrostatic for FH/π interactions. Similarly, for a given type of XH/π interaction there can be variation in the electrostatic component with changes in hybridization. For instance, whereas sp_3-hybridized CH/π interactions (*e.g.* CH_4···benzene) are largely dispersion-driven, there is a significant contribution from electrostatic effects in sp-hybridized CH/π interactions (*e.g.* acetylene···benzene).

One final, less well-appreciated non-covalent interaction that has emerged as a key factor in a surprising number of organic systems is the CH···O interaction. These non-classical hydrogen bonds were recently reviewed by Johnston and Cheong[152] and have been shown to be key stereocontrolling elements in a wide range of organocatalyzed reactions.

The presence of a formal charge on one or more interacting species can significant impact the strength and geometry of these non-covalent interactions. For instance, in 2002, Cannizzaro and Houk[181] reported remarkably strong CH···O interactions in $R_3N^+C–H\cdots O=C$ complexes, which are important in the context of molecular recognition and stereoselective catalysis. Moreover, this enhanced interaction was predicted to persist even in water. Subsequent work by Scheiner *et al*.[182-183] has

examined the impact of ionic charge more broadly, considering a number of model non-covalent interactions. In 2014, Nepal and Scheiner[182] examined the impact of ionic charge on CH/π interactions in model complexes of tetraalkylammonium cations with benzene (see Figure III-3), finding that such complexes are considerably more strongly bound than their neutral counterparts. Similarly, computations revealed that complexes of methylamines and thioethers with *N*-methyaetamide (NMA) are strengthened considerably by adding an additional methyl group to the proton donor. These effects are tempered somewhat by polar solvents, but the ionic complexes were predicted to retain their favored status even in water.

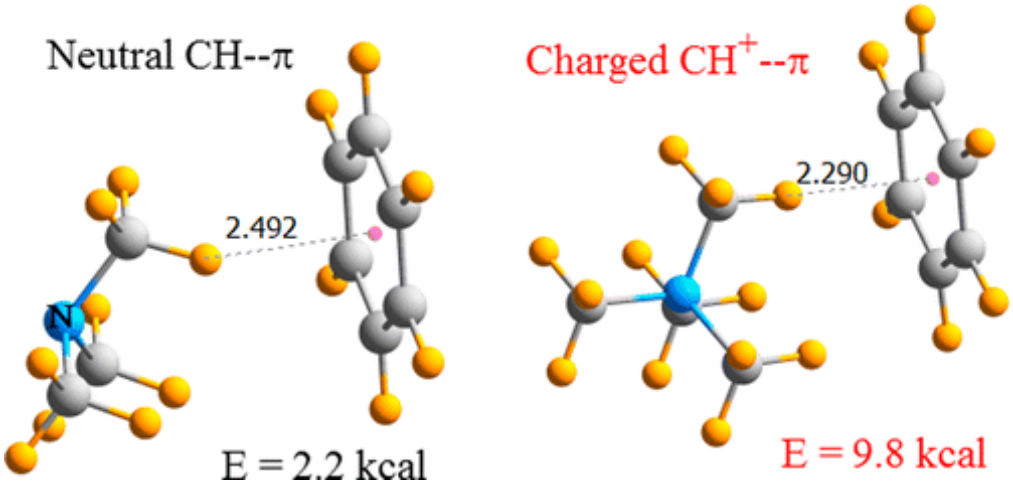

Figure III-3. Model complexes studied by Nepal and Scheiner[182] to understand the impact of charge on CH/π interactions. Reprinted from American Chemical Society.

In cases where both interacting molecules bear formal charges, one must be careful not to convolute the strength of a specific non-covalent interaction with the overall intermolecular Coulombic interaction between two charged species. For instance, in 2011, D'Oria and Novoa[184] introduced the concept of cation-anion hydrogen

bonds, which exhibit binding energies sometimes exceeding 200 kcal/mol! However, these complexes are cases in which the interacting species bear complementary ionic charges, and the vast majority of the reported gas-phase interaction energies are simply the result of the Coulombic interactions between two species. The hydrogen bonding interactions themselves are likely not much stronger than conventional hydrogen bonds (see Figure III-4).

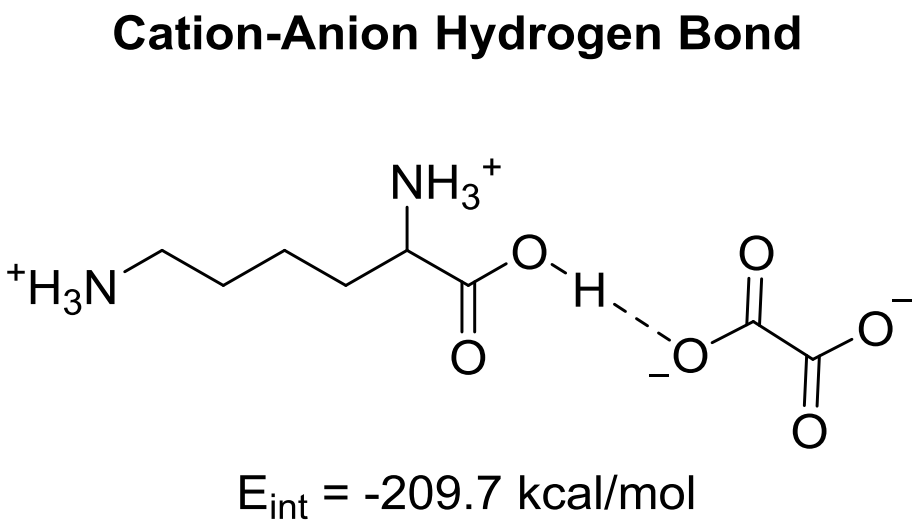

Figure III-4. Example of a cation-anion hydrogen bond from D'Oria and Novoa.[184]

3.3. Methods to Study Non-Covalent Interactions

Much of our understanding of non-covalent interactions involving aromatic rings stems from experimental probes of these interactions. In particular, a number of groups have devised molecular balances and various supramolecular complexes that enable the experimental quantitation of non-covalent interactions.[185-193] For instance, Shimizu and co-workers[185] recently designed a molecular balance to probe the deuterium isotope effect on CH/π interactions, finding that this effect is either very small or non-

existent. Many other torsional balance systems have provided unprecedented insight into the nature of non-covalent interactions, including the effects of solvents.[191-193] Much of the work in this area was reviewed in 2010 by Cockroft and co-workers.[194]

Complementary information has been gleaned from gas-phase computational studies of both model non-covalent complexes and more realistic systems. However, the application of popular electronic structure methods to systems in which non-covalent interactions play key roles is rife with pitfalls.[148] For more than a decade, the venerable B3LYP functional was the workhorse of computational quantum chemistry. By providing relatively reliable structures, thermochemistry, and reaction barrier heights at a modest computational cost, B3LYP was the obvious choice for the vast majority of computational studies of medium-sized organic molecules. However, significant weaknesses in B3LYP became apparent as attention turned to larger molecular systems. The major weakness stemmed from the inability of B3LYP and other conventional DFT to functionals to capture dispersion effects.

For instance, B3LYP and other conventional functionals predict purely repulsive interaction potentials for the benzene sandwich dimer, whereas reliable *ab initio* methods indicate a binding energy of nearly 2 kcal/mol (see Figure III-5). Until about a decade ago, capturing dispersion-driven non-covalent interactions required the use of computationally demanding *ab initio* methods. In particular, coupled cluster theory [*e.g.* CCSD(T)] with large basis sets has been applied to many model non-covalent complexes to provide benchmark-quality interaction potentials. Conventional second-order Møller-Plesset perturbation theory (MP2), which is considerably cheaper and can be applied to

relatively large molecular systems, tends to overestimate dispersion interactions. However, the spin-component-scaled variant, SCS-MP2,[195] largely corrects this deficiency and has been used to provide reliable interaction energies for many non-covalent complexes.

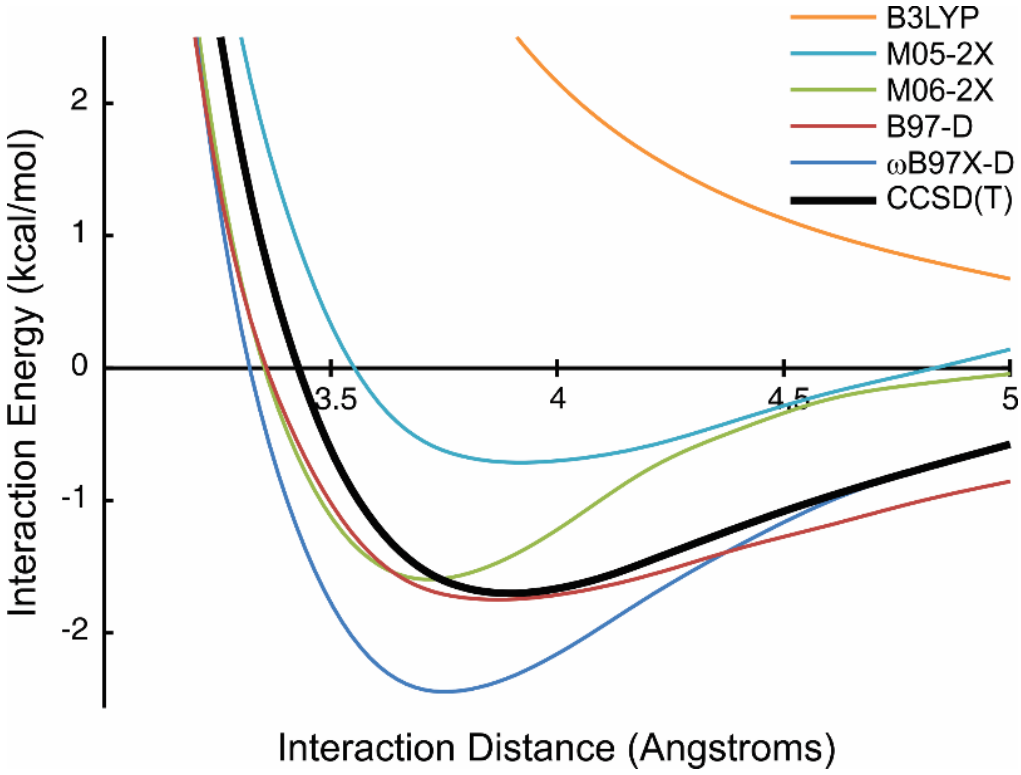

Figure III-5. Interaction potentials for the benzene sandwich dimer computed using popular DFT functionals compared to benchmark CCSD(T) data from Sherrill and co-workers.[196] All DFT computations utilized the 6-311+G(*d*,*p*) basis set.

Fortunately, there have been a number of advances in DFT methods in the last decade, and many functionals are now available for reliable studies of non-covalent interactions in organic systems. The most popular approaches employ the semi-empirical dispersion corrections of Grimme and co-workers (so-called –D functionals, *e.g.* B97-D, ωB97X-D, *etc.*)[19, 21] and the M05 and M06 suites of functionals from

Truhlar and co-workers (*e.g.* M05-2X and M06-2X).[85, 87, 197-200] Such methods provide varying degrees of accuracy when applied to model stacked systems (see Figure III-5) and have proved reliable when applied to large organic systems in which dispersion-driven non-covalent interactions play key roles. Consequently, these methods are now widely used in the computational organic chemistry community. However, it should be noted that the M06 family of functionals is particularly sensitive to the choice of integration grid, and the use of the default integration grid in many popular electronic structure packages can lead to substantial errors in both predicted reaction energies and interaction energies.[201-204] Other computational tools available for quantifying individual non-covalent interactions in organic systems including Bader's quantum theory of atoms-in-molecules (QTAIM) and the natural bond orbital (NBO) approach of Weinhold *et al*.[205-206]

There are also a number of qualitative tools that are widely used to understand non-covalent interactions in organic systems. Chief among these are molecular electrostatic potential plots (ESPs, see Figure III-6). Unfortunately, these ESP plots are often misinterpreted and misused. The primarily problem arises from the connections between the electron density and the ESP. Many organic chemists conflate the electrostatic potential in a region with the local electron density. Common descriptions such as "electron-rich" and "electron-poor" only serve to exacerbate this problem. However, electrostatic potentials and electron densities are distinct, and, while they often track each other, there are countless examples where they do not. Most importantly, a change in the ESP in some region of space does not necessarily indicate a change in the

electron density in the corresponding region. This can be seen most clearly for aromatic molecules; in 2009, Wheeler and Houk[207] showed that substituent effects on the ESPs of substituted arenes are dominated by the through-space effects of the substituents, not any substantial changes in the π-electron density of the arene. For instance, the drastic differences among the ESPs over the centroids of the rings shown in Figure III-6 are due almost entirely to the through-space electrostatic effects of the substituents; any small differences in the π-electron densities of these rings have an almost negligible impact. Similarly, Wheeler and Bloom[208] showed that changes in the ESPs above the centroids of many *N*-heterocycles are not due to changes in the π-electron density, as is commonly assumed.

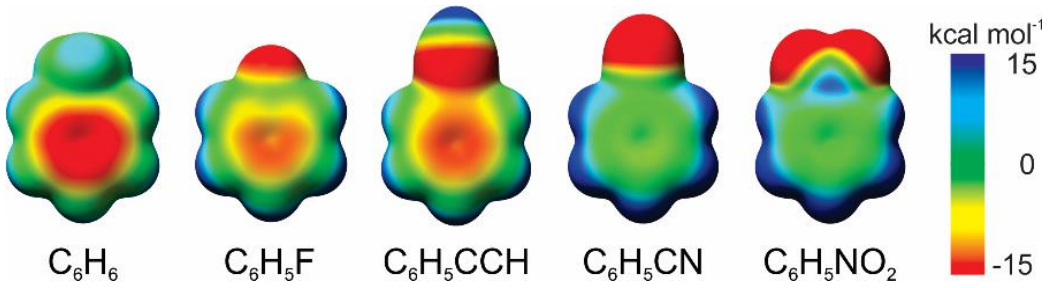

Figure III-6. Molecular electrostatic potentials (ESPs) of several monosubstited benzenes. Reprinted from American Chemical Society.

Finally, Yang *et al*. introduced the now widely-used NCI method,[29, 209] which provides a graphical representation of repulsive and attractive inter- and intramolecular interactions based on an analysis of the electron density and its gradient. The resulting "NCI plots" provide a useful guide for comparing weak inter- and intramolecular interactions among different organic systems.

3.4. Examples of Non-Covalent Interactions in Organic Synthesis

Having established the broad range of computational tools that are now available to study non-covalent interactions in the context of organic systems, we next discuss representative examples in which insight into non-covalent interactions has can be gleaned from careful computational studies.

3.4.1 Non-Covalent Interaction as a Conformational Controlling Elements

Intramolecular non-covalent interactions can have considerable impact on the conformations of organic molecules. For instance, Nishio and co-workers[151] have provided intriguing examples of the impact of non-covalent interactions on molecular conformations, even suggesting that some well-established phenomena like the alkyl ketone effect and anomeric effect are artifacts of stabilizing non-covalent interactions. Similarly, work by Nishio *et al*.[150, 210-211] also suggested that the relatively small energy difference between axial and equatorial conformers of halogenated cyclohexanes, as compared to alkyl cyclohexanes, may be ascribed to stabilizing 1,3-diaxial X···H non-covalent interactions.

Nishio *et al*.[212] have also shown that non-covalent interactions play key roles in the conformations of larger molecules. For instance, levopimaric acid adopts in folded conformation, as opposed to the more sterically relieved extended conformation one might expect (see Figure III-7). Nishio *et al*.[213] showed computationally that for model compounds, the folded conformer benefits from stabilizing CH/π interactions between the conjugated diene ring and nearby methyl group.

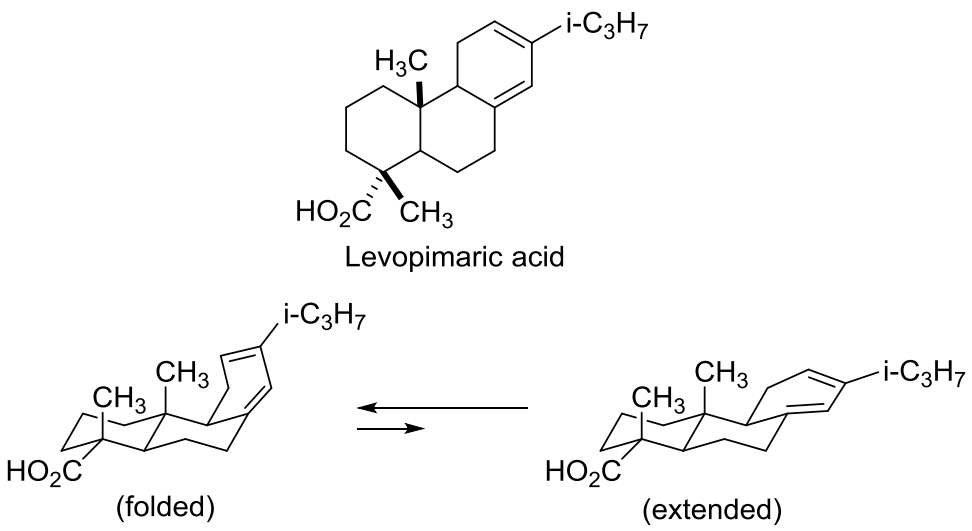

Figure III-7. Folded and extended conformers of levopimaric acid studied by Nishio *et al*., who showed computationally that CH/π interaction stabilize the folded conformer.

Scheiner, Smith *et al*.[214] have also presented a compelling study in which they demonstrated the switching of conformational preference in flouroamides through non-covalent CH···O interactions. α-flouroamides are known to have a strong tendency to adopt *trans*-planar conformations in which the fluorine is *anti* to the carbonyl, minimizing electrostatic repulsion (see Figure III-8a).[215] However Smith *et al*.[214] envisioned that gradually increasing fourine substitution, along with the incorporation of a suitable proton acceptor, could override this inharent conformational bias. A computed torsional potential energy scan for model fluoroamides confirmed that the conformer with a *trans*-planar OCCF dihedral angle is favored by 6 kcal/mol over the corresponding *cis*-planar conformation in the case of $CH_3NHCOCH_2F$; for $CH_3NHCOCHF_2$ this energy difference is reduced to 4 kcal/mol. A more elaborate system was then devised in which a carbamate group was installed that could interact

with the CHXF group through CH···O interactions (see Figure III-8b). Ultiumately, extensive computational analyses demonstrated that this CH···O interaction was sufficient to overcome the inherent bias for trans-planar configurations of fluoramides and render the two planar conformations roughly isoenergetic (See Figure III-8c).

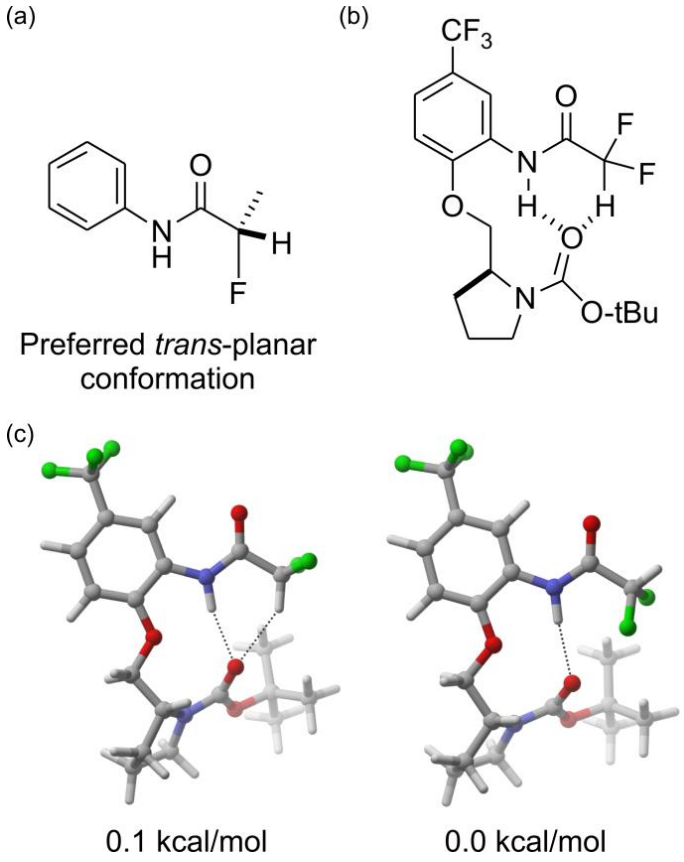

Figure III-8. (a) Strongly preferred *trans*-planar conformer of α-fluoroamides; (b) modified system devised by Scheiner, Smith *et al*.[214] to prove the ability of CH···O interactions to impact conformations; (c) lowest-lying computed conformers, in which the *cis*-planar conformer is nearly isoenergetic with the *trans*-planar conformer due to favorable CH···O interactions in the former.

3.4.2 Non-Covalent Interaction in Supramolecular Systems

Non-covalent interactions play vital roles in supramolecular chemistry, and non-covalent interactions involving aromatic rings have proved particular useful in sensing

applications. For instance, Johnson *et al.*[216] reported a tripodal urea based receptors that shows excellent selectivity towards nitrates. They observed that anion-binding by this receptor followed the general trend $NO_3^- > Cl^- > Br^- > I^-$. However, this substrate specificity is lost in the absence of the three fluorines of the central phenyl ring. This suggested that an anion-π interaction between the bound anion and central phenyl ring, which would only be favorable in the case of the trifluorophenyl case, is important for selectivity (see Figure III-9).

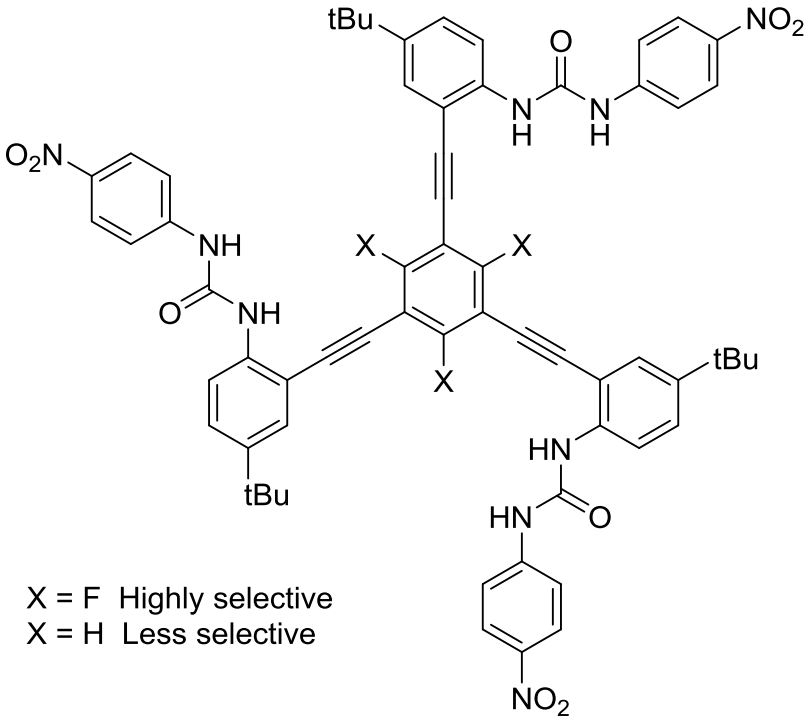

Figure III-9. Tripodal urea based anion receptor of Johnson *et al.*[216]

Other anion-binding receptors have been designed that rely on anion-π interactions, including the anion receptor cage based on triazine linked by trialkylamines pioneered by Mascal *et al.*,[217] the naphthalene diimide (NDI) based fluoride sensor by

Saha *et al.*,[218] the NDI based prism and macrobicyclic cyclophane derivative of Stoddart *et al.*,[219-220] and the NDI based "anion-π slides" of Matile and coworkers.[221]

3.4.3 Non-Covalent Interactions in Organic Reactions

Non-covalent interactions have also emerged as a powerful strategy for controlling the outcomes of organic reactions, with applications across both catalytic and non-catalytic transformations. A number of groups have reviewed this area;[38, 108, 152-154] here, we present several selective examples of organic reactions in which various non-covalent interactions play vital roles.

Tambar, Tantillo, and coworkers documented the key roles of various weak interaction in the enantioselectivity of a phosphoric acid catalyzed aromatic aza-Claisen rearrangement.[222] Through computations, they showed that the catalyst engages with the substrate via NH···O and CH···O interactions; the 9-anthracenyl group of the catalyst blocks the bottom *Si* face, forcing the reaction to take place on the less crowded *Re* face. Moreover, it was shown that the higher selectivity in the case of aromatic substituents, compared to aliphatic substituents, can be attributed to additional stabilizing edge-to-face CH/π interactions in former cases (see Figure III-10).

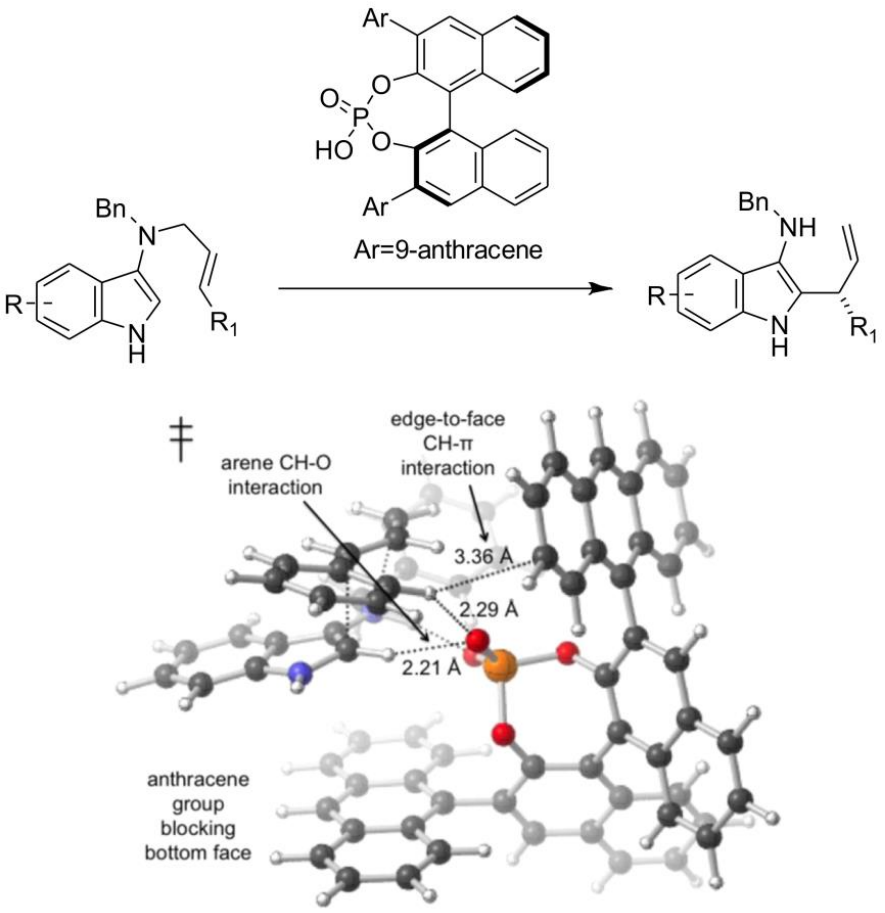

Figure III-10. Phosphoric acid catalyzed aromatic aza-Claisen of Tantillo, Tambar, and co-workers, along with their computed TS structure featuring a number of pivotal non-covalent interactions. Reprinted from American Chemical Society.

Nagasawa and co-workers[223] examined the role of non-covalent interactions in the stereoselectivity of an oxidative kinetic resolution of a tetralone derived β-ketoester using a guanidine-bisurea organocatalyst. In addition to hydrogen bonding interactions, dispersion-driven CH /π and π-stacking interactions played a crucial role in stabililizing the TS leading to the favored isomer (see Figure III-11). Although they did not quantify the impact of individual non-covalent interactions, their overall predicted free energy

differences between diastereomeric TS structures were in perfect agreement with experimental stereoselectivities.

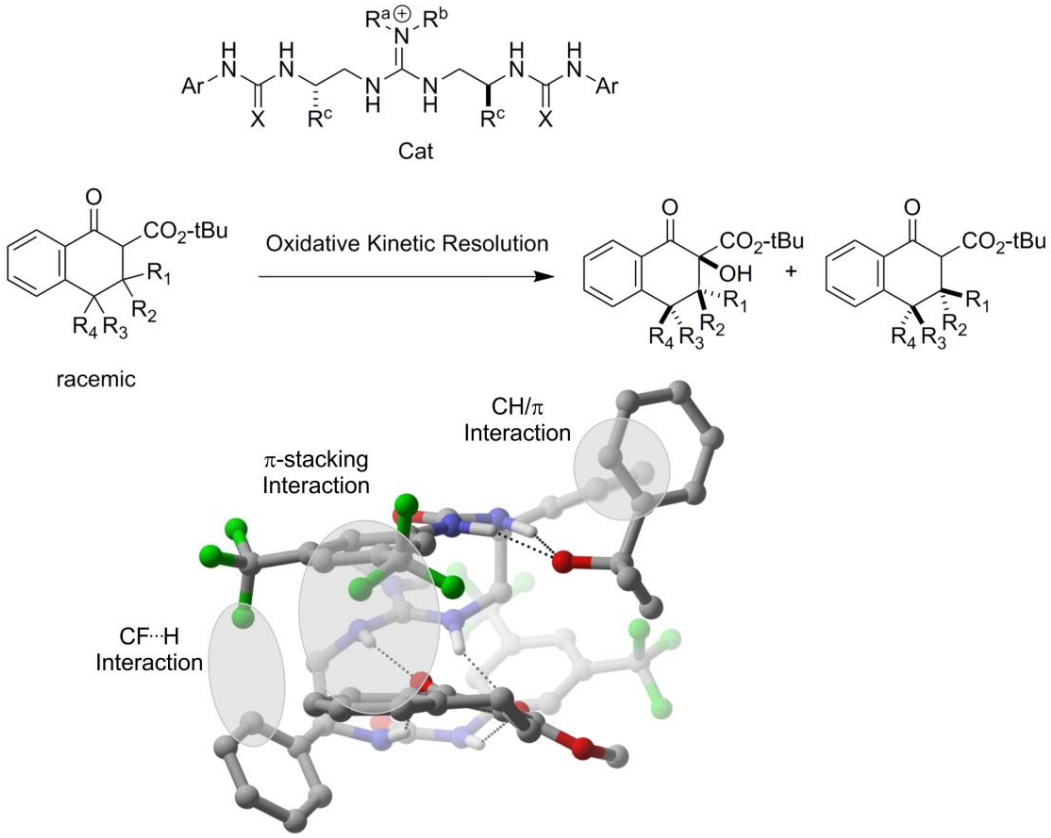

Figure III-11. Oxidative kinetic resolution of Nagasawa and co-workers, along with a key TS structure featuring non-conventional CF···H, π-stacking, and CH/π interactions.

Finally, we note that a thorough understanding of non-covalent interactions can pave the way for the design improved catalysts. Cheong, Schedt and co-workers[224] used their understanding of non-classical hydrogen bonds (NCHBs) to design an imidazolium-derived *N*-heterocyclic carbine catalyst for asymmetric homoenolate additions to acyl phosphonates. They envisioned that formation of the major (*S*,*S*) and minor (*R*,*R*) enantiomeric products stem from the nucleophilic attack of the acyl

phosphonate carbonyl by the homoenol, whereby differential stabilization of the phosphonyl oxygen by the aryl protons of the catalyst through NCHBs is mainly responsible for the observed stereoselectivity. A careful computational analysis of competing transition states revealed a number of important non-covalent contacts stabilizing the TS structures leading to both the major and minor products. This analysis suggested that methyl substitutions at the *meta* positions of the terminal phenyl would further destabilize the TS structure leading to minor enantiomer, which was then demonstrated experimentally (see Figure III-12). Replacing these methyl groups with even bulkier ethyl groups further increased the *er* to 94:6.

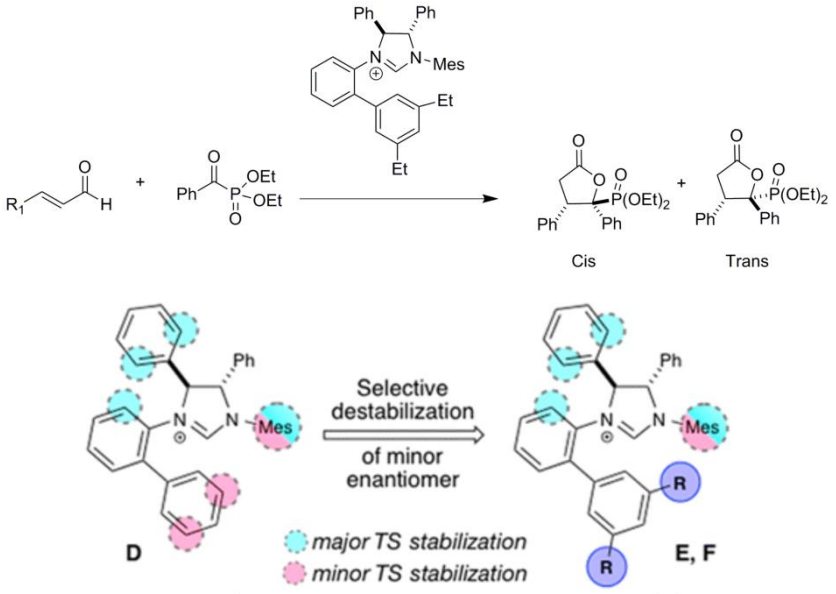

Figure III-12. NHC-catalyzed asymmetric homoenolate additions to acyl phosphonates, along with the computationally-derived strategy for enhancing stereoselectivity.

3.4.3 Non-Covalent Interactions in Biology Systems

Non-covalent interactions play vital roles in myriad biological systems,[225] impacting everything from the structure and stability of DNA and proteins to the binding

of ligands by proteins. As such, understanding these non-covalent interactions is important for understanding biological function and for the design of pharmaceuticals. Understanding π-stacking interactions is particularly important within the context of drug design. For instance, Klebe and co-workers[226] developed a potent inhibitor for aldol reductase featuring a *m*-nitrophenyl ring. X-Ray data revealed that the binding of this inhibitor is driven in large part by the stacking interaction of this *m*-nitrohphenyl ring with Trp111 chain in the binding pocket (see Figure III-13). Moreover, removal of the nitro group eroded the binding affinity by almost an order of magnitude, demonstrating the importance of substituent effects on π-stacking interactions and their subsequent impact on ligand binding.

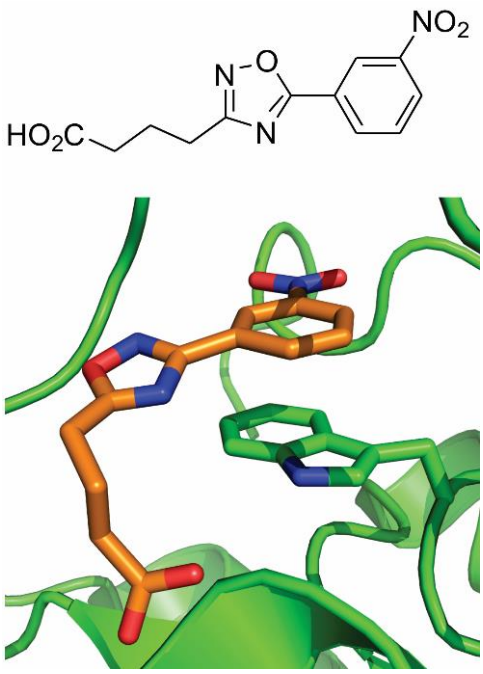

Figure III-13**.** Aldol reductase inhibitor from Klebe and co-workers[226] whose binding is driven in part by a π-stacking interaction between a nitrophenyl ring and Trp111 (PDB code: 2IKG).

π-stacking interactions are also important in DNA-intercalation phenomena, which have been widely studied using computational quantum chemistry.[227-230] For example, Hobza and co-workers[228] studied π-stacking interactions of four intercalators used in antitumor chemotherapy, showing that the binding is driven by a combination of electrostatic and dispersion interactions. Hargis *et al*.[230] studied the stacking interactions of DNA-base pairs with benzo[a]pyrene diol epoxide, (+)BaP-DE2, which the major carcinogenic component of tobacco smoke and soot (see Figure III-14). DFT optimizations showed that in some of the most favorable non-covalent complexes with the GC base pair, the epoxide is positioned for nucleophilic attack by the exocyclic amine of guanine. This provided a potential explanation for the strong tendency of this carcinogen to form covalent adducts to GC-rich regions of double stranded DNA.

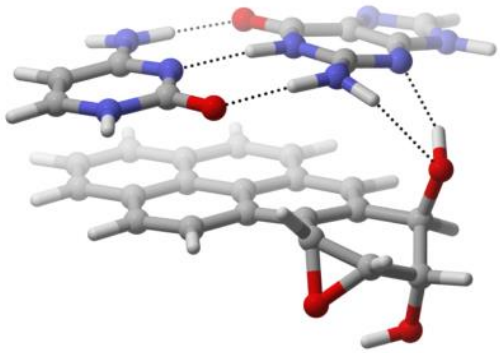

Figure III-14. Stacked complex of benzo[a]pyrene diol epoxide with the GC base pair in which the exocyclic amino group of guanine is ideally positioned for backside nucleophilic attack of the epoxide, from Hargis *et al*.[230]

Other non-covalent interactions abound in biological systems. For instance, Tantillo and coworkers[231] have probed the role of CH/π interactions as modulators of carbocation structure, with important implications in the panoply of cation-

rearrangements operative terpene biosynthesis. Efficacy of inhibition of the peroxisome proliferator activated receptors(PPAR) with its selective inhibitor partly reasoned due to favorable SH···π interaction[232] while the inhibitor binding to Chk1 kinase is operative via the putative involvement of CH···O and NH···π interactions[233]. CH···O interaction known to be involve catalytic mechanisms of numerous enzymes including serine proteases and methyltransferases.[234]

Finally, we note rapidly growing interest in anion–π interactions in biological systems, driven in large part by computational analyses of the PDB that have revealed many close contacts between anions and aromatic rings. Such structural studies are often accompanied by DFT or MP2 studies of the underlying non-covalent interactions. In 2013, Frontera and coworkers deciphered the key involvement of anion- π interactions Flavin dependent oxidoreductases.[235] X-ray crystal structure analysis along with DFT computations indicates that π-system of flavin adenine dinucleotide plays a key role to stabilize the anionic intermediate via an anion-π interaction. Similarly, the inhibition of ureate oxidate by cyanide has been explained based on attractive anion-π interactions between the CN^- anion and uric acid moiety.[236]

3.5. Practical Considerations

Modern DFT methods have opened the door for reliable studies of a broad range of organic systems in which non-covalent interactions play key roles. However, such studies must be carried out with due caution, since the description of these dispersion-driven interactions are not well-described by many once-popular methods. Although the impact of dispersion interactions might fortuitously cancel for a given system,

explaining the surprisingly good results derived from many older functionals such as B3LYP in many cases, in general it is mandatory to account for dispersion effects in any organic systems beyond a few dozen atoms. Luckily, there are now many widely-available DFT functionals that provide good descriptions of these interactions. In general, the 2nd and 3rd generation empirical dispersion corrections from Grimme *et al*. (the so-called -D2 and –D3 methods)[19, 21] are the simplest to employ, and can be paired with any well-behaved DFT functional. We have found that the B97-D functional,[19, 237] when paired with a triple-ζ basis set (such as def2-TZVP),[238] provides reliable predictions across many different non-covalent interactions and organic systems. Moreover, when paired with density fitting techniques, B97-D computations are inexpensive and can be routinely applied to systems with 100s of atoms or to 1000s of systems with dozens of atoms. However, as always, one must be careful to reliably capture all properties of interest. In this regard, it should be noted that B97-D provides reaction barrier heights and overall reaction thermochemistry that are often in significant error relative to experiment or more robust computational methods. More sophisticated functionals, including ωB97X-D,[239] ameliorate many of these problems, providing accurate predictions for non-covalent interactions, kinetics, and reaction thermochemistry. Of course, this comes with some increase in computational cost.

CHAPTER IV

CHIRAL PHOSPHORIC ACID CATALYSIS: FROM NUMBERS TO INSIGHTS[*]

4.1. Introduction

Chiral phosphoric acid (CPA) catalysed reactions, interest in which has grown considerably over the last dozen years (see Figure IV-1A),[11] have opened up previously inaccessible enantioselective synthetic routes and now constitute a key area of growth in the field of organocatalysis. Despite this progress, considerable gaps in our understanding of the modes of activation and stereoinduction in these reactions remain. In recent years, computational studies have unravelled key aspects of these reactions, providing insight into their often high degrees of activity and stereoselectivity and paving the way for more effective CPA catalysed transformations.

Paton and co-workers[240] recently provided a tutorial review on the computational modelling of stereoselective organic reactions, covering both computational methods as well as fundamental concepts important for understanding stereoselectivity (kinetic vs. thermodynamic stereoselectivity, the Curtin-Hammett principle, *etc*). Here we provide a detailed account by delving more deeply into computational studies of CPA catalysed reactions in particular, showing how careful analyses of computed transition state (TS) structures can help turn numbers into insights. We commence with an outline of the computational tools that can be used to understand CPA catalysed reactions.

---

[*] Adapted with permission from "Chiral Phosphoric Acid Catalysis: from numbers to insights" by R.Maji, S.C. Mallojalla and S. E. Wheeler, 2018. *Chem. Soc. Rev.*. **47**, 1142. Copyright 2018 Royal Chemical Society.

Subsequently, we describe various factors impacting stereoselectivity followed by qualitative models that have been developed to predict the stereochemical outcomes of these reactions. Next, we discuss the primary activation modes operative in these reactions as well as important categories of CPA catalysed reactions in which computational studies have proved vital to understanding stereoselectivity. This is followed by examples in which computations have provided a deeper understanding of other mechanistic aspects of these reactions. We conclude by highlighting outstanding challenges and areas that deserve special attention. Although this review is focused primarily on CPAs, selected examples of similar axially chiral phosphoramidites and phosphoramides are also included (see Figure IV-1B), since computational chemistry has also provided important insights into these related transformations.

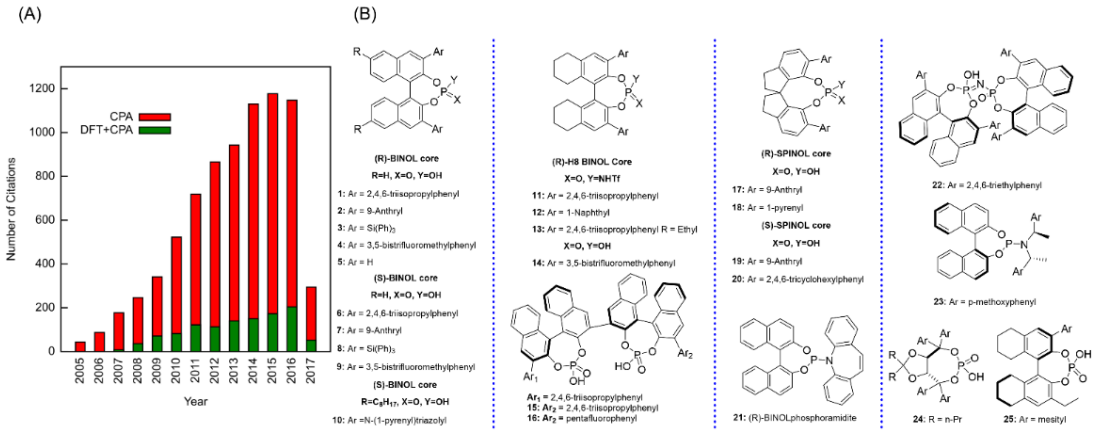

Figure IV-1 (A) Growth in the number of papers on CPA-catalysed reactions; (B) Chiral phosphoric acids (CPAs) and similar catalysts discussed in this work.

4.2. Theoretical methods and tools to analyze reactivities and selectivities

4.2.1 Computational Methods

Quantum chemical methods applicable to large organic systems have matured considerably in recent years, and the relative free energies of transition states for complex organic reactions can be computed with remarkable accuracy. Such methods include combined quantum mechanics/molecular mechanics (QM/MM) and QM/QM methods as well as Kohn-Sham density functional theory (DFT), which is well-suited for systems with 50-100 atoms. In QM/MM-based methods, such as ONIOM, parts of the system are treated quantum mechanically whereas other components (typically those not directly involved in the reaction) are treated using classical MM methods. A decade ago, such methods were widely employed to study CPA-catalysed reactions out of necessity. In these studies, the phosphoric acid moiety of the catalyst and the reactants were typically treated at the DFT level while the remaining components of the catalyst were treated at the MM level. However, with continued advances in computational hardware (following Moore's Law) and algorithms, reactions catalysed by large CPAs can now be treated entirely with DFT.

Such applications of DFT need to be done with care, however, to ensure that the many dispersion-driven noncovalent interactions operative in these systems (*vide infra*) are treated accurately. For example, the B3LYP functional, which for many years was the workhorse of computational organic chemistry, fails to account for dispersion-like interactions and can subsequently provide inaccurate results for CPA catalysed reactions. Luckily, the last decade has witnessed tremendous advancements in DFT methods that

capture dispersion-driven interactions. Chief among these are the empirical dispersion corrections from Grimme *et al*. (the so-called –D methods), which can be coupled with any well-behaved DFT functional (B3LYP, B97, TPSS, *etc*.). The continuum solvent models PCM and SMD have proved sufficient (and necessary!) for many of these reactions, although inclusion of explicit solvent is sometimes required.

In general, stereoselectivity depends on the difference in free energy between competing transition states, $\Delta\Delta G^{\ddagger}$. However, we note that many authors utilize enthalpies (or even electronic energies) due to errors associated with computing the entropic contributions to $\Delta\Delta G^{\ddagger}$. Once structures of key TS structures have been optimized, the battle has only begun, and one must turn to other computational tools in order to understand the origin of the energy difference between stereocontrolling transition states. Such tools are described in the following sections.

4.2.2 Distortion-interaction and fragmentation studies

Distortion-interaction analysis (or the activation-strain model), was introduced to explain trends in barrier heights of bimolecular reactions.[241] In such analyses, the reaction barrier ($\Delta E^{\ddagger}$) is decomposed into the energy required to distort the reactants into the TS geometry (ΔE_{dist}) and the interaction energy between these distorted fragments ($\Delta E_{int} = \Delta E^{\ddagger} - \Delta E_{dist}$). Distortion-interaction has also proved useful in explaining the difference in energy between stereocontrolling TS structures in asymmetric reactions. In such applications, the reaction barrier is decomposed into the energy required to distort the reacting substrates and catalyst into their TS geometries and the interaction energy between the distorted substrates and catalyst. It is important to note that in contrast to

the original applications to bimolecular reactions, in which ΔE_{int} reflected the extent of formation of the forming/breaking bonds, in applications to asymmetric reactions ΔE_{int} reflects the noncovalent interactions between the substrate and catalyst; any differences in the extent of formation of forming/breaking bonds is included in the substrate distortion energy.

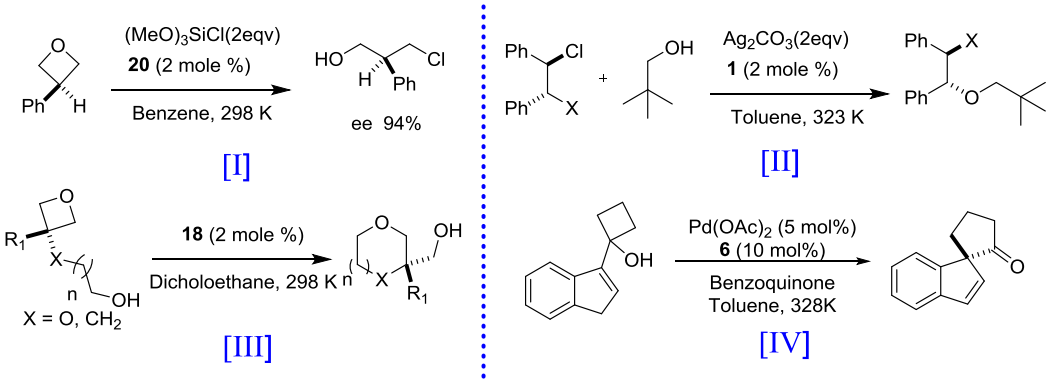

Scheme IV-1. Reactions demonstrating the use of distortion-interaction analysis to explain stereoinduction.[242-245]

Distortion-interaction analyses can be complemented by fragmentation studies, in which selected portions of optimized TS structures (*e.g.* aryl-substituents) are removed and replaced with hydrogens while holding the rest of the structure fixed.[244, 246] This can help pinpoint differences in interaction energies between similar stereocontrolling structures by systematically eliminating sources of noncovalent interactions. It should be noted, however, that such fragmentations often lead to only qualitative predictions of the strengths of these interactions; that is, the act of severing covalent bonds can lead to significant changes in the resulting interaction energies. The result is that the sum of

individual interaction energies is not always in strict agreement with the interaction energies computed for the intact TS structures.

Within the framework of distortion-interaction analyses, the stereoselectivity of CPA-catalysed reactions can be distortion-controlled, interaction-controlled, or controlled by both distortion and interaction energies. Among distortion-controlled reactions, stereoselectivity can arise from differences in either catalyst or substrate distortion, or both. For instance, Champagne and Houk[242] showed that distortion of the catalyst is mainly responsible for stereoselectivity in intermolecular oxetane ring-openings by *in situ* generated HCl (Scheme IV-1, reaction I). By excising the flanking aryl groups on the catalyst, they further showed that the excess catalyst distortion in TS_{minor} arises primarily from the phosphoric acid functionality of the catalyst. On the other hand, Duarte *et al.*[243] showed that in chiral phosphate mediated desymmetrizations of aziridinium and episulfonium ions (Scheme IV-1, reaction II), the stereoselectivity is primarily a result of excess substrate distortion in the TS leading to the minor stereoisomer.

With regard to interaction-controlled reactions, Maji *et al.*[244] showed that the selectivity of reaction III (Scheme IV-1) is governed primarily by differences in interaction energies between the catalyst and substrates. Finally, Jindal *et al.*[245] provided a recent example in which both distortion and interactions control selectivity (Scheme 1, reaction IV). In this Pd(II)-Brønsted acid catalysed migratory ring expansion of an indenylcyclobutanol, DFT computed structures for the stereodetermining step exhibit a nearly orthogonal arrangement of two chiral phosphates around Pd in TS_{major}, while

TS_{minor} shows a nearly coplanar arrangement. The square planer geometry around the Pd in the latter case leads to greater distortion than seen for TS_{major}. Furthermore, TS_{major} enjoys more C–H···π interactions compared to its counterpart and hence enjoys more favourable interactions.

Despite its demonstrated utility, distortion-interaction analyses alone do not always provide a comprehensive understanding of the mode of stereoinduction in CPA-catalysed reactions, since such analyses fail to quantify the separate contributions of steric interactions, dispersion interactions, and electrostatic interactions to the energy difference between stereocontrolling TSs.

4.2.3 AIM analysis and NCI plots

A number of computational tools have been developed to identify noncovalent interactions by analysing electron densities. In the atoms-in-molecules (AIM) framework, the presence of a bond path and bond critical point (BCP) along the bond path has been deemed an indicator of bonding interactions between two atoms. The stereoselectivity of several CPA-catalysed reactions has been attributed to differential noncovalent interaction based in part on the use of AIM to pinpoint crucial noncovalent contacts. For instance, Sunoj and co-workers[247-248] used AIM to identify the weak interactions responsible for stereoinduction in several CPA-catalysed reactions. In the case of an asymmetric sulfoxidation reaction,[247] preferential *Re* facial addition was explained by the greater number of favourable noncovalent contacts, as identified by AIM (Figure IV-2).

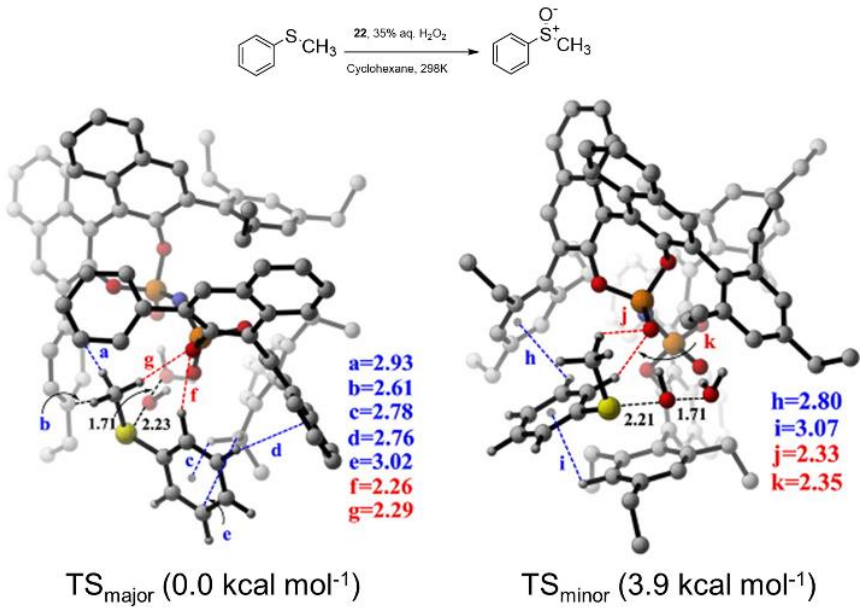

Figure IV-2**.** Stereocontrolling TS for CPA Catalysed asymmetric sulfoxidation reaction along with their relative free energies in kcal mol^{-1}.[247]

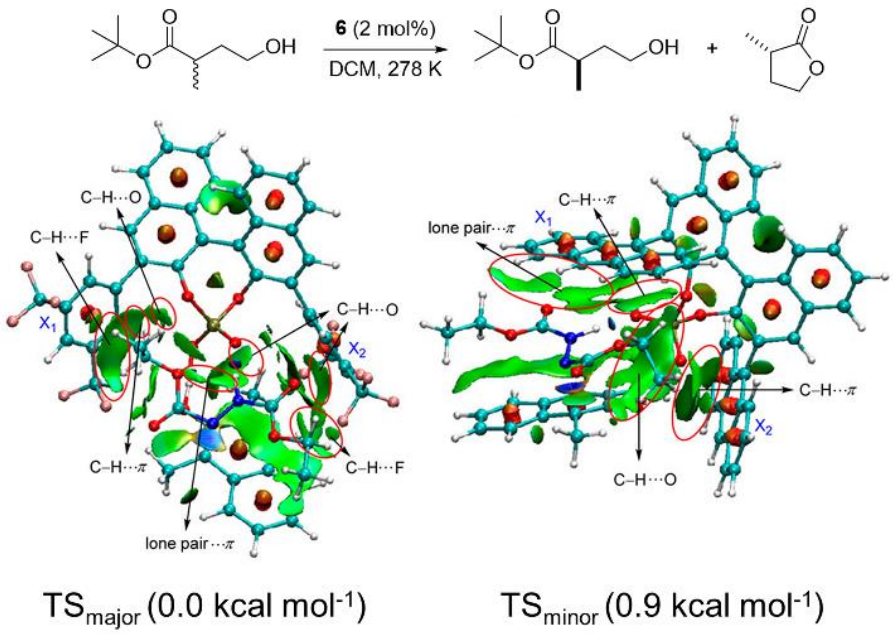

Figure IV-3. NCI analysis (blue, strong attraction; green, weak interaction; red, strong repulsion) of stereocontrolling TSs for CPA catalysed kinetic resolution of hydroxyl ester along with their relative free energies in kcal mol^{-1}.[249] Reprinted from American Chemical Society.

Noncovalent interactions can also be visualized by using the noncovalent interaction (NCI) index of Yang and co-workers,[209] which is also based on analyses of the electron density. Plots of the NCI index provide a qualitative mapping of inter- and intramolecular noncovalent interactions, with colours differentiating attractive and repulsive interactions. This enables a quick comparison of the dominant interactions operative in competing TSs. For instance, Changotra *et al.*[249] used NCI plots in their study of CPA catalysed kinetic resolutions of hydroxyl esters (Figure IV-3). Comparison of NCI plots for the major and minor TS structures reveals the presence of significantly more stabilizing dispersion-like interactions (green surfaces) in the former than in the latter.

4.2.4 NBO and Electrostatic potentials

Finally, natural bond orbital (NBO) analyses and analyses of ESPs provide means of quantifying specific noncovalent interactions in CPA-catalysed reactions. These approaches are particularly useful in unravelling the impact of competing noncovalent interactions in TS structures. For example, in their study of chiral phosphate mediated desymmetrizations (Scheme IV-1, reaction II), Duarte and Paton[243] utilised NBO second-order perturbation theory to quantify a key CH···O interaction between the catalyst and substrate (Figure IV-4A). Similarly, Paton and co-workers[250] also identified an important arene metal interaction in both the rate and stereodetermining oxidative coupling TS in the course of designing a chiral phosphoramadite ligand for a stereoselective Rh-catalysed [5+2] ynamide cycloaddition. In this case, NBO analysis

enabled the quantification of π-d donation and d to π* back-bonding in this reaction (Figure IV-4B), providing key insights that formed the basis for the design of a modified ligand that provided enhanced selectivity.

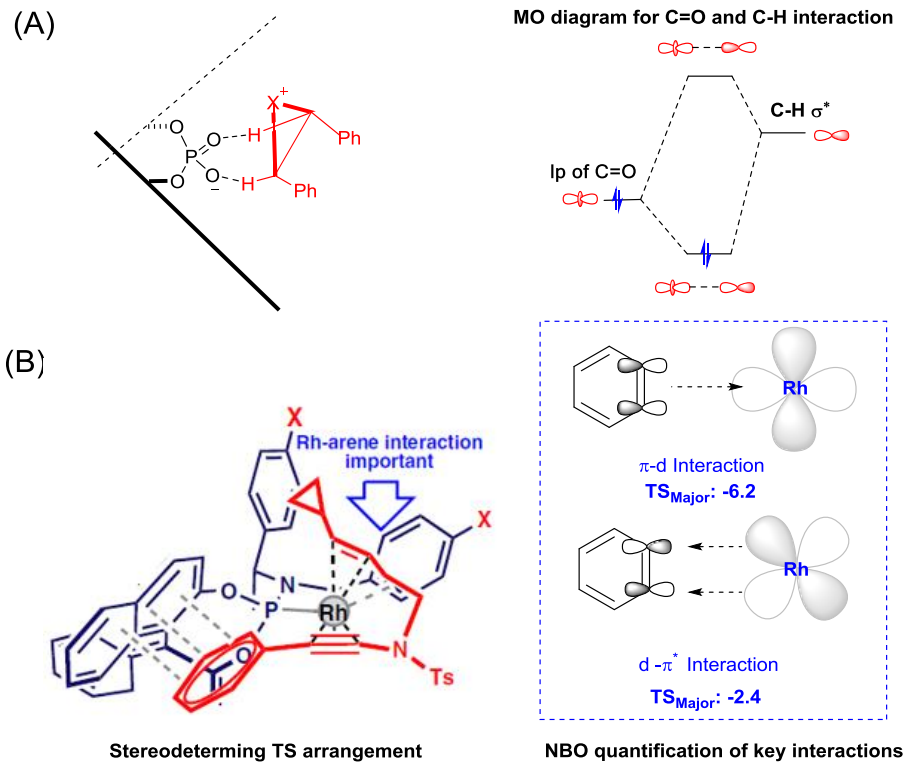

Figure IV-4**.** NBO quantification of interactions in CPA catalysis[243, 250]

An estimate of electrostatic interactions can be gleaned from computed ESPs of stereocontrolling TSs. The ESP is the electrostatic interaction that a positive test charge would experience at a point in space near a molecule, and reflects the balance between the repulsion of this test charge by the nuclei and the attraction by the molecular electron density. Since the ESP at a given point depends on the electron density everywhere in space, even a remote change in the electron density distribution can impact the ESP at a given point. As such, one should be cautious not to conflate changes in the ESP with

local changes in the electron density. In general, the electrostatic interaction between two molecules or molecular fragments can be approximated as the product of the charges due to one molecule (or fragment) with the ESP arising from the other molecule (or fragment). In this way, the electrostatic contributions of interactions in competing stereocontrolling TS structures can be compared in a semi-quantitative fashion.

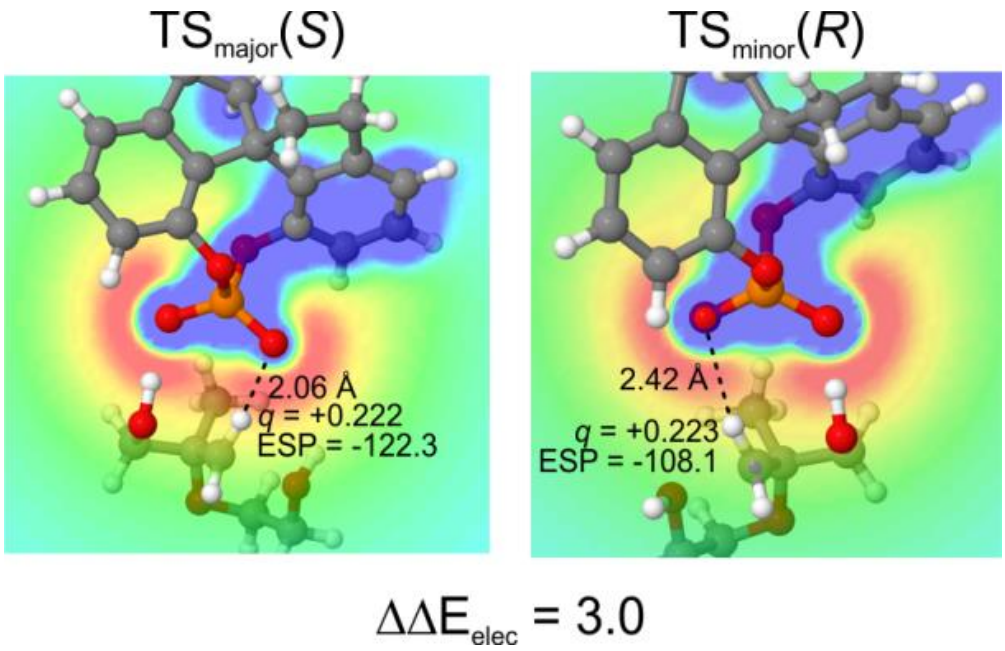

Figure IV-5**.** Quantification of relative electrostatic stabilization (ΔΔE, in kcal mol^{-1}) of a key proton in competing stereocontrolling TS structures.[244] The NPA charge (*e*) of this proton and ESP (in kcal/mol) due to the phosphate at the position of this proton are also provided.

For example, Maji *et al*.[244] used ESPs to quantify the contribution of electrostatic interactions to the energy difference between stereocontrolling TS structures in intramolecular oxetane ring openings. They found that a key proton resides in a more favourable electrostatic environment in TS$_{major}$ than in TS$_{minor}$ (see Figure IV-5). More precisely, the ESP at the position of this in TS$_{major}$ and TS$_{minor}$ (Figure IV-5) is –122.3

and –108.1 kcal/mol, respectively. Taking the product of these ESPs with the corresponding NPA charges reveals a 3.0 kcal/mol preferential electrostatic stabilization of the former.

4.3. Key stereodetermining factors in CPA catalyzed reaction

4.3.1 Steric environment

The steric environment around the chiral phosphoric acid framework has long been considered the dominant determining factor for stereoselectivity of CPA catalysed reactions. The presence of aryl side chains in the 3,3' positions of CPAs creates a well-defined, tuneable chiral binding cavity for the reacting substrates. As such, many explanations of the stereoselectivity of CPA-catalysed reactions hinge on the destabilization of the disfavoured TS through steric interactions of the substrates with the flanking aryl groups of the catalyst. This is the basic presumption behind the "Quadrant Projection" and "Goodman Projection" models described below in Section 4.4.

Reid and Goodman[251] have championed the idea that steric interactions between substrates and CPA catalysts can be broadly divided into *proximal* and *remote* steric effects (Figure IV-6A). Moreover, they showed that these effects can be quantified based on readily computed energetic and geometric parameters of CPA catalyst components. In particular, proximal steric effects are captured by two physical parameters: 1) *A* values for the distal substituents, which correspond to the thermodynamic difference between diaxial and diequitorial conformations of 1,3-disubstituted cyclohexanes; and 2) rotational barriers of the aryl side chains, which capture the energy required for rotation

around the central C-C bond to circumvent the destabilizing eclipsing interaction between attached R groups with the hydrogens of the opposing aryl ring. Remote steric interactions, on the other hand, can be described by the so-called AREA angle (A Remote Environmental Angle). AREA(θ) is defined as the smallest angle between the vector *p* (which goes from the midpoint of the naphthol oxygens to the Ph) and all possible *c* vectors (which extend from the Ph to each atom on the 3,3'-substituents).

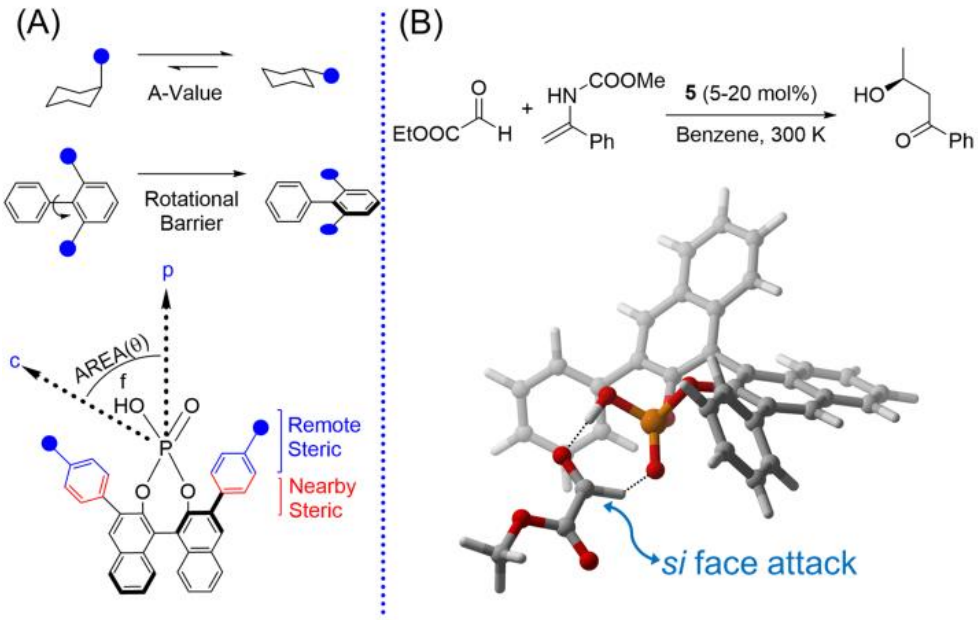

Figure IV-6**.** (A) Key steric parameters identified by Reid and Goodman[251] or CPA catalysed reactions. (B) Key stereocontrolling TS for a CPA-catalysed aza-ene reaction between glyoxylate and ene-carbamates.[252]

Steric interactions can impact stereoselectivity through two limiting mechanisms. Typically, these interactions destabilize one TS relative to competing TSs. In extreme cases, steric interactions can completely eliminate access to one prochiral face of a substrate in a pre-formed substrate/catalyst complex. The former category is widely

represented in the examples of CPA-catalysed reactions discussed in Section 6. As far as the second group, Terada *et al*.[252] rationalised the enantioselectivity of a CPA-catalysed aza-ene reaction between glyoxylate and ene-carbamate based on DFT computations (see Figure IV-6B). They reported that the two H-bonds between the catalyst and glyoxolate in the pre-reaction complex forces a coplanar orientation of the substrate with the phosphoric acid moiety. Based on these results, they argued that the *re* face of the aldehyde is shielded by the aryl side chain of the catalyst, thereby promoting nucleophilic attack of the carbamate from the *si* face.

Steric interactions can be difficult to quantify, since frequently it is distortion effects that arise to avoid steric interactions that drive selectivity, not the steric interactions themselves. For instance, the confined size and shape of the binding cavity of CPAs often induces significant distortion of either the catalyst or substrates to avoid significant steric clashes; the two distortion-guided reactions[242-243] described in Section 2.2 are examples. This effect can be particularly pronounced for CPA's that are relatively rigid (*e.g.* SPINOL derived CPAs). The excellent performance of axially chiral imidodiphosphoric acids,[247] with respect to their monomeric counterparts, can also be attributed in part to the greater ability of these more confined binding pockets to discriminate between stereoisomers via steric effects.

4.3.2 Noncovalent Interactions

The last decade has seen an increasing appreciation of the importance of attractive noncovalent interactions in organic systems in general and CPA catalysed reactions in particular.[253-254] The presence of heteroatoms bearing significant partial

charges as well as aryl groups that flank the reacting centre in CPAs can lead to myriad stabilizing noncovalent interactions in the stereocontrolling TSs. These interactions include π-stacking, CH···π, C=O···H, C-H···O, and lone-pair···π interactions, among others. Recent advances in our understanding of these interactions have enabled their use as key design elements CPA-catalysed reactions.[253]

Recently-reported reactions from the Toste and Sigman groups[253] demonstrate the power of noncovalent interactions to dictate the stereochemical outcome of CPA-catalysed reactions. For instance, they showed[253] that a stacking interaction between a triazole on the catalyst and an aryl component of the substrate was pivotal in an enantioselective oxidative amination (Scheme IV-2, reaction I). They also demonstrated[253] an enantiodivergent fluorination of allylic alcohols that exploits lone-pair···π interactions (Scheme IV-2, reaction II).

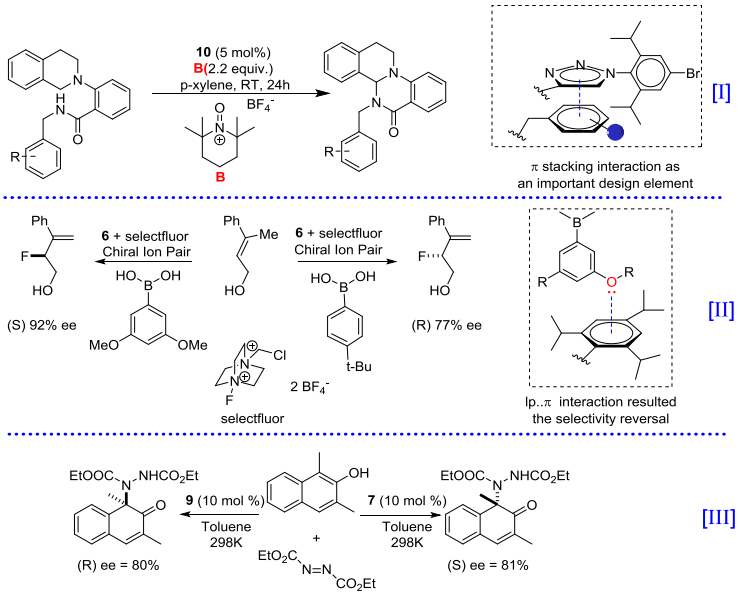

Scheme IV-2**.** Steric Exploitation of noncovalent interaction to design new stereoselective reaction.[253] CPA dependent stereo reversal in asymmetric dearomative amination of β-naphthols.[255]

Noncovalent interactions can also lead to reversal of selectivity. For example, Changotra *et al*.[255] demonstrated the potential for noncovalent interactions to dictate the stereochemical outcome of an asymmetric dearomative amination of β-naphthols (Scheme 2, reaction III). In this case, changing the aryl substituent on the CPA from 3,5-$(CF_3)_2$-C_6H_3 (**4**) to 9-anthryl (**2**) lead to a reversal in selectivity. This was explained in terms of the change in preferred orientation of the substrate within catalyst cavity. With **4**, the substrates were positioned perpendicular to the 3,3' substituents while with **2** they adopt a nearly parallel orientation. This, in turn, changed the pattern of noncovalent interactions from predominantly C–H···F to C–H···π in the stereocontrolling transition states, leading to the observed stereoreversal.

Often, the role of attractive noncovalent interactions in stereoinduction is obvious when examining the competing TS structures; a strongly stabilizing interaction might be present in the preferred TS but completely absent in the disfavoured TS. For instance, Tambar and co-workers[222] documented the role of noncovalent interactions in the enantioselectivity of a CPA catalysed aza-Claisen rearrangement (Figure IV-7A). Through computations, they showed that the catalyst engages with the substrate via NH···O and CH···O interactions; the 9-anthracenyl group of the catalyst then blocks the bottom *si* face, forcing the reaction to take place on the less crowded *re* face. Moreover, it was shown that the higher selectivity in the case of aromatic substituents, compared to aliphatic ones, can be attributed to stabilizing edge-to-face CH···π interactions in the former case.

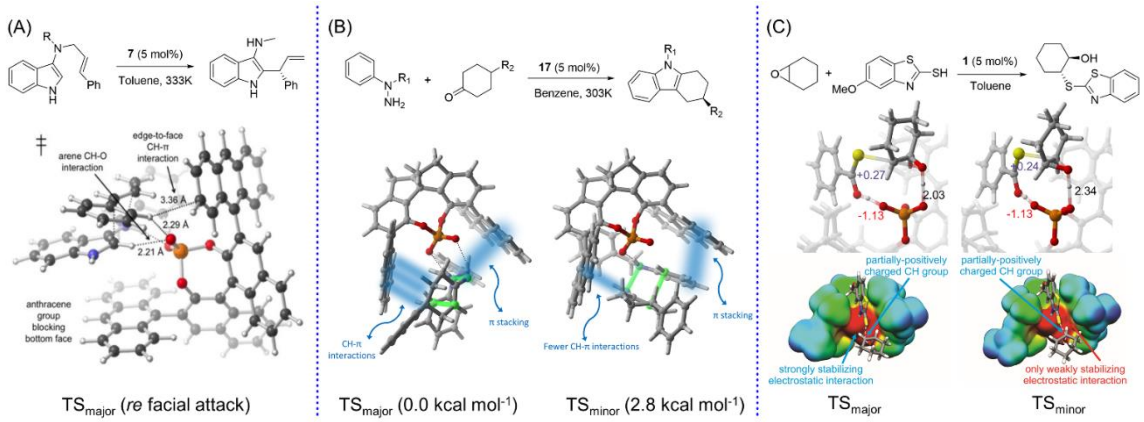

Figure IV-7. (A) CPA-catalysed aza-Claisen rearrangement.184. (B) DFT computed stereodetermining TSs of CPA-catalysed Fischer Indolization along with the free energies in kcal mol-1.188 (C) CPA-catalysed intermolecular epoxide openings.

However, in some cases the role of noncovalent interactions in stereoinduction is less clear, since many competing attractive interactions can be present in both the major and minor TSs. In such cases, one must quantify the individual interactions to pinpoint those primarily responsible for preferential stabilization of the favoured TS. For instance, Seguin and Wheeler[118] recently studied the CPA catalysed Fischer indole reaction in Figure IV-7B, identifying the two lowest lying TSs for the stereocontrolling [3,3]-sigmatropic rearrangement. TS_{major} was found to be 2.8 kcal/mol lower in free energy than TS_{minor}, providing reasonable agreement with the observed selectivity. Distortion-interaction analysis of these TS structures provided an interaction energy difference of 4.8 kcal/mol, which was partitioned into contributions from different noncovalent interactions via fragmentation. It was observed that while H-bonding interactions favour TS_{major}, π-stacking interactions between the substrate and anthryl

groups favour the minor TS. The dominant factor in this reaction turned out to be CH···π interactions, which favour the major TS by an overwhelming 5 kcal/mol.

A relatively unexplored property of CPA catalysts is their ability to achieve stereodifferentiation by constraining the orientation of the reacting substrates within the highly heterogeneous electrostatic environment of the binding cavity and thereby preferentially stabilizing one transition state over others. Often, CPAs protonate the substrate, and the subsequent TS structures correspond to ion-pairs. In many cases, the 3,3'-aryl groups of the CPA create a narrow cleft that restricts the orientation of the reacting substrates within the chiral electrostatic environment of the depronated catalyst. This can result in the preferential electrostatic stabilization of fleeting or permanent partial charges in the reacting substrates. Given the strength of electrostatic interactions compared to dispersion-driven interactions, for example, even small differences in the orientation of the substrate between two competing TS structures can have a substantial impact on enantioselectivity. Seguin *et al.*[246] and Maji *et al.*[244] have noted such examples in the context of CPA-catalysed epoxide and oxetane ring-openings, respectively. In both cases, examination of the ESPs of the competing TS structures proved informative (see Figure IV-7C), as did quantifying the electrostatic stabilization of key C-H groups in these structures (as described in Section 2.4). In the case of the asymmetric ring-opening of epoxides (Figure IV-7C), the TS structure leading to the preferred isomer is preferentially stabilized by electrostatic interactions of the C-H undergoing nucleophilic attack (which bears a significant partial positive charge during the TS) by the phosphoryl

oxygen of the deprotonated catalyst.[246] This electrostatic mode of stabilization in epoxide ring openings gained further support from a later study by List *et al*.[256]

4.3.3 Phosphoric acid pK_a

The judicious tuning of catalyst acidity has also proved fruitful as a path to catalyst optimization. For instance, Houk *et al*.[257] observed that the acidity of the Brønsted acid catalyst is crucial for the efficiency of ($3^+ + 2$) cycloadditions of hydrazones with alkenes; lower acidic phosphoric acids are ineffective, while more acidic chiral *N*-triflylphosphoramides proved highly selective. They analysed[257] these reactions using DFT, showing that the superior performance of *N*-triflylphosphoramidite based catalysts over CPAs can be attributed to distortion effects. That is, because of the higher acidity of the phosphoramidite, the cycloaddition TS requires little distortion of the ion pair complex. The inability of CPAs to protonate the hydrazones leads to greater distortion to achieve the TS geometry. Similarly, dithio-analogues of CPAs, whose pK_a's are generally lower than the corresponding CPAs, have proved effective in a number of transformations. In general, both yield and selectivity often suffer when these various acid catalysts with pK_a's outside of an ideal window for a given reaction are used.

Despite significant progress, a proper physical organic basis behind such pK_a-dependence remains elusive. One way to understand these effects would be to determine the acidity of these CPAs and correlate these with reactivity. However, the difficulty of experimentally determining reliable pK_a's of these catalysts hinders such studies. Gratifyingly, recent theoretical work by Cheng *et al*.[258-259] has provided DFT-based predictions of pK_a's for CPA catalysts in DMSO to a precision of ~0.4 pK_a units,

offering a possible route to more definitive studies of structure-activity relationship and rational tuning of CPA-like catalysts. Moreover, this computational approach is applicable to CPAs in presence of other catalysts, opening the door to tuning the CPA pK_a's in the context of cooperative catalysis.

4.4. Models to predict stereochemical outcomes

A primary aim of many computational studies is the development of a general, predictive model of the stereochemical outcome of reactions. One of the earliest such models was the Quadrant Projection of Himo[260] and Terada,[261] which has formed the foundation for explanations of a wide array of CPA-catalysed reactions. In Quadrant Projection, the catalyst is viewed along the C_2-axis (Figure IV-8), resulting in the aryl substituents on the catalyst occupying two of four 'quadrants'. The preferred TS structure is generally the one in which the substrates are positioned in the unoccupied quadrants, providing a simple visual tool for a qualitative understanding of stereoselectivity. This quadrant model was modified by Goodman *et al.*,[262] and has been used to develop a general predictive model of imine hydrogenation reactions. In the so-called Goodman Projection (Figure IV-8), the catalyst is oriented such that the BINOL oxygens are in the plane of the page, leaving the phosphoryl group lying above and below the page along with the aryl substituents. This provides an alternative visualization of steric interactions between the substrates and catalyst. These quadrant models have formed the basis for more specific predictive models of the stereochemical outcome of particular reactions. Representative examples are discussed below.

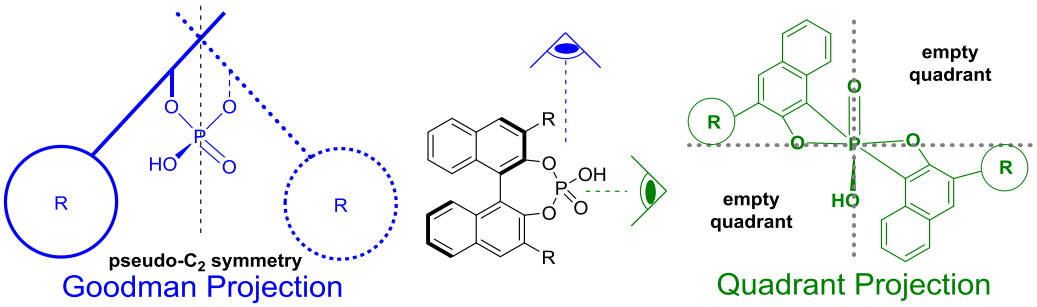

Figure IV-8. Goodman Projection and Quadrant projection of a CPA catalyst.[260, 262]

It is important to recognize that increasing steric demand does not always translate into greater selectivity; instead, it can stop the reaction altogether or even reverse the sense of stereoinduction. One case, from Reid and Goodman,[251] involves the transfer hydrogenation of an imine (Figure IV-9), in which reversal of stereoselectivity is observed depending on the size of the 3,3'-substituents. Reid and Goodman[251] proposed a model, based on their remote and proximal steric parameters (Figure IV-6), that can be used to predict the outcome of this complex CPA catalysed transformations. In this reaction, the imine can be oriented in two different ways with respect to the 3,3' groups (Type 1 and Type 2). Moreover, the imine can be in either a cis (Z) or trans (E) conformation based on internal steric demand, leading to four unique TS arrangements for such reactions (two of which are shown in Figure IV-9). Among these, Type 1E and Type 2Z furnish the (S)-product while Type 1Z and Type 2E afford the (R)-product. ONIOM computations indicate that for catalysts **6** and **8**, Type 1 is preferred. However, these computations also show that Type 1Z is preferred with catalyst **6** but Type 1E is preferred with **8**. This was explained in terms of the strikingly different steric parameters for these two catalysts. For **8**, the catalyst cavity is of a medium size, and the

E conformation is preferred over Z in order to reduce internal steric interactions in the imine. For **6**, on the other hand, the larger 3,3'-groups result in a much smaller catalyst cavity and the steric interactions between the R groups and the aryl side chains outweigh the energetic cost of internal steric repulsions. The result is a preference for Type 1Z and a reversal of stereoselectivity compared to **8**.

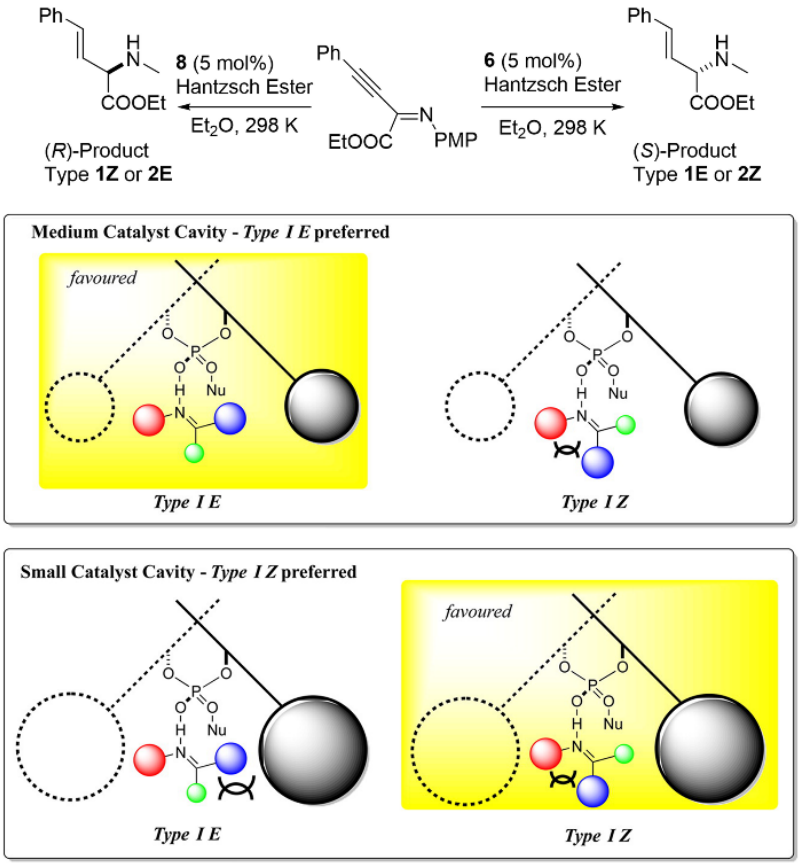

Figure IV-9. (A) Model to account for proximal and distal steric requirements in bifunctional CPA-catalysed reactions of imines.[263] Reprinted from American Chemical Society.

Goodman *et al*.[264] and Houk and co-workers[265] have both studied CPA catalysed allylation and propargylation reactions, showing that these reactions proceed via cyclic,

six membered chair-like transition states. Two distinct TS models have been proposed to explain the selectivity (see Figure IV-10). In both models, the Brønsted acidic functionality of the CPA activates the boronate ester through a hydrogen bond. While the pseudo-equatorial oxygen of the boronate is activated in Houk's model, the pseudo-axial oxygen of the boronate is activated in Goodman's model. Furthermore, in Goodman's model the formyl hydrogen interacts with the Lewis basic part of the CPA, while in Houk's model electrostatic interactions are responsible for orienting the aldehyde. Further studies showed that transition states corresponding to these two models are of comparable energy for formation of the major isomer, indicating that both models are potentially relevant to formation of this stereoisomer. However, Houk's model was found to be the dominant pathway for formation of the minor isomer. While steric interactions are primarily responsible for the stereoselectivity in Goodman's model, stereoselectivity in Houk's model is due to distortion of the catalyst to avoid steric interactions.

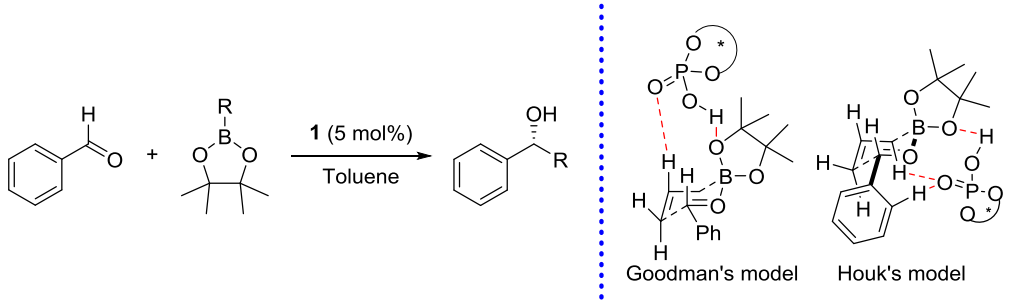

Figure IV-10**.** CPA catalysed allylation and propargylation of aldehydes.[264]

Champagne and Houk[242] proposed a working model for intermolecular oxetane openings (Scheme IV-1, reaction I) based on Quadrant Projection.[242] According to their

model (Figure IV-11), the nucleophile and the leaving group occupy the empty quadrants in TSs leading to both the major and minor products, which projects the larger substituent of the oxetane *anti* to the catalyst. From this projection, one can predict the preferred isomer considering the overall steric interaction. The TS that would suffer minimum steric repulsion between the substituent of the oxetane (blue sphere) and the substituents at the para position of the catalyst walls (black spheres) is predicted to be favoured. This simple model is remarkably successful at predicting the stereochemical outcome for other intermolecular oxetane openings and amination reactions without any further computations.

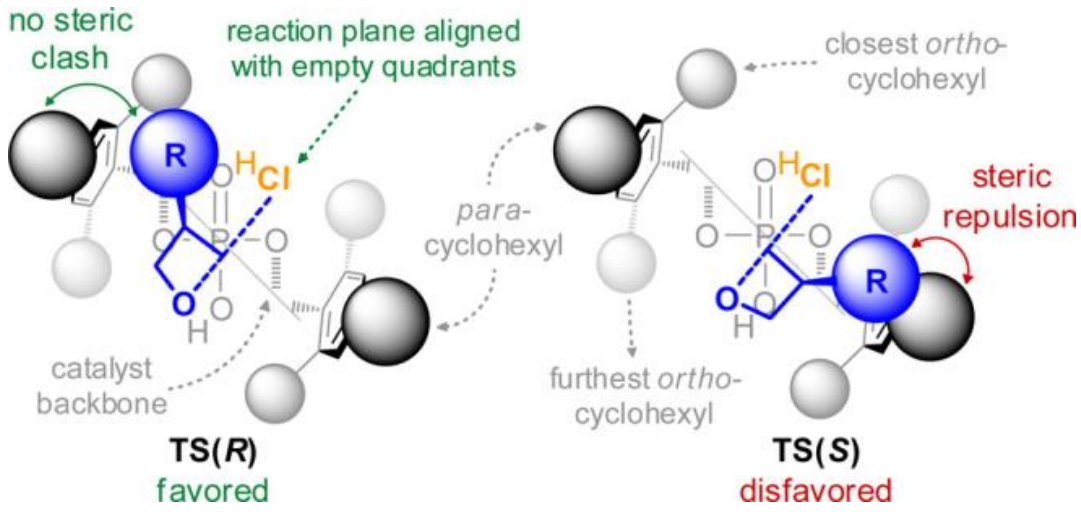

Figure IV-11. Stereochemical model to predict the outcome of an intermolecular oxetane openings .[242] Reprinted from American Chemical Society.

Despite the success of this model, it failed to explain the outcome of intramolecular oxetane desymmetrizations. In light of this, Maji *et al.*[244] recently proposed two new models (Figure IV-12) that explain the stereoselectivity of these reactions. The difference is that in these intramolecular reactions, the coordination of

both the electrophile and nucleophile with the acid and basic sites of the CPA requires significant substrate distortion. The result is a qualitatively different activation mode in these intramolecular reactions (see below) and a qualitatively different origin of selectivity. Moreover, the presence or absence of a chelating group (*e.g* OH) leads to qualitatively different TS arrangements than seen for substrates without chelating groups.

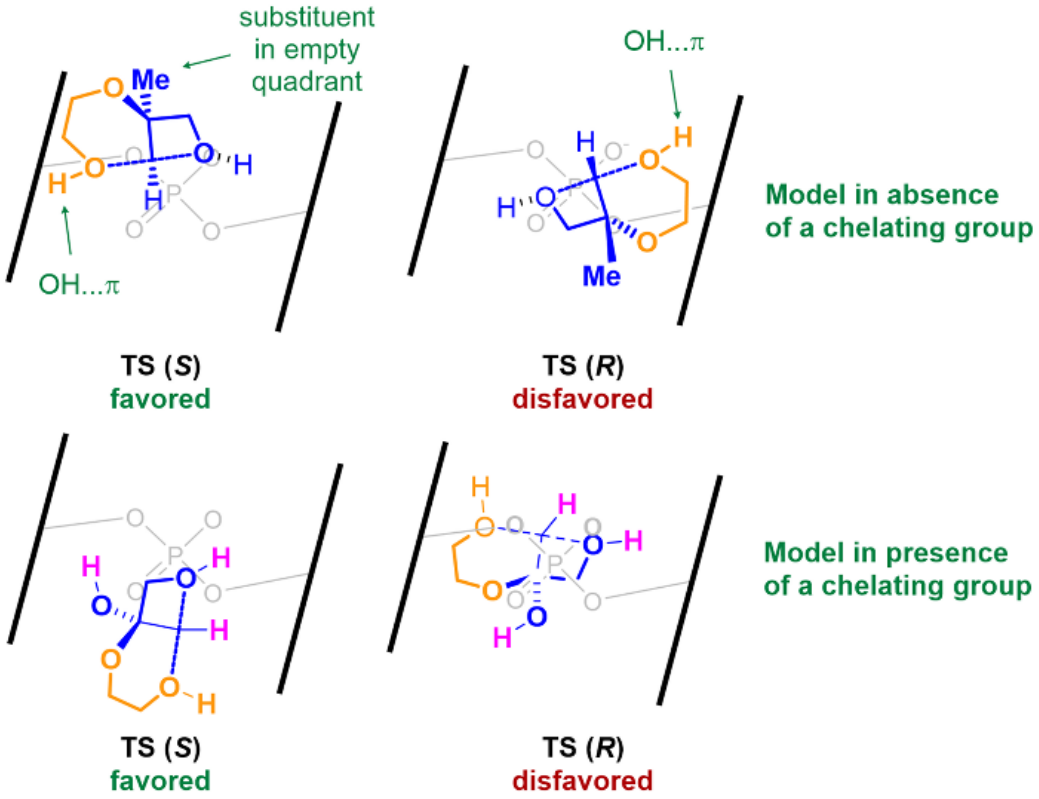

Figure IV-12. Two different models for intramolecular oxetane opening.[244]

4.5. Overview of binding and activation modes

Understanding the binding and activation mode is vital for designing new CPA catalysed reactions. In conventional CPA-catalysed reactions, activation occurs by the

lowering of the LUMO energy of the substrate through either hydrogen bonding or protonation by the phosphoric acid. This has traditionally been thought to occur via two primary modes, dual activation and bifunctional (either inter- or intramolecular) activation (Figure IV-13A).

However, computations have revealed additional activation and binding modes, broadening the scope of CPA catalysed reactions. For example, while CPA activation typically involves two-point contact (which is generally thought to impart greater selectivity), Calleja *et al*.[266] showed the feasibility of one point coordination in the context of an asymmetric Povarov reaction (Figure IV-13B). DFT computations indicated the favourability of an atypical one point coordination between the imine and the chiral phosphoric acid that maximizes π-stacking interactions while minimizing steric interactions in the transition state. In a similar spirit, Maji *et al*.[244] recently reported (Figure IV-13C) a distortion-guided activation mode in the case of intramolecular oxetane openings (Scheme IV-1, reaction III). In the preferred TS, the phosphoric acid activates the oxetane through an OH···O hydrogen bonding interaction while the aryl substituent of the catalyst activates the nucleophilic oxygen via an OH···π interaction. This "oxetane activation" mode was shown to be more favourable than more conventional activation modes, which can be understood in terms of the relative distortion energies of the substrates in the corresponding TS structures. For the traditional bifunctional activation mode, the substrate distortion is substantial due to the ring strain required to engage in two OH···O interactions with the catalyst. This strain is largely alleviated in oxetane activation, in which one OH···O interaction is replaced with

a CH···O interaction. The lack of distortion in this mode more than compensates for the relative weakness of the CH···O interaction compared to an OH···O hydrogen bond.

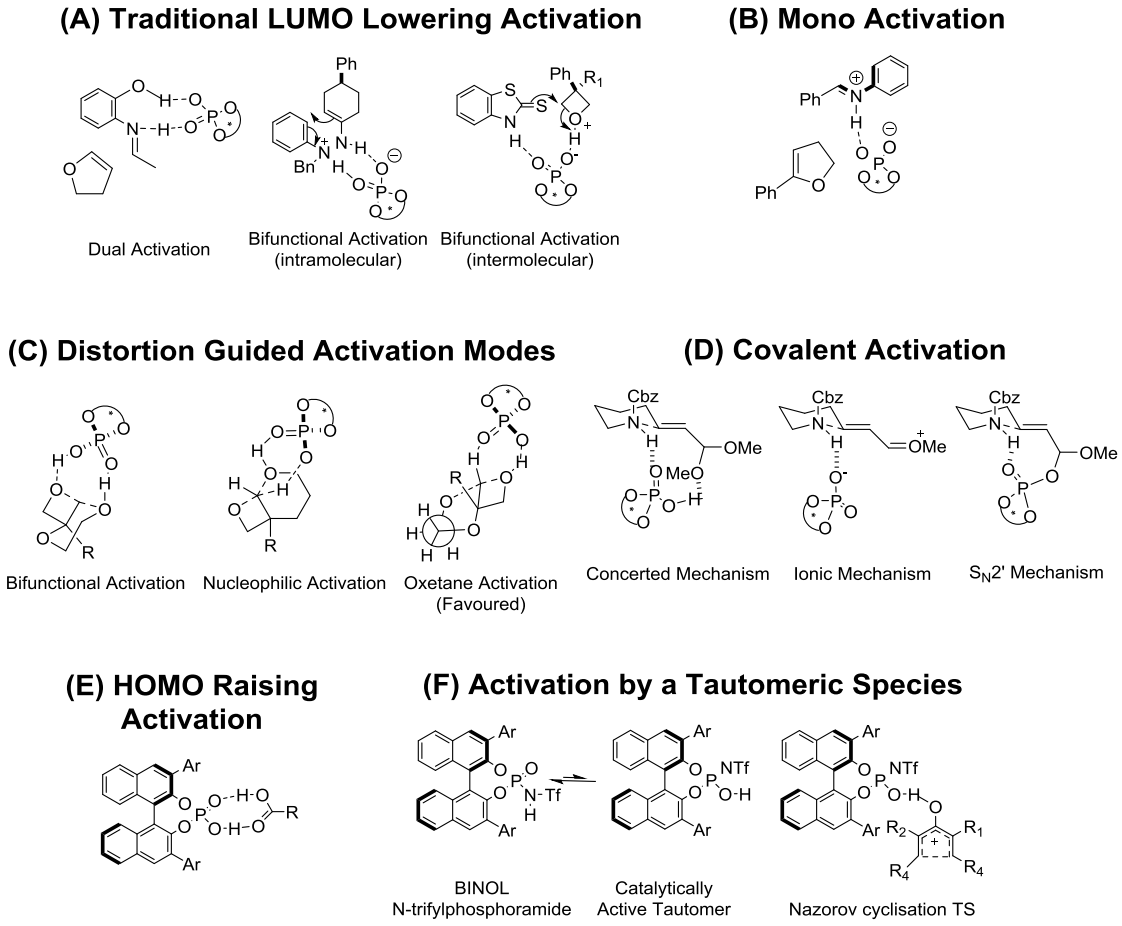

Figure IV-13. Various activation modes in CPA catalysis identified through computational studies.

While CPA catalysis typically occurs via noncovalent activation of the substrates, computations have also identified examples of covalent activation. This is somewhat unexpected, as the formation of covalent bonds typically leads to the deactivation of CPA-based catalysts. However, Nagorny, *et al.*[267] studied the CPA catalysed synthesis of piperidines through an intramolecular cyclization of unsaturated

acetals. They showed that an unexpected SN2' pathway is favoured over the expected concerted or ionic mechanisms (Figure IV-13D).

Recent computational and experimental work from Thiel, List, *et al*.[256] has revealed that CPAs can also activate substrates by raising the HOMO energy. In contrast to the more common LUMO lowering pathway, computed FMO energies reveal that the HOMO energy of acetic acid is increased upon complexation with TRIP while the energy of the LUMO remains almost unchanged (Figure IV-13E). This represents a potentially powerful new mode of activation for CPA catalysed reactions.

New binding modes of chiral phosphoramides have also been identified through computations. While the active form of chiral phosphoramides is typically thought to be the more stable amide tautomer (*i.e*. NHX and P═O),[257] Krenske and co-workers[268] showed that the active form of a BINOL-*N*-triflylphosphoramide catalysed enantioselective Nazarov cyclization is the less-stable tautomer containing a P(═NTf)OH group (Figure IV-13F). This was attributed to the more facile protonation of the substrate from an OH compared to NH, which occurs concomitantly with ring closure. Interconversion between tautomers was predicted to be fast, relative to electrocyclization, making this process viable under Curtin-Hammett conditions.

4.6. Reactions involving phosphoric acid

Having discussed computational tools, qualitative models, and the major activation modes operative in CPA catalysis, we now turn to representative examples of CPA catalysed transformations that have been analysed computationally. Stereoselective CPA catalysed reactions can generally be grouped into five categories: Brønsted acid

catalysis, chiral counterion catalysis, chiral anion phase transfer catalysis, chiral cooperative catalysis, and chiral relay catalysis. While the literature on CPA catalysis is dominated by Brønsted-acid mediated reactions, computational studies have also been applied to these other categories. Below, we mainly focus on Brønsted-acid mediated catalysis (Sec. 4. 6.1), followed by a more abbreviated discussion of other modes (Sec. 4.6.2).

4.6.1 Brønsted acid catalysis

4.6.1.1 Asymmetric hydrogenations

DFT has been applied to a number of CPA-catalysed hydrogenations. For example, Simón and Goodman[269] studied a Hantzsch ester mediated hydrogenation, revealing that the bifunctional activation mode is preferred. Based on this bifunctional activation, the selectivity of this reaction was explained in terms of a three-point model based on steric interactions. In the case of acyclic imines, E-Z interconversion is rapid and the reaction proceeds through the Z-conformer to avoid steric interactions between the incoming nucleophile and the catalyst. This model is supported by analyses of the Goodman Projection of the computed TS structures. Phenylimine forms a complex with the phosphoric acid through hydrogen bonding, leaving the bulky substituents oriented away from the 3,3'-substituents of the catalyst. The Brønsted acid functionality of the catalyst then activates the nucleophile, completing the three-point contact model. Because they cannot freely interconvert between *E* and *Z* conformations, the stereochemistry in the case of cyclic imines is dictated by the stereochemistry of the imine in order to minimize steric interactions (Figure IV-14).

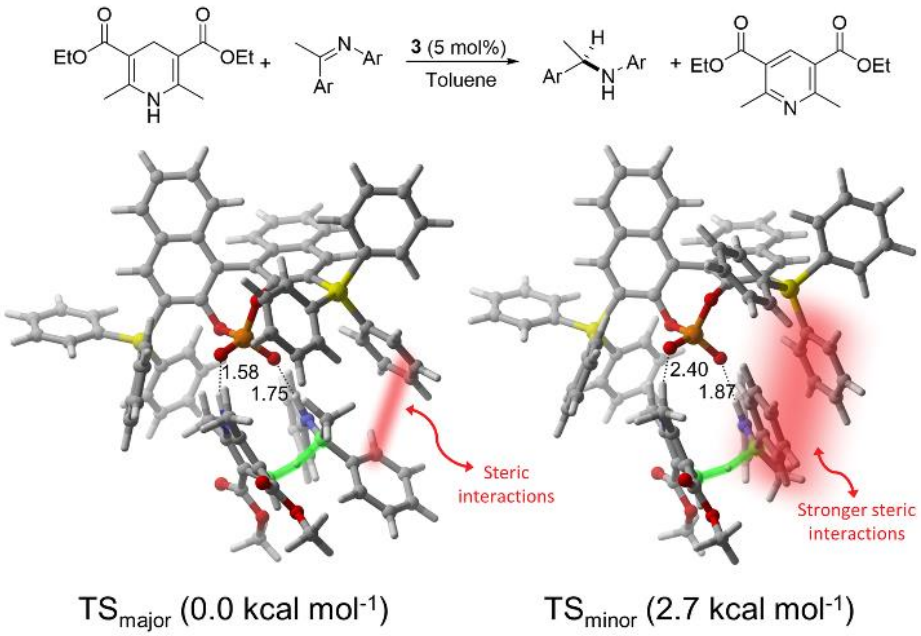

Figure IV-14. Stereodetermining TSs of CPA catalysed Hantzsch ester mediated hydrogenation along with their free energies in kcal mol^{-1}. [269]

4.6.1.2 Kinetic resolutions and dynamic kinetic resolutions

Akiyama *et al.*[270] utilized CPA-catalysed transfer hydrogenation for the oxidative kinetic resolution of indolines. DFT studies suggested a cyclic TS in which the Brønsted acidic proton activates the ketimine while the Lewis basic phosphoryl oxygen hydrogen bonds with the indoline N-H, thus activating both substrates. Examining the Quadrant Projection suggests that the *syn* ketimine is favoured over the *anti* ketimine due to steric factors (Figure IV-15), explaining the observed stereoselectivity.

Nimmagadda *et al.*[271] recently reported the synthesis of chiral oxime ethers via the dynamic kinetic resolution (DKR) of cyclohexanones catalysed by metal salts of CPAs. Computed structures for the stereocontrolling transition states revealed a shape complementarity between the reacting substrates and chiral binding pocket of the

catalyst in the case of the TS leading to the major stereoisomer. This resulted in more favourable NH···O and CH···π interactions in this TS, which lead to the observed stereoselectivity (Figure IV-16).

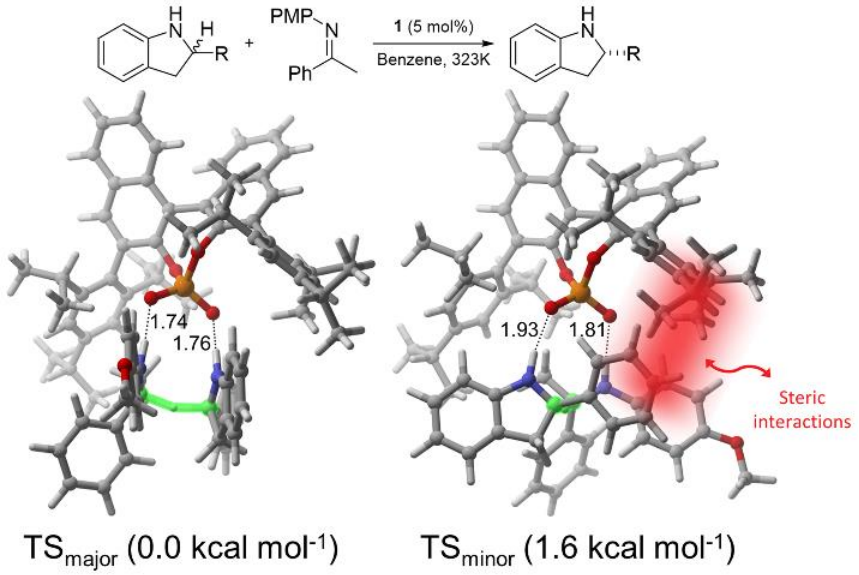

Figure IV-15. TS showing key interactions in the oxidative kinetic resolution of indolines along with their relative electronic energies in kcal mol^{-1}.[270]

4.6.1.3 Desymmetrization

Intramolecular and intermolecular desymmetrizations of epoxides and oxetanes have been studied computationally by a number of groups.[242, 244, 256, 272-273] Some aspects of these reactions have already been discussed in the sections above; below, we briefly summarize key findings along with two other desymmetrization reactions. Ajitha and Huang[272] first studied the asymmetric ring-opening of *meso* epoxides using DFT. They reported that the reaction proceeds via a concerted bifunctional pathway where a C-H···O interaction combined with steric effects govern the enantioselectivity. Subsequently, Seguin and Wheeler[246] performed a more extensive study of nine reactions/catalyst

combinations, arriving at a slightly different understanding of these reactions (Figure IV-7C). They argued that the difference in CH···O distance observed by Ajitha and Huang[272] is a consequence of other noncovalent interactions, and does not account for the free energy difference between the stereocontrolling TSs. Instead, they explained the preferential nucleophilic attack of one carbon over the other to the different electrostatic environments of the two carbons of the epoxide within the heterogenous electrostatic environment of the deprotonated catalyst. This resulted in the preferential electrostatic stabilization of a transient positive charge in the major TS, which ultimately gave rise to the observed stereoselectivity.

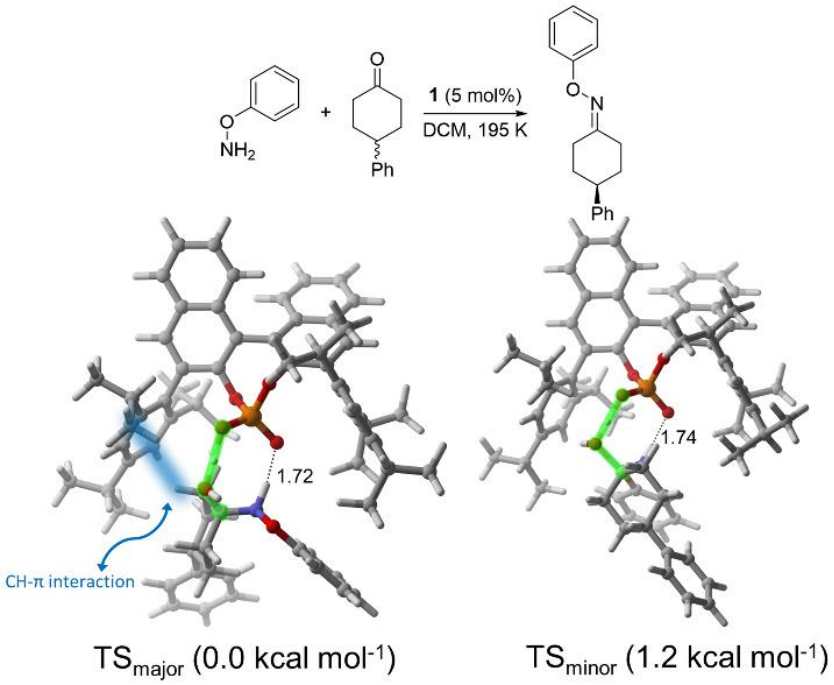

Figure IV-16. DFT optimized TS structures leading to the favoured and disfavoured stereoisomeric oxime ethers along with relative free energies in kcal mol^{-1}.[271]

Seguin and Wheeler[273] and Champagne and Houk[242] independently studied the catalytic enantioselective intermolecular desymmetrizations of oxetanes, arriving at disparate conclusions regarding the origin of selectivity. Champagne and Houk[242] pinpointed catalyst distortion as the primary contributor to selectivity in intermolecular oxetane desymmetrizations by HCl, proposing a general model for stereoinduction in such reactions. On the other hand, Seguin and Wheeler[273] examined four examples of oxetane ring openings by mercaptobenzothaizoles (see a representative example in Figure IV-17), showing that the mode of stereoinduction and TS structures changed markedly with small variation in substrate and catalyst. Overall, they reported that stereoselectivity is governed by the interplay of many relatively modest noncovalent interactions, precluding the development of a general stereochemical model. Similarly, Maji *et al*.[244] recently showed that the stereoselectivity of intramolecular oxetane desymmetrization (Scheme IV-1, reaction III) is controlled primarily by competing electrostatic and π-stacking interactions. Unlike the epoxide desymmetrizations studied by Seguin and Wheeler,[246] the impact of electrostatic interactions in these oxetane desymmetrizations depends on nature of the chelating group.

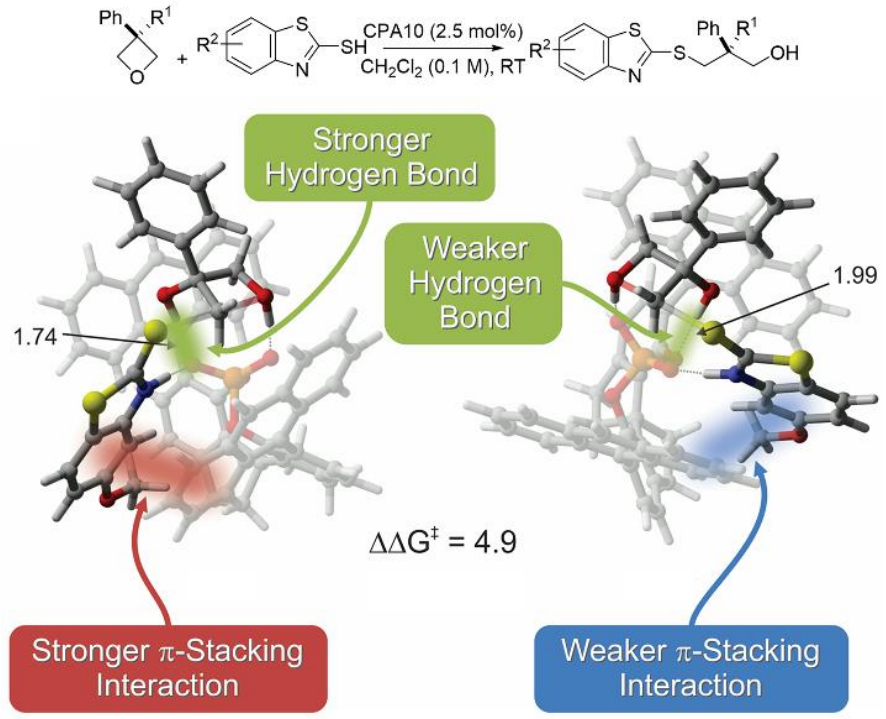

Figure IV-17. Intramolecular oxetane openings by marcaptobenzothiazoles,[273] in which the left structures leads to the major product. (Relative free energies in kcal mol^{-1})

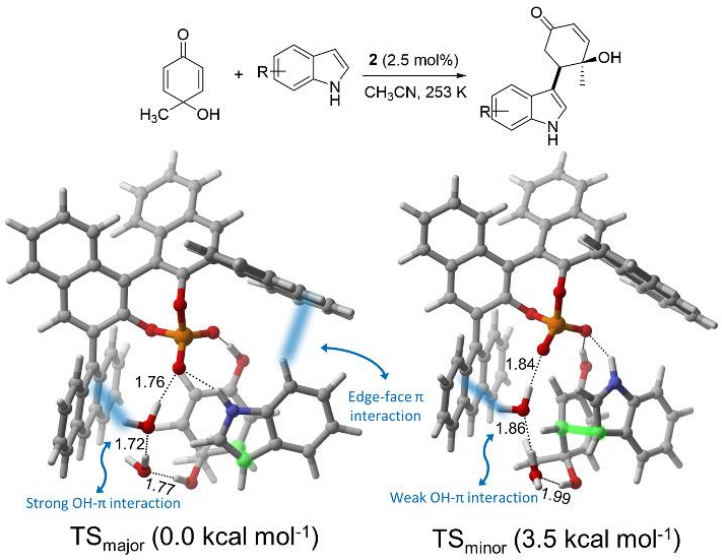

Figure IV-18**.** TSs showing major interactions involved in CPA catalysed FC alkylation along with their computed free energies in kcal mol^{-1}.[274]

Garcia *et al*.[274] studied the desymmetrization of cyclohexadiones via a Fridel-Crafts alkylation experimentally (Figure IV-18), finding that the exclusion of water from the reaction decreased both the rate and enantioselectivity. DFT computations provided a compelling explanation for this intriguing experimental outcome. First, the experimental data could be reproduced only if two explicit water molecules were included in the computations. The associated TS structures revealed two important roles of water. First, the presence of water results in a more compact catalyst cavity in the major TS. Second, water preferentially stabilizes the major TS by engaging in an OH···π interaction with the anthracenyl substituent on the catalyst. TS_{major} is further stabilized by an edge-to-face aryl-aryl interaction between the indole and the other anthracenyl group (Figure IV-18).

Houk *et al*.[275] studied the CPA catalysed oxidative desymmetrization of substituted diols via oxidative cleavage of benzylidineacetals (Figure IV-19). To explore the origin of enantioselectivity, the authors used a model biphenol-derived CPA to study the key proton-transfer TS. The computed free energy of TS_{major} was 2.0 kcal/mol lower than that of TS_{minor}, in good agreement with the 95% *ee* obtained experimentally. Given the lack of obvious steric interactions in these two competing TS structures, the authors argued that stereodifferentiation arises from the orientation of the *p*-methoxyphenyl (PMP) group of the substrate relative to the bulky aryl substituent on the catalyst. While these two aryl groups are distant in the minor TS, they engage in a stabilizing T-shaped interaction in TS_{major}. This aryl–aryl interaction was shown to contribute the majority of the energetic preference for TS_{major}. Given the importance of this interaction, the authors predicted that replacement of the PMP group in the original

substrate with methyl would significantly erode the enantioselectivity. This was validated experimentally.

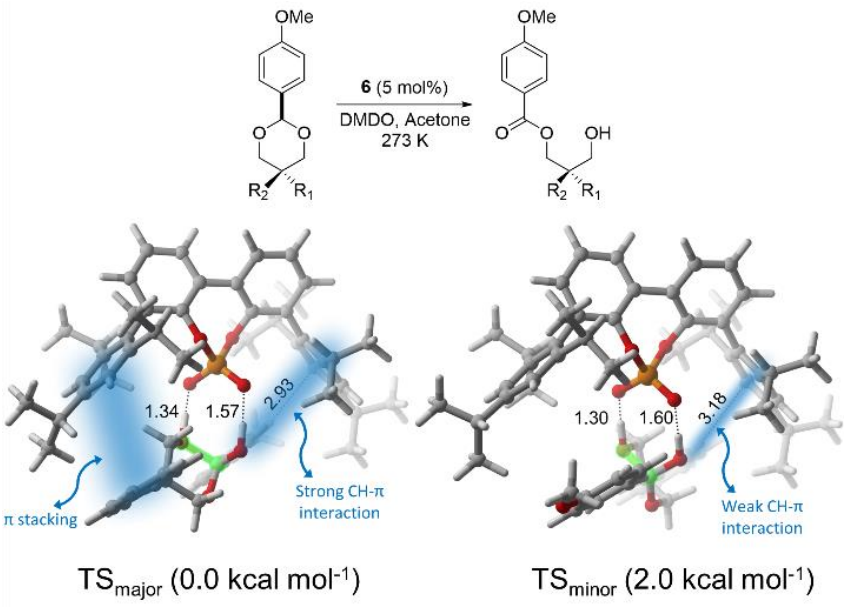

Figure IV-19. Stereodetermining TSs for oxidative desymmetrization of benzylidineacetals, along with their relative free energies in kcal mol^{-1}.[275]

4.6.1.4 Pericyclic reactions

Bis-phosphoric acids have been shown to be more acidic than monophosphoric acids, and can form extensive hydrogen bonding networks. Terada *et al.*[276] exploited these features to develop bis-phosphoric acid based catalysts (**21** and **22** in Figure IV-1), demonstrating their efficacy in an asymmetric Diels-Alder cycloaddition (Figure IV-20). Computations suggest that the (*S, R, S*) atropodiasteriomer of the symmetric catalyst (**21**) is favoured and the chiral environment provided by this catalyst is distinct from that of the corresponding CPA due to the hydrogen bonding network. Steric interactions between the substrates and the aryl substituent on the catalyst were pinpointed as the

source of stereoselectivity. The impact of electron withdrawing groups on one of the aryl substituents was investigated by considering the C_1-symmetric CPA catalyst **22**. Computed TS structures showed that the introduction of this electron-deficient aryl group perturbs the chiral reacting space by altering the pK_a of the adjacent phosphoric acid proton. This example not only demonstrates the use of computations to probe electronic effects and noncovalent interactions in CPA catalysis, but also demonstrates the importance of properly tuning pK_a in CPA catalysed reactions.

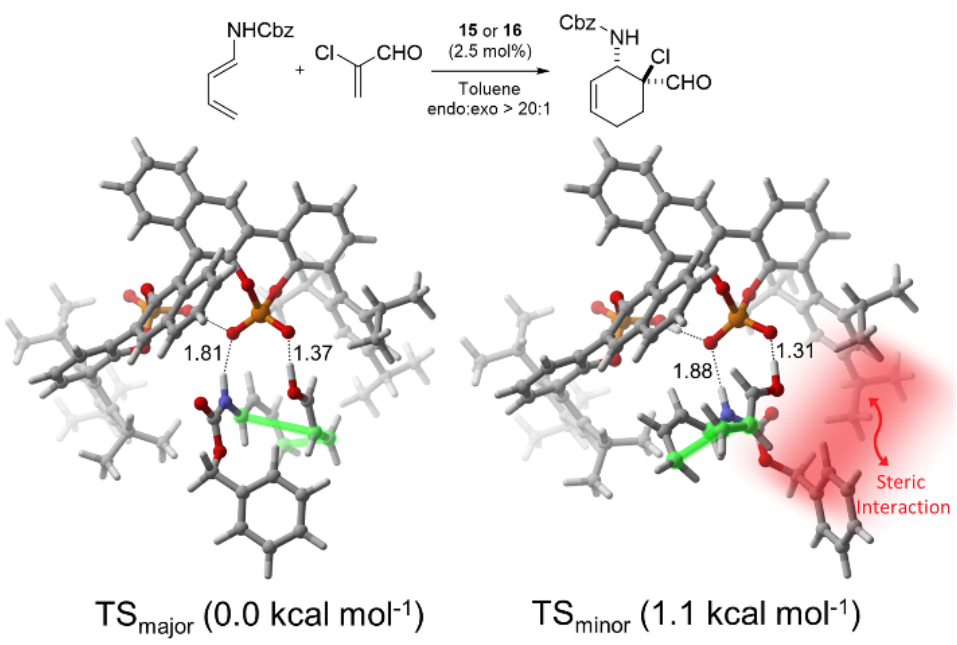

Figure IV-20. C_2-symmetric bis-phosphoric acid catalysed Diels Alder reaction from Terada and co-worker's along with their free energies in kcal mol^{-1}.[276]

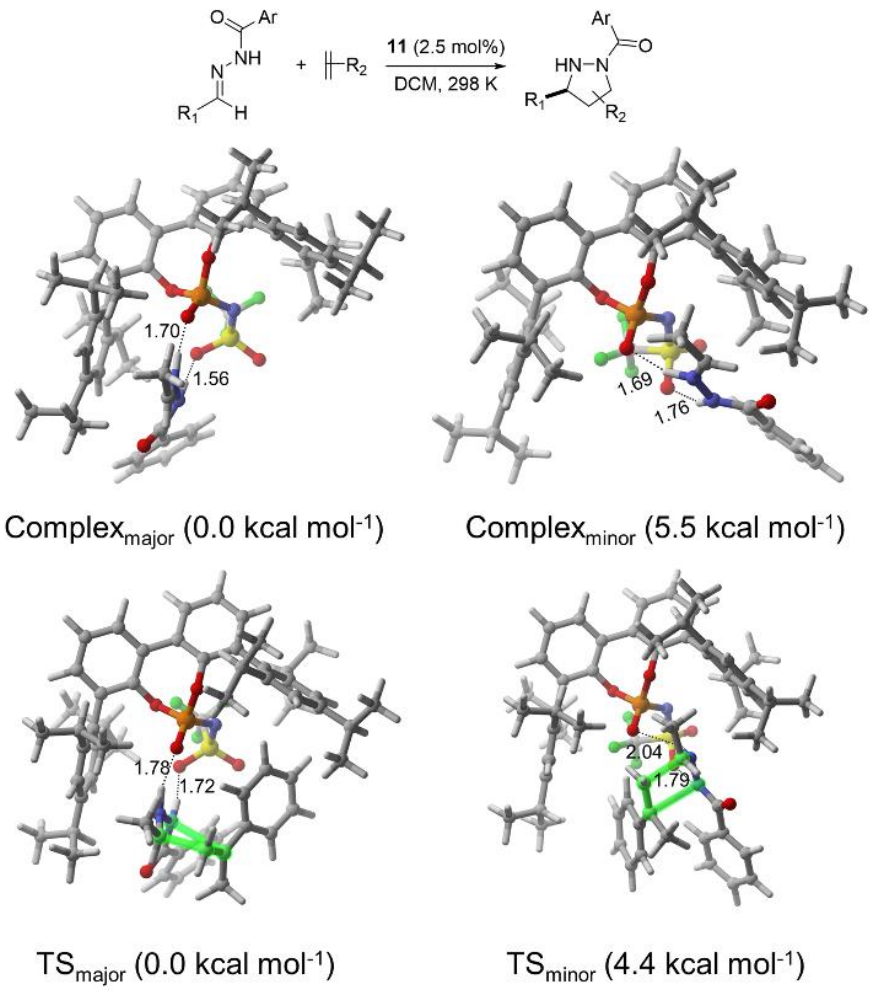

Figure IV-21. DFT optimized ion pair complexes and stereodetermining TSs of *N*-Triflylphosphoramide catlaysed ($3^+ + 2$) cycloaddition along with their free energies in kcal mol^{-1}.[257]

Houk and co-workers[257] addressed several issues related to *N*-triflylphosphoramide catalysed ($3^+ + 2$) cycloadditions between hydrazine and alkenes (Figure IV-21), including the preferred protonation state and reaction pathway, the origin of stereoinduction, and the relatively poor selectivity in the case of ethyl vinyl thioethers. Initial protonation of the hydrazone by the *N*-triflylphosphoramide produces an ion pair that subsequently undergoes a ($3^+ + 2$) cycloaddition with the alkene. This is preferred

over the alternative (3 + 2) cycloaddition involving the analogous azomethine imine due to greater stability of the hydrazine compared to the azomethine imine. The origin of enantioselectivity was ascribed to the steric demand of the bulky substituents of the catalyst, which leaves only one pro-chiral face of the hydrazonium available for alkene approach. Consistent with this model, the low enantioselectivity of ethyl vinyl thioethers, compared to α-methyl styrene, can be explained by its smaller size; the large binding pocket of [H8]-BINOL-based triflylphosphoramide does not provide the same high degree of enantioselectivity as in the case of α-methyl styrene.

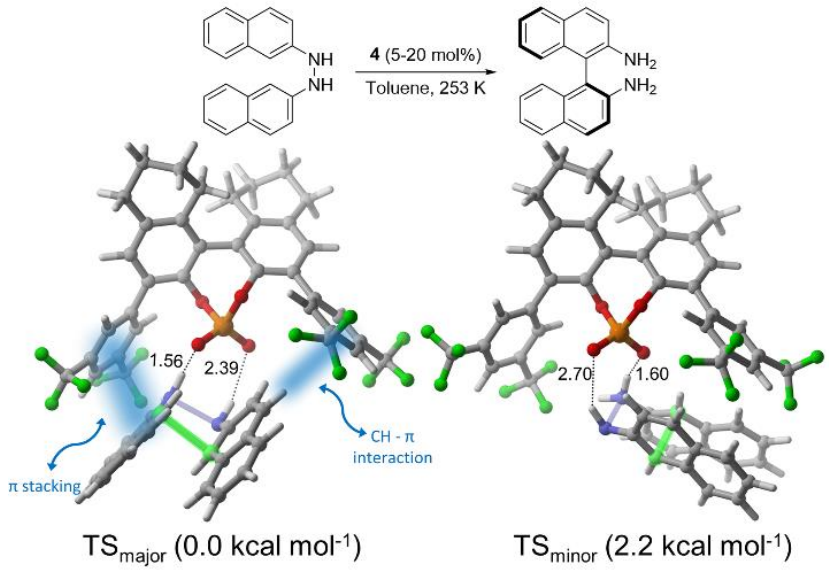

Figure IV-22**.** DFT-optimized CPA catalysed TSs of [3,3] sigmatropic rearrangement of *N,N*'-diaryl hydrazines along with their free energies in kcal mol^{-1} from Kürti *et al.*[42]

The importance of electronic effects in CPA-catalysed pericyclic reactions was demonstrated by Kürti *et al.*[120] in their enantioselective BINAM synthesis. They ascribed the stereoselectivity in the key [3,3]-sigmatropic shift transition states to both steric and electronic effects (Figure IV-22). The chiral counterion creates an asymmetric binding

pocket for the protonated substrate. In addition, the electron-withdrawing CF_3 groups of the catalyst lead to enhanced CH···π and π–stacking interactions that favour TS_{major}. Consistent with this model, replacing the CF_3 groups in this catalyst with Me resulted in decreased stereoselectivity.

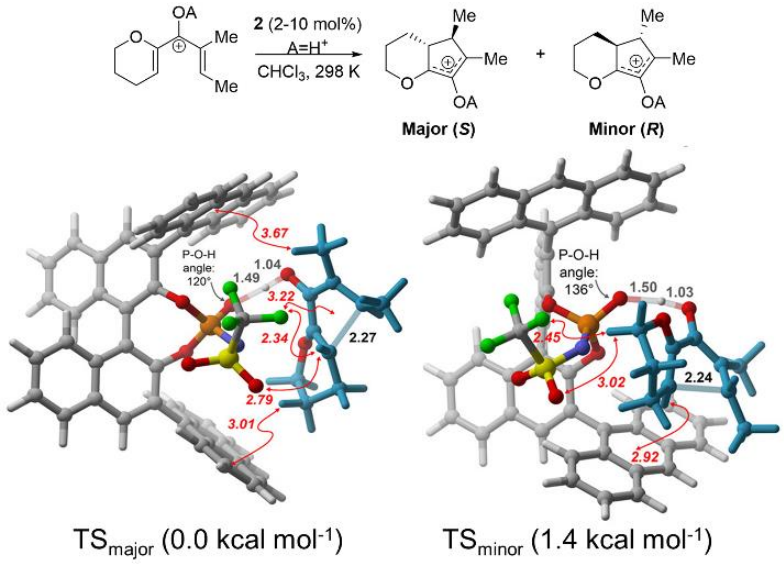

Figure IV-23**.** DFT-optimized TSs of chiral phosphonamide catalysed Nazorov cyclization of dihydropyranyl vinyl ketones with relative free energies in kcal mol^{-1}.[268]

Krenske and co-workers[268] recently reported on the enantioselectivities of Nazarov cyclizations of three classes of divinylketones by chiral phosphoramide based catalysts. They found that the selectivity is dependent on a combination of factors, including catalyst distortion, the degree of proton transfer, intramolecular substrate stabilization, and a wide range of intermolecular noncovalent interactions (CH···π, cation−π, CH···O, CH···F, and cation–lone pair interactions) between the substrate and catalyst in the transition state. All of these interactions depended on a tight fit of the cyclizing divinyl ketone into the chiral binding pocket of the catalyst, and the selectivity

was attributed to the greater catalyst distortion in TS_{minor} due to widening of the P-O-H angle in order to accommodate the substrate within the catalyst cavity (Figure IV-23).

4.6.2 Alternate Mode of Catalysis

There are a number of other modes of catalysis open to CPAs and related catalysts. For instance, the ability of these catalysts to work cooperatively with other catalysts has garnered significant interest in the last decade; computational studies can provide key insights that aid the development of such complex catalytic systems. Several examples in this area have recently been highlighted by Sunoj and co-workers[125] so here we present two new examples where phosphoric acid or phosphoramide based catalysts work cooperatively to achieve high selectivity, as well as other novel modes of CPA catalysis.

Grayson *et al*.[277] studied Ru and CPA cooperativity in the context of the asymmetric hydroxyalkylation of butadienes (Scheme IV-3, reaction I). Based on DFT computations, they reasoned that the chiral phosphate dependent steroselectivity results from a CH···O interaction between the phosphoryl oxygen and the formyl proton of the aldehyde in the case of TADDOL derived catalysts. With this favourable CH···O interaction in place, the *syn* selectivity can be understood by the preferential reaction of (Z)-s-crotylruthenium with aldehydes in which the crotyl methyl group is placed in a pseudo-axial position to alleviate *gauche* interactions with the aldehyde. On the contrary, for BINOL-derived catalysts this CH···O interaction is not present, since its formation would lead to a steric clash between the chiral phosphine and the chiral phosphate

ligand. Consequently, with these catalysts nucleophilic attack occurs on the opposite prochiral face of the aldehyde, leading to *anti* selectivity.

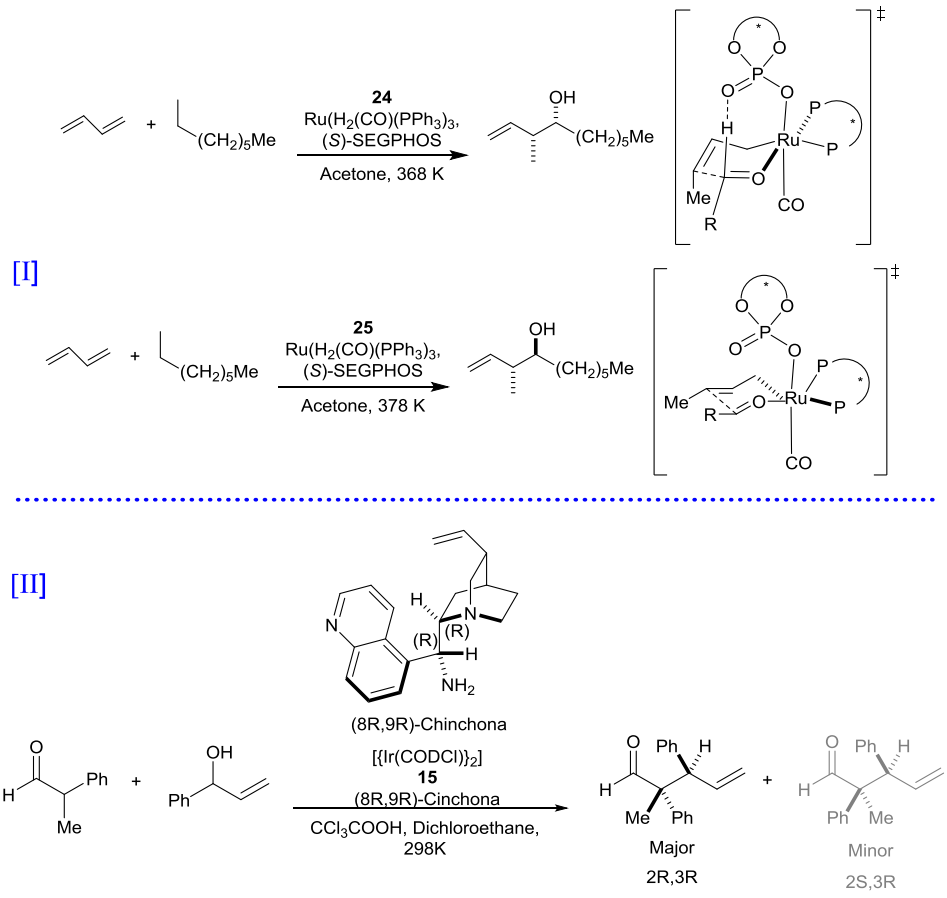

Scheme IV-3**.** Stereodivergence in hydroxy alkylation of butadienes using cooperative catalysis (reaction I)[277] and cooperative dual catalytic asymmetric α-allylation (reaction II).[248]

Bhaskararao and Sunoj[248] studied the stereodivergence in an asymmetric α–allylation reaction under the cooperative action of a chiral Ir-phosphoramidite and cinchona amine (Scheme IV-3, reaction II). One intriguing aspect of this reaction is the ability to alter the chirality of each stereocentre of the product by employing the enantiomer of the corresponding catalyst. For instance, when the (*R*,*R*)-cinchona is used

with (*R*)-phosphoramidite, the major product has a (2*R*,3*R*) configuration at the the α and β–centres. These configurations can be inverted simply by using the (*S*,*S*)-cinchona and (*S*)-phosphoramidite. Computational analysis indicates that the configuration of the β carbon is determined during the formation of an Ir-π-allyl intermediate. Consistent with experiment, the lowest energy TS leading to the (2*R*,3*R*) product involves *re* facial addition of (*R*,*R*)-cinchona-enamine to the *si* face of the Ir-(R)-phosphoramidite intermediate. Transition states corresponding to *si*-*si* and *si*-*re* additions were significantly higher in energy, which is consistent with the experimentally observed high enantio- and diastereoselectivity. These energy differences were attributed to the preferential stabilization of one TS through π-stacking and CH···π interactions.

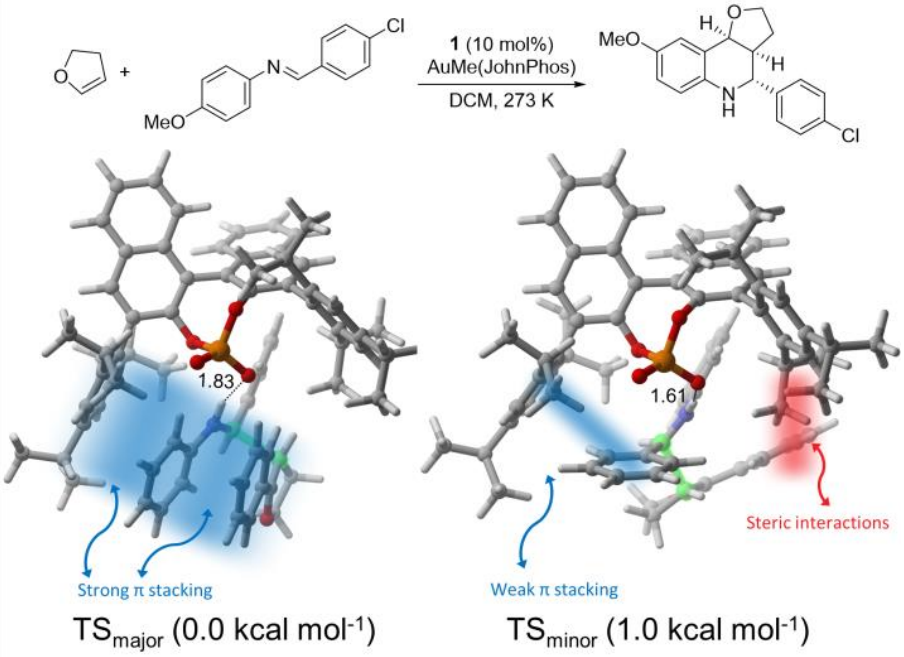

Figure IV-24. Stereodetermining TSs for the three component orthogonal relay catalysis along with the relative free energies in kcal mol^{-1}.[266]

Rodriguez and co-workers[266] recently highlighted the importance of π-stacking and steric interactions in Au and CPA mediated orthogonal relay catalysis in the enantioselective synthesis of hexahydrofuro[3,2-c] quinolones via a Pavarov reaction. The authors showed that the reaction follows a stepwise pathway rather than the commonly assumed concerted pathway. Computations further showed that the TS leading to the major *exo* product is stabilized by π-stacking interactions while also minimizing steric interactions (Figure IV-24). The reduced selectivity in toluene was attributed to the destabilization of a key π–π–π interaction in TS_{major} due to competitive stacking interactions with the solvent.

Jindal and Sunoj[278] studied a multicatalytic allylation reaction, showing that the chiral phosphate serves as a counterion rather than a ligand for Pd. In particular, they demonstrated that Pd-bis-phosphine was the active species and, due to its larger volume, the chiral phosphoric acid can only interact as a counterion. Consequently, chirality transfer takes place through an outer sphere effect.

Finally, Paton and co-workers[243] recently performed the first theoretical study of asymmetric chiral anion phase transfer (CAPT) catalysis for *meso* aziridinium and episulfonium ring openings using both QM and Molecular dynamics (MD) simulations. Their study offers valuable insights into ion-pairing, ring-opening, and catalyst deactivation pathways. Explicitly solvated classical MD simulations and QM computations were used to explore possible ion-pairing geometries and to compute reliable interaction energies. Their results showed that the formation and stability of the ion pair is dramatically reduced with increased solvent polarity. TS computations further

indicated that the stereoselectivity of the ring opening is mainly controlled by distortion of the substrate. Computed pathways for catalyst deactivation showed that under normal stoichiometric condition catalyst deactivation can be competitive with ring opening, thereby necessitated the use of excess alcohol.

4.7 Other mechanistic insights

Computational chemistry has also provided mechanistic insights into CPA catalysis beyond stereoselectivity. For instance, computations have been used to identify and explain preferred reaction pathways, to identify the nature of intermediates among several possibilities, and to uncover new, unexpected pathways.

For example, Jindal and Sunoj[279] found that ligand exchange was critical to determine the low-energy pathway for a Pd(II))-Brønsted acid catalysed migratory asymmetric ring expansion of an indenylcyclobutanol to a spirocyclic indane. Of the two mechanistic possibilities examined, a Wacker-type pathway (involving a semi-pinacol ring expansion followed by reductive elimination) was found to be energetically favoured over the alternative allylic pathway (in which ring expansion of a Pd-π allyl intermediate occurs after the initial allylic C-H activation). Computations further indicated that the replacement of the native acetate ligands on Pd by phosphate and water stabilized a crucial TS structure. Remarkably, the authors showed that a phosphate mediated C-H activation pathway is more favourable than the widely accepted acetate-assisted activation. The phosphoric acid was shown to play a dual role in this process; during the first step, it is bound to the Pd as a ligand, lowering the energy, while in the

second step it remains in the outer sphere and relays the indenyl β-proton to the Pd bound phosphate.

Similarly, Paton *et al*.[250] studied two potential mechanisms for a Rh-catalysed stereoselective [5+2]-cycloisomerization of ynamide vinyl cyclopropanes. In contrast to previous studies, their computations supported a revised mechanistic sequence in which an irreversible, stereodetermining C-C coupling between the reactants takes place before the metal insertion into the vinyl cyclopropane.

Thiel and co-workers[280] offered a revised view of the Brønsted acid-catalysed cyclization of an α,β-unsaturated hydrazine. Although this reaction had previously been classified as a 6π electrocyclization, computations suggest a non-pericyclic nature. In view of the computational results, they argued that this reaction can either be classified as a pseudo-pericyclic reaction or a 5 *endo*-polar mechanism in which the lone pair of nitrogen attacks the allylic group.

MD simulations have also provided key insights into the dynamics of CPA catalysed reactions. For instance, Houk *et al*.[281] used MD simulations to characterize C-H···O interactions in CPA catalysed allylborations, corroborating their previous model (Figure IV-10). In the gas phase, they showed that there is a significant enhancement of C-H···O and O-H···O interactions moving from the reactant to the TS; this effect is present but much weaker in toluene due to solvent caging. This was attributed to the build-up of partial charge during the transition state due to the forming B···O bond. This charge separation leads to an increase in the acidity of the benzaldehyde H and basicity of the allylboronate oxygen, which in turn enhances the C-H···O and O-H···O interactions

in the TS relative to reactants and products. Finally, Zimmerman and co-workers[282] recently used MD simulations to probe the potential of a short-lived oxocarbenium intermediate along the concerted path in a (6,6)-spiroketalization. MD trajectories starting at the concerted TS structure revealed a short overall reaction time, which is consistent with a concerted asynchronous mechanism that avoids this oxocarbenium intermediate. These MD trajectories also indicated that alcohol deprotonation and ring closure occur simultaneously.

4.8 Future directions

As documented above, our understanding of CPA catalysed reactions has witnessed tremendous growth over the last decade, driven in part by computational studies. Despite these advancements, some aspects of these reactions remain relatively unexplored and we wish to point out a few areas where computational studies can provide a foundation for future development.

First, modern quantum chemistry can aid in the design of reactions that are still relatively underdeveloped. For instance, it has been observed that highly reactive electrophiles are incompatible with CPA catalysis, presumably due to background decomposition pathways in which the catalyst is engaged in an undesired nucleophilic attack to form an inactive alkylated species. List *et al*.[256] recently circumvented this problem in the CPA-catalysed conversion of epoxides to thiiranes through the formation of a heterodimer that prevents catalyst deactivation. Computational studies can potentially generalize this approach to other, related systems. On the other hand, reactions of inert substrates (*e.g.* C-H functionalization, or activation of inert C-C bonds)

still pose a formidable challenge in CPA catalysed reactions, representing an area in which computations can play a leading role. Although there have been promising examples of cooperative catalysts in recent years, there is still a lack of mechanistic understanding of these transformations. Rigorous computational analyses of such reactions are likely to pave the way for further developments. Along these lines, the predictions of pK_a's of CPA catalysts from Cheng *et al*.,[23,24] either as an independent catalysts or in presence of another catalyst, could prove fruitful in the development of new reactions.

Secondly, a proper understanding of stereodetermining TS structures can facilitate the *de novo* design of CPA catalysts. Sunoj and co-workers[283] provided a pioneering example of the power of such design efforts in which they predicted stereoselectivities for new catalysts for an asymmetric diamination reaction. Going a step further, Anderson *et al*.[250] recently demonstrated the computationally-guided improvement of selectivity in enantio- and diastereoselective ynamide [5+2] cycloisomerizations. Our hope is that continued developments will open up the doors for the more routine use of computational chemistry in the design of CPA-based catalysts.

Finally, recent studies have shown that stereoselectivity sometimes arises from the complex interplay of a number of factors. Often in such cases, application of conventional computational tools alone is insufficient to untangle the many contributing factors. Sigman and co-workers[284] have demonstrated the power of combining experimental and computational data through the identification of multi-parameter linear free energy relationships as a means of identifying the many factors that impact

stereoselectivity in complex CPA catalysed reactions. Such studies represent the forefront of combined experimental/computational studies of CPA-catalysed reactions.

4.9 Conclusions

Computational chemistry has made enormous strides in the last few years explaining the origin of activity and selectivity of CPA catalysed reactions, which in turn can inform the design of new reactions. We hope this tutorial review will not only provide an overview of the methods and techniques at the disposal of the computational organic chemist, but will also help guide both synthetic chemists and budding computational organic chemists hoping to make maximal use of computational data in research into CPA catalysed reactions. Together, this will aid future studies of chiral phosphoric acid catalysed reactions.

CHAPTER V

IMPORTANCE OF ELECTROSTATIC EFFECTS IN THE STEREOSELECTIVITY OF NHC CATALYZED KINETIC RESOLUTIONS*

5.1. Introduction

N-heterocyclic carbenes (NHCs) have emerged as powerful organocatalysts in a number of enantioselective transformations,[9, 285-289] including kinetic resolutions (KR)[290-291] and dynamic kinetic resolutions (DKR).[292-298] While the appeal of NHCs alone continues to expand, their use in cooperative catalysis[125, 299-301] involving organocatalysts, Lewis acids, and metals,[258, 302-315] and as additives,[316-320] provides further incentive to their theoretical study.[11, 116, 321-335] A molecular level understanding of these processes holds the key for the improvement of existing protocols and the design of new reactions.[224, 336]

NHC-catalyzed kinetic resolutions of alcohols and amines remain at the forefront of catalytic applications, and three strategies have emerged in recent years (see Scheme 1). In 2013, Yamada *et al*.[337] demonstrated the KR of cyclic diols catalyzed by **1** (reaction I), which requires the presence of an achiral co-catalyst (4-dimethylaminobenzoic acid, **1a**). Work by Bode, *et al*.[338-340] used an achiral NHC (**2**) paired with a chiral co-catalyst (**2a**, Scheme V-1) to achieve the KR of cyclic amines (reaction II). Finally, in 2014 Zhao *et al*.[341] demonstrated the KR of axially-chiral

* Adapted with permission from "Importance of Electrostatic Effects in the Stereoselectivity of NHC-Catalyzed Kinetic Resolution" by R.Maji and S. E. Wheeler, 2017. *J. Am. Chem. Soc.* **139**, 12441. Copyright 2017 American Chemical Society.

BINOL-derivatives catalyzed by chiral NHC **3** (reaction III). Catalyst **3**, derived from **1** by the removal of the nitro group and replacement of Ph with a mesityl group, proved highly selected in the KR of a number of BINOL-derivatives (see Table V-1), with selectivity factors (S) of 52 and 116 for (±)-**4** and (±)-**5**, respectively.[341] Unlike reactions I and II, reaction III does not require an added co-catalyst. Instead, by using BzO as a leaving group on the acylating agent, instead of Br as in reaction I, the requisite benzoic-acid co-catalyst is generated as a byproduct of the reaction. Moreover, whereas reaction I does not proceed in the case of *trans*-2-methoxycyclohexanol,[337] reaction III does proceed with methylated substrates [*e.g.* (±)-**6**], albeit with reversed and drastically reduced selectivity (see Table V-1).

Previous computational studies[337, 342] have provided some insights into the role of additives and the origin of selectivity in reactions I and II. For instance, Yamada *et al*.[337] used density functional theory (DFT) to study reaction I. They reported that additive **1a** forms crucial hydrogen bonding interactions with the diol during the acylation step. The importance of these two hydrogen bonds was corroborated by the experimental finding that for methylated substrates the KR does not proceed. However, the role of this additive in other aspects of this reaction, including the stereoselectivity and overall reaction rate, was not addressed. Kozlowski, *et al*.[342] examined reaction II computationally, reporting a novel concerted pathway for amide bond formation and attributing the stereoselectivity to a gearing effect driven by steric interactions. The origin of activity and selectivity in reaction III has not previously been addressed.

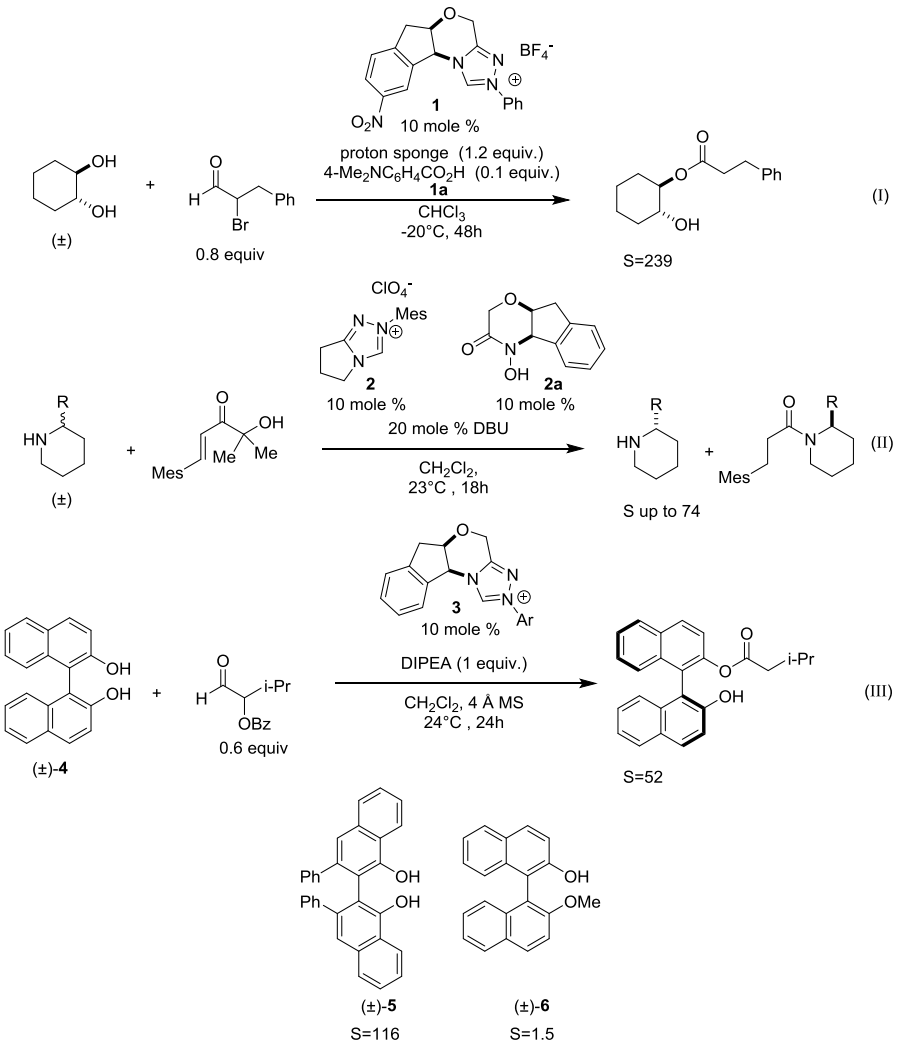

Scheme V-1. Three strategies for the kinetic resolution of chiral alcohols and amines catalyzed by NHCs from Yamada et al. (reaction I),[337,343] Bode, et al. (reaction II),[338-340] and Zhao et al. (reaction III).[341]

Despite these previous computational studies,[9,12] a number of important questions about these three NHC-catalyzed kinetic resolutions remain. First, what roles does BzO^- (used as an additive in reaction I and generated *in situ* in reaction III) play in

reactions I and III? Second, what is the origin of stereoselectivity in reaction III, and why is the selectivity reversed in the case of (±)-**6**? Third, what role do the additives play in all three reactions with regard to both catalytic activity and selectivity? Finally, is there a common unifying feature of these three NHC catalyzed kinetic resolutions that can point toward a more general understanding of these powerful transformations? To address these questions, we explored the catalytic cycle for the KR of (±)-**4**, (±)-**5**, and (±)-**6** catalyzed by **3** computationally, and re-examined key aspects of reactions I and II. The results reveal a shared electrostatic mode of stereoinduction in all three transformations, as well as by-product mediated co-catalysis in the case of reaction III.

5.2. Results and Discussion

Table V-1. Experimental and M06-2X/6-311+G(d,p)//B3LYP/6-31+G(d) predicted selectivity factors (S) and relative free energy barriers for the KR of (±)-4, (±)-5, and (±)-6 catalyzed by **3**.[a]

Diol	Exptl. S	Exptl. $\Delta\Delta G^{\ddagger}$	Theor. S	Theor. $\Delta\Delta G^{\ddagger}$
(±)-**4**	52	2.3	42	2.2
(±)-5	116	2.8	>200	4.5
(±)-6	1.5[b]	-0.2	2.8[b]	-0.6

[a](*S*)-isomer favored except where noted. The theoretical $\Delta\Delta G^{\ddagger}$ values are Boltzmann-weighted relative free energy barriers.
[b](*R*)-isomer favored

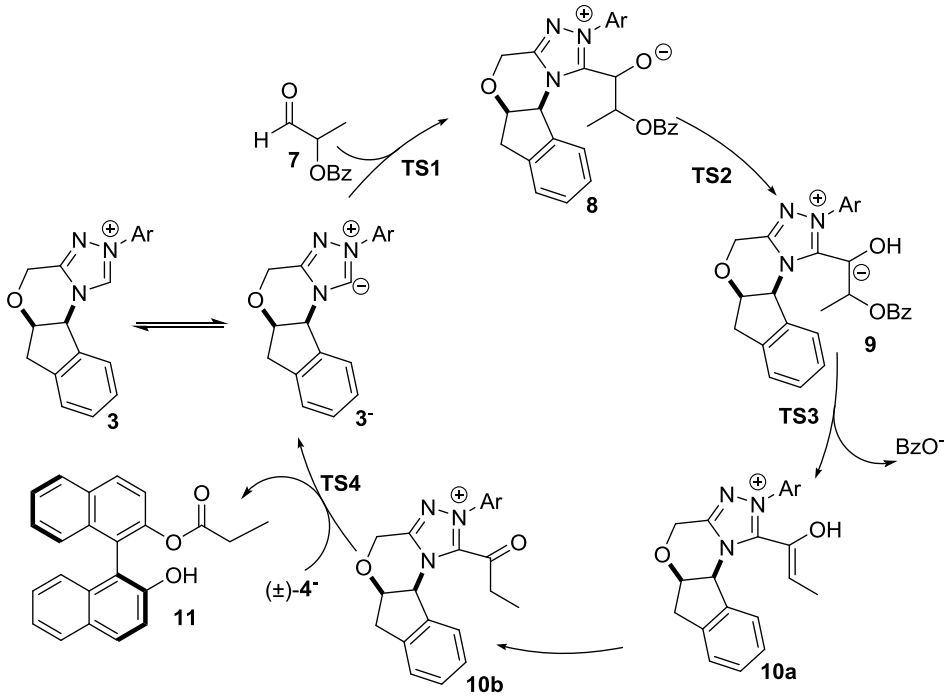

Scheme V-2. Catalytic cycle for the KR of (±)-4catalyzed by **3**.

The free energy profile (see Figure V-1) for the KR of (±)-**4** catalyzed by **3** (see Scheme V-2) was computed at the M06-2X/6-311+G(*d*,*p*)//B97-D/TZV(2*d*,2*p*) level of theory based on a simplified version of **3** (Ar = Ph).[344] The catalytic cycle commences with the nucleophilic addition of the deprotonated NHC (**3**$^-$) to the aldehyde (**7**), leading to a zwitterionic intermediate (**8**) via **TS1**. We considered several possibilities for **TS1** : addition to the *si* face of the aldehyde is slightly favored over the *re* face (10.8 vs 11.3 kcal/mol, relative to separated reactants). The resulting zwitterionic intermediate can then undergo a direct proton shift via **TS2** (Figure V-2a) to form the Breslow intermediate (**9**); however, the associated barrier is a prohibitive 53.4 kcal/mol, relative to separated starting materials.[345] Consequently, we considered proton transfers facilitated by species present in the reaction mixture, including BzOH (which is

generated during the reaction) and the deprotonated BINOL-derived substrate (*i.e.*, **4**$^-$), in addition to stepwise mechanisms. Ultimately, we found that the BzOH-assisted proton transfer has the lowest barrier (13.4 kcal/mol, relative to starting materials). This proceeds by a barrierless protonation of the alkoxide in **8** by BzOH followed by the deprotonation of the adjacent carbon via **TS2**···**BzOH** (see Figure V-2a). Thus, in reaction III the benzoic acid by-product plays a key catalytic role, similar to that of catechol additives reported by Rovis *et al*.[317] and the in situ generated phenol byproducts reported by Sunoj *et al*.[322, 324]

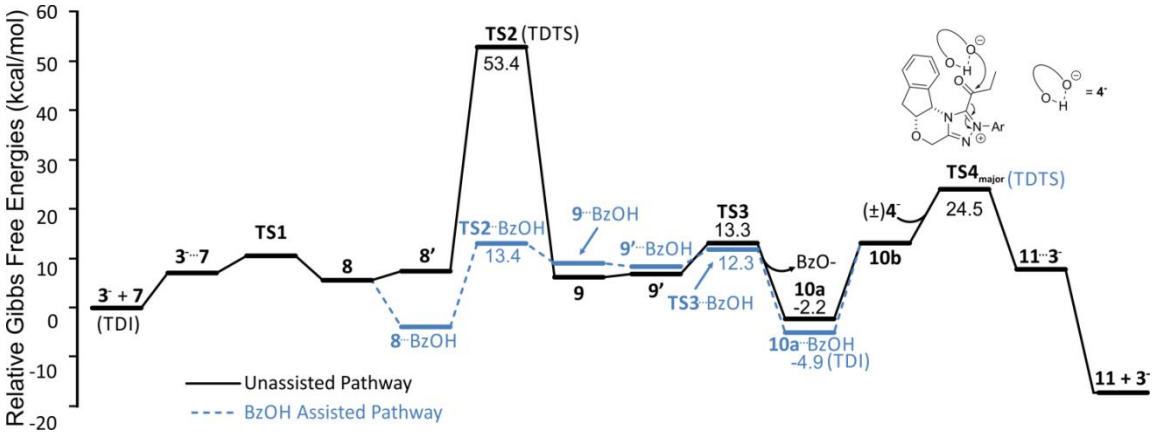

Figure V-1**.** M06-2X/6-311G+(d,p)//B97-D/TZV(2d,2p) computed free energy profile for the KR of (±)-**4**catalyzed by **3** along BzOH assisted (gray) and unassisted (black) pathways. The TOF determining TS (TDTS) and TOF determining intermediate (TDI) for both pathways are marked in the corresponding colors. Key free energy values are provided in kcal/mol.

Subsequently, **10b** is stereoselectively intercepted by the BINOL-derivative, resulting in kinetic resolution via **TS4**. Depending on the protonation state of the incoming nucleophile, two distinct mechanisms are viable: a cationic pathway (in the case of a neutral diol) or a zwitterionic pathway (if the diol is deprotonated). Considering

the pK_a of the species present in the medium, and given the previous precedence that phenols can be deprotonated by an NHC,[346] a zwitterionic pathway is more likely. The associated TS for formation of the major stereoisomer is 24.5 kcal/mol higher in free energy than the starting materials.

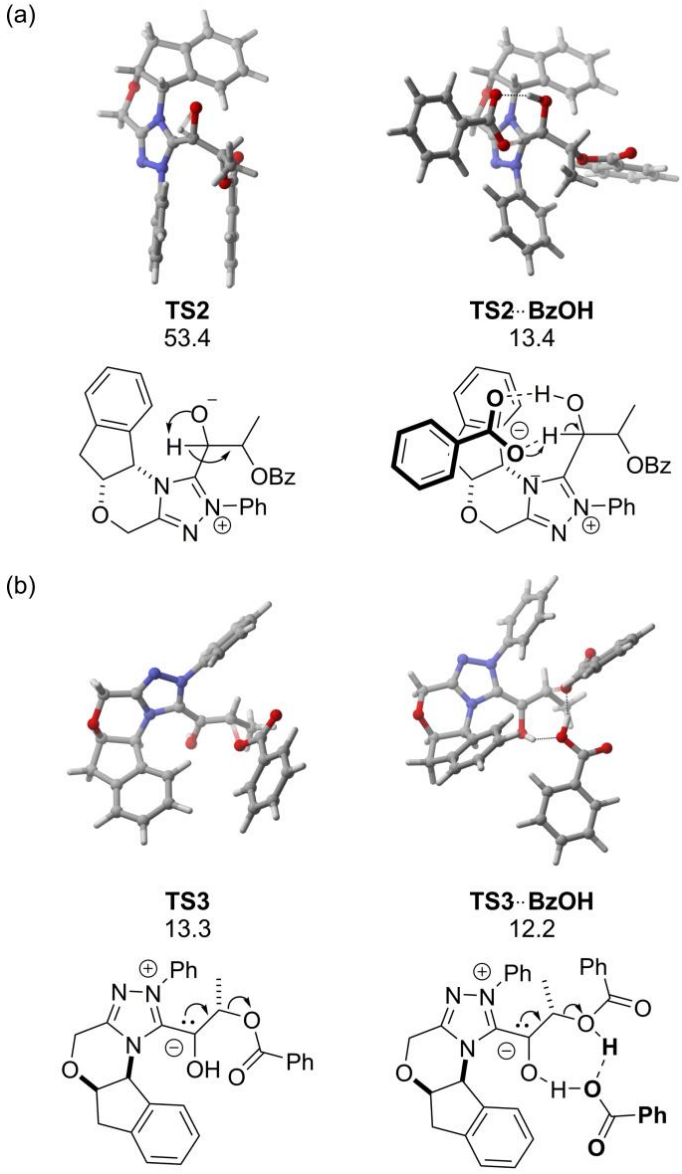

Figure V-2**.** B97-D/TZV(2d,2p)optimized unassisted and BzOH assisted structures for (a) **TS2** and (b) **TS3** for reaction III.

We have analyzed the Gibbs free energy profile for reaction III (Figure V-1) using the energetic span model.[347] In the absence of any explicit participation of BzOH, **3**$^-$ + **7** is the TOF determining intermediate (TDI) while the TOF determining TS (TDTS) is **TS2**. This leads to an overall free energy span of 53.4 kcal/mol. In the presence of BzOH, however, the stereoselective acylation by the deprotonated BINOL (**TS4**) is the TDTS and **10a** the TDI. The effective span in this case is 29.4 kcal/mol (for formation of the major stereoisomer). Consequently, the participation of the BzOH by-product as a co-catalyst not only lowers the activation energy of the proton transfer, reducing the energetic span by 24.0 kcal/mol, but also renders the acyl transfer step (**TS4**) both rate determining and stereoselectivity determining.

As noted above, reactions I and II require the addition of a co-catalyst. For reaction II, the chiral hydroxamic acid co-catalyst (**2a**) is the active acylating agent and Kozlowski *et al*.[342] clearly delineated its impact on rate. In particular, they reported that in the rate-limiting acyl transfer step, **2a** is involved in a concerted, seven membered transition state. This results in an overall activation energy of 22.7 kcal/mol; the next lowest-lying pathway identified involves water relay catalysis, which is almost 11 kcal/mol higher in energy.

In the case of reaction I, the role of the benzoic acid co-catalyst (**1a**) has not been fully explored. Overall, the mechanism for reaction I is similar to that shown in Scheme 2. Furthermore, in view of our present finding regarding the role of BzOH in reaction III, as well as previous reports,[11, 329] we anticipated that **1a** facilitates the key proton transfer to generate the active acylating agent in this reaction (analogous to **TS2** in

Scheme V-2). Indeed, computations indicate a step-wise proton transfer in which **1a** first protonates the alkoxide and the conjugate base of **1a** then deprotonates the adjacent carbon (see Figure V-3).[348] Overall, the explicit participation of **1a** in this proton shift lowers the predicted free energy barrier by 40.1 kcal/mol, compared to the direct, unassisted proton transfer (52.4 kcal/mol). Thus, the viability of both reactions I and III depends on a co-catalyst assisted proton transfer. The difference, of course, is that in reaction I this co-catalyst must be added, whereas the BzOH byproduct serves this role in reaction III.

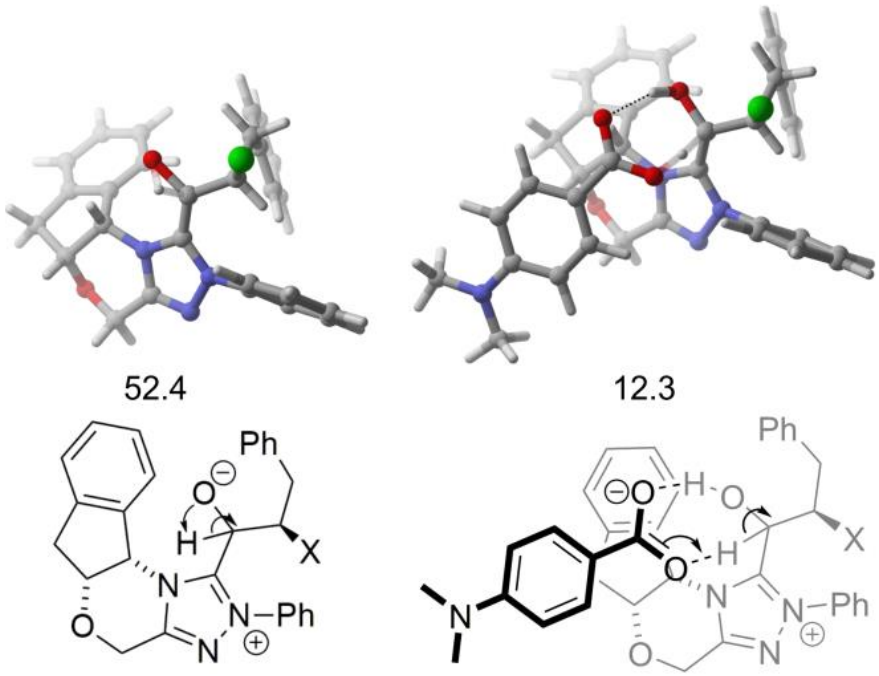

Figure V-3. B97-D/TZV(2d,2p)optimized unassisted (left) and assisted proton shift to form the active acylating agent in reaction I. In the computed TS structures, X = Cl (X = Br in the experiment).

We next set out to unravel the mode of stereoinduction in the acyl transfer step for the KR of (±)-**4,** (±)-**5**, and (±)-**6** catalyzed by **3**, and to compare this with the origin of selectivity in reactions I and II. For this, we considered the full catalyst **3** (Ar = mesityl). Four distinct conformers were considered[349] for the KR of (±)-**4** using various level of theory (see Appendix A additional details). All of the methods considered provided qualitatively similar results; however, M06-2X/6-311+G(d,p)//B3LYP/6-31+G(d) provided slightly better agreement with the experimental selectivity factors so will be discussed exclusively below.

Theoretical *S* values and Boltzmann weighted relative free energy barriers, $\Delta\Delta G^{\ddagger}$,[350] are provided in Table 1 for the KR of (±)-**4,** (±)-**5**, and(±)-**6** catalyzed by **3**. Overall, the theoretical *S* values are in very good agreement with experiment,[341] correctly capturing the enhanced selectivity for (±)-**5** and reduced and reversed of selectivity for (±)-**6**, compared to (±)-**4**.[351]

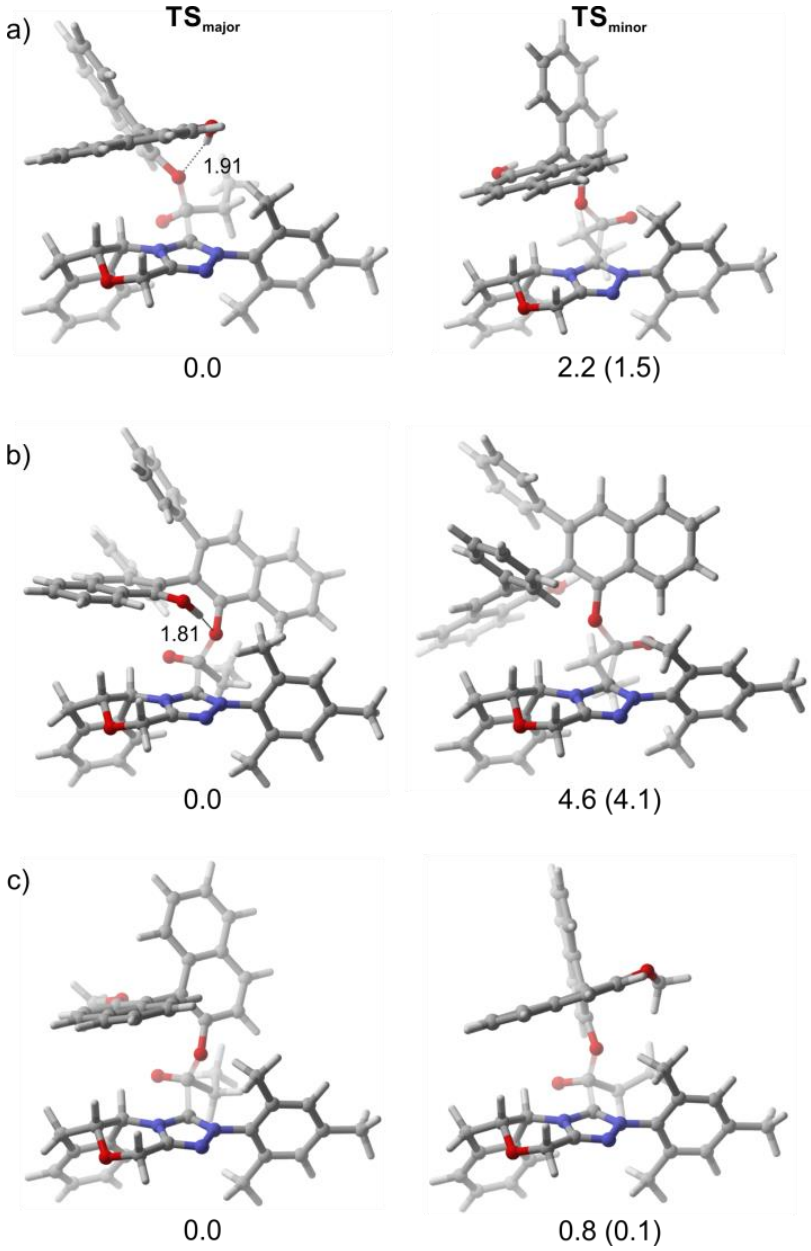

Figure V-4. B3LYP/6-31+G(d) optimized primary stereocontrolling TS structures for the KR of (a) (±)-4, (b)(±)-5, and (c)(±)-6 catalyzed by 3(*i.e.* TS4 in Scheme V-2). Key bond distances shown in Angstroms; relative free energies and electronic energies (in parentheses) are provided in kcal/mol. Note that the selectivity in (c) is opposite that in (a) and (b).

For the KR of (±)-**4**, the stereoselectivity is primarily controlled by two transition states, one leading to the major stereoisomer (**TS$_{major}$**) and one leading to the minor stereoisomer(**TS$_{minor}$**). These TS structures differ by 2.2 kcal/mol in free energy, which is dominated by the energetic component ($\Delta\Delta E^{\ddagger}$ = 1.5 kcal/mol). Topological analyses by AIM[30, 352-353] reveal a number of crucial non-covalent contacts, including CH···π, C=O···H, C-H···O, and lone-pair···π interactions. However, the most glaring difference between **TS$_{minor}$** and **TS$_{major}$** is the presence of a strong, charge-assisted OH···O hydrogen bond in the latter but not the former (see Figure V-4). This leads to substantial stabilization of **TS$_{major}$** over **TS$_{minor}$**. Notably, were the diol not deprotonted, one would not expect this H-bonding interaction to be present.[354] The impact of this interaction can be seen more clearly from distortion-interaction analysis by considering the relative energies of the BINOL substrate in the geometries of the two TS structures; in **TS$_{major}$**, the substrate is 4.4 kcal/mol lower in energy than in **TS$_{minor}$**. Other, compensative effects, including non-covalent interactions that preferentially stabilize **TS$_{minor}$**, lead to the net energy difference of 1.5 kcal/mol.

The drastically reduced selectivity in the case of the KR of (±)-**6** provides further corroboration of the importance of this hydrogen bonding interaction in the stereoselectivity of reaction III, since the presence of an Me group in **6** precludes formation of this key O···H-O interaction (Figure V-4c). The result is that non-covalent interactions are balanced in the two primary stereocontrolling TS structures. The balancing of non-covalent interactions, combined with the similar steric environments of these TS structures (See Appendix A more details), lead to **TS$_{major}$** and **TS$_{minor}$** being

nearly isoenergetic ($\Delta\Delta E^{\ddagger}$ = 0.1 kcal/mol), and reaction III being unselective in the KR of **6**.

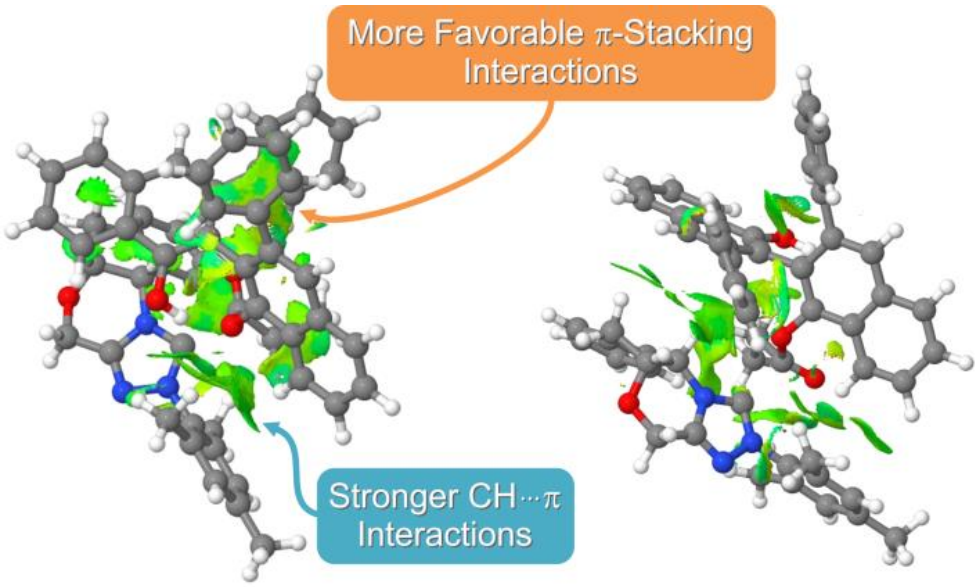

Figure V-5. Comparison of NCI plots for the two primary stereo controlling TS structures for the KR of (±)-5 catalyzed by 3[isosurface generated (-0.03- 0.03)].

The stereocontrolling TS structures for the KR of (±)-**5** are depicted in Figure V-4b. Both the energy and free energy difference between $\mathbf{TS_{minor}}$ and $\mathbf{TS_{major}}$ are larger than for **4**, in agreement with the experimentally observed enhanced selectivity. As with **4**, the formation of a critical hydrogen bond in $\mathbf{TS_{major}}$ provides substantial preferential stabilization as gleaned from distortion-interaction analysis. Moreover, for **5** there are additional, dispersion-driven non-covalent interactions that provide further stabilization of $\mathbf{TS_{major}}$, compared to $\mathbf{TS_{minor}}$. This is captured by AIM analysis (see Appendix A more details), as well as the NCI analysis of Yang and co-workers.[29, 209] For instance, Figure V-5 shows substantially greater dispersion-driven π-stacking and CH/π interactions between the substrate and catalyst in $\mathbf{TS_{major}}$ than in $\mathbf{TS_{minor}}$, which nicely

mirrors the result of the AIM analysis. Overall, the exceptional selectivity in the KR of (±)-**5** catalyzed by **3** adds to the growing list of examples of NHC-catalyzed reactions in which sundry non-covalent interactions (π-stacking, CH/π, hydrogen-bonding, *etc*.) work in concert to preferentially stabilize a given TS structure.[321-325, 329]

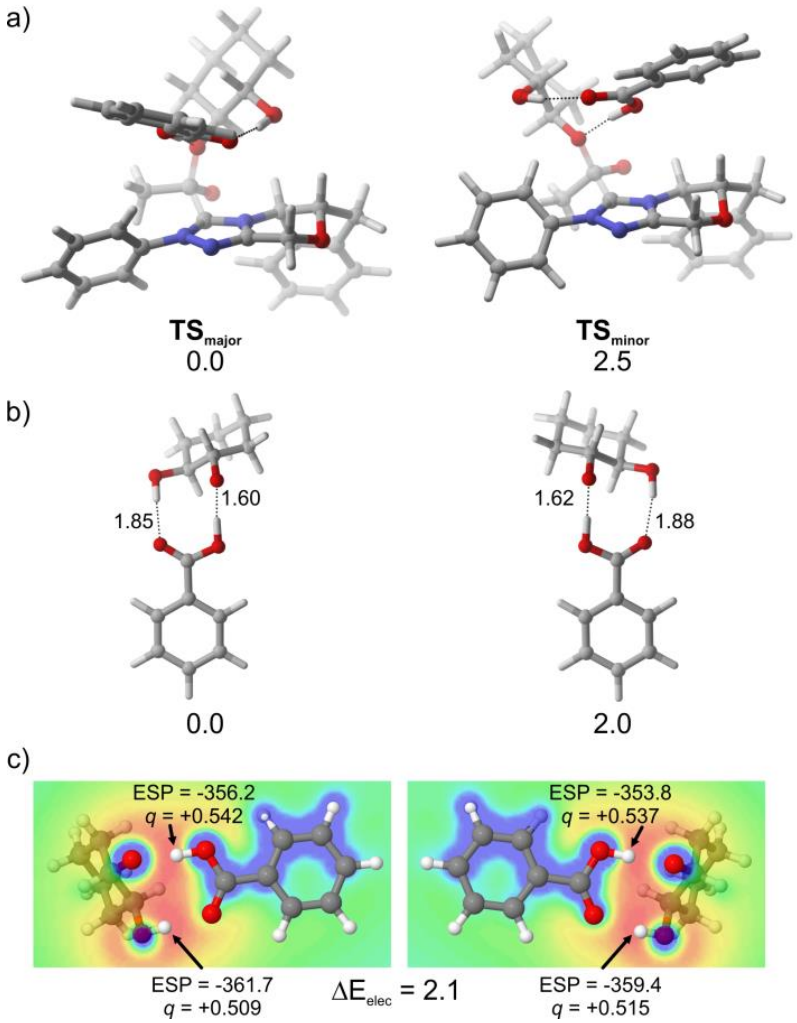

Figure V-6. (a) Primary stereocontrolling TS structures for reaction I from Yamada *et al*.[337] [computed at the B3LYP/6-31G(*d*,*p*) level of theory] along with relative energies in kcal/mol. (b) Model TS structures derived from those in (a), along with the corresponding relative energies in kcal/mol. (c) Electrostatic potential in due to the structures in (b) in the absence of the protons involved in hydrogen bonding(red = -375 kcal/mol; blue = 0 kcal/mol) along with values of the ESP at the positions of the protons

(in kcal/mol), atomic charges on the protons (q), and the total difference in electrostatic stabilization (ΔE_{elec}) in kcal/mol.

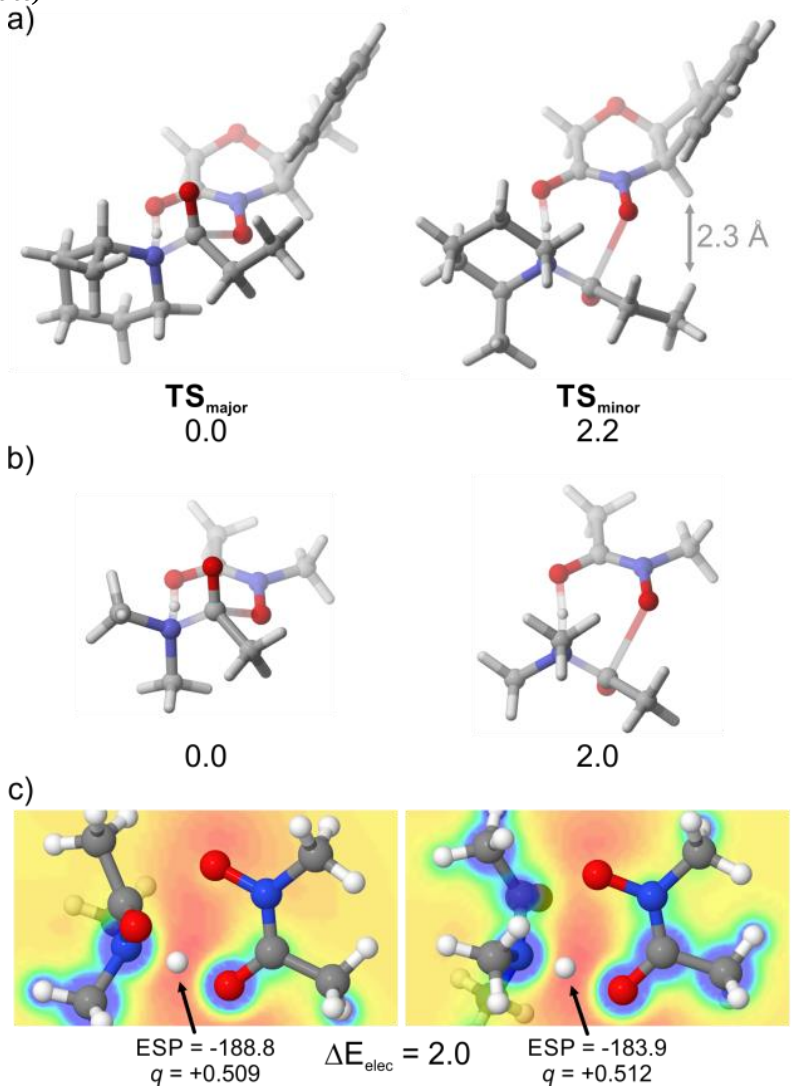

Figure V-7. (a) Primary stereocontrolling TS structures for reaction II from Kozlowski *et al*.[342] [computed at the M06-2X/6-311G(*d*,*p*) level of theory] along with relative energies in kcal/mol. (b) Model TS structures derived from those in (a), along with the corresponding relative energies in kcal/mol. (c) Electrostatic potential in the N-H-O plane arising from the model structures in (b) in the absence of the proton being transferred (red = -200 kcal/mol; blue = +400 kcal/mol). Values of the ESP at the positions of the protons are given in kcal/mol, along with the atomic charge (q) on the protons, and the total difference in electrostatic stabilization (ΔE_{elec}) in kcal/mol.

In light of the above results for reaction III, we re-examined the previously reported stereocontrolling TS structures reported by Yamada *et al*.[337] (Figure V-6) and

by Kozlowski, *et al*.[342] (Figure V-7) for reactions I and II, respectively. For reaction III, the lack of an OH···O hydrogen bonding interaction in $\mathbf{TS_{minor}}$ provided a clear driver of stereoselectivity. For reaction I, the origin of the 2.5 kcal/mol energy difference is less obvious, since the TS structures leading to both the major and minor stereoisomers exhibit 8-membered, charge-assisted hydrogen bond networks (see Figure V-6). However, closer examination of these structures reveals slightly more favorable geometries for the hydrogen bonding interactions in $\mathbf{TS_{major}}$. Indeed, consideration of truncated models in which these hydrogen bond networks are isolated from the remainder of the TS structures reveals that 2.0 kcal/mol of the energy difference between $\mathbf{TS_{minor}}$ and $\mathbf{TS_{major}}$ arises from differences in these hydrogen bonding interactions (See Figure V-6b). The large energetic impact of these subtle geometrical differences stems from the charged-assisted nature of these hydrogen bond networks, whose strengths vary much more strongly than their neutral counterparts.[183, 355-360]

The energetic difference in these H-bond interactions was quantified using NBO-based second order perturbation analysis[361] and AIM,[362] providing qualitatively similar results (2.2 kcal/mol for NBO and 1.7 kcal/mol for AIM), further supporting the above analysis. However, the differences in these hydrogen bond networks can also be examined from an electrostatic perspective. The electrostatic potential (ESP) due to the model hydrogen-bonding networks in Figure V-6b, *without the two protons*, are plotted in Figure V-6c. The presence of heteroatoms and the charged nature of these hydrogen-bond networks result in highly heterogeneous electrostatic environments for the two shared protons. The small differences in proton positions leads to both protons being in

more favorable electrostatic environments in **TS$_{major}$** than in **TS$_{minor}$**. The resulting difference in electrostatic stabilization is 2.1 kcal/mol, favoring **TS$_{major}$**, providing a third, independent confirmation of the importance of these hydrogen bonding interactions on the stereoselectivity of reaction I. Moreover, this electrostatic view gives a simple physical understanding of this energy differences in terms of the preferential electrostatic stabilization of **TS$_{major}$,** compared to **TS$_{minor}$**.

Similar to reaction I, there are subtle differences in the position of the transferring proton in the stereocontrolling TS structures for reaction II. Furthermore, the electrostatic environment arising from the numerous heteroatoms and charged nature of this H-bond network result in the transferring proton being in a more favorable electrostatic environment in **TS$_{major}$** than in **TS$_{minor}$** (see Figure V-7c). Quantifying In reaction II, the origin of stereoselectivity is also somewhat enigmatic. Kozlowski *et al*.[342] attributed the 2.2 kcal/mol enthalpy difference between the lowest-lying TS structures leading to the minor and major stereoisomers to transannular steric interactions between the NHC ring hydrogen and terminal hydrogen of ethyl group (see Figure V-7). However, Cheong *et al*.[363] have quantified the energetic consequences of similar interactions, finding that an H···H contact of 2.3 Å only imparts an energetic cost of ~0.25 kcal/mol. This is well short of the 2.2 kcal/mol enthalpy difference reported by Kozlowski *et al*.[342] Consistent with this, consideration of the model systems in Figure V-7b, in which this putative steric clash has been removed, the energy difference between **TS$_{major}$** and **TS$_{minor}$** is only reduced to 2.0 kcal/mol. This suggests that there is another source of energetic separation between these key TS structures.

Similar to reaction I, there are subtle differences in the position of the transferring proton in the stereocontrolling TS structures for reaction II. Furthermore, the electrostatic environment arising from the numerous heteroatoms and charged nature of this H-bond network result in the transferring proton being in a more favorable electrostatic environment in $\mathbf{TS_{major}}$ than in $\mathbf{TS_{minor}}$ (see Figure V-7c). Quantifying the difference in electrostatic stabilization of the proton results in an energy difference of 2.0 kcal/mol, favoring $\mathbf{TS_{major}}$. Thus, the bulk of the 2.2 kcal/mol difference in enthalpy between $\mathbf{TS_{major}}$ and $\mathbf{TS_{minor}}$, which underlies the stereoselectivity of reaction II, can be attributed to the preferential electrostatic stabilization of the transferring proton in the favored transition state.

After addressing the origin of stereoselectivity in these three NHC catalyzed KRs, we wondered whether similar effects are also operative in any examples of NHC-catalyzed DKRs. Chi and co-workers[297] recently reported a NHC-catalyzed DKR of carboxylic esters (see Scheme V-2). Based on DFT computations, Chi *et al*.[297] proposed that the TS leading to the minor stereoisomer was destabilized by steric interactions (see Figure V-8a). Once again, considering model TS structures in which this steric interaction has been removed, along with other peripherial groups, leaves the energy difference largely intact (3.6 kcal/mol; see Figure V-8b). That is, steric interactions account for relatively little of the 5 kcal/mol energy difference. Instead, there is a network of CH···O interactions[152] that all favor $\mathbf{TS_{major}}$, which are ultimately responsible for the stereoselectivity of this NHC-catalyzed DKR.

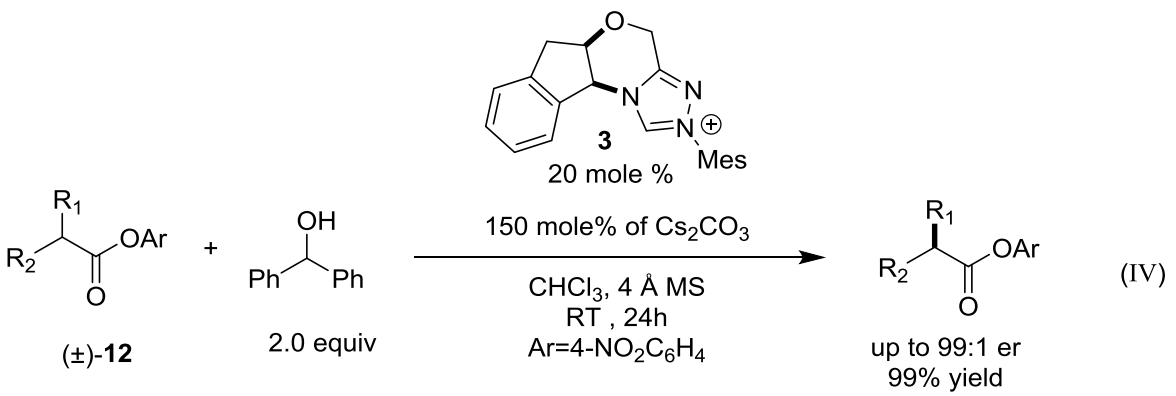

Scheme V-3. DKR of α,α-disubstituted esters from Chi et al.[297]

The nature of the key hydrogen bonding interactions are different in reactions I and II and IV. For instance, reaction I features a cyclic hydrogen bond network that is distant from the key bond forming reactions, whereas for reaction II the key hydrogen bond network is directly involved in the bond forming/breaking step. Reaction IV, on the other hand, relies on the collective effects of three hydrogen-bonding interactions that are again somewhat distant from the key bond forming/breaking events in the transition state. Moreover, these reactions involve different types of hydrogen bonds: an NH···O interaction, a charge assisted OH···O interaction, and CH···O interactions[152] for reactions I, II, and IV, respectively. These three examples are also distinct from the kinetic resolution reported by Cheong *et al*.[296] in which the stereoselectivity was attributed to the electrostatic stabilization of a fleeting charge in the TS by the catalyst.

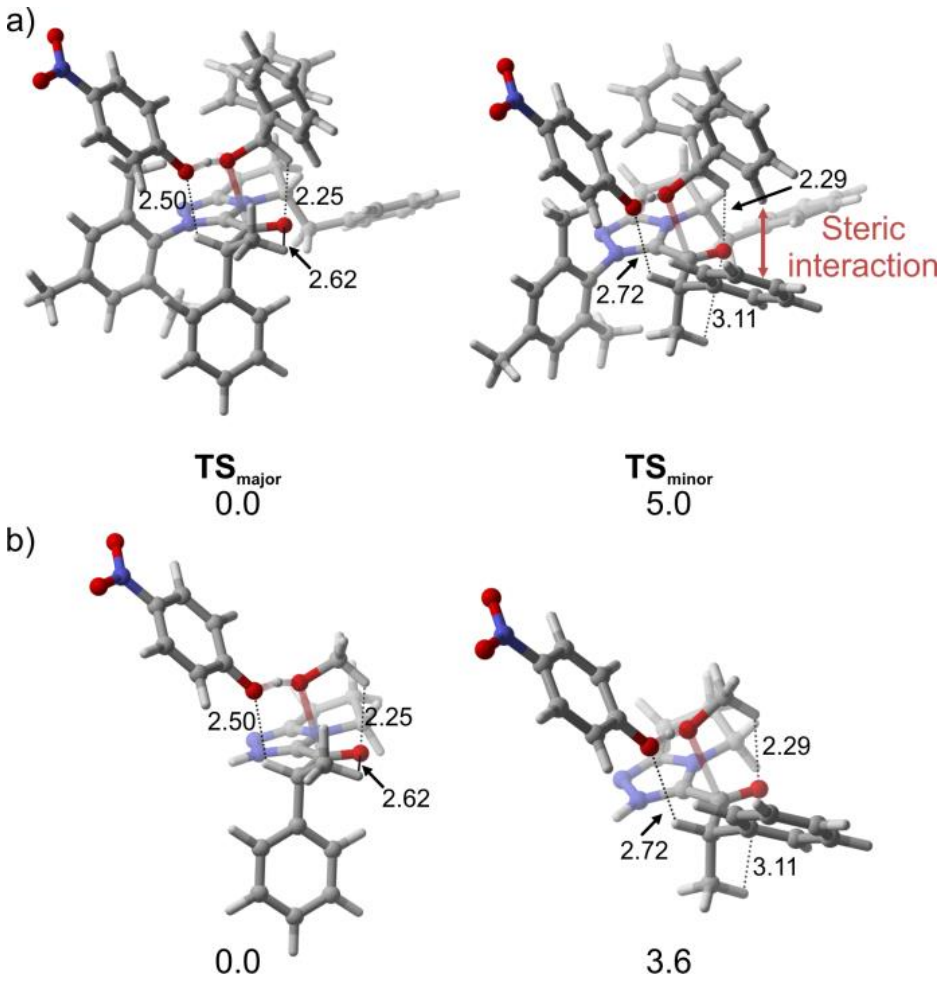

Figure V-8. (a) Primary stereocontrolling TS structures for reaction IV computed at the B3LYP/6-31G(d) level of theory, from Chi *et al.*,[297] along with relative gas-phase energies in kcal/mol. Key CH…O interaction distances are shown in Angstroms. (b) Model TS structures derived from those in (a), along with the corresponding relative energies in kcal/mol.

Despite these differences, by considering the electrostatic environment of the protons involved in these hydrogen-bond networks, we arrive at a consistent, electrostatically-driven understanding of the stereoselectivity of these three reactions. In all cases, the TS structure leading to the major stereoisomer is preferentially stabilized because key protons are located in more favorable electrostatic environments. One can

view the stereoselectivity of reaction III in a similar light—the presence of a charge-assisted OH···O interaction in $\mathbf{TS_{major}}$ and its absence in $\mathbf{TS_{minor}}$ is simply an extreme case of a single proton being in a more favorable electrostatic environment in the favored TS compared to the disfavored TS. Indeed, quantifying the electrostatic stabilization of that proton in $\mathbf{TS_{major}}$ and $\mathbf{TS_{minor}}$ for the KR of (±)-**4** catalyzed by **3**, one finds an energy difference of 1.0 kcal/mol favoring $\mathbf{TS_{major}}$. This is in reasonable agreement with the electronic energy difference of 1.5 kcal/mol.

Examples of electrostatically-driven selectivity of NHC-catalyzed transformations have been previously documented,[296, 332, 364-367] which stem from the unique electronic character of NHCs. For instance, Bode, Schoenebeck, *et al.*[364] explained the selectivity of an NHC-catalyzed Claisen rearrangement by the electrostatic stabilization of the favored TS structure. Houk, Rovis, *et al.*[332, 367] reasoned the improved reactivity and selectivity of flourinated NHC catalysts in an asymmetric Setter reaction due to preferential electrostatic interactions between catalyst and substrates. Similarly, Studer *et al.*[365-366] explained chemoselective acylation of an alcohol in the presence of an amine by the more electrostatic nature of hydrogen bonding. Finally, Cheong, Scheidt, *et al.*[336] very recently showed the importance of electrostatic stabilization in an NHC-catalyzed annulation. Furthermore, the importance of charge-assisted hydrogen bonds in Brønsted-acid catalyzed reactions have recently been demonstrated experimentally by Gschwind *et al.*[368] Taken together, these findings point toward a much greater role of electrostatic effects in the selectivity of NHC catalyzed transformations than is widely assumed.

5.3. Conclusions

N-heterocyclic carbenes have emerged as powerful organocatalysts for kinetic resolutions and dynamic kinetic resolutions.[290-298, 337-341] However, a number of key questions regarding the origin of catalytic activity and selectivity of several recently reported KRs of diols and amines had not been fully resolved. We used modern computational tools to examine three NHC-catalyzed kinetic resolutions (Scheme 1). First, we unveiled the full role of BzO^- in the KR of BINOL-derivatives catalyzed by a chiral NHC (reaction III), which is an *in situ*-generated additive that obviates the need for an added co-catalyst as in other, similar transformations. Furthermore, in this reaction the BINOL-derived substrate is deprotonated, enabling the formation of a key intramolecular hydrogen bond in the favored TS structure and leading to high degrees of selectivity; when the substrate is methylated, this hydrogen bonding interaction is absent and selectivity is lost. In the case of VANOL-derived substrates, additional non-covalent interactions work in concert with this hydrogen bonding interaction, leading to further enhanced selectivity. Zhao *et al*.[369] recently reported an NHC-catalyzed acylative desymmetrization in which the stereoselectivity depended on a combination of a similar intramolecular H-bond combined with steric effects. In all three KRs examined here, the co-catalyst plays key roles; it facilitates a key proton transfer in both reactions I and III, substantially lowering the activation energies.

A reexamination of previously reported[9,12] stereocontrolling TS structures for reactions I, II and IV also revealed a new view of the origin of their selectivities. In each case, there are cyclic hydrogen bond networks in both the favored and disfavored TS

structures; however, these hydrogen bonds are more favorable in the TS structure leading to the major isomer. These disparate examples were all explained based on a simple electrostatic model—the protons involved in these charge-assisted hydrogen bond networks are in more favorable electrostatic environments in the TS structures leading to the major stereoisomer.

The importance of such subtle, electrostatically-driven non-covalent interactions in these four reactions exemplifies the similarities between many organocatalysts and enzymes, as envisioned by Jacobsen and others,[13, 253, 370-371] since many enzymes induce selectivity through the interaction of reacting substrates within a chiral, heterogeneous electrostatic environment.[372-374] These four NHC-catalyzed reactions join the growing list of organocatalysts that achieve selectivity through stabilizing electrostatic interactions,[112, 152, 246, 332, 336, 357, 364-367, 375-387] and emphasize the power of using favorable non-covalent interactions, rather than steric effects, to simultaneously achieve high degrees of activity and selectivity. Hopefully, the insights uncovered in this study will not only have implications for the design of more effective NHC catalysts, but can also help to guide judicious choice of protic additives[388] and exploitation of favorable electrostatic interactions.

5.4. Theoretical Methods

We considered several levels of theory, including B97-D/TZV(2*d*,2*p*), B3LYP/6-31+G(*d*), B3LYP-D3/6-31+G(*d*), ωB97XD/6-31+G(*d*), and M06-2X/6-31+G(*d*). Solvent effects (dichloromethane) were accounted with CPCM unless specified otherwise.[389-390] Transition state structures were verified by the presence of a single

imaginary vibrational frequency. The presented theoretical free energy differences ($\Delta\Delta G^{\ddagger}$) correspond to the difference in free energy between the lowest-lying transition state structures for each reaction/catalyst combination based on an extensive search of possible conformations of the catalyst and substrates (see Appendix A more details). It is assumed that these reactions are under Curtin-Hammett control, and that the enantioselectivity is dictated by $\Delta\Delta G^{\ddagger}$ for the stereocontrolling step (*vide infra*). In view of multiple reactive conformers for each isomer, presented free energy differences are based on a Boltzmann weighting of conformations of each TS structure. Thermal free energy corrections were based on the quasi-rigid rotor/harmonic oscillator (quasi-RRHO) approximation of Grimme.[391] The overall energetic profile of the catalytic cycle was analyzed by applying energetic span model.[347] Distortion-interaction analysis was performed on B3LYP/6-31G(*d*)optimized geometries following the protocol of Ess and Houk[31, 392] (or equivalently, the activation-strain model of Bickelhaupt*et al*.[393-394]). We also performed AIM analyses to identify important non-covalent interactions.[30, 352-353] Topological analysis of the electron density distribution is performed using electron densities computed at the CPCM-B3LYP/6-31G(*d*) level of theory. NCI plots were also used to visualize dispersion-driven non-covalent interactions.[29, 209] The electrostatic stabilization of key protons in stereocontrolling TS structures was quantified by taking the product of the electrostatic potential (ESP) due to all other atoms evaluated at the position of the proton with the NPA atomic charge of the proton in the intact TS structure, as done previously by Lu and Wheeler.[395] Molecular structure figures were generated using CYLview.[396] All computations were performed using Gaussian 09[397]

and the B97-D computations employed density fitting techniques. For the analyses of previously reported TS structures,[297, 337, 342] we used the same levels of theory as found in the corresponding references, for consistency.

CHAPTER VI

ACTIVATION MODE AND ORIGIN OF SELECTIVITY OF SELECTIVITY IN CHIRAL PHOSPHORIC ACID CATALYZED OXACYCLE FORMATION BY INTRAMOLECULAR OXETANE DESYMMETRIZATION*

6.1. Introduction

The desymmetrization of achiral and *meso* compounds is a powerful route to enantiopure molecules, and has consequently received significant attention.[5, 398] While intermolecular oxetane openings provide access to 2,3-disubstituted propan-1-ols,[399] intramolecular variants of this reaction can incorporate these scaffolds into cyclic structures. Numerous strategies for enantioselective oxetane openings have been developed, involving organocatalysts,[400-402] Lewis acids,[403] and metals.[404-406] A more complete understanding of key stereocontrolling factors in such reactions, as well as deeper mechanistic insights, will help to expand the scope of these synthetic protocols. Computational quantum chemistry has emerged as a powerful means of achieving such insights across many classes of organocatalyzed reactions,[224] including those catalyzed by chiral phosphoric acids (CPAs).[407] The last decade has witnessed significant progress in our understanding of CPA-catalyzed reactions,[247, 260, 408-412] particularly in terms of their preferred activation mode and origins of stereoselectivity.[11] Complemented by experimental work by Gschwind *et al*.,[413-415] theoretical studies have provided key

*Adapted with permission from "Activation Mode and Origin of Selectivity in Chiral Phosphoric Acid Catalyzed Oxacycle Formation by Intramolecular Oxetane Desymmetrization" by R.Maji, P.A. Champagne, K.N.Houk and S. E. Wheeler, *ACS Catal.* **7**, 7332. Copyright 2017 American Chemical Society.

insights into the binding modes of these catalysts and the development of intuitive models that enable the prediction and rationalization of stereochemical outcomes for many of these reactions.[260, 263, 416] The general consensus is that CPA-catalyzed reactions typically operate via a 'bifunctional' activation mode[247, 249, 262, 417] in which the electrophile and nucleophile are simultaneously activated through interactions with the Brønsted acidic and basic sites of the catalyst.[11] Concurrently, the understanding of the origin of stereoselectivity of these reactions has gradually shifted from a view anchored in repulsive steric interaction to more nuanced models based on the interplay of numerous attractive and repulsive non-covalent interactions between the catalyst and substrates.[36, 118, 222, 246, 275, 418-424]

Recently, Seguin and Wheeler[273] and Champagne and Houk[242] presented theoretical studies of CPA-catalyzed intermolecular oxetane ring openings, reaching disparate conclusions regarding the relative importance of distortion effects and non-covalent interactions. In particular, Seguin and Wheeler[273] found that electrostatic interactions guided the selectivity of oxetane ring openings in the case of mercaptobenzothiazole nucleophiles,[425] while Champagne and Houk[242] reported a distortion-guided steric outcome for HCl mediated oxetane ring openings.[426] The latter study provided a general model of selectivity for oxetane desymmetrizations, which correctly explains the major enantiomer observed in various published reactions of oxetanes, including the one studied by Seguin and Wheeler.[273]

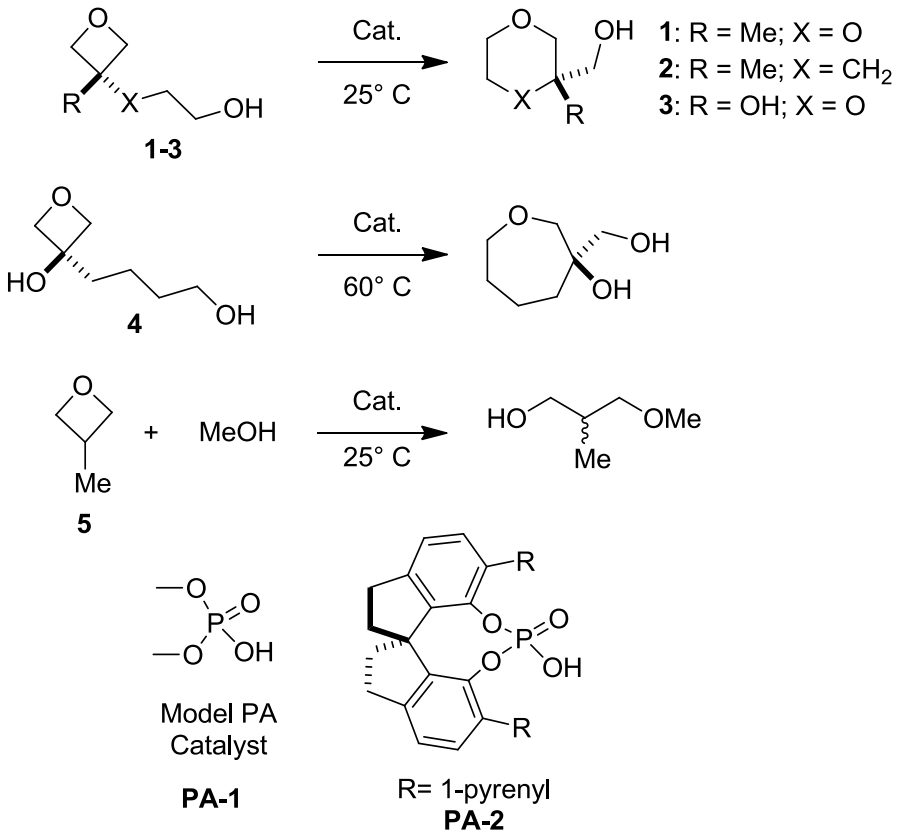

Scheme VI-1. Organocatalytic cascade Intramolecular oxetane ring opening reactions from Sun *et al*.[427] (substrates 1-4), along with a model intermolecular oxetane ring opening (substrate 5).

However, this general model of selectivity was not directly applicable to Sun's intramolecular openings of 3,3-disubstituted oxetanes (Scheme VI-1).[427] Intrigued by this limitation of the model, and in line with our overlapping interests in CPA-catalyzed reactions,[118, 246, 265, 271, 275, 428] we pursued a joint theoretical study of the intramolecular oxetane desymmetrizations in Scheme 1.[427] These reactions provide direct access to enantioenriched 1,4-dioxanes and other related oxacycles that are abundant in natural products and pharmaceuticals. For these reactions, (*R*)-SPINOL-derived catalyst **PA-2** was the most selective, and good yields of the desired products were usually obtained at

room temperature. To explain the experimental selectivity, Sun *et al.*[427] assumed the conventional bifunctional activation mode, where the stereochemical outcome could be predicted through consideration of steric interactions. However, since our recently-developed steric model could not account for the observed selectivity[242] we expected to find some caveat to this explanation.

6.2. Methods

All DFT computations were carried out using Gaussian 09.[429] Geometry optimizations and vibrational frequency computations were conducted at the B97D/TZV(2d,2p) level of theory, with single point energy refinements at the M06-2X/6-311+G(d,p) level. Solvent effects (dichloroethane) were accounted for with SMD for all geometry optimizations, vibrational frequency computations, and single-point energies unless specified otherwise.[430] Stereoselectivities were based on the relative free energies of the lowest-lying transition state (TS) structures leading to the minor and major stereoisomers ($\Delta\Delta G^{\ddagger}$), under the assumption that these reactions are under Curtin-Hammett control. Transition state structures were verified by the presence of a single imaginary vibrational frequency. The theoretical free energy differences for each reaction/catalyst combination are based on an extensive search of possible conformations of the catalyst and substrates (see Appendix B more details). Thermal free energy corrections were based on the quasi-rigid rotor/harmonic oscillator (quasi-RRHO) approximation of Grimme.[431] The overall energetic profile of the catalytic cycle was analyzed by applying the energetic span model.[347] Distortion/interaction analysis was performed on the B97-D/TZV(2*d*,2*p*) optimized geometries following the protocol

of Ess and Houk[31, 392] (or equivalently, the activation-strain model of Bickelhaupt *et al*.[393-394]). AIM analyses have been employed to identify important non-covalent interactions,[30, 352-353] and the strength of various hydrogen bonding interactions were quantified using the method by Espinosa and coworkers.[362] NCI plots were also used to visualize dispersion-driven non-covalent interactions as proposed by Yang and coworkers.[29, 209] Atomic charges were computed using natural population analysis (NPA).[361] The electrostatic stabilization was quantified by taking the product of the electrostatic potential (ESP) due to all other atoms evaluated at the position of a proton with the NPA atomic charge of the proton in the intact TS structure, as done previously by Lu and Wheeler.[395] Molecular structure figures were generated using CYLview.[396]

6.3. Results and Discussion

To evaluate the possible activation modes in CPA-catalyzed intramolecular oxetane desymmetrizations, we first considered the reaction of substrate **1** catalyzed by phosphoric acid dimethyl ester (**PA-1**) as a model catalyst.[432] Three low-energy binding modes were identified, and the most stable conformations for each mode are shown in **Figure** VI-**1** in a rotated Goodman[263] and Terada-Himo quadrant[260, 433] projections. These projections are related by a 90° rotation along the x-axis. A nearly linear arrangement of the leaving group, substituted carbon, and nucleophile is observed in all three cases, as expected for an S_N2-like opening of the oxetane. In these transition states, proton transfer to the oxetane oxygen is complete, while the nucleophilic alcohol is still almost intact (both O–H bonds are between 0.97 – 1.03 Å), an effect related to the weak acidity of alcohols. The result is that these TSs are essentially ion-pairs of the protonated

substrate and deprotonated catalyst.[414-415, 434-435] Notably, the chair-like conformation of the forming 6-membered ring is always the most favorable. After the TS, IRC analysis shows that the cationic product is deprotonated by the catalyst phosphate to form a neutral product-complex spontaneously. In addition to the expected "bifunctional activation" (**BA**) mode,[242, 246, 273] we found two unprecedented modes where the catalyst interacts with only one of the two OH groups. In the "nucleophile activation" (**NA**) mode, only the nucleophile OH is bound to the phosphate, while in the "oxetane activation" (**OA**) mode, the oxetane OH is bound to the phosphate. In both cases however, the second oxygen of the catalyst engages in a CH···O interaction with the carbon undergoing substitution. Surprisingly, in this intramolecular system, **OA** is the most favorable activation mode, with an activation free energy of 32.7 kcal/mol compared to separated reactants. This is 0.9 and 1.1 kcal/mol smaller than the activation free energy for the **BA** and **NA** modes, respectively. Although the **OA** mode is preferred for this reaction, due to the lack of a substantial energy difference we were unable to eliminate the other possible activation modes at this stage.

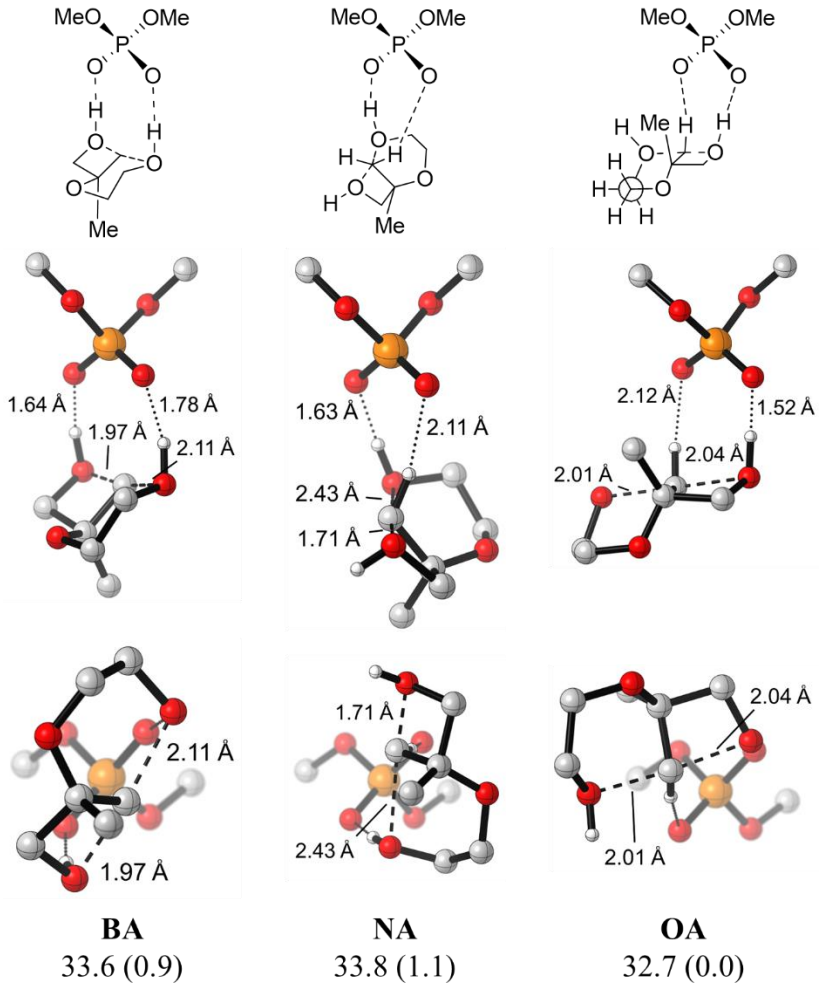

Figure VI-1.Three activation modes of substrate **1** catalyzed by **PA-1**, shown in their rotated Goodman (middle row) and quadrant (bottom row) projections, with their (relative) free energies of activation (in kcal/mol). Non-critical hydrogens are omitted for clarity (note that in the Goodman projection for the OA mode, a proton is obscured by the nucleophilic oxygen). The TSs shown lead to the (*S*)-product.The 3,3′-aryl groups (Ar) serve primarily to create a restrictive binding groove that orients the substrates within the electrostatic environment of the catalyst.

The **BA** mode has two strong OH···O hydrogen bonds between the catalyst oxygens and the substrate, yet has similar energies to **NA** or **OA**. To understand this effect, we conducted a distortion/interaction analysis at the SMD-M06-2X/6-311+G(d,p) level of theory (Table VI-1). We compared the relative energies of distortion of the

catalyst ($^{\Delta\Delta E^{cat}_{dist}}$) and substrate ($^{\Delta\Delta E^{sub}_{dist}}$) components, as well as the actual (ΔE_{int}) and relative ($\Delta\Delta E_{int}$) interaction energies between these two parts, setting the **BA** mode as our standard (0.0 kcal/mol).

Table VI-1**.** Relative distortion/interaction analysis (in kcal/mol).

TS	**$\Delta\Delta E^{‡}$**	**$\Delta\Delta E_{dist}^{cat}$**	**$\Delta\Delta E_{dist}^{Sub}$**	**ΔE_{int}**	**$\Delta\Delta E_{int}$**
BA	0.0	0.0	0.0	38.0	0.0
NA	0.4	-0.3	-14.4	-22.9	15.1
OA	-0.6	0.0	-9.9	-28.7	9.3

No difference in the catalyst distortion was identified by this analysis, but drastically different substrate distortion energies were found. Interestingly, the **BA** mode requires the most substrate distortion, whereas the **NA** and **OA** modes require 14.4 and 9.9 kcal/mol less substrate distortion, respectively. However, this reduced distortion for **NA** and **OA** comes at the cost of reduced interaction energies with the catalyst, as expected from the different binding patterns exhibited by these activation modes (Figure VI-1). For **OA**, the reduction in interaction energy is only slightly smaller (9.3) than the savings from distortion (-9.9), making it the best activation mode by a mere 0.6 kcal/mol.

The distortion required for the intramolecular ring system of **1** can be explained by the nature of the forming 6-membered ring, which involves all sp^3-hybridized atoms. This precludes the alignment of the oxetane and nucleophile O–H bonds required to simultaneously engage in strong hydrogen bonding interactions with the phosphate catalyst in the **BA** mode (**Figure** VI-**2**). Instead, significant distortions of the oxetane and chair-like rings are required for these hydrogen bonds to align. To prove this, we computed TS structures for the reaction of substrate **5** with methanol, again catalyzed by

model catalyst **PA-1** (**Figure** VI-**3**). In this case, easy alignment of both OH groups was expected (**Figure** VI-**2**).

Indeed, for this model system, the **BA** mode is at least 3.2 kcal/mol more favorable than either **NA** or **OA**. When these intermolecular TS structures are compared to those of Figure VI-1, the **NA** and **OA** modes have identical alignments of the nucleophilic and electrophilic parts of the reaction, relative to the catalyst structure. Therefore, for these modes, the intra- or intermolecular nature of the TS has no effect. However, the **BA** TS is organized in a strikingly different way in Figures 1 and 3, which indicates that it is arranged differently, depending on whether the reaction is intramolecular (distorted) or intermolecular (not distorted). Therefore, i*n the absence of unfavorable distortion, the conventional bifunctional mode is the preferred mode of activation for the opening of oxetanes catalyzed by phosphoric acids.*

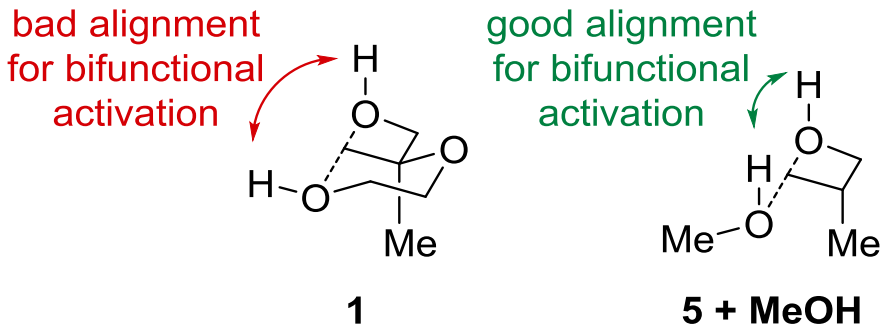

Figure VI-2**.** Different alignments of the OH groups for intra- and intermolecular oxetane desymmetrizations.

Having established the plausibility of several potential binding modes for intramolecular oxetane ring openings, we next considered four examples using the full catalyst **PA-2**. Theoretical *ee*'s are presented in Table 2; we are pleased to observe

remarkable agreement with the experimental stereoselectivities,[427] capturing not only the reduced stereoselectivity for substrates 3 and 4 but also reasonable reproduction of experimental values in all cases. Computed *ee* values are 1-16% lower than experimental, representing a maximum error of 0.6 kcal/mol.

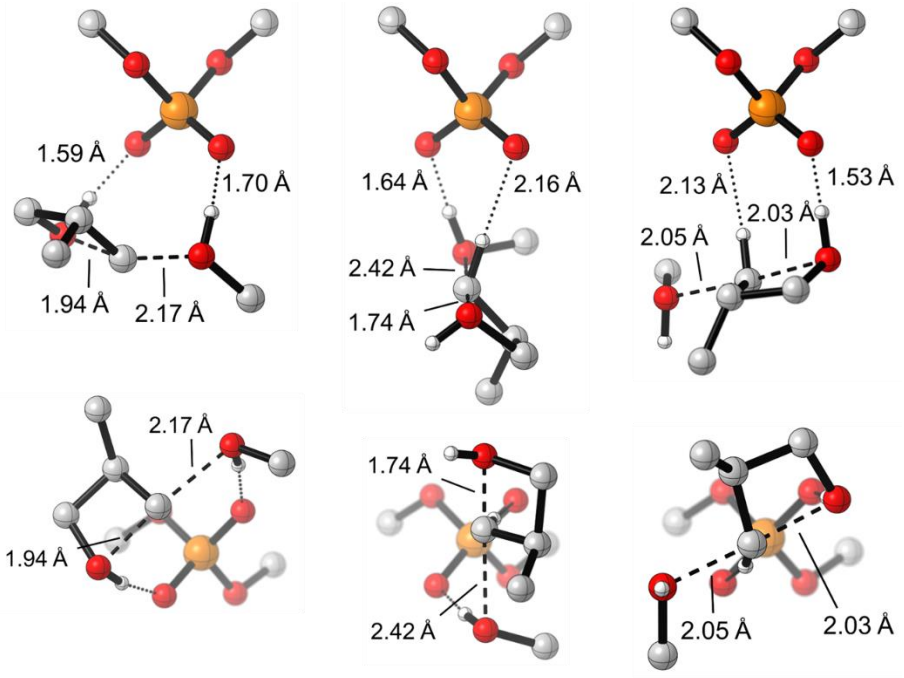

Figure VI-3**.** Rotated Goodman and quadrant projections of the three activation modes, for the reaction of **5** with MeOH, catalyzed by **PA-1**. Non-critical hydrogens are removed for clarity. (Relative) free energies of activation are displayed below the structures, in kcal/mol.

For the reaction of substrate **1** catalyzed by the real catalyst **PA-2**, the same three activation modes can be located, but their relative energies are significantly different from those computed for **PA-1** (**Figure** VI-**4**). Notably, **OA** is even more strongly favored over the other activation modes for the real catalyst than for the model catalyst,

indicating that the flanking pyrenyl groups provide greater stabilization to the TS for the **OA** mode. We find that in both **NA** and **OA**, the OH group that is not bound to the PA moiety is engaged in an OH···π interaction with one of the flanking pyrenyl groups of the catalyst, partially offsetting the decreased interaction energy inherent to these two activation modes (see above). Of interest, the arrangement of the substrate relative to the catalyst structure is almost identical, *whether the real or model catalyst is used*, except for slight variations that allow a more efficient OH···π overlap.

Table VI-2**.** Experimental[427] and theoretical *ee*'s and corresponding relative free energies (in kcal/mol) for substrates **1**-**4** catalyzed by **PA-2**.[a]

Substrate	ee	ΔΔG‡	ee	ΔΔG‡
1	98	2.7	94	2.1
2	91	1.8	90	1.8
3	86	1.5	78	1.3
4	67	1.1	51	0.7

[a]All reactions at 298K except for substrate **4** (333K).

Additional insights regarding this preferred binding mode can be gleaned from distortion/interaction analysis. As in the model TS structures, interaction energies favor the **BA** mode, in large part because of the presence of two OH···O hydrogen bonds; however, this comes at the expense of distortion of the substrate in order to align these two hydrogen bonds with the phosphate oxygens. In the **OA** mode, the less favorable hydrogen bonding interactions are compensated by the lack of distortion. Moreover, in this mode there is an additional stabilization afforded by the OH···π interaction between the nucleophilic OH and one of the pyrenyl substituents on the catalyst. The net result is that for reactions catalyzed by **PA-2**, the TS structures corresponding to the **BA** mode are thermodynamically unimportant and these reactions proceed almost entirely via **OA**.

We note that these trends are consistent regardless of the DFT method employed (see Appendix B more details).

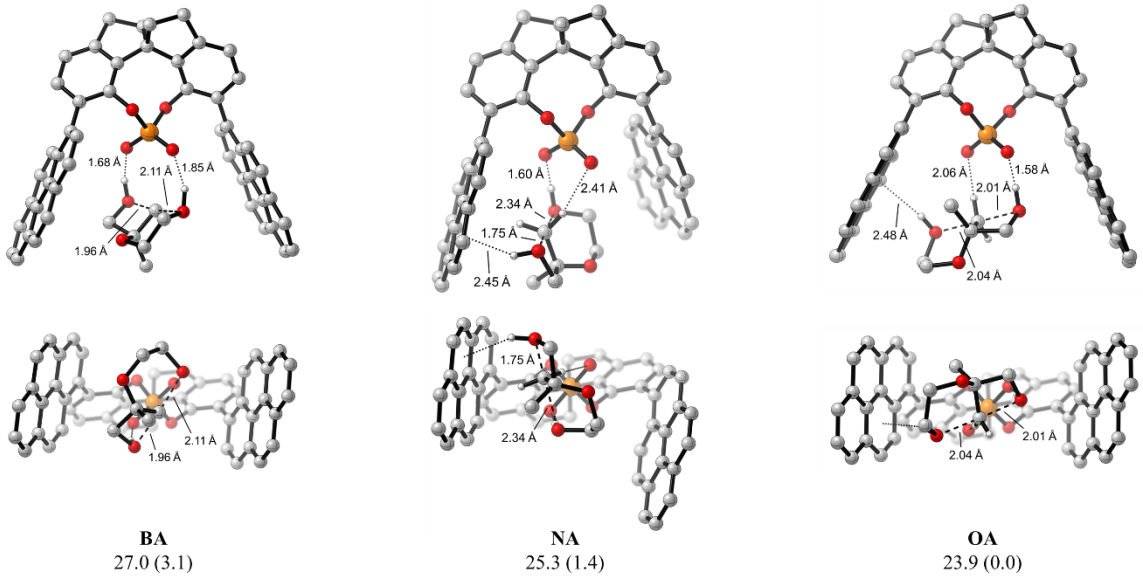

Figure VI-4**.** Lowest-energy TSs for reaction of substrate **1** catalyzed by **PA-2** for the three activation modes, shown in their rotated Goodman (top row) and quadrant (bottom row) projections. The structures shown lead to the major (*S*) product found experimentally. (Relative) free energies of activation are given below the structures, in kcal/mol. Key bond lengths are highlighted. Non-critical hydrogen atoms are omitted for clarity.

Considering the overall free energy profile for reaction of **1**, the energetic span[347] for the catalyzed reaction is 23.9 kcal/mol and the reaction is exergonic by 20.7 kcal/mol (see Appendix B more details). This relatively low energetic span can be contrasted with the uncatalyzed reaction (47.3 kcal/mol), or the span resulting from the model catalyst **PA-1** (32.7 kcal/mol). In other words, the non-covalent stabilization of the rate-limiting TS provided by the aryl substituents on the catalyst is a vital component of the catalytic activation of this reaction; the phosphoric acid functionality alone does not lower the

barrier enough to render this intramolecular oxetane ring opening viable at room temperature.

Finally, we turn to understanding the mode of stereoinduction for the reaction of substrates **1**-**4** catalyzed by **PA-2**. The lowest-lying TS structures leading to the major (*S*) and minor (*R*) stereoisomers are shown in Figures 5 and 6 for substrates **1** and **3**, respectively (see Appendix B for TS structures for **2** and **4**). First, these favored TS structures correspond to the **OA** mode, in which the oxetane interacts with the catalyst via OH···O and C–H···O interactions with the phosphate. It is instructive to compare the substrate orientations in these TS structures for **PA-2** with the corresponding structures for the model catalyst **PA-1** (see Figure VI-5). For **1**, in the TS leading to the major (*S*) product, the reacting substrate adopts an arrangement that is almost identical to that seen for the model catalyst (Figure VI-5a). A slight shift of the substrate and rotation of the nucleophilic OH orient this hydroxyl group towards the nearby pyrene, leading to a more stabilizing OH···π interaction. However, in the TS leading to the minor (*R*) product the substrate is oriented differently in the model and real catalysts (Figure VI-5b). To achieve a moderately good OH···π overlap, the substrate is rotated within the pocket, which has the effect of elongating and thus weakening the CH···O interaction that is characteristic of the **OA** mode [2.42 Å in TS(*R*) vs 2.06 Å in TS(*S*)]. Furthermore, if the substrate were to adopt the orientation seen with the model catalyst in the pocket of **PA-2**, the methyl substituent would be in close contact with the wall of the catalyst. This further incentivizes the above-mentioned rotation.

Overall, due to the two-point binding of the TSs in **OA**, which imposes a predictable arrangement of the substrate, the TS leading to the major stereoisomer positions the nucleophilic OH group in an arrangement favorable for OH···π interaction, while the TS leading to the minor enantiomer has to rotate to engage in such an interaction. Based on the importance of these stabilizing OH···π interactions in these TS structures (see above), a model can be developed to qualitatively explain the sense of the observed enantioselectivity. This model is shown in **Figure** VI-**7a**.

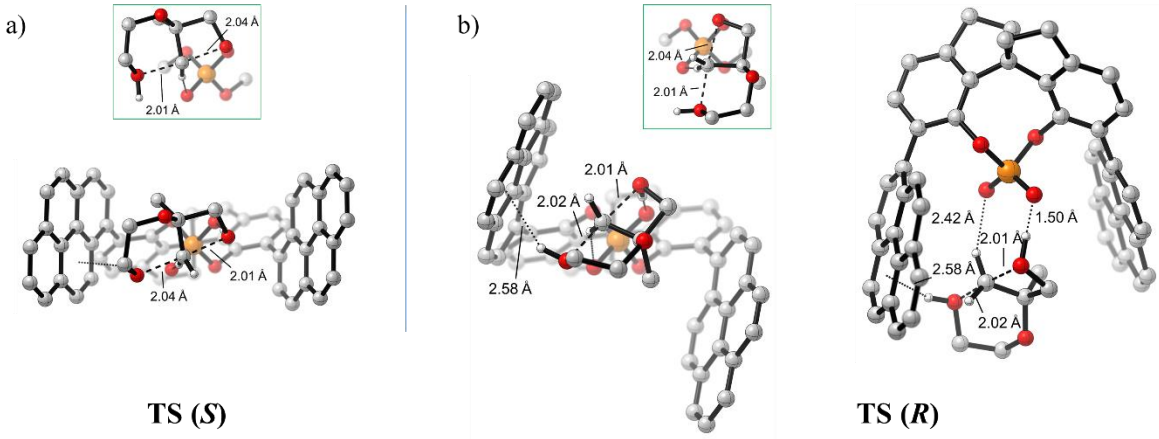

Figure VI-5. Lowest-lying stereocontrolling TS structures for the reaction of **1** catalyzed by **PA-2**. a) Quadrant projection of the TS structures leading to the major (*S*)-product. Inset: Lowest-energy (*S*) TS structure with model catalyst **PA-1**. b) Quadrant (left) and rotated Goodman (right) projections of the TS structures leading to the minor (*R*) product. Inset: Lowest-energy (*R*) TS structure with the model catalyst. Non-critical hydrogens are omitted for clarity.

As the **OA** mode uses a relatively weak CH···O interaction to bind the substrate to the catalyst, any possibly stronger interaction has the potential to displace this CH···O interaction and alter the substrate orientation. For instance, substrates **3** and **4** feature an OH group at the 3-position, which is capable of hydrogen bonding with the catalyst. Figure VI-6 shows that in the lowest-energy TS structures of **3** with **PA-2**, the substrate

is oriented to allow the protonated oxetane and 3-OH groups to interact with the phosphate moiety. However, as this new binding mode is governed by these two non-covalent interactions, the expected arrangements of the TSs are predictable. This allows us to draw another model to explain the observed selectivity for these substrates (**Figure** VI-**7b**). This model is once again based on the fact that the OH···π interaction is crucial to stabilize the TSs, such that the minor TSs will have to rearrange in the catalyst pocket to maximize this interaction.

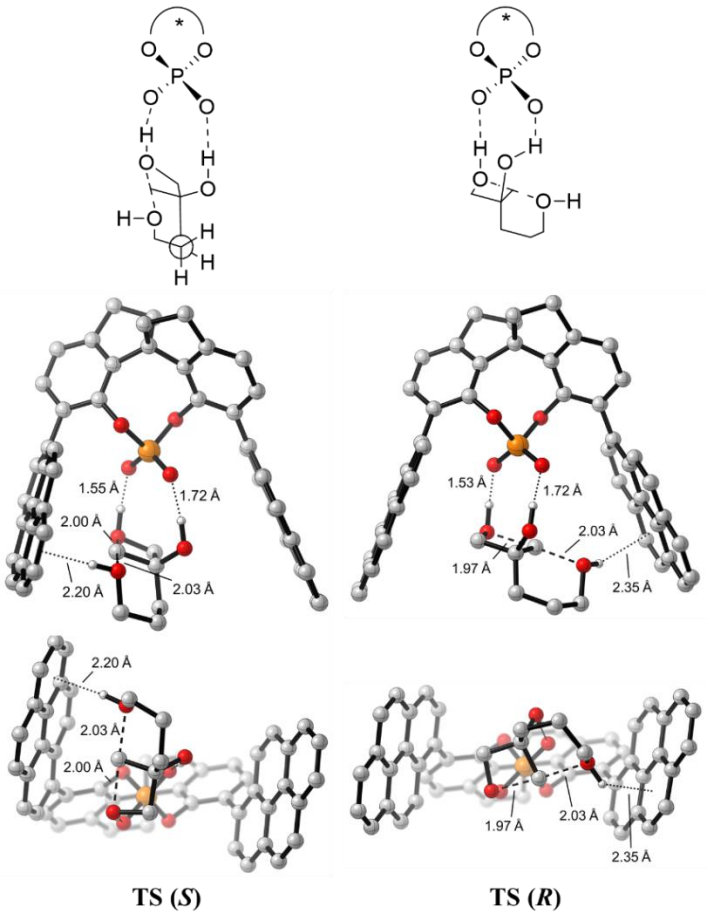

Figure VI-6**.** Most favorable TS structures leading to each enantiomer for the reaction of **3** catalyzed by **PA-2**. Structures are shown in their rotated Goodman (middle row) and quadrant (bottom row) projections, with non-critical hydrogens removed for clarity.

Distortion/interaction analyses[31, 392-393] provide further quantitative insight into the mode of stereoinduction in these reactions, adding to the above discussion and the associated models in Figure VI-7. Gas-phase energy differences between the lowest-lying TS structures leading to the minor and major stereoisomers, $\Delta\Delta E^{\ddagger}$ (Table VI-3), follow a similar trend to the $\Delta\Delta G^{\ddagger}$ values from Table 2, indicating only a small impact of solvent and entropic effects on stereoselectivity. To understand the origin of these gas-phase energy differences, they were decomposed into the difference in energy required to distort the catalyst ($^{\Delta\Delta E^{cat}_{dist}}$) and substrates ($^{\Delta\Delta E^{sub}_{dist}}$) into the corresponding TS geometries, and the difference in interaction energies between these distorted species (see Table VI-**3**). For substrates **1**-**3**, substrate distortion favors formation of the minor stereoisomer (for **4**, substrate distortion has no significant effect); however, these effects are overshadowed by the catalyst distortion, which favors the TS structures leading to the major stereoisomer. In all cases, the largest driver of stereoselectivity is differences in interaction energies between the substrates and catalyst, which favor the TS structures leading to the major stereoisomer.

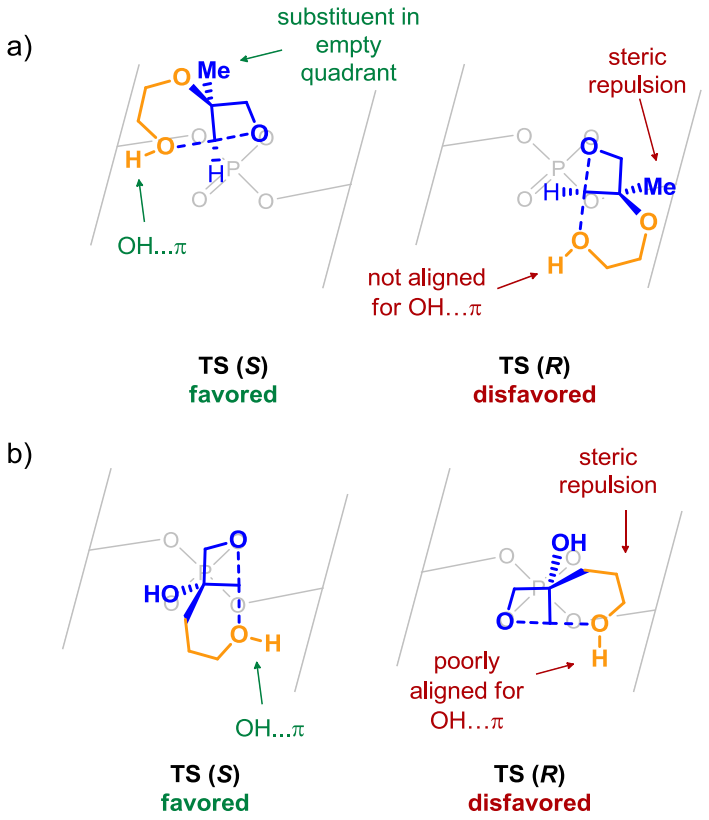

Figure VI-7**.** Models depicting the expected arrangements of substrates **1** (a) and **3** (b) relative to the binding pocket of a CPA catalyst. Comparison of these structures allow a qualitative understanding of which enantiomer will be favored.

Table VI-3**.** Differences in gas-phase energies ($\Delta\Delta E^{\ddagger}$) between the stereocontrolling TS structures, decomposition of $\Delta\Delta E^{\ddagger}$ into distortion ($^{\Delta\Delta E^{cat}_{dist}}$ and $^{\Delta\Delta E^{sub}_{dist}}$) and interaction ($\Delta\Delta E_{int}$) energies, and approximate decomposition of $\Delta\Delta E_{int}$ into contributions from non-covalent interactions of the substrates with the aryl ($^{\Delta\Delta E^{Ar}_{int}}$) and phosphoric acid ($^{\Delta\Delta E^{Phos}_{int}}$) components of the catalyst.

Substrate	$\Delta\Delta E^{\ddagger}$	$\Delta\Delta E_{dist}^{cat}$	$\Delta\Delta E_{dist}^{Sub}$	$\Delta\Delta E_{int}$	ΔE_{int}^{Ar}	$\Delta\Delta E_{int}^{Phos}$
1	4.8	2.9	-1.0	2.9	-0.1	4.1
2	5.5	2.1	-0.9	4.4	3.2	1.2
3	1.1	0.5	-0.5	1.1	2.9	-1.3
4	1.6	0.6	0.2	0.8	2.6	-2.5

These interaction energy contributions to $\Delta\Delta E^{\ddagger}$ were further probed by considering truncated model systems in which the substrate interacts with either the

pyrenyl groups ($^{\Delta\Delta E_{int}^{Ar}}$) or phosphoric acid functionality ($^{\Delta\Delta E_{int}^{Phos}}$), in the geometries of the stereocontrolling TS structures (see Table 3). These models provide a rough separation of the contribution of non-covalent interactions with the aryl substituents and phosphoric acid functionality to $\Delta\Delta E_{int}$, respectively. For substrate **1**, non-covalent interactions between the substrate and pyrenyl groups have no net impact on stereoselectivity; instead, the energy difference between the stereocontrolling TS structures arises from differences in non-covalent interactions with the phosphoric acid component of the catalyst. This is consistent with the model in Figure VI-7a. For substrate **1**, both stereocontrolling TSs feature similar OH···π interactions with the aryl walls of the catalyst, but in the minor TS the CH···O interaction is elongated to afford the proper geometry. This is reflected in $^{\Delta\Delta E_{int}^{Phos}}$. Substrates **2**-**4** are more complicated, since non-covalent interactions with the aryl substituents and phosphoric acid functionality both impact the stereoselectivity. While interactions with the aryl groups favor the major TS for all three of these substrates, interactions with the phosphate favor the major TS for **2** but the minor TS for substrates **3** and **4**. Analyses by AIM[26b,33] and NCI[29, 209] support the finding that non-covalent interactions of the substrate with the aryl walls of the catalyst preferentially stabilize the major TS and enhance the stereoselectivity. In particular, while non-covalent interactions abound in both the major and minor TS, AIM and NCI indicated that the major TS features stronger CH···π, OH···π, and (in the case of substrates **3** and **4**) lone pair···π interactions than the minor TS. Differences in the interactions of the substrate with the phosphoric acid functionality, which favor formation of the major stereoisomer for **1** and **2** but the minor stereoisomer for **3** and **4**,

can be understood by considering the partial atomic charges and geometries of the corresponding TS structures. In the **OA** mode, the early protonation of the substrate by the catalyst leads to substantial partial positive charges on the hydrogens of the carbon being attacked; these charges will interact with the chiral electrostatic environment created by the deprotonated catalyst, as observed recently by Seguin and Wheeler[246] and List *et al*.[256] for CPA catalyzed epoxide desymmetrizations. These electrostatic contributions are associated with the CH···O interactions between the substrate and catalysts in the major and minor TS structures. For substrates **1** and **2**, there is a greater positive charge and a shorter CH···O distance in the TS leading to the major stereoisomer, compared to the minor product (see Figure VI-8). This trend is reversed for substrates **3** and **4**, for which the TS leading to the minor stereoisomer exhibits a geometry more compatible with electrostatic stabilization via this CH···O interaction.

These electrostatic effects can be quantified approximately by considering the interaction of these atomic charges with the electrostatic potential arising from the deprotonated catalyst (see Figure VI-8). The resulting difference in electrostatic interactions for substrate **1**, accounting for the CH···O and OH···O interactions, is +2.8 kcal/mol (favoring the major stereoisomer); for substrate **3** (accounting for both OH···O interactions and the CH···O), the difference in electrostatic stabilization is -1.9 kcal/mol (favoring the minor stereoisomer). This can be contrasted with the aforementioned work[246, 256] on CPA-catalyzed epoxide ring openings, where the stereoselectivity was uniformly enhanced by the electrostatic stabilization of the TS structure leading to the major stereoisomer.

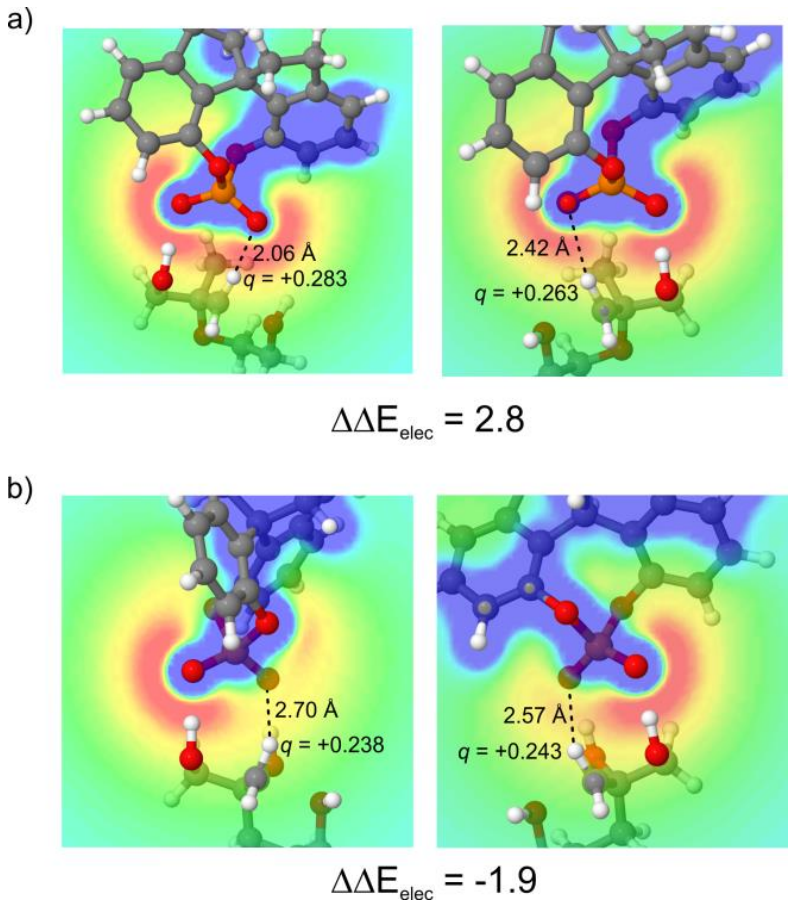

Figure VI-7. Electrostatic potentials due to the deprotonated catalyst in the plane of key hydrogens (red = -150.0 kcal/mol; blue = 0.0 kcal/mol). The difference in electrostatic stabilization for substrate **1** (a) and **3** (b) of the key CH and OH group(s) ($\Delta\Delta E_{elec}$) is also shown in kcal/mol.

6.4. Conclusions

We have shown that the activation mode for chiral phosphoric acid-catalyzed intramolecular oxetane ring openings differs qualitatively from that for intermolecular oxetane ring openings, and is contrary to popular reactivity models for CPA-catalyzed reactions in general. The origin of this is straightforward: intramolecular oxetane desymmetrizations with all-sp^3 rings require significant substrate distortion in order for both the electrophile and nucleophile to engage in OH···O hydrogen bonds with the

Brønsted acidic and basic sites of the catalyst. Instead, the favored activation mode for a series of intramolecular oxetane ring openings involves activation of only the oxetane by the phosphoric acid functionality; the nucleophile is mildly activated by OH···π interactions with a flanking pyrenyl group of the catalyst. This is corroborated by studies of a model intermolecular oxetane ring opening, for which the conventional bifunctional activation mode is favored.

From a mechanistic point of view, the intramolecular oxetane desymmetrization involves general acid catalysis. We have developed two models that qualitatively explain and predict which enantiomer will be favored for each type of substrate. Stereoselectivity of these reactions is driven primarily by differences in non-covalent interactions of the substrates with both the aryl substituents and phosphoric acid functionality of the catalysts. We showed that depending on the nature of groups attached, electrostatic interactions of the reacting oxetane with the chiral electrostatic environment of the deprotonated catalyst can either enhance or decrease the stereoselectivity. These intramolecular oxetane openings add to the growing list of organocatalysts that achieve selectivity through stabilizing non-covalent[14, 101, 112, 121, 248, 254, 322, 436-440] and electrostatic interactions.[152, 246, 357, 364-365, 375-383, 441-442] We envision that the insights into the mode of stereoinduction in these reactions will prove useful in improving the scope and efficiency of related reactions.

CHAPTER VII

UNDESTANDING THE REACTIVITY AND SELECTIVITY OF FLUXIONAL CHIRAL DMAP CATALYZED KINETIC RESOLUTIONS

7.1. Introduction

The biological relevance of chiral alcohols has driven the development of many methods for their kinetic resolution (KR), which have been subjected to numerous experimental and theoretical studies.[443-445] Among available strategies for the KR of alcohols, chiral 4-dimethylaminopyridine (DMAP) catalyzed KRs are particularly appealing due to their operational simplicity, high turnover, and environmental friendliness.[10, 446] Studying such reactions computationally not only enriches our understanding of these processes but also creates opportunities to improve their efficiency.

In continuation of our efforts to understand the stereoselectivity of organocatalyzed reactions,[14] particularly in the context of KRs,[271, 447] we have examined the KR of axially chiral biaryls reported by Sibi and co-workers in 2014 (Scheme VII-1).[448] In this reaction, chiral DMAP catalyst **A** serves as a highly selective catalyst when paired with isobutyric anhydride as the acylating agent. Although there have been previous computational studies of other KRs of alcohols,[143, 449-452] the reaction in Scheme VII-1 presents a number of unique features. First, it is the seminal example of an organocatalyzed KR that provides excellent selectivity for axially chiral alcohols, yet has not been explored computationally. Second, it exhibits high degrees of selectivity despite the use of a highly-fluxional chiral catalyst. This is contrary to the conventional wisdom

that more rigid catalysts should provide better selectivity, raising key questions regarding the interplay of catalyst flexibility and selectivity. Finally, Sibi *et al.*[448] observed that biaryl alcohols with electron-rich substituents at the β'-position exhibit much higher selectivities than those with electron-poor ones. Although this was explained in terms of a possible non-covalent interaction between these substituents and the N-acyl group, the established precedent of $\pi^{\cdots}\pi^{+}$ interactions in similar acylation reactions[143, 449, 452] raises the possibility that these substituent effects are due to the modulation of $\pi^{\cdots}\pi^{+}$ interactions in the stereocontrolling transition state (TS).

7.2. Theoretical Methods

Computations were performed using Gaussian 09.[453] Free energies were computed within the quasi-RRHO approximation of Grimme.[454] Additional computational details can be found in Appendix C.

7.3. Results and Discussion

First, we tackle one of the most perplexing aspects of this reaction, the ability of an apparently fluxional catalyst to impart high degrees of stereoselectivity. The conformations of catalyst **A** were explored initially using molecular mechanics (MM), identifying 15 potential low-lying conformers. Subsequent geometry optimization using five different DFT functionals identified three distinct low-lying conformations; two of these are predicted to be present in solution at room temperature and rapidly inter-converting; this supports Sibi's characterization of this catalyst as highly fluxional. The energetic ordering of the three lowest lying conformations is dependent on the DFT employed due to differences in the ability of these methods to capture dispersion-like

interactions (two these key conformers are depicted in Figure VII-1). To assess the performance of these different DFT methods, the low-lying conformers were compared with the crystal structure of DMAP catalyst **A**.[455] Overall, B97D/TZV(2*d*,2*p*) and M06-2X/6-31G(d) provided structures with the smallest root mean squared deviation (RMSD). Of the three low-lying conformations, conformer **Y**, which features a stabilizing π-stacking interaction (Figure VII-1a), is higher in energy than the conformers **X** (Figure VII-1a) and **Z** (see Appendix C). The lowest-lying conformation (**X**) is stabilized by a CH–π interaction.

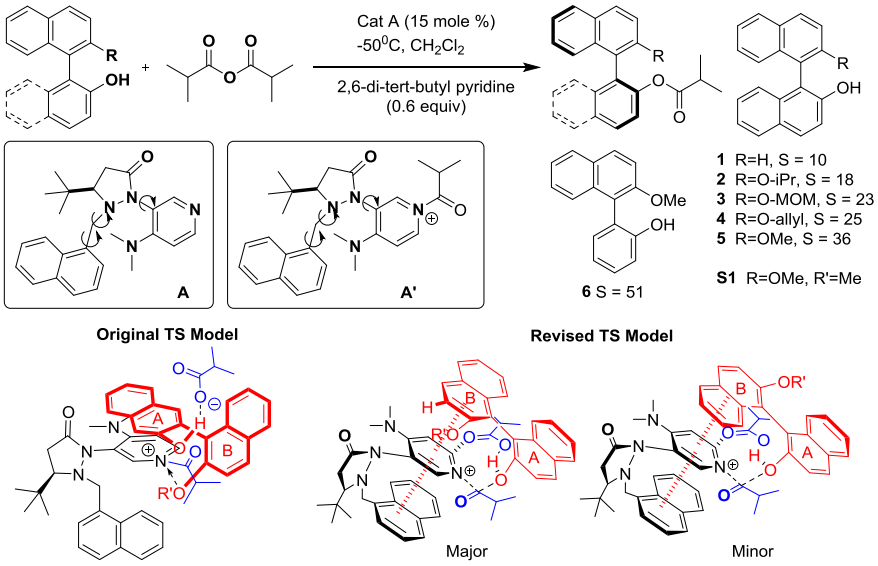

Scheme VII-1**.** (a) DMAP-catalysed kinetic resolution of chiral biaryls from Sibi *et al.*[448] as well as Sibi's original TS model (bottom left) and our revised TS model (bottom right).

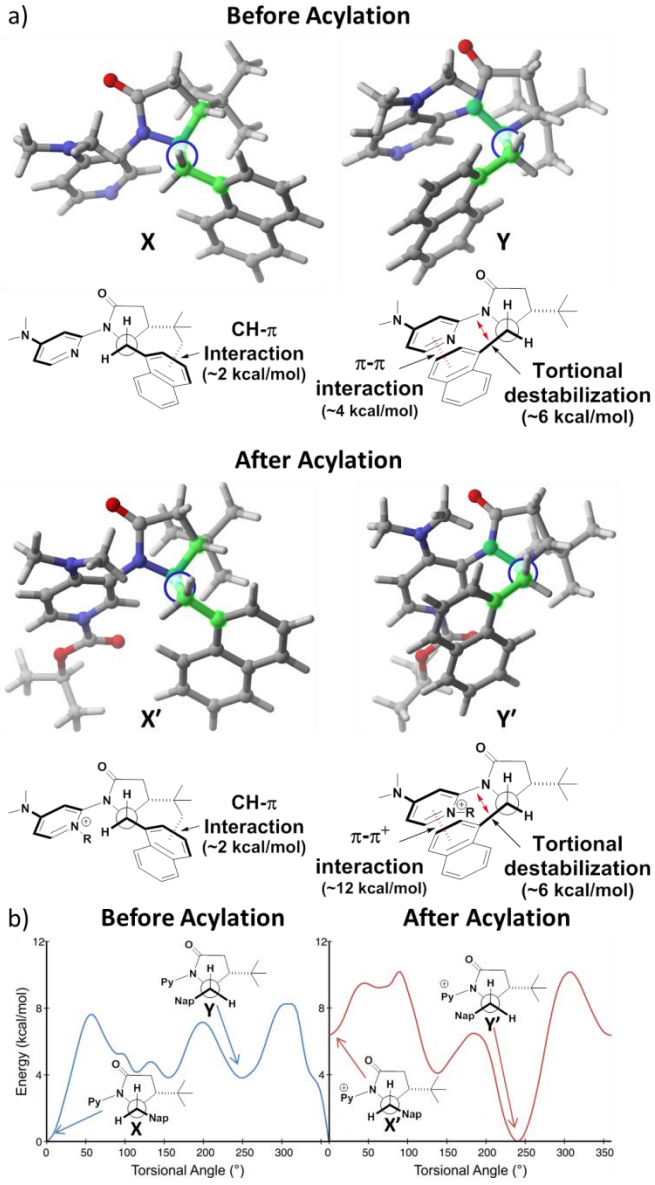

Figure VII-1. a) Key conformations of catalyst **A** before and after acylation. b) Torsional potential of the catalyst before and after the reaction

Given the literature precedent,[10, 143] we presumed that *in situ* generated acylated DMAP (**A**′) is the active catalyst in the reaction in Scheme VII-1. Therefore, we identified 15 low-lying conformers of **A**′ using MM which were further subjected to

geometry optimizations using different DFT methods. The energetic ordering of the low-lying conformations changes dramatically going from **A** to **A′** (See Appendix C). Conformer **Y′**, which is the acylated analogue of **Y**, is considerably lower in energy than the other conformers and will be the only conformation present in solution. This can be attributed to the highly-favorable π-π^+-stacking interaction between the N-acyl pyridinium and naphthyl group in this conformation. This electrostatically-enhanced stacking interaction is far more stabilizing than the CH$\cdots\pi$ interactions present in conformer **X′**. Thus, even though the catalyst itself (**A**) is highly fluxional, π-π^+ stacking interactions lock the activated catalyst (**A′**) into a single conformation (**Y′**).

To further understand these conformational preferences and the reduction in fluxionality upon acylation, we quantified the two primary non-covalent interactions operative in conformers **X** and **Y**. These two conformations can be interconverted by rotating around the highlighted C–N bond in Figure VII-1. The energy of catalyst **A** as a function of the CNCH dihedral angle both before and after acylation is plotted in Figure VII-1b. Conformers **X** and **X′** are stabilized in part by CH-π interactions between the *tert*-butyl and napthyl groups. Conformers **Y** and **Y′**, on the other hand, exhibit π-π interactions between the napthyl group and the pyridine and pyridinium rings, respectively (Figure VII-1). In the latter case, this interaction is expected to be significantly stronger due to the formal charge on the pyridinium. Symmetry adapted perturbation theory (SAPT) was employed at the SAPT0/jun-cc-pVDZ level to quantify these non-covalent interactions between individual components of **A** and **A′** in these two conformations (see Table C3 in Appendix C). Before acylation, the stacking interaction

between the pyridine and naphthalene groups in **Y** is 2.3 kcal more favorable than the CH-π interaction in **X**. Given that conformation **X** is ~4 kcal/mol lower in energy than **Y**, there must be ~6 kcal/mol of torsional destabilization of **Y** due to the eclipsed conformation around the C–N bond. Upon acylation, the strength of the resulting π-π^+ interaction in **Y′** is now 9.9 kcal/mol more favorable than the CH-π interaction in **X′**, overcoming the torsional destabilization. These data show that the bulk of this enhancement is due to electrostatic effects. In other words, the electrostatically-driven π-π^+ interaction in **Y′** controls the conformation of the activated catalyst,[141, 456-460] overriding the intrinsic conformational preference for **X**/**X′**. [214, 461]

Next, we turn to the mode of catalysis. Previous work by Zipse *et al*.[462-463] and Bourissou *et al*.[464] showed that both nucleophilic and base catalyzed pathways can be viable for these reactions depending on nature of the alcohol. In this case, there are two distinct base-catalyzed mechanisms (involving either four or six membered cyclic transition states) as well as a nucleophilic pathway (the acylation TS for each path is depicted in Figure VII-2b). We have explored these three mechanistic possibilities for the DMAP catalyzed acylation of (±)-**1** at the M06-2X/6-311+G(*d*,*p*)//CPCM-B97-D/TZV(2*d*,2*p*) level of theory,[465] modeling the isobutyrate as acetate. In contrast to the work of Sibi and co-workers,[448] in which it was assumed that the isobutyrate acts solely by deprotonating the alcohol, we find that this counterion plays a much more central role in all three mechanisms considered by taking part in key hydrogen-bonding networks. For formation of both the major and minor enantiomer, the base-catalyzed pathways are 8-10 kcal/mol higher in free energy than the nucleophilic pathway (see Figure VII-2a).

Notably, for the nucleophilic pathway the acylation of DMAP (TS1) is rate determining while the subsequent nucleophilic acyl transfer step (TS2) determines the stereoselectivity. This is contrary to other alcohols, for which the acyl transfer step has been found to be rate determining.[462-463, 466] In line with the previous work from Zipse and coworkers,[463] we find that DMAP acylation via a ternary complex is even higher in free energy than the two base catalyzed pathways.[467]

The favorability of the acyl transfer step in the nucleophilic pathway over the base-catalyzed pathways can be understood in terms of competing non-covalent interactions. There are two main non-covalent interactions at play in these TS structures (Figure VII-2b), which were quantified through both a fragment-based disconnection approach as well as by AIM analysis.[30, 468] First, in all three TS structures there is a stacking interaction between a naphthyl group of the substrate and the pyridinium. This stacking interaction is more stabilizing in the base-catalyzed TSs than the nucleophilic TS. This can be explained the full formal positive charge on the pyridinium in the base-catalyzed pathways, compared to the partial positive charge in the nucleophilic pathway due to the breaking N-acyl bond. This leads to enhanced $\pi\ldots\pi^{+}$ interactions in the former cases. However, this effect is overshadowed by the presence of a more favorable network of hydrogen bonds involving the counteranion. In the nucleophilic TS there are a greater number of homonuclear charged assisted hydrogen bonds (CAHB) compared to the less favorable heteronuclear charge assisted hydrogen bonds operative in the base-catalyzed TSs.[359] This is corroborated by AIM-based analyses.[362, 469]

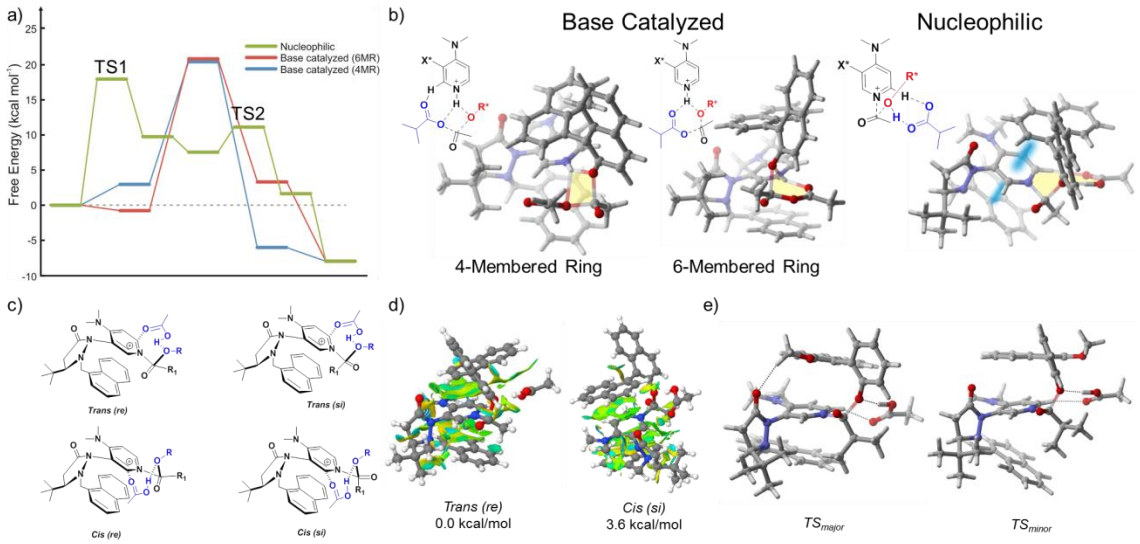

Figure VII-2. (a) M06-2X/6-311+G(d,p)//B97-D/TZV(2d,2p) computed free energy profiles for the KR of (±)-**1** catalysed by **A** via three mechanisms (formation of major enantiomer). (b) transition states for acylation steps in each mechanism (c) possible orientations of the N-acyl group and relative positions of alcohol and isobutyrate counter-ion (modeled here as acetate); (d) NCI plot showing the greater number of dispersion-driven non-covalent interactions in the lower-lying *Trans*(*re*) configuration; (e) Stereocontrolling TS structures for the KR of (±)-**6** catalyzed by **A**.

For the preferred nucleophilic pathway, there are four distinct relative orientations of the catalyst, alcohol, isoburyrate, and *N*-acyl group (See Figure VII-2c).[463] In each case, the counterion (modeled here as acetate) engages on a hydrogen bond with the alcohol and a CH···O interaction with DMAP. An extensive conformational search for both atropisomers of alcohol **1** revealed that the Trans(*re)* orientation is strongly favored. This can be attributed to the presence of additional stabilizing non-covalent interactions compared to the other conformations, as seen by comparing the corresponding NCI plots[29, 209] in Figure VII-2d and through AIM analysis (See Appendix C).

The resulting TS model is depicted in Scheme VII-1, and can be contrasted with the previously reported model from Sibi and coworkers.[448] There are three marked differences. First, Sibi *et al*.[448] proposed that the fluxional napthylmethyl group of the catalyst blocks both the back and side of the pyridinium ring. This was based on the crystal structure of the unactivated catalyst, for which conformation **X** is preferred (see Figure VII-1). However, as noted above, in the preferred conformation of the acylated catalyst (**Y**) the napthyl component of the catalyst engaged in a strong $\pi\cdots\pi^+$ interaction with the pyridinium that renders this group immobile. Furthermore, Sibi *et al*.[448] proposed that naphthalene ring A from the substrate, which bears the hydroxyl group (see Scheme VII-1), lies atop the pyridinium. Instead, we find a three-layer $\pi\cdots\pi^+\cdots\pi$ stacking interaction involving the naphthyl and pyridinium components of the catalyst and naphthyl ring B of the substrate. While this interaction is present in both the major and minor TS (see Scheme VII-1), the location of the OR′ substituent on ring B differs between these two transition states. This suggests that the observed substituent effects could arise from substituent-induced modulation of this π-π^+ stacking interaction.[39, 470-471] Second, while Sibi *et al*. proposed that the isobutyrate acts solely as a base, we find that it not only abstracts the alcohol proton to facilitate the acylation step but is simultaneously engaged in a cyclic hydrogen-bonding interaction. In these transition states, the proton of the reacting alcohol has been completely transferred to the isobutyrate counterion. The resulting acid plays a crucial role in the TS by engaging in two distinct hydrogen bonding interactions (one ionic and one C-H$\cdots$O interaction, forming a nine-membered cyclic H-bonding network) with the substrate and the core of

the catalyst along with other, weaker non-covalent interactions. In many ways, this arrangement is reminiscent of carboxylate assisted C-H activation in transition metal catalysis.[472] Third, while Sibi proposed that the OR′ group potentially coordinates with the *N*-acyl group, we find no such interaction. The net result is a highly-constrained TS geometry in which there are myriad intra- and intermolecular non-covalent contacts (SI for detailed discussion). Thus, even though the unactivated catalyst is highly fluxional, in the stereocontrolling TS the entire system becomes rigid.

Table VII-1**.** Experimental and theoretical selectivity favors (S) and relative free energy barriers computed at the M06-2X/6-311+G(d,p)//B97-D/TZV(2d,2p) level of theory (223 K) for the KR of substrates (±)**1-6** catalyzed by **A**.[a]

Axial biaryl	Exp. S	Exp. $\Delta\Delta G^{\ddagger}$	Theor. S	Theor. $\Delta\Delta G^{\ddagger}$
(±)-**1**	10	1.0	10	1.0
(±)-**2**	18	1.3	14	1.2
(±)-**3**	23	1.4	18	1.3
(±)-**4**	25	1.4	26	1.4
(±)-**5**	36	1.6	34	1.6
(±)-**6**	51	1.8	>100	3.1

[a](*S*)-isomer favoured.

Having established the key reactive conformer for the stereoselectivity determining step, we next consider the stereoselectivities for six substrates using catalyst **A** (see Table VII-1). These six substrates show marked changes in selectivities stemming from minor changes in substituent. We used isobutyrate as the acylating group, but still used acetate as the counteranion. TS structures were computed using several DFT methods for substrate **1** (S = 10) to explore which method provides the best agreement with experiment. Ultimately, we found that M06-2X/6-311+G(d,p)//CPCM-B97-D/TZV(2d,2p) performs best and was applied to the five other substrates. We observe

excellent agreement between the computed and experimental selectivities for all but one substrate (**6**); in this last case, although we overestimate the selectivity we still capture the overall trend (see Table VII-1). The stereocontrolling TS structures for the KR of (±)-**6** are depicted in Figure VII-2e.

Previous work by Houk, Birman and co-workers[143, 449, 452] have established cation-π interactions as the drivers of selectivity in similar acylative KRs. To understand the origin of stereoselectivity for the KR of **1**-**6** catalyzed by **A**, and to probe the role of different non-covalent interactions, we analyzed truncated models of the stereochemistry-determining acyl transfer TS structures. In particular, we considered structures in which the π-π^+ interaction involving the B ring of the substrate was eliminated and in which the acetate counterion was removed (see Table 2). First, we note that the energy difference between the stereocontrolling TS structures follows the same trend as the free energy difference. The computed energy differences with the π-π^+ interaction removed show that while this interaction plays a significant role in the selectivity for most of the substrates (**2**, **3**, **4**, and **6**) it plays no role in others (**1** and **5**). At the same time, non-covalent interactions with the acetate counterion, which include H···O interactions with the alcohol and the CH···O interactions with the catalyst as well as more subtle dispersion-driven interactions with the B naphthyl group of the substrate, enhance the stereoselectivity for some of the substrates (**1** and **5**, and to some extent **6**) but not others (**2** and **4**). For **3**, the non-covalent interactions with the acetate hinder the selectivity, reducing the energy difference between the major and minor TS from 2.7 to 1.1 kcal/mol. Overall, these data indicate that the selectivity of the KR of **1**-**6** catalyzed

by **A** depends on both π-π^+ interactions between the substrate and catalyst and the various non-covalent interactions involving the counteranion. For instance, for **1**, non-covalent interactions with the acetate favor the major stereoisomer while the π–π^+ interactions favor the minor stereoisomer, leading to the overall low selectivity favor of 10. This can be contrasted with **6**, for which both the π–π^+ interactions and interactions with the acetate favor the major isomer, leading to the high selectivity favor of 51.

The changes in the π–π^+ interactions in these stereocontrolling TS structures do not appear to arise from effects of the substituents on the stacking interactions themselves. Instead, the substituents engage in other non-covalent interactions with the catalyst. For instance, in TS_{major} for **6** (see Figure VII-2e) there is a stabilizing CH···O interaction between the methoxy group and the carbonyl oxygen of the catalyst. Similar interactions are present in TS_{major} for the other substrates. In the minor TS, on the other hand, the oxygen of this methoxy group is positioned over acetatic acid, which presumably destabilizes TS_{minor}.

Table VII-2**.** Computed energy difference between the minor and major stereocontrolling TS structures ($\Delta\Delta E^{\ddagger}$), in structures with the B ring of the substrate removed ($\Delta\Delta E^{\ddagger}$ without stacking), and in structures with the acetate counterion removed ($\Delta\Delta E^{\ddagger}$ without acetate).

Axial biaryl	$\Delta\Delta E^{\ddagger}$	$\Delta\Delta E^{\ddagger}$ without stacking	$\Delta\Delta E^{\ddagger}$ without acetate
(±)-**1**	0.2	0.4	-0.7
(±)-**2**	0.4	-0.7	0.5
(±)-**3**	1.1	-0.1	2.7
(±)-**4**	1.8	0.4	1.9
(±)-**5**	2.5	2.4	1.6
(±)-**6**	3.1	1.5	2.7

This new view of the role of substituents in this reaction can be used to understand the selectivities of other substrates. For example, Sibi *et al*.[448] noted that the selectivity is lower for substrates with a BOC substituent. This can be explained by the disruption of the CH···O interaction between the α-hydrogen of the substituent and the carbonyl group of the catalyst, which helps stabilize the major TS structures for the other substrates. Similarly, the computed TS structures suggest that b-substituents will also disrupt this CH…O interaction, which would lead to reduced selectivity for β-substituted biaryls. Indeed, the computed selectivity for a hypothetical substrate featuring a β-methyl group (**S1**, predicted S = 13) is reduced compared to the analogous structure without a β-substituent (**5**, for which the predicted S is 34).

7.4. Conclusions

In conclusion, we have presented the first theoretical study of the KR of axially chiral biaryls catalyzed by fluxionally chiral DMAP. Overall, the data reveal a rich interplay of non-covalent interactions that underlie nearly all aspects of this reaction. First, even though the catalyst itself is highly fluxional, exhibiting two interconverting conformations at room temperature, the active, acylated form of the catalyst is conformationally rigid due to electrostatically-driven π–π^+ interactions. This rigidity, combined with a network of other non-covalent interactions, underlie the high degrees of stereoselectivity. Our data also support a nucleophilic mode of catalysis, which is rendered more favourable than alternative, base-catalyzed mechanisms due to the impacts of non-covalent interactions. Finally, we showed near quantitative reproduction of experimental selectivities for six substrates and developed a stereochemical model of

this reaction in which π–π^+ interactions, a hydrogen-bonding network involving the counteranion, and a key CH…O interaction between the a-hydrogens of substituents independently control the stereoselectivity. These latter interactions can be used to explain the selectivity of other substrates, including those that have not yet been tested experimentally. Overall, the competition of many non-covalent interactions operative in this reaction underscore the resemblance of many small organocatalysts to enzymes in which selectivity and reactivity are modulated through the subtle effects of myriad stabilizing non-covalent interactions.[438]

CHAPTER VIII

CONCLUSIONS

The case studies in this dissertation underscore the importance of non-covalent interactions in stereoselectivity of asymmetric organocatalytic reactions. These studies serve as a testament to the failure of the popular view of stereoselectivity, which places an undue emphasis on steric factors. An overriding message of this dissertation is that non-covalent interactions can be harnessed more often in asymmetric catalysis. Given the widespread availability of new computational tools that can reliably capture dispersion-driven non-covalent interactions, which have been extensively reviewed in Chapters II, III and IV, the time is long overdue that the origins of selectivity be subjected to more rigorous analyses.

By combining key insights provided by computational chemistry with experimental investigations, tremendous advances can be made in the design of more effective catalysts. With a desire to help make that bridge, in the first few chapters we have provided a synopsis of the many computational and conceptual tools at the disposal of the computational organic chemist to encourage such collaborative interactions. Throughout, the emphasis is on moving from the numbers provided by computations to the insights valued by chemists working on the development of new catalytic reactions. These Chapters should not only foster cooperation between computational and experimental chemists, but will also help advanced undergraduates and those just entering the field, as well researchers seeking an introduction to the latest computational techniques that can add value to their own research.

In Chapter V, we examined three *N*-heterocyclic carbene (NHC) catalyzed kinetic resolutions (KR) and one dynamic kinetic resolution (DKR) using modern density functional theory methods to identify the origin of catalytic activity and selectivity and the role of co-catalysts in these reactions. The results reveal electrostatic interactions as the common driver of selectivity. Furthermore, in the case of a recently described KR of BINOL-derivatives, a computational examination of the full catalytic cycle reveals that a benzoic acid by-product changes the turnover limiting transition state, obviating the need for an added co-catalyst. Together, these data provide key insights into the activity and selectivity of NHC-catalyzed kinetic resolutions, underscoring the importance of electrostatic interactions as a driver of selectivity

Next, we employed DFT methods to elucidate the activation mode and origin of stereoselectivity in chiral phosphoric acid-catalyzed intramolecular oxetane desymmetrizations. Computed enantioselectivities are in excellent agreement with experiment. An unexpected, distortion-driven activation mode was observed, instead of the usual "bifunctional activation." This mode is only favored for some intramolecular oxetane openings, highlighting an exception to known models. Stereoselectivity in these reactions can be explained by the balance of favorable non-covalent interactions of the substrates with both the aryl substituents and phosphoric acid functionality of the catalysts.

Finally, we studied the first KR of axially chiral biaryls reported by Sibi and co-workers using a fluxional chiral DMAP catalysis. Computational analyses reveal that the intrinsic fluxionality of the catalyst is lost after acylation due to electrostatically-driven

π–π^+ interactions, while the mode of catalysis is governed by competing non-covalent interactions. We propose a revised transition state model in which both the conformation and stereoselectivity are governed by non-covalent interactions.

Overall, this work emphasizes the importance of electrostatically governed non-covalent interactions in asymmetric catalysis. These studies have filled some of the gaps in our understanding of the means by which these interactions can be modulated, allowing us to more fully harness their power in organic reactions. These insights will contribute to ongoing efforts to exploit electrostatic based effects in the design of new catalysts, including via *in silico* catalyst design.

Another intriguing aspect of these reactions that was revealed in this work is the parallel between enzymes and small molecular catalysis: in both cases reactivity has been shown to be modulated by subtle interactions with minute precisions. It is well documented that Nature exploits electrostatic based TS organization and stabilizations in enzyme catalysis like serine proteases (oxyanion holes) and acetyl choline esterase. Much to our delight, we showed that a number of small-molecule organocatalysts also demonstrate an uncanny ability to control mechanism and selectivity through the subtle interplay of non-covalent interactions.

Although the computational studies described in this dissertation were inspired by previous experiments, our hope is that the detailed molecular insights that emerged from them will guide future experiments. We believe that increasing the synergy between theory and experiments will usher a new era in asymmetric catalysis in years ahead.

REFERENCES

1. LaPlante, S. R.; Fader, L. D.; Fandrick, K. R.; Fandrick, D. R.; Hucke, O.; Kemper, R.; Miller, S. P. F.; Edwards, P. J., Assessing Atropisomer Axial Chirality in Drug Discovery and Development. *Journal of Medicinal Chemistry* **2011,** *54* (20), 7005-7022.

2. Robinson, D. E. J. E.; Bull, S. D., Kinetic resolution strategies using non-enzymatic catalysts. *Tetrahedron: Asymmetry* **2003,** *14* (11), 1407-1446.

3. John M., K.; Jay F., L.; Eric N., J., Practical Considerations in Kinetic Resolution Reactions. *Advanced Synthesis & Catalysis* **2001,** *343* (1), 5-26.

4. Pellissier, H., Recent developments in dynamic kinetic resolution. *Tetrahedron* **2008,** *64* (8), 1563-1601.

5. Zeng, X.-P.; Cao, Z.-Y.; Wang, Y.-H.; Zhou, F.; Zhou, J., Catalytic Enantioselective Desymmetrization Reactions to All-Carbon Quaternary Stereocenters. *Chemical Reviews* **2016,** *116* (12), 7330-7396.

6. List, B., Introduction: Organocatalysis. *Chem. Rev.* **2007,** *107* (12), 5413-5415.

7. MacMillan, D. W. C., The advent and development of organocatalysis. *Nature* **2008,** *455* (7211), 304-308.

8. Seayad, J.; List, B., Asymmetric organocatalysis. *Org. Biomol. Chem.* **2005,** *3* (5), 719-724.

9. Flanigan, D. M.; Romanov-Michailidis, F.; White, N. A.; Rovis, T., Organocatalytic Reactions Enabled by N-Heterocyclic Carbenes. *Chemical Reviews* **2015,** *115* (17), 9307-9387.

10. Wurz, R. P., Chiral Dialkylaminopyridine Catalysts in Asymmetric Synthesis. *Chemical Reviews* **2007,** *107* (12), 5570-5595.

11. Parmar, D.; Sugiono, E.; Raja, S.; Rueping, M., Complete Field Guide to Asymmetric BINOL-Phosphate Derived Brønsted Acid and Metal Catalysis: History and Classification by Mode of Activation; Brønsted Acidity, Hydrogen Bonding, Ion Pairing, and Metal Phosphates. *Chemical Reviews* **2014,** *114* (18), 9047-9153.

12. Gu, Y.; Kar, T.; Scheiner, S., Fundamental Properties of the CH···O Interaction: Is It a True Hydrogen Bond? *J. Am. Chem. Soc.* **1999,** *121* (40), 9411-9422.

13. Knowles, R. R.; Jacobsen, E. N., Attractive Noncovalent Interactions in Asymmetric Catalysis: Links between Enzymes and Small Molecule Catalysts. *Proc. Natl. Acad. Sci. USA* **2010,** *107*, 20678-20685.

14. Wheeler, S. E.; Seguin, T. J.; Guan, Y.; Doney, A. C., Noncovalent Interactions in Organocatalysis and the Prospect of Computational Catalyst Design. *Accounts of Chemical Research* **2016,** *49* (5), 1061-1069.

15. Calais, J.-L., Density-functional theory of atoms and molecules. R.G. Parr and W. Yang, Oxford University Press, New York, Oxford, 1989. IX + 333 pp. Price £45.00. *Int. J. Quantum Chem.* **1993,** *47* (1), 101-101.

16. Tsuzuki, S.; Lüthi, H. P., Interaction energies of van der Waals and hydrogen bonded systems calculated using density functional theory: Assessing the PW91 model. *J. Chem. Phys.* **2001,** *114* (9), 3949-3957.

17. Cerny, J.; Hobza, P., The X3LYP extended density functional accurately describes H-bonding but fails completely for stacking. *Phys Chem Chem Phys* **2005,** *7* (8), 1624-1626.

18. Johnson, E. R.; Wolkow, R. A.; DiLabio, G. A., Application of 25 density functionals to dispersion-bound homomolecular dimers. *Chemical Physics Letters* **2004,** *394* (4–6), 334-338.

19. Grimme, S., Semiempirical GGA-Type Density Functional Constructed with a Long-Range Dispersion Correction. *J. Comp. Chem.* **2006,** *27*, 1787-1799.

20. Goerigk, L.; Grimme, S., A thorough benchmark of density functional methods for general main group thermochemistry, kinetics, and noncovalent interactions. *Phys Chem Chem Phys* **2011,** *13* (14), 6670-6688.

21. Grimme, S.; Antony, J.; Ehrlich, S.; Krieg, H., A Consistent and Accurate *ab Initio* Parametrization of Density Functional Dispersion Correction (DFT-D) for the 94 Elements H-Pu. *J. Chem. Phys.* **2010,** *132*, 154104.

22. Goerigk, L.; Kruse, H.; Grimme, S., Benchmarking Density Functional Methods against the S66 and S66x8 Datasets for Non-Covalent Interactions. *ChemPhysChem* **2011,** *12* (17), 3421-3433.

23. Zhao, Y.; Truhlar, D. G., The M06 suite of density functionals for main group thermochemistry, thermochemical kinetics, noncovalent interactions, excited states, and

transition elements: two new functionals and systematic testing of four M06-class functionals and 12 other functionals. *Theor. Chem. Acc.* **2008,** *120* (1), 215-241.

24. Peverati, R.; Truhlar, D. G., Improving the Accuracy of Hybrid Meta-GGA Density Functionals by Range Separation. *J. Phys. Chem. Lett.* **2011,** *2* (21), 2810-2817.

25. Grimme, S., Density functional theory with London dispersion corrections. *WIREs Comput Mol. Sci.* **2011,** *1* (2), 211-228.

26. Curtin, D. Y., *Rec. Chem. Prog.* **1954,** *15*, 111−128.

27. Eyring, H., The Activated Complex in Chemical Reactions. *J. Chem. Phys.* **1935,** *3* (2), 107-115.

28. Schrödinger Release 2016-3: MacroModel, v., Schrödinger, LLC, New York, NY, 2016.

29. Contreras-García, J.; Johnson, E. R.; Keinan, S.; Chaudret, R.; Piquemal, J.-P.; Beratan, D. N.; Yang, W., NCIPLOT: A Program for Plotting Noncovalent Interaction Regions. *Journal of Chemical Theory and Computation* **2011,** *7* (3), 625-632.

30. Bader, R. F. W., Atoms in molecules. *Acc. Chem. Res.* **1985,** *18* (1), 9-15.

31. Ess, D. H.; Houk, K. N., Distortion/Interaction Energy Control of 1,3-Dipolar Cycloaddition Reactivity. *Journal of the American Chemical Society* **2007,** *129* (35), 10646-10647.

32. Bickelhaupt, F. M.; van Zeist, W. J., The activation strain model of chemical reactivity. *Org. Biomol. Chem.* **2010,** *8* (14), 3118-3127.

33. Jones, G. B., π Shielding in organic synthesis. *Tetrahedron* **2001,** *57* (38), 7999-8016.

34. Lu, T.; Wheeler, S. E., Harnessing weak interactions for enantioselective catalysis. *Science* **2015,** *347*, 719-720.

35. Copeland, G. T.; Miller, S. J., Selection of Enantioselective Acyl Transfer Catalysts from a Pooled Peptide Library through a Fluorescence-Based Activity Assay: An Approach to Kinetic Resolution of Secondary Alcohols of Broad Structural Scope. *J. Am. Chem. Soc.* **2001,** *123*, 6495-6502.

36. Krenske, E. H.; Houk, K. N., Aromatic Interactions as Control Elements in Stereoselective Organic Reactions. *Acc. Chem. Res.* **2013,** *46*, 979-989.

37. Wagner, J. P.; Schreiner, P. R., London Dispersion in Molecular Chemistry—Reconsidering Steric Effects. *Angew. Chem. Int. Ed.* **2015,** *54* (42), 12274-12296.

38. Zhao, Y.; Cotelle, Y.; Sakai, N.; Matile, S., Unorthodox Interactions at Work. *J. Am. Chem. Soc.* **2016,** *138*, 4270-4277.

39. Wheeler, S. E.; Bloom, J. W. G., Toward a More Complete Understanding of Noncovalent Interactions Involving Aromatic Rings. *The Journal of Physical Chemistry A* **2014,** *118* (32), 6133-6147.

40. Wheeler, S. E.; Bloom, J. W. G., Toward a More Complete Understanding of Noncovalent Interactions Involving Aromatic Rings. *J. Phys. Chem. A* **2014,** *118* (32), 6133-6147.

41. Salonen, L. M.; Ellermann, M.; Diederich, F., Aromatic Rings in Chemical and Biological Recognition: Energetics and Structures. *Angew. Chem. Int. Ed.* **2011,** *50*, 4808-4842.

42. Meyer, E. A.; Castellano, R. K.; Diederich, F., Interactions with Aromatic Rings in Chemical and Biological Recognition. *Angew. Chem. Int. Ed.* **2003,** *42*, 1210-1250.

43. Martinez, C. R.; Iverson, B. L., Rethinking the Term "π-Stacking". *Chem. Sci.* **2012,** *3*, 2191-2201.

44. Raju, R. K.; Bloom, J. W. G.; An, Y.; Wheeler, S. E., Substituent Effects in Non-Covalent Interactions with Aromatic Rings: Insights from Computational Chemistry. *ChemPhysChem* **2011,** *12*, 3116-3130.

45. Wheeler, S. E., Understanding Substituent Effects in Non-Covalent Interactions Involving Aromatic Rings. *Acc. Chem. Res.* **2013,** *46*, 1029-1038.

46. Hunter, C. A.; Sanders, J. K. M., The Nature of π-π Interactions. *J. Am. Chem. Soc.* **1990,** *112*, 5525-5534.

47. Hunter, C. A.; Lawson, K. R.; Perkins, J.; Urch, C. J., Aromatic Interactions. *J. Chem. Soc., Perkin Trans. 2* **2001**, 651-669.

48. Carver, F. J.; Hunter, C. A.; Livingstone, D. J.; McCabe, J. F.; Seward, E. M., Substituent Effects on Edge-to-Face Aromatic Interactions. *Chem. Eur. J.* **2002,** *8*, 2848-2859.

49. Cockroft, S. L.; Hunter, C. A.; Lawson, K. R.; Perkins, J.; Urch, C., J., Electrostatic Control of Aromatic Stacking Interactions. *J. Am. Chem. Soc.* **2005,** *127*, 8594-8595.

50. Cockroft, S. L.; Perkins, J.; Zonta, C.; Adams, H.; Spey, S. E.; Low, C. M. R.; Vinter, J. G.; Lawson, K. R.; Urch, C. J.; Hunter, C. A., Substituent Effects on Aromatic Stacking Interactions. *Org. Biomol. Chem.* **2007,** *5*, 1062-1080.

51. Cockroft, S. L.; Hunter, C. A., Desolvation and Substituent Effects in Edge-to-Face Aromatic Interactions. *Chem. Commun.* **2009**, 3961-3963.

52. Sinnokrot, M. O.; Sherrill, C. D., Unexpected Substituent Effects in Face-to-Face π-Stacking Interactions. *J. Phys. Chem. A* **2003,** *107*, 8377-8379.

53. Sinnokrot, M. O.; Sherrill, C. D., Substituent Effects in π-π Interactions: Sandwich and T-Shaped Configurations. *J. Am. Chem. Soc.* **2004,** *126*, 7690-7697.

54. Ringer, A. L.; Sinnokrot, M. O.; Lively, R. P.; Sherrill, C. D., The Effect of Multiple Substituents on Sandwich and T-Shaped π-π Interactions. *Chem. Eur. J.* **2006,** *12*, 3821-3828.

55. Ringer, A. L.; Sherrill, C. D., Substituent Effects in Sandwich Configurations of Multiply Substituted Benzene Dimers Are Not Solely Governed By Electrostatic Control. *J. Am. Chem. Soc.* **2009,** *131*, 4574-4575.

56. Bloom, J. W. G.; Wheeler, S. E., Taking Aromaticity out of Aromatic Interactions. *Angew. Chem. Int. Ed.* **2011,** *50*, 7847-7849.

57. Wheeler, S. E., Local Nature of Substituent Effects in Stacking Interactions. *J. Am. Chem. Soc.* **2011,** *133*, 10262-10274.

58. Raju, R. K.; Bloom, J. W. G.; Wheeler, S. E., Broad Transferability of Substituent Effects in π-Stacking Interactions Provides New Insights into Their Origin. *J. Chem. Theory Comput.* **2013,** *9*, 3479-3490.

59. Watt, M.; Hardebeck, L. K. E.; Kirkpatrick, C. C.; Lewis, M., Face-to-Face Arene-Arene Bidning Energies: Dominated by Dispersion but Predicted by Electrostatic

and Dispersion/Polarizability Substituent Constants. *J. Am. Chem. Soc.* **2011,** *133*, 3854-3862.

60. Parrish, R. M.; Sherrill, C. D., Quantum-Mechanical Evaluation of π–π versus Substituent−π Interactions in π Stacking: Direct Evidence for the Wheeler–Houk Picture. *J. Am. Chem. Soc.* **2014,** *136* (50), 17386-17389.

61. Grimme, S., Do Special Noncovalent π-π Stacking Interactions Really Exist? *Angew. Chem. Int. Ed.* **2008,** *47*, 3430-3434.

62. Sinnokrot, M. O.; Sherrill, C. D., High-Accuracy Quantum Mechanical Studies of π-π Interactions in Benzene Dimers. *J. Phys. Chem. A* **2006,** *110*, 10656-10668.

63. Cozzi, F.; Cinquini, M.; Annunziata, R.; Dwyer, T.; Siegel, J. S., Polar/π Interactions between Stacked Aryls in 1,8-Diarylnaphthalenes. *J. Am. Chem. Soc.* **1992,** *114*, 5729-5733.

64. Cozzi, F.; Cinquini, M.; Annunziata, R.; Siegel, J. S., Dominance of Polar/π over Charge-Transfer Effects in Stacked Phenyl Interactions. *J. Am. Chem. Soc.* **1993,** *115*, 5330-5331.

65. Cozzi, F.; Ponzini, F.; Annunziata, R.; Cinquini, M.; Siegel, J. S., Polar Interactions between Stacked π Systems in Fluorinated 1,8-Diarylnaphthalenes: Importance of Quadrupole Moments in Molecular Recognition. *Angew. Chem. Int. Ed.* **1995,** *34*, 1019-1020.

66. Cozzi, F.; Siegel, J. S., Interaction between Stacked Aryl Groups in 1,8-Diarylnaphthalenes: Dominance of Polar/π over Charge-Transfer Effects. *Pure Appl. Chem.* **1995,** *67*, 683-689.

67. Cozzi, F.; Annunziata, R.; Benaglia, M.; Cinquini, M.; Raimondi, L.; Baldridge, K. K.; Siegel, J. S., Through-Space Interactions between Face-to-Face, Center-to-Edge Oriented Arenes: Importance of Polar–π Effects *Org. Biomol. Chem.* **2003,** *1*, 157-162.

68. Wheeler, S. E.; Houk, K. N., Substituent Effects in the Benzene Dimer are Due to Direct Interactions of the Substituents with the Unsubstituted Benzene. *J. Am. Chem. Soc.* **2008,** *130*, 10854-10855.

69. Kodama, Y.; Nishihata, K.; Nishio, M.; Nakagawa, N., Attractive interaction between aliphatic and aromatic systems. *Tet. Lett.* **1977,** *18* (24), 2105-2108.

70. Tsuzuki, S.; Fujii, A., Nature and physical origin of CH/π interaction: significant difference from conventional hydrogen bonds. *Phys. Chem. Chem. Phys.* **2008,** *10*, 2584-2594.

71. Tsuzuki, S.; Uchimaru, T.; Mikami, M., Magnitude and Nature of Carbohydrate–Aromatic Interactions in Fucose–Phenol and Fucose–Indole Complexes: CCSD(T) Level Interaction Energy Calculations. *J. Phys. Chem. A* **2011,** *115* (41), 11256-11262.

72. Shibasaki, K.; Fujii, A.; Mikami, N.; Tsuzuki, S., Magnitude of the CH/π interaction in the gas phase: Experimental and theoretical determination of the accurate interaction energy in benzene-methane. *J. Phys. Chem. A* **2006,** *110* (13), 4397-4404.

73. Tsuzuki, S.; Honda, K.; Uchimaru, T.; Mikami, M.; Tanabe, K., The magnitude of the CH/π interaction between benzene and some model hydrocarbons. *J. Am. Chem. Soc.* **2000,** *122* (15), 3746-3753.

74. Bloom, J. W. G.; Raju, R. K.; Wheeler, S. E., Physical Nature of Substituent Effects in XH/π Interactions. *J. Chem. Theory and Comput.* **2012,** *8*, 3167-3174.

75. Dougherty, D. A., Cation-π Interactions in Chemistry and Biology: A New View of Benzene, Phe, Tyr, and Trp. *Science* **1996,** *271*, 163-168.

76. Mecozzi, S.; West, A. P., Jr.; Dougherty, D. A., Cation-π Interactions in Simple Aromatics: Electrostatics Provide a Predictive Tool. *J. Am. Chem. Soc.* **1996,** *118*, 2307-2308.

77. Ma, J. C.; Dougherty, D. A., The Cation-π Interaction. *Chem. Rev.* **1997,** *97*, 1303-1324.

78. Gallivan, J. P.; Dougherty, D. A., Cation-π Interactions in Structural Biology. *Proc. Natl. Acad. Sci. USA* **1999,** *96*, 9459-9464.

79. Dougherty, D. A., The Cation−π Interaction. *Acc. Chem. Res.* **2013,** *46*, 885-893.

80. Giese, M.; Albrecht, M.; Rissanen, K., Experimental investigation of anion-[small pi] interactions - applications and biochemical relevance. *Chemical Communications* **2016,** *52* (9), 1778-1795.

81. Rutledge, L. R.; Churchill, C. D. M.; Wetmore, S. D., A Preliminary Investigation of the Additivity of π-π or π^{+}-π Stacking and T-Shaped Interactions between Natural or Damaged DNA Nucleobases and Histidine *J. Phys. Chem. B* **2010,** *114*, 3355-3367.

82. Tsuzuki, S.; Mikama, M.; Yamada, S., Origin of Attraction, Magnitude, and Directionality of Interactions in Benzene Complexes with Pyridinium Cations. *J. Am. Chem. Soc.* **2007,** *129*, 8656-8662.

83. Grimme, S., Accurate Description of van der Waals Complexes by Density Functional Theory Including Empirical Corrections. *J. Comp. Chem.* **2004,** *25*, 1463-1473.

84. Grimme, S., Density Functional Theory with London Dispersion Corrections. *WIREs Comp. Mol. Sci.* **2011,** *1*, 211-228.

85. Zhao, Y.; Schultz, N. E.; Truhlar, D. G., Design of Density Functionals by Combining the Method of Constraint Satisfaction with Parametrization for Thermochemistry, Thermochemical Kinetics, and Noncovalent Interactions. *J. Chem. Theory and Comput.* **2006,** *2*, 364-382.

86. Zhao, Y.; Truhlar, D. G., A new local density functional for main-group thermochemistry, transition metal bonding, thermochemical kinetics, and noncovalent interactions. *J. Chem. Phys.* **2006,** *125*, 194101.

87. Zhao, Y.; Truhlar, D. G., The M06 Suite of Density Functionals for Main Group Thermochemistry, Thermochemical Kinetics, Noncovalent interactions, Excited States, and Transition Elements: Two New Functionals and Systematic Testing of Four M06 Functionals and Twelve Other Functionals. *Theo. Chem. Acc.* **2008,** *120*, 215-241.

88. McNeil, A. J.; Müller, P.; Whitten, J. E.; Swager, T. M., Conjugated Polymers in an Arene Sandwich. *J. Am. Chem. Soc.* **2006,** *128*, 12426-12427.

89. Wheeler, S. E.; McNeil, A. J.; Müller, P.; Swager, T. M.; Houk, K. N., Probing Substituent Effects in Aryl−Aryl Interactions Using Stereoselective Diels−Alder Cycloadditions. *Journal of the American Chemical Society* **2010,** *132* (10), 3304-3311.

90. El-azizi, Y.; Schmitzer, A.; Collins, S. K., Exploitation of Perfluorophenyl–Phenyl Interactions for Achieving Difficult Macrocyclizations by Using Ring-Closing Metathesis. *Angewandte Chemie* **2006,** *118* (6), 982-987.

91. Collins, S. K.; El-Azizi, Y.; Schmitzer, A. R., Development of Perfluoroarene−Arene Interactions for Macrocyclic En-yne Metathesis and the Total Synthesis of Macrocyclic Natural Products. *J. Org. Chem.* **2007,** *72* (17), 6397-6408.

92. El-Azizi, Y.; Zakarian, J. E.; Bouillerand, L.; Schmitzer, A. R.; Collins, S. K., Exploiting Non-Covalent Interactions in Synthesis: Macrocyclization Employing Amide-Based Auxiliaries. *Advanced Synthesis & Catalysis* **2008,** *350* (14-15), 2219-2225.

93. Bolduc, P.; Jacques, A.; Collins, S. K., Efficient Macrocyclization Achieved via Conformational Control Using Intermolecular Noncovalent π-Cation/Arene Interactions. *Journal of the American Chemical Society* **2010,** *132* (37), 12790-12791.

94. Yamakawa, M.; Yamada, I.; Noyori, R., CH/π Attraction: The Origin of Enantioselectivity in Transfer Hydrogenation of Aromatic Carbonyl Compounds Catalyzed by Chiral η6-Arene-Ruthenium(II) Complexes. *Angew. Chem. Int. Ed.* **2001,** *40* (15), 2818-2821.

95. Noyori, R.; Yamakawa, M.; Hashiguchi, S., Metal−Ligand Bifunctional Catalysis: A Nonclassical Mechanism for Asymmetric Hydrogen Transfer between Alcohols and Carbonyl Compounds. *J. Org. Chem.* **2001,** *66* (24), 7931-7944.

96. Yamakawa, M.; Ito, H.; Noyori, R., The Metal−Ligand Bifunctional Catalysis: A Theoretical Study on the Ruthenium(II)-Catalyzed Hydrogen Transfer between Alcohols

and Carbonyl Compounds. *Journal of the American Chemical Society* **2000,** *122* (7), 1466-1478.

97. Matsuoka, A.; Sandoval, C. A.; Uchiyama, M.; Noyori, R.; Naka, H., Why p-Cymene? Conformational Effect in Asymmetric Hydrogenation of Aromatic Ketones with a η6-Arene/Ruthenium(II) Catalyst. *Chem. Asian J.* **2015,** *10* (1), 112-115.

98. Santoni, G.; Mba, M.; Bonchio, M.; Nugent, W. A.; Zonta, C.; Licini, G., Stereoselective Control by Face-to-Face Versus Edge-to-Face Aromatic Interactions: The Case of C3-TiIV Amino Trialkolate Sulfoxidation Catalysts. *Chemistry – A European Journal* **2010,** *16* (2), 645-654.

99. Santoni, G.; Mba, M.; Bonchio, M.; Nugent, W. A.; Zonta, C.; Licini, G., Stereoselective Control by Face-to-Face Versus Edge-to-Face Aromatic Interactions: The Case of C3-TiIV Amino Trialkolate Sulfoxidation Catalysts. *Chem. Eur. J.* **2010,** *16* (2), 645-654.

100. Bahmanyar, S.; Houk, K. N.; Martin, H. J.; List, B., Quantum Mechanical Predictions of the Stereoselectivities of Proline-Catalyzed Asymmetric Intermolecular Aldol Reactions. *Journal of the American Chemical Society* **2003,** *125* (9), 2475-2479.

101. Armstrong, A.; Boto, R. A.; Dingwall, P.; Contreras-Garcia, J.; Harvey, M. J.; Mason, N. J.; Rzepa, H. S., The Houk-List transition states for organocatalytic mechanisms revisited. *Chemical Science* **2014,** *5* (5), 2057-2071.

102. Bakr, B. W.; Sherrill, C. D., Analysis of transition state stabilization by non-covalent interactions in the Houk–List model of organocatalyzed intermolecular Aldol

additions using functional-group symmetry-adapted perturbation theory. *Phys. Chem. Chem. Phys.* **2016,** *18* 10297-10308.

103. Zhao, Q.; Lam, Y.-h.; Kheirabadi, M.; Xu, C.; Houk, K. N.; Schafmeister, C. E., Hydrophobic Substituent Effects on Proline Catalysis of Aldol Reactions in Water. *The Journal of Organic Chemistry* **2012,** *77* (10), 4784-4792.

104. Allemann, C.; Gordillo, R.; Clemente, F. R.; Cheong, P. H.-Y.; Houk, K. N., Theory of Asymmetric Organocatalysis of Aldol and Related Reactions: Rationalizations and Predictions. *Accounts of Chemical Research* **2004,** *37* (8), 558-569.

105. Gordillo, R.; Houk, K. N., Origins of Stereoselectivity in Diels−Alder Cycloadditions Catalyzed by Chiral Imidazolidinones. *Journal of the American Chemical Society* **2006,** *128* (11), 3543-3553.

106. Brazier, J. B.; Evans, G.; Gibbs, T. J. K.; Coles, S. J.; Hursthouse, M. B.; Platts, J. A.; Tomkinson, N. C. O., Solution Phase, Solid State, and Theoretical Investigations on the MacMillan Imidazolidinone. *Organic Letters* **2009,** *11* (1), 133-136.

107. Gonzalez-James, O. M.; Kwan, E. E.; Singleton, D. A., Entropic Intermediates and Hidden Rate-Limiting Steps in Seemingly Concerted Cycloadditions. Observation, Prediction, and Origin of an Isotope Effect on Recrossing. *Journal of the American Chemical Society* **2012,** *134* (4), 1914-1917.

108. Krenske, E. H., Aromatic interactions in asymmetric catalysis: control of enantioselectivity in Diels-Alder reactions catalysed by camphor-derived hydrazides. *Organic & Biomolecular Chemistry* **2013,** *11* (32), 5226-5232.

109. Lemay, M.; Ogilvie, W. W., Aqueous Enantioselective Organocatalytic Diels−Alder Reactions Employing Hydrazide Catalysts. A New Scaffold for Organic Acceleration. *Organic Letters* **2005,** *7* (19), 4141-4144.

110. Lemay, M.; Ogilvie, W. W., Mechanistic Studies of Hydrazide-Catalyzed Enantioselective Diels−Alder Reactions. *The Journal of Organic Chemistry* **2006,** *71* (12), 4663-4666.

111. Lemay, M.; Aumand, L.; Ogilvie, W. W., Design of a Conformationally Rigid Hydrazide Organic Catalyst. *Advanced Synthesis & Catalysis* **2007,** *349* (3), 441-447.

112. Holland, M. C.; Paul, S.; Schweizer, W. B.; Bergander, K.; Mück-Lichtenfeld, C.; Lakhdar, S.; Mayr, H.; Gilmour, R., Noncovalent Interactions in Organocatalysis: Modulating Conformational Diversity and Reactivity in the MacMillan Catalyst. *Angewandte Chemie International Edition* **2013,** *52* (31), 7967-7971.

113. Kemppainen, E. K.; Sahoo, G.; Piisola, A.; Hamza, A.; Kótai, B.; Pápai, I.; Pihko, P. M., Mukaiyama–Michael Reactions with trans-2,5-Diarylpyrrolidine Catalysts: Enantioselectivity Arises from Attractive Noncovalent Interactions, Not from Steric Hindrance. *Chemistry – A European Journal* **2014,** *20* (20), 5983-5993.

114. Seebach, D.; Grošelj, U.; Schweizer, W. B.; Grimme, S.; Mück-Lichtenfeld, C., Experimental and Theoretical Conformational Analysis of 5-Benzylimidazolidin-4-one Derivatives – a 'Playground' for Studying Dispersion Interactions and a 'Windshield-Wiper' Effect in Organocatalysis. *Helvetica Chimica Acta* **2010,** *93* (1), 1-16.

115. Langdon, S. M.; Legault, C. Y.; Gravel, M., Origin of Chemoselectivity in N-Heterocyclic Carbene Catalyzed Cross-Benzoin Reactions: DFT and Experimental Insights. *The Journal of Organic Chemistry* **2015,** *80* (7), 3597-3610.

116. Allen, S. E.; Mahatthananchai, J.; Bode, J. W.; Kozlowski, M. C., Oxyanion Steering and CH−π Interactions as Key Elements in an N-Heterocyclic Carbene-Catalyzed [4 + 2] Cycloaddition. *Journal of the American Chemical Society* **2012,** *134* (29), 12098-12103.

117. Parmar, D.; Sugiono, E.; Raja, S.; Rueping, M., Complete Field Guide to Asymmetric BINOL-Phosphate Derived Brønsted Acid and Metal Catalysis: History and Classification by Mode of Activation; Brønsted Acidity, Hydrogen Bonding, Ion Pairing, and Metal Phosphates. *Chem. Rev.* **2014,** *114*, 9047-9153.

118. Seguin, T. J.; Lu, T.; Wheeler, S. E., Enantioselectivity in Catalytic Asymmetric Fischer Indolizations Hinges on the Competition of π-Stacking and CH/π Interactions. *Organic Letters* **2015,** *17* (12), 3066-3069.

119. Müller, S.; Webber, M. J.; List, B., The Catalytic Asymmetric Fischer Indolization. *J. Am. Chem. Soc.* **2011,** *133*, 18534-18437.

120. Li, G.-Q.; Gao, H.; Keene, C.; Devonas, M.; Ess, D. H.; Kürti, L., Organocatalytic Aryl–Aryl Bond Formation: An Atroposelective [3,3]-Rearrangement Approach to BINAM Derivatives. *J. Am. Chem. Soc.* **2013,** *135* (20), 7414-7417.

121. Johnston, C. P.; Kothari, A.; Sergeieva, T.; Okovytyy, S. I.; Jackson, K. E.; Paton, R. S.; Smith, M. D., Catalytic enantioselective synthesis of indanes by a cation-directed 5-endo-trig cyclization. *Nat Chem* **2015,** *7* (2), 171-177.

122. Anderson, C. D.; Dudding, T.; Gordillo, R.; Houk, K. N., Origin of Enantioselection in Hetero-Diels−Alder Reactions Catalyzed by Naphthyl-TADDOL. *Organic Letters* **2008,** *10* (13), 2749-2752.

123. Quallich, G. J.; Woodall, T. M., Diphenyloxazaborolidine a new catalyst for enantioselective reduction of ketones. *Tet. Lett.* **1993,** *34*, 4145-4148.

124. Korenaga, T.; Kadowaki, K.; Sakai, T., Effect of conformational control of chiral oxazaborolidine by π–π stacking interaction of a pentafluorophenyl group toward asymmetric borane reduction. *Journal of Fluorine Chemistry* **2007,** *128* (5), 557-561.

125. Jindal, G.; Kisan, H. K.; Sunoj, R. B., Mechanistic Insights on Cooperative Catalysis through Computational Quantum Chemical Methods. *ACS Catalysis* **2015,** *5* (2), 480-503.

126. Tang, W.; Johnston, S.; Iggo, J. A.; Berry, N. G.; Phelan, M.; Lian, L.; Bacsa, J.; Xiao, J., Cooperative Catalysis through Noncovalent Interactions. *Angewandte Chemie International Edition* **2013,** *52* (6), 1668-1672.

127. Xu, H.; Zuend, S. J.; Woll, M. G.; Tao, Y.; Jacobsen, E. N., Asymmetric Cooperative Catalysis of Strong Brønsted Acid–Promoted Reactions Using Chiral Ureas. *Science* **2010,** *327* (5968), 986-990.

128. Zhao, Y.; Domoto, Y.; Orentas, E.; Beuchat, C.; Emery, D.; Mareda, J.; Sakai, N.; Matile, S., Catalysis with Anion–π Interactions. *Angewandte Chemie International Edition* **2013,** *52* (38), 9940-9943.

129. Zhao, Y.; Beuchat, C.; Domoto, Y.; Gajewy, J.; Wilson, A.; Mareda, J.; Sakai, N.; Matile, S., Anion−π Catalysis. *Journal of the American Chemical Society* **2014,** *136* (5), 2101-2111.

130. Zhao, Y.; Sakai, N.; Matile, S., Enolate chemistry with anion–π interactions. *Nat. Commun.* **2014,** *5*.

131. Miros, F. N.; Zhao, Y.; Sargsyan, G.; Pupier, M.; Besnard, C.; Beuchat, C.; Mareda, J.; Sakai, N.; Matile, S., Enolate Stabilization by Anion–π Interactions: Deuterium Exchange in Malonate Dilactones on π-Acidic Surfaces. *Chem. Eur. J.* **2015**, 2648-2657.

132. Lu, T.; Wheeler, S. E., Quantifying the Role of Anion−π Interactions in Anion−π Catalysis. *Organic Letters* **2014,** *16* (12), 3268-3271.

133. Zhao, Y.; Benz, S.; Sakai, N.; Matile, S., Selective acceleration of disfavored enolate addition reactions by anion-[small pi] interactions. *Chem. Sci.* **2015**.

134. Zhao, Y.; Cotelle, Y.; Avestro, A.-J.; Sakai, N.; Matile, S., Asymmetric Anion-π Catalysis: Enamine Addition to Nitroolefins on π-Acidic Surfaces. *Journal of the American Chemical Society* **2015,** *137* (36), 11582-11585.

135. Yamada, S.; Fossey, J. S., Nitrogen cation–π interaction in asymmetric organocatalytic synthesis. *Org. Biomol. Chem.* **2011,** *9*, 7275-7281.

136. Kojima, S.; Hiroike, K.; Ohkata, K., Stereoselective synthesis of activated cyclopropanes with an α-pyridinium acetamide bearing an 8-phenylmenthyl group as the chiral auxiliary. *Tetrahedron Letters* **2004,** *45* (18), 3565-3568.

137. Kojima, S.; Fujitomo, K.; Shinohara, Y.; Shimizu, M.; Ohkata, K., Stereoselective formation of activated cyclopropanes with pyridinium ylides bearing a (−)-8-phenylmenthyl group as the chiral auxiliary. *Tetrahedron Letters* **2000,** *41* (50), 9847-9851.

138. Yamada, S.; Misono, T.; Tsuzuki, S., Cation−π Interactions of a Thiocarbonyl Group and a Carbonyl Group with a Pyridinium Nucleus. *Journal of the American Chemical Society* **2004,** *126* (31), 9862-9872.

139. Yamada, S.; Misono, T.; Iwai, Y., Kinetic resolution of sec-alcohols by a new class of pyridine catalysts having a conformation switch system. *Tetrahedron Letters* **2005,** *46* (13), 2239-2242.

140. Yamada, S.; Misono, T.; Iwai, Y.; Masumizu, A.; Akiyama, Y., New Class of Pyridine Catalyst Having a Conformation Switch System: Asymmetric Acylation of Various sec-Alcohols. *J. Org. Chem.* **2006,** *71* (18), 6872-6880.

141. Yamada, S.; Morita, C., Face-Selective Addition to a Cation−π Complex of a Pyridinium Salt: Synthesis of Chiral 1,4-Dihydropyridines. *Journal of the American Chemical Society* **2002,** *124* (28), 8184-8185.

142. Wei, Y.; Held, I.; Zipse, H., Stacking interactions as the principal design element in acyl-transfer catalysts. *Organic & Biomolecular Chemistry* **2006,** *4* (22), 4223-4230.

143. Li, X.; Liu, P.; Houk, K. N.; Birman, V. B., Origin of Enantioselectivity in CF3−PIP-Catalyzed Kinetic Resolution of Secondary Benzylic Alcohols. *Journal of the American Chemical Society* **2008,** *130* (42), 13836-13837.

144. Yang, X.; Bumbu, V. D.; Liu, P.; Li, X.; Jiang, H.; Uffman, E. W.; Guo, L.; Zhang, W.; Jiang, X.; Houk, K. N.; Birman, V. B., Catalytic, Enantioselective N-Acylation of Lactams and Thiolactams Using Amidine-Based Catalysts. *Journal of the American Chemical Society* **2012,** *134* (42), 17605-17612.

145. Birrell, J. A.; Desrosiers, J.-N.; Jacobsen, E. N., Enantioselective Acylation of Silyl Ketene Acetals through Fluoride Anion-Binding Catalysis. *Journal of the American Chemical Society* **2011,** *133* (35), 13872-13875.

146. Yeung, C. S.; Ziegler, R. E.; Porco, J. A.; Jacobsen, E. N., Thiourea-Catalyzed Enantioselective Addition of Indoles to Pyrones: Alkaloid Cores with Quaternary Carbons. *Journal of the American Chemical Society* **2014,** *136* (39), 13614-13617.

147. Burns, N. Z.; Witten, M. R.; Jacobsen, E. N., Dual Catalysis in Enantioselective Oxidopyrylium-Based [5 + 2] Cycloadditions. *J. Am. Chem. Soc.* **2011,** *133* (37), 14578-14581.

148. Müller-Dethlefs, K.; Hobza, P., Noncovalent Interactions: A Challenge for Experiment and Theory. *Chem. Rev.* **2000,** *100*, 143-168.

149. Salonen, L. M.; Ellermann, M.; Diederich, F., Aromatic Rings in Chemical and Biological Recognition: Energetics and Structures. *Angew. Chem. Int. Ed.* **2011,** *50* (21), 4808-4842.

150. Takahashi, O.; Kohno, Y.; Nishio, M., Relevance of Weak Hydrogen Bonds in the Conformation of Organic Compounds and Bioconjugates: Evidence from Recent Experimental Data and High-Level ab Initio MO Calculations. *Chemical Reviews* **2010,** *110* (10), 6049-6076.

151. Nishio, M., CH/π hydrogen bonds in organic reactions. *Tetrahedron* **2005,** *61* (29), 6923-6950.

152. Johnston, R. C.; Cheong, P. H.-Y., C-HO non-classical hydrogen bonding in the stereomechanics of organic transformations: theory and recognition. *Organic & Biomolecular Chemistry* **2013,** *11* (31), 5057-5064.

153. Singh, S. K.; Das, A., The n [rightward arrow] [small pi]* interaction: a rapidly emerging non-covalent interaction. *Phys. Chem. Chem. Phys.* **2015,** *17* (15), 9596-9612.

154. Kennedy, C. R.; Lin, S.; Jacobsen, E. N., The Cation–π Interaction in Small-Molecule Catalysis. *Angew. Chem. Int. Ed.* **2016,** *DOI: 10.1002/anie.201600547*.

155. Wheeler, S. E., Understanding Substituent Effects in Non-Covalent Interactions Involving Aromatic Rings. *Acc. Chem. Res.* **2013,** *46*, 1029-1038.

156. Wheeler, S. E.; Bloom, J. W. G., Toward a More Complete Understanding of Non-Covalent Interactions Involving Aromatic Rings. *J. Phys. Chem. A* **2014,** *118*, 6133-6147.

157. Sinnokrot, M. O.; Sherrill, C. D., High-Accuracy Quantum Mechanical Studies of π-π Interactions in Benzene Dimers. *J. Phys. Chem. A* **2006,** *110*, 10656-10668.

158. Watt, M.; Hardebeck, L. K. E.; Kirkpatrick, C. C.; Lewis, M., Face-to-Face Arene-Arene Binding Energies: Dominated by Dispersion but Predicted by Electrostatic and Dispersion/Polarizability Substituent Constants. *J. Am. Chem. Soc.* **2011,** *133*, 3854-3862.

159. Sinnokrot, M. O.; Sherrill, C. D., Unexpected Substituent Effects in Face-to-Face π-Stacking Interactions. *J. Phys. Chem. A* **2003,** *107*, 8377-8379.

160. Sinnokrot, M. O.; Sherrill, C. D., Substituent Effects in π-π Interactions: Sandwich and T-Shaped Configurations. *J. Am. Chem. Soc.* **2004,** *126*, 7690-7697.

161. Arnstein, S. A.; Sherrill, C. D., Substituent Effects in Parallel-Sisplaced π-π Interactions. *Phys. Chem. Chem. Phys.* **2008,** *10*, 2646-2655.

162. Hohenstein, E. G.; Duan, J.; Sherrill, C. D., Origin of the Surprising Enhancement of Electrostatic Energies by Electron-Donating Substituents in Substituted Benzene Sandwich Dimers. *J. Am. Chem. Soc.* **2011,** *133*, 13244-13247.

163. Parrish, R. M.; Sherrill, C. D., Quantum-Mechanical Evaluation of pi-pi versus Substituent-pi Interactions in pi Stacking: Direct evidence for the Wheeler-Houk Picture. *J. Am. Chem. Soc.* **2014,** *136*, 17386-17389.

164. Cozzi, F.; Cinquini, M.; Annunziata, R.; Dwyer, T.; Siegel, J. S., Polar/π Interactions between Stacked Aryls in 1,8-Diarylnaphthalenes. *J. Am. Chem. Soc.* **1992,** *114*, 5729-5733.

165. Cozzi, F.; Cinquini, M.; Annunziata, R.; Siegel, J. S., Dominance of Polar/π over Charge-Transfer Effects in Stacked Phenyl Interactions. *J. Am. Chem. Soc.* **1993,** *115*, 5330-5331.

166. Cozzi, F.; Annunziata, R.; Benaglia, M.; Cinquini, M.; Raimondi, L.; Baldridge, K. K.; Siegel, J. S., Through-Space Interactions between Face-to-Face, Center-to-Edge Oriented Arenes: Importance of Polar–π Effects *Org. Biomol. Chem.* **2003,** *1*, 157-162.

167. Hunter, C. A.; Sanders, J. K. M., The Nature of π-π Interactions. *J. Am. Chem. Soc.* **1990,** *112*, 5525-5534.

168. Hunter, C. A.; Lawson, K. R.; Perkins, J.; Urch, C. J., Aromatic Interactions. *J. Chem. Soc., Perkin Trans. 2* **2001**, 651-669.

169. Cockroft, S. L.; Hunter, C. A.; Lawson, K. R.; Perkins, J.; Urch, C., J., Electrostatic Control of Aromatic Stacking Interactions. *J. Am. Chem. Soc.* **2005,** *127*, 8594-8595.

170. Cockroft, S. L.; Perkins, J.; Zonta, C.; Adams, H.; Spey, S. E.; Low, C. M. R.; Vinter, J. G.; Lawson, K. R.; Urch, C. J.; Hunter, C. A., Substituent Effects on Aromatic Stacking Interactions. *Org. Biomol. Chem.* **2007,** *5*, 1062-1080.

171. Wheeler, S. E., Local Nature of Substituent Effects in Stacking Interactions. *J. Am. Chem. Soc.* **2011,** *133*, 10262-10274.

172. Raju, R. K.; Bloom, J. W. G.; Wheeler, S. E., Broad Transferability of Substituent Effects in π-Stacking Interactions Provides New Insights into Their Origin. *J. Chem. Theory Comput.* **2013,** *9*, 3479-3490.

173. Dougherty, D. A., The Cation−π Interaction. *Acc. Chem. Res.* **2013,** *46*, 885-893.

174. Dougherty, D. A., Physical Organic Chemistry on the Brain. *J. Org. Chem.* **2008,** *73*, 3667-3673.

175. Cubero, E.; Luque, F. J.; Orozco, M., Is polarization important in cation-π interactions? *Proc. Natl. Acad. Sci. USA* **1998,** *95*, 5976-5980.

176. Geronimo, I.; Singh, N. J.; Kim, K. S., Can Electron-Rich π Systems Bind Anions? *J. Chem. Theory and Comput.* **2011,** *7*, 825-829.

177. Mecozzi, S.; West, A. P., Jr.; Dougherty, D. A., Cation-π Interactions in Simple Aromatics: Electrostatics Provide a Predictive Tool. *J. Am. Chem. Soc.* **1996,** *118*, 2307-2308.

178. Wheeler, S. E.; Houk, K. N., Substituent Effects in Cation/π Interactions and Electrostatic Potentials above the Center of Substituted Benzenes Are Due Primarily to through-Space Effects of the Substituents. *J. Am. Chem. Soc.* **2009,** *131*, 3126-3127.

179. Wheeler, S. E.; Houk, K. N., Are Anion/π Interactions Actually a Case of Simple Charge-Dipole Interactions? *J. Phys.Chem. A* **2010,** *114*, 8658-8664.

180. ZHang, X.; Dai, H.; Yan, H.; Zou, W.; Cremer, D., B–H···π Interaction: A New Type of Nonclassical Hydrogen Bonding. *J. Am. Chem. Soc.* **2016,** *138*, 4334-4337.

181. Cannizzaro, C. E.; Houk, K. N., Magnitudes and Chemical Consequences of R3N+─C−H···OC Hydrogen Bonding. *J. Am. Chem. Soc.* **2002,** *124*, 7163-7169.

182. Nepal, B.; Scheiner, S., Effect of Ionic Charge on the CH···π Hydrogen Bond. *J. Phys. Chem. A* **2014,** *118* (40), 9575-9587.

183. Adhikari, U.; Scheiner, S., Magnitude and Mechanism of Charge Enhancement of CH··O Hydrogen Bonds. *J. Phys. Chem. A* **2013,** *117* (40), 10551-10562.

184. D'Oria, E.; Novoa, J. J., Cation–Anion Hydrogen Bonds: A New Class of Hydrogen Bonds That Extends Their Strength beyond the Covalent Limit. A Theoretical Characterization. *J. Phys. Chem. A* **2011,** *115*, 13114-13123.

185. Zhao, C.; Parrish, R. M.; Smith, M. D.; Pellechia, P. J.; Sherrill, C. D.; Shimizu, K. D., Do Deuteriums Form Stronger CH−π Interactions? *Journal of the American Chemical Society* **2012,** *134* (35), 14306-14309.

186. Oki, M., 1,9-Disubstituted triptycenes: an excellent probe for weak molecular interactions. *Accounts of Chemical Research* **1990,** *23* (11), 351-356.

187. Gung, B. W.; Xue, X.; Reich, H. J., The Strength of Parallel-Displaced Arene−Arene Interactions in Chloroform. *The Journal of Organic Chemistry* **2005,** *70* (9), 3641-3644.

188. Carroll, W. R.; Pellechia, P.; Shimizu, K. D., A Rigid Molecular Balance for Measuring Face-to-Face Arene−Arene Interactions. *Organic Letters* **2008,** *10* (16), 3547-3550.

189. Yamada, S.; Yamamoto, N.; Takamori, E., A Molecular Seesaw Balance: Evaluation of Solvent and Counteranion Effects on Pyridinium−π Interactions. *Organic Letters* **2015,** *17* (19), 4862-4865.

190. Motherwell, W. B.; Moïse, J.; Aliev, A. E.; Nič, M.; Coles, S. J.; Horton, P. N.; Hursthouse, M. B.; Chessari, G.; Hunter, C. A.; Vinter, J. G., Noncovalent Functional-Group–Arene Interactions. *Angew. Chem. Int. Ed.* **2007,** *46* (41), 7823-7826.

191. Yang, L.; Brazier, J. B.; Hubbard, T. A.; Rogers, D. M.; Cockroft, S. L., Can Dispersion Forces Govern Aromatic Stacking in an Organic Solvent? *Angew. Chem. Int. Ed.* **2015,** *55*, 912-916.

192. Muchowska, K. B.; Adam, C.; Mati, I. K.; Cockroft, S. L., Electrostatic Modulation of Aromatic Rings via Explicit Solvation of Substituents. *J. Am. Chem. Soc.* **2013,** *135* (9976-9979).

193. Yang, L.; Adam, C.; Cockroft, S. L., Quantifying Solvophobic Effects in Nonpolar Cohesive Interactions. *J. Am. Chem. Soc.* **2015,** *137*, 10084-10087.

194. Mati, I. K.; Cockroft, S. L., Molecular Balances for Quantifying Non-Covalent Interactions. *Chem. Soc. Rev.* **2010,** *39*, 4195-4205.

195. Grimme, S., Improved second-order Møller–Plesset perturbation theory by separate scaling of parallel- and antiparallel-spin pair correlation energies. *J. Chem. Phys.* **2003,** *118*, 9095-9102.

196. Sinnokrot, M. O.; Sherrill, C. D., Highly Accurate Coupled Cluster Potential Energy Curves for the Benzene Dimer: Sandwich, T-Shaped, and Parallel-Displaced Configurations. *J. Phys. Chem. A* **2004,** *108*, 10200-10207.

197. Zhao, Y.; Truhlar, D. G., Density Functional for Spectroscopy: No Long-Range Self-Interaction Error, Good Performance for Rydberg and Charge-Transfer States, and Better Performance on Average than B3LYP for Ground States. *J. Phys. Chem. A* **2006,** *110*, 13126.

198. Zhao, Y.; Truhlar, D. G., A new local density functional for main-group thermochemistry, transition metal bonding, thermochemical kinetics, and noncovalent interactions. *J. Chem. Phys.* **2006,** *125*, 194101.

199. Zhao, Y.; Truhlar, D. G., Density Functionals for Noncovalent Interaction Energies of Biological Importance. *J. Chem. Theory Comput.* **2007,** *3*, 289-300.

200. Zhao, Y.; Truhlar, D. G., Density Functionals with Broad Applicability in Chemistry. *Acc. Chem. Res.* **2008,** *41*, 157-167.

201. Gräfenstein, J.; Cremer, D., Efficient Density-Functional Theory Integrations by Locally Augmented Radial Grids. *J. Chem. Phys.* **2007,** *127*, 164113.

202. Gräfenstein, J.; Izotov, D.; Cremer, D., Avoiding Singularity Problems Associated with Meta-GGA (Generalized Gradient Approximation) Exchange and Correlation Functionals Containing the Kinetic Energy Density. *J. Chem. Phys.* **2007,** *127*, 214103.

203. Johnson, E. R.; Becke, A. D.; Sherrill, C. D.; DiLabio, G. A., Oscillations in Meta-Generalized-Gradient Approximation Potential Energy Surfaces for Dispersion-Bound Complexes. *J. Chem. Phys.* **2009,** *131*, 034111.

204. Wheeler, S. E.; Houk, K. N., Integration Grid Errors for Meta-GGA-Predicted Reaction Energies: Origin of Grid Errors for the M06 Suite of Functionals. *J. Chem. Theory Comput.* **2010,** *6*, 395-404.

205. Foster, J. P.; Weinhold, F., Natural Hybrid Orbitals. *J. Am. Chem. Soc.* **1980,** *102*, 7211-7218.

206. Reed, A. E.; Curtiss, L. A.; Weinhold, F., Intermolecular interactions from a natural bond orbital, donor-acceptor viewpoint. *Chem. Rev.* **1988,** *88*, 899-926.

207. Wheeler, S. E.; Houk, K. N., Through-Space Effects of Substituents Dominate Molecular Electrostatic Potentials of Substituted Arenes. *J. Chem. Theory Comput.* **2009,** *5*, 2301-2312.

208. Wheeler, S. E.; Bloom, J. W. G., Anion-π Interactions and Positive Electrostatic Potentials of N-Heterocycles Arise from the Positions of the Nuclei, not Changes in the π-electron Distribution. *Chem. Commun.* **2014,** *50*, 11118-11121.

209. Johnson, E. R.; Keinan, S.; Mori-Sánchez, P.; Contreras-García, J.; Cohen, A. J.; Yang, W., Revealing Noncovalent Interactions. *Journal of the American Chemical Society* **2010,** *132* (18), 6498-6506.

210. Takahashi, O.; Yasunaga, K.; Gondoh, Y.; Kohno, Y.; Saito, K.; Nishio, M., The Conformation of 2-Phenylpropionaldehyde and Alkyl 1-Phenylethyl Ketones as Evidenced by Ab Initio Calculations. Relevance of the CH/π and CH/O Interactions in Stereochemistry. *Bulletin of the Chemical Society of Japan* **2002,** *75* (8), 1777-1783.

211. Takahashi, O.; Yamasaki, K.; Kohno, Y.; Ueda, K.; Suezawa, H.; Nishio, M., The Origin of the Relative Stability of Axial Conformers of Cyclohexane and Cyclohexanone Derivatives: Importance of the CH/n and CH/π Hydrogen Bonds. *Bulletin of the Chemical Society of Japan* **2009,** *82* (2), 272-276.

212. Nishio, M.; Umezawa, Y.; Fantini, J.; Weiss, M. S.; Chakrabarti, P., CH-[small pi] hydrogen bonds in biological macromolecules. *Physical Chemistry Chemical Physics* **2014,** *16* (25), 12648-12683.

213. Takahashi, O.; Yamasaki, K.; Kohno, Y.; Ueda, K.; Suezawa, H.; Nishio, M., The conformation of levopimaric acid investigated by high-level ab initio MO calculations. Possibility of the CH/π hydrogen bond. *Tetrahedron* **2009,** *65* (17), 3525-3528.

214. Jones, C. R.; Baruah, P. K.; Thompson, A. L.; Scheiner, S.; Smith, M. D., Can a C–H···O Interaction Be a Determinant of Conformation? *Journal of the American Chemical Society* **2012,** *134* (29), 12064-12071.

215. W. Banks, J.; S. Batsanov, A.; A. K. Howard, J.; O'Hagan, D.; S. Rzepa, H.; Martin-Santamaria, S., The preferred conformation of [small alpha]-fluoroamides. *Journal of the Chemical Society, Perkin Transactions 2* **1999,** (11), 2409-2411.

216. Watt, M. M.; Zakharov, L. N.; Haley, M. M.; Johnson, D. W., Selective Nitrate Binding in Competitive Hydrogen Bonding Solvents: Do Anion–π Interactions Facilitate Nitrate Selectivity? *Angewandte Chemie International Edition* **2013,** *52* (39), 10275-10280.

217. Mascal, M.; Yakovlev, I.; Nikitin, E. B.; Fettinger, J. C., Fluoride-Selective Host Based on Anion–π Interactions, Ion Pairing, and Hydrogen Bonding: Synthesis and Fluoride-Ion Sandwich Complex. *Angewandte Chemie International Edition* **2007,** *46* (46), 8782-8784.

218. Guha, S.; Saha, S., Fluoride Ion Sensing by an Anion−π Interaction. *Journal of the American Chemical Society* **2010,** *132* (50), 17674-17677.

219. Schneebeli, S. T.; Frasconi, M.; Liu, Z.; Wu, Y.; Gardner, D. M.; Strutt, N. L.; Cheng, C.; Carmieli, R.; Wasielewski, M. R.; Stoddart, J. F., Electron Sharing and Anion–π Recognition in Molecular Triangular Prisms. *Angewandte Chemie International Edition* **2013,** *52* (49), 13100-13104.

220. Hafezi, N.; Holcroft, J. M.; Hartlieb, K. J.; Dale, E. J.; Vermeulen, N. A.; Stern, C. L.; Sarjeant, A. A.; Stoddart, J. F., Modulating the Binding of Polycyclic Aromatic Hydrocarbons Inside a Hexacationic Cage by Anion–π Interactions. *Angewandte Chemie International Edition* **2015,** *54* (2), 456-461.

221. Perez-Velasco, A.; Gorteau, V.; Matile, S., Rigid Oligoperylenediimide Rods: Anion–π Slides with Photosynthetic Activity. *Angewandte Chemie International Edition* **2008,** *47* (5), 921-923.

222. Maity, P.; Pemberton, R. P.; Tantillo, D. J.; Tambar, U. K., Brønsted Acid Catalyzed Enantioselective Indole Aza-Claisen Rearrangement Mediated by an Arene CH–O Interaction. *Journal of the American Chemical Society* **2013,** *135* (44), 16380-16383.

223. Odagi, M.; Furukori, K.; Yamamoto, Y.; Sato, M.; Iida, K.; Yamanaka, M.; Nagasawa, K., Origin of Stereocontrol in Guanidine-Bisurea Bifunctional Organocatalyst That Promotes α-Hydroxylation of Tetralone-Derived β-Ketoesters: Asymmetric Synthesis of β- and γ-Substituted Tetralone Derivatives via Organocatalytic Oxidative Kinetic Resolution. *Journal of the American Chemical Society* **2015,** *137* (5), 1909-1915.

224. Jang, K. P.; Hutson, G. E.; Johnston, R. C.; McCusker, E. O.; Cheong, P. H. Y.; Scheidt, K. A., Asymmetric Homoenolate Additions to Acyl Phosphonates through Rational Design of a Tailored N-Heterocyclic Carbene Catalyst. *Journal of the American Chemical Society* **2014,** *136* (1), 76-79.

225. Cerny, J.; Hobza, P., Non-covalent interactions in biomacromolecules. *Physical Chemistry Chemical Physics* **2007,** *9* (39), 5291-5303.

226. Steuber, H.; Heine, A.; Klebe, G., Structural and Thermodynamic Study on Aldose Reductase: Nitro-substituted Inhibitors with Strong Enthalpic Binding Contribution. *Journal of Molecular Biology* **2007,** *368* (3), 618-638.

227. Li, S.; Cooper, V. R.; Thonhauser, T.; Lundqvist, B. I.; Langreth, D. C., Stacking Interactions and DNA Intercalation. *J. Phys. Chem. B* **2009,** *113*, 11166-11172.

228. Řeha, D.; Kabeláč, M.; Ryjáček, F.; Šponer, J.; Šponer, J. E.; Elstner, M.; Suhai, S.; Hobza, P., Intercalators. 1. Nature of Stacking Interactions between Intercalators (Ethidium, Daunomycin, Ellipticine, and 4'6-Diaminide-2-phenylindole) and DNA Base Pairs. *Ab Initio* Quantum Chemical, Density Functional Theory, and Empirical Potential Study. *J. Am. Chem. Soc.* **2002,** *124*, 3366-3376.

229. Langner, K. M.; Kedzierski, P.; Sokalski, W. A.; Leszczynski, J., Physical Nature of Ethidium and Proflavine Interactions with Nucleic Acid Bases in the Intercalation Plane *J. Phys. Chem. B* **2006,** *110*, 9720-9727.

230. Hargis, J. C.; Schaefer, H. F.; Houk, K. N.; Wheeler, S. E., Non-Covalent Interactions of a Benzo[a]pyrene Diol Epoxide with DNA Base Pairs: Insight into the Formation of Adducts of (+)-BaP DE-2 with DNA. *J. Phys. Chem. A* **2010,** *114*, 2038-2044.

231. Hong, Y. J.; Tantillo, D. J., C-H[small pi] interactions as modulators of carbocation structure - implications for terpene biosynthesis. *Chemical Science* **2013,** *4* (6), 2512-2518.

232. Grether, U.; Bénardeau, A.; Benz, J.; Binggeli, A.; Blum, D.; Hilpert, H.; Kuhn, B.; Märki, H. P.; Meyer, M.; Mohr, P.; Püntener, K.; Raab, S.; Ruf, A.; Schlatter, D., Design and Biological Evaluation of Novel, Balanced Dual PPARα/γ Agonists. *ChemMedChem* **2009,** *4* (6), 951-956.

233. Foloppe, N.; Fisher, L. M.; Francis, G.; Howes, R.; Kierstan, P.; Potter, A., Identification of a buried pocket for potent and selective inhibition of Chk1: Prediction and verification. *Bioorganic & Medicinal Chemistry* **2006,** *14* (6), 1792-1804.

234. Fick, R. J.; Kroner, G. M.; Nepal, B.; Magnani, R.; Horowitz, S.; Houtz, R. L.; Scheiner, S.; Trievel, R. C., Sulfur–Oxygen Chalcogen Bonding Mediates AdoMet Recognition in the Lysine Methyltransferase SET7/9. *ACS Chemical Biology* **2015**.

235. Bauzá, A.; Quiñonero, D.; Deyà, P. M.; Frontera, A., On the Importance of Anion–π Interactions in the Mechanism of Sulfide:Quinone Oxidoreductase. *Chemistry – An Asian Journal* **2013,** *8* (11), 2708-2713.

236. Estarellas, C.; Frontera, A.; Quiñonero, D.; Deyà, P. M., Relevant Anion–π Interactions in Biological Systems: The Case of Urate Oxidase. *Angewandte Chemie International Edition* **2011,** *50* (2), 415-418.

237. Becke, A., Density-Functional Thermochemistry. V. Systematic Optimization of Exchange-Correlation Functionals. *J. Chem. Phys.* **1997,** *107*, 8554-8560.

238. Weigend, F.; Ahlrichs, R., Balanced basis sets of split valence, triple zeta valence and quadruple zeta valence quality for H to Rn: Design and assessment of accuracy. *Phys. Chem. Chem. Phys.* **2005,** *7*, 3297-3305.

239. Chai, J.-D.; Head-Gordon, M., Systematic Optimization of Long-Range Corrected Hybrid Density Functionals. *J. Chem. Phys.* **2008,** *128*, 084106.

240. Peng, Q.; Duarte, F.; Paton, R. S., Computing organic stereoselectivity - from concepts to quantitative calculations and predictions. *Chem. Soc. Rev.* **2016,** *45* (22), 6093-6107.

241. Bickelhaupt, F. M.; Houk, K. N., Analyzing Reaction Rates with the Distortion/Interaction-Activation Strain Model. *Angew. Chem. Int. Ed.* **2017,** *56* (34), 10070-10086.

242. Champagne, P. A.; Houk, K. N., Origins of Selectivity and General Model for Chiral Phosphoric Acid-Catalyzed Oxetane Desymmetrizations. *Journal of the American Chemical Society* **2016,** *138* (38), 12356-12359.

243. Duarte, F.; Paton, R. S., Molecular Recognition in Asymmetric Counteranion Catalysis: Understanding Chiral Phosphate-Mediated Desymmetrization. *Journal of the American Chemical Society* **2017,** *139* (26), 8886-8896.

244. Maji, R.; Champagne, P. A.; Houk, K. N.; Wheeler, S. E., Activation Mode and Origin of Selectivity in Chiral Phosphoric Acid-Catalyzed Oxacycle Formation by Intramolecular Oxetane Desymmetrizations. *ACS Catalysis* **2017,** *7* (10), 7332-7339.

245. Jindal, G.; Sunoj, R. B., Deciphering the Origin of Stereoinduction in Cooperative Asymmetric Catalysis Involving Pd(II) and a Chiral Brønsted Acid. *Organic Letters* **2015,** *17* (12), 2874-2877.

246. Seguin, T. J.; Wheeler, S. E., Electrostatic Basis for Enantioselective Brønsted-Acid-Catalyzed Asymmetric Ring Openings of meso-Epoxides. *ACS Catalysis* **2016,** *6* (4), 2681-2688.

247. Jindal, G.; Sunoj, R. B., Axially Chiral Imidodiphosphoric Acid Catalyst for Asymmetric Sulfoxidation Reaction: Insights on Asymmetric Induction. *Angewandte Chemie International Edition* **2014,** *53* (17), 4432-4436.

248. Bhaskararao, B.; Sunoj, R. B., Origin of Stereodivergence in Cooperative Asymmetric Catalysis with Simultaneous Involvement of Two Chiral Catalysts. *Journal of the American Chemical Society* **2015,** *137* (50), 15712-15722.

249. Changotra, A.; Sunoj, R. B., Origin of Kinetic Resolution of Hydroxy Esters through Catalytic Enantioselective Lactonization by Chiral Phosphoric Acids. *Org. Lett.* **2016,** *18* (15), 3730-3733.

250. Straker, R. N.; Peng, Q.; Mekareeya, A.; Paton, R. S.; Anderson, E. A., Computational ligand design in enantio- and diastereoselective ynamide [lsqb]5+2[rsqb] cycloisomerization. *Nat. Commun.* **2016,** *7*, 10109.

251. Reid, J. P.; Goodman, J. M., Goldilocks Catalysts: Computational Insights into the Role of the 3,3′ Substituents on the Selectivity of BINOL-Derived Phosphoric Acid Catalysts. *Journal of the American Chemical Society* **2016,** *138* (25), 7910-7917.

252. Terada, M.; Soga, K.; Momiyama, N., Enantioselective Activation of Aldehydes by Chiral Phosphoric Acid Catalysts in an Aza-ene-type Reaction between Glyoxylate and Enecarbamate. *Angewandte Chemie International Edition* **2008,** *47* (22), 4122-4125.

253. Toste, F. D.; Sigman, M. S.; Miller, S. J., Pursuit of Noncovalent Interactions for Strategic Site-Selective Catalysis. *Accounts of Chemical Research* **2017,** *50* (3), 609-615.

254. Sunoj, R. B., Transition State Models for Understanding the Origin of Chiral Induction in Asymmetric Catalysis. *Accounts of Chemical Research* **2016,** *49* (5), 1019-1028.

255. Changotra, A.; Das, S.; Sunoj, R. B., Reversing Enantioselectivity Using Noncovalent Interactions in Asymmetric Dearomatization of β-Naphthols: The Power of 3,3′ Substituents in Chiral Phosphoric Acid Catalysts. *Org. Lett.* **2017,** *19* (9), 2354-2357.

256. Monaco, M. R.; Fazzi, D.; Tsuji, N.; Leutzsch, M.; Liao, S.; Thiel, W.; List, B., The Activation of Carboxylic Acids via Self-Assembly Asymmetric Organocatalysis: A Combined Experimental and Computational Investigation. *Journal of the American Chemical Society* **2016,** *138* (44), 14740-14749.

257. Hong, X.; Küçük, H. B.; Maji, M. S.; Yang, Y.-F.; Rueping, M.; Houk, K. N., Mechanism and Selectivity of N-Triflylphosphoramide Catalyzed (3+ + 2) Cycloaddition between Hydrazones and Alkenes. *Journal of the American Chemical Society* **2014,** *136* (39), 13769-13780.

258. Yang, C.; Xue, X.-S.; Jin, J.-L.; Li, X.; Cheng, J.-P., Theoretical Study on the Acidities of Chiral Phosphoric Acids in Dimethyl Sulfoxide: Hints for Organocatalysis. *The Journal of Organic Chemistry* **2013,** *78* (14), 7076-7085.

259. Yang, C.; Xue, X.-S.; Li, X.; Cheng, J.-P., Computational Study on the Acidic Constants of Chiral Brønsted Acids in Dimethyl Sulfoxide. *The Journal of Organic Chemistry* **2014,** *79* (10), 4340-4351.

260. Marcelli, T.; Hammar, P.; Himo, F., Phosphoric Acid Catalyzed Enantioselective Transfer Hydrogenation of Imines: A Density Functional Theory Study of Reaction Mechanism and the Origins of Enantioselectivity. *Chemistry – A European Journal* **2008,** *14* (28), 8562-8571.

261. Gridnev, I. D.; Kouchi, M.; Sorimachi, K.; Terada, M., On the mechanism of stereoselection in direct Mannich reaction catalyzed by BINOL-derived phosphoric acids. *Tetrahedron Letters* **2007,** *48* (3), 497-500.

262. Simón, L.; Goodman, J. M., A Model for the Enantioselectivity of Imine Reactions Catalyzed by BINOL−Phosphoric Acid Catalysts. *The Journal of Organic Chemistry* **2011,** *76* (6), 1775-1788.

263. Reid, J. P.; Simón, L.; Goodman, J. M., A Practical Guide for Predicting the Stereochemistry of Bifunctional Phosphoric Acid Catalyzed Reactions of Imines. *Accounts of Chemical Research* **2016,** *49* (5), 1029-1041.

264. Grayson, M. N.; Pellegrinet, S. C.; Goodman, J. M., Mechanistic Insights into the BINOL-Derived Phosphoric Acid-Catalyzed Asymmetric Allylboration of Aldehydes. *Journal of the American Chemical Society* **2012,** *134* (5), 2716-2722.

265. Wang, H.; Jain, P.; Antilla, J. C.; Houk, K. N., Origins of Stereoselectivities in Chiral Phosphoric Acid Catalyzed Allylborations and Propargylations of Aldehydes. *The Journal of Organic Chemistry* **2013,** *78* (3), 1208-1215.

266. Calleja, J.; Gonzalez-Perez, A. B.; de Lera, A. R.; Alvarez, R.; Fananas, F. J.; Rodriguez, F., Enantioselective synthesis of hexahydrofuro[3,2-c] quinolines through a multicatalytic and multicomponent process. A new "aromatic sandwich" model for BINOL-phosphoric acid catalyzed reactions. *Chemical Science* **2014,** *5* (3), 996-1007.

267. Sun, Z.; Winschel, G. A.; Zimmerman, P. M.; Nagorny, P., Enantioselective Synthesis of Piperidines through the Formation of Chiral Mixed Phosphoric Acid

Acetals: Experimental and Theoretical Studies. *Angewandte Chemie International Edition* **2014,** *53* (42), 11194-11198.

268. Lovie-Toon, J. P.; Tram, C. M.; Flynn, B. L.; Krenske, E. H., Mechanisms of Carbonyl Activation by BINOL N-Triflylphosphoramides: Enantioselective Nazarov Cyclizations. *ACS Catal.* **2017,** *7* (5), 3466-3476.

269. Simón, L.; Goodman, J. M., Theoretical Study of the Mechanism of Hantzsch Ester Hydrogenation of Imines Catalyzed by Chiral BINOL-Phosphoric Acids. *Journal of the American Chemical Society* **2008,** *130* (27), 8741-8747.

270. Saito, K.; Shibata, Y.; Yamanaka, M.; Akiyama, T., Chiral Phosphoric Acid-Catalyzed Oxidative Kinetic Resolution of Indolines Based on Transfer Hydrogenation to Imines. *Journal of the American Chemical Society* **2013,** *135* (32), 11740-11743.

271. Nimmagadda, S. K.; Mallojjala, S. C.; Woztas, L.; Wheeler, S. E.; Antilla, J. C., Enantioselective Synthesis of Chiral Oxime Ethers: Desymmetrization and Dynamic Kinetic Resolution of Substituted Cyclohexanones. *Angewandte Chemie International Edition* **2017,** *56* (9), 2454-2458.

272. Ajitha, M. J.; Huang, K.-W., Role of keto-enol tautomerization in a chiral phosphoric acid catalyzed asymmetric thiocarboxylysis of meso-epoxide: a DFT study. *Organic & Biomolecular Chemistry* **2015,** *13* (45), 10981-10985.

273. Seguin, T. J.; Wheeler, S. E., Competing Noncovalent Interactions Control the Stereoselectivity of Chiral Phosphoric Acid Catalyzed Ring Openings of 3-Substituted Oxetanes. *ACS Catalysis* **2016,** *6* (10), 7222-7228.

274. García-García, C.; Ortiz-Rojano, L.; Álvarez, S.; Álvarez, R.; Ribagorda, M.; Carreño, M. C., Friedel–Crafts Alkylation of Indoles with p-Quinols: The Role of Hydrogen Bonding of Water for the Desymmetrization of the Cyclohexadienone System. *Organic Letters* **2016,** *18* (9), 2224-2227.

275. Meng, S.-S.; Liang, Y.; Cao, K.-S.; Zou, L.; Lin, X.-B.; Yang, H.; Houk, K. N.; Zheng, W.-H., Chiral Phosphoric Acid Catalyzed Highly Enantioselective Desymmetrization of 2-Substituted and 2,2-Disubstituted 1,3-Diols via Oxidative Cleavage of Benzylidene Acetals. *J. Am. Chem. Soc.* **2014,** *136* (35), 12249-12252.

276. Momiyama, N.; Funayama, K.; Noda, H.; Yamanaka, M.; Akasaka, N.; Ishida, S.; Iwamoto, T.; Terada, M., Hydrogen Bonds-Enabled Design of a C1-Symmetric Chiral Brønsted Acid Catalyst. *ACS Catalysis* **2016,** *6* (2), 949-956.

277. Grayson, M. N.; Krische, M. J.; Houk, K. N., Ruthenium-Catalyzed Asymmetric Hydrohydroxyalkylation of Butadiene: The Role of the Formyl Hydrogen Bond in Stereochemical Control. *Journal of the American Chemical Society* **2015,** *137* (27), 8838-8850.

278. Jindal, G.; Sunoj, R. B., Mechanistic Insights on Cooperative Asymmetric Multicatalysis Using Chiral Counterions. *The Journal of Organic Chemistry* **2014,** *79* (16), 7600-7606.

279. Jindal, G.; Sunoj, R. B., Importance of Ligand Exchanges in Pd(II)-Brønsted Acid Cooperative Catalytic Approach to Spirocyclic Rings. *Journal of the American Chemical Society* **2014,** *136* (45), 15998-16008.

280. Heggen, B.; Patil, M.; Thiel, W., Cyclization of an α,β-Unsaturated hydrazone catalyzed by a BINOL-phosphoric acid: Pericyclic or not? *Journal of Computational Chemistry* **2016,** *37* (2), 280-285.

281. Grayson, M. N.; Yang, Z.; Houk, K. N., Chronology of CH···O Hydrogen Bonding from Molecular Dynamics Studies of the Phosphoric Acid-Catalyzed Allylboration of Benzaldehyde. *Journal of the American Chemical Society* **2017,** *139* (23), 7717-7720.

282. Khomutnyk, Y. Y.; Argüelles, A. J.; Winschel, G. A.; Sun, Z.; Zimmerman, P. M.; Nagorny, P., Studies of the Mechanism and Origins of Enantioselectivity for the Chiral Phosphoric Acid-Catalyzed Stereoselective Spiroketalization Reactions. *Journal of the American Chemical Society* **2016,** *138* (1), 444-456.

283. Jindal, G.; Sunoj, R. B., Rational design of catalysts for asymmetric diamination reaction using transition state modeling. *Organic & Biomolecular Chemistry* **2014,** *12* (17), 2745-2753.

284. Orlandi, M.; Toste, F. D.; Sigman, M. S., Multidimensional Correlations in Asymmetric Catalysis through Parameterization of Uncatalyzed Transition States. *Angewandte Chemie International Edition* **2017,** *56* (45), 14080-14084.

285. Enders, D.; Niemeier, O.; Henseler, A., Organocatalysis by N-Heterocyclic Carbenes. *Chemical Reviews* **2007,** *107* (12), 5606-5655.

286. Bugaut, X.; Glorius, F., Organocatalytic umpolung: N-heterocyclic carbenes and beyond. *Chemical Society Reviews* **2012,** *41* (9), 3511-3522.

287. Ryan, S. J.; Candish, L.; Lupton, D. W., Acyl anion free N-heterocyclic carbene organocatalysis. *Chemical Society Reviews* **2013,** *42* (12), 4906-4917.

288. Hopkinson, M. N.; Richter, C.; Schedler, M.; Glorius, F., An overview of N-heterocyclic carbenes. *Nature* **2014,** *510* (7506), 485-496.

289. Menon, R. S.; Biju, A. T.; Nair, V., Recent advances in employing homoenolates generated by N-heterocyclic carbene (NHC) catalysis in carbon-carbon bond-forming reactions. *Chemical Society Reviews* **2015,** *44* (15), 5040-5052.

290. Li, G.-Q.; Li, Y.; Dai, L.-X.; You, S.-L., Enantioselective Synthesis of cis-4-Formyl-β-lactams via Chiral N-Heterocyclic Carbene-Catalyzed Kinetic Resolution. *Advanced Synthesis & Catalysis* **2008,** *350* (9), 1258-1262.

291. Wang, M.; Huang, Z.; Xu, J.; Chi, Y. R., N-Heterocyclic Carbene-Catalyzed [3+4] Cycloaddition and Kinetic Resolution of Azomethine Imines. *Journal of the American Chemical Society* **2014,** *136* (4), 1214-1217.

292. Wu, Z.; Li, F.; Wang, J., Intermolecular Dynamic Kinetic Resolution Cooperatively Catalyzed by an N-Heterocyclic Carbene and a Lewis Acid. *Angewandte Chemie International Edition* **2015,** *54* (5), 1629-1633.

293. Goodman, C. G.; Walker, M. M.; Johnson, J. S., Enantioconvergent Synthesis of Functionalized γ-Butyrolactones via (3 + 2)-Annulation. *J. Am. Chem. Soc.* **2015,** *137* (1), 122-125.

294. Zhao, C.; Li, F.; Wang, J., N-Heterocyclic Carbene Catalyzed Dynamic Kinetic Resolution of Pyranones. *Angewandte Chemie International Edition* **2016,** *55* (5), 1820-1824.

295. Cohen, D. T.; Eichman, C. C.; Phillips, E. M.; Zarefsky, E. R.; Scheidt, K. A., Catalytic Dynamic Kinetic Resolutions with N-Heterocyclic Carbenes: Asymmetric Synthesis of Highly Substituted β-Lactones. *Angewandte Chemie International Edition* **2012,** *51* (29), 7309-7313.

296. Johnston, R. C.; Cohen, D. T.; Eichman, C. C.; Scheidt, K. A.; Ha-Yeon Cheong, P., Catalytic kinetic resolution of a dynamic racemate: highly stereoselective [small beta]-lactone formation by N-heterocyclic carbene catalysis. *Chemical Science* **2014,** *5* (5), 1974-1982.

297. Chen, X.; Fong, J. Z. M.; Xu, J.; Mou, C.; Lu, Y.; Yang, S.; Song, B.-A.; Chi, Y. R., Carbene-Catalyzed Dynamic Kinetic Resolution of Carboxylic Esters. *Journal of the American Chemical Society* **2016,** *138* (23), 7212-7215.

298. Goodman, C. G.; Johnson, J. S., Dynamic Kinetic Asymmetric Cross-Benzoin Additions of β-Stereogenic α-Keto Esters. *J. Am. Chem. Soc.* **2014,** *136* (42), 14698-14701.

299. Cohen, D. T.; Scheidt, K. A., Cooperative Lewis acid/N-heterocyclic carbene catalysis. *Chem. Sci.* **2012,** *3* (1), 53-57.

300. Allen, A. E.; MacMillan, D. W. C., Synergistic catalysis: A powerful synthetic strategy for new reaction development. *Chemical Science* **2012,** *3* (3), 633-658.

301. Wang, M. H.; Scheidt, K. A., Cooperative Catalysis and Activation with N-Heterocyclic Carbenes. *Angewandte Chemie International Edition* **2016,** *55* (48), 14912-14922.

302. Wang, M. H.; Cohen, D. T.; Schwamb, C. B.; Mishra, R. K.; Scheidt, K. A., Enantioselective β-Protonation by a Cooperative Catalysis Strategy. *Journal of the American Chemical Society* **2015,** *137* (18), 5891-5894.

303. Izquierdo, J.; Orue, A.; Scheidt, K. A., A Dual Lewis Base Activation Strategy for Enantioselective Carbene-Catalyzed Annulations. *Journal of the American Chemical Society* **2013,** *135* (29), 10634-10637.

304. Youn, S. W.; Song, H. S.; Park, J. H., Asymmetric Domino Multicatalysis for the Synthesis of 3-Substituted Phthalides: Cinchonine/NHC Cooperative System. *Organic Letters* **2014,** *16* (3), 1028-1031.

305. Bera, S.; Samanta, R. C.; Daniliuc, C. G.; Studer, A., Asymmetric Synthesis of Highly Substituted β-Lactones through Oxidative Carbene Catalysis with LiCl as Cooperative Lewis Acid. *Angewandte Chemie International Edition* **2014,** *53* (36), 9622-9626.

306. Raup, D. E. A.; Cardinal-David, B.; Holte, D.; Scheidt, K. A., Cooperative catalysis by carbenes and Lewis acids in a highly stereoselective route to γ-lactams. *Nat Chem* **2010,** *2* (9), 766-771.

307. Cohen, D. T.; Cardinal-David, B.; Scheidt, K. A., Lewis Acid Activated Synthesis of Highly Substituted Cyclopentanes by the N-Heterocyclic Carbene Catalyzed Addition of Homoenolate Equivalents to Unsaturated Ketoesters. *Angew. Chem. Int. Ed.* **2011,** *50* (7), 1678-1682.

308. Ozboya, K. E.; Rovis, T., Enamine/carbene cascade catalysis in the diastereo- and enantioselective synthesis of functionalized cyclopentanones. *Chemical Science* **2011,** *2* (9), 1835-1838.

309. Lathrop, S. P.; Rovis, T., Asymmetric Synthesis of Functionalized Cyclopentanones via a Multicatalytic Secondary Amine/N-Heterocyclic Carbene Catalyzed Cascade Sequence. *Journal of the American Chemical Society* **2009,** *131* (38), 13628-13630.

310. Li, J.-L.; Sahoo, B.; Daniliuc, C.-G.; Glorius, F., Conjugate Umpolung of β,β-Disubstituted Enals by Dual Catalysis with an N-Heterocyclic Carbene and a Brønsted Acid: Facile Construction of Contiguous Quaternary Stereocenters. *Angewandte Chemie International Edition* **2014,** *53* (39), 10515-10519.

311. Zhao, X.; DiRocco, D. A.; Rovis, T., N-Heterocyclic Carbene and Brønsted Acid Cooperative Catalysis: Asymmetric Synthesis of trans-γ-Lactams. *Journal of the American Chemical Society* **2011,** *133* (32), 12466-12469.

312. Guo, C.; Fleige, M.; Janssen-Müller, D.; Daniliuc, C. G.; Glorius, F., Cooperative N-Heterocyclic Carbene/Palladium-Catalyzed Enantioselective Umpolung Annulations. *Journal of the American Chemical Society* **2016,** *138* (25), 7840-7843.

313. Schlepphorst, C.; Maji, B.; Glorius, F., Ruthenium-NHC Catalyzed α-Alkylation of Methylene Ketones Provides Branched Products through Borrowing Hydrogen Strategy. *ACS Catalysis* **2016,** *6* (7), 4184-4188.

314. Dugal-Tessier, J.; O'Bryan, E. A.; Schroeder, T. B. H.; Cohen, D. T.; Scheidt, K. A., An N-Heterocyclic Carbene/Lewis Acid Strategy for the Stereoselective Synthesis of

Spirooxindole Lactones. *Angewandte Chemie International Edition* **2012,** *51* (20), 4963-4967.

315. Wang, Z.-Y.; Ding, Y.-L.; Wang, G.; Cheng, Y., Chiral N-heterocyclic carbene/Lewis acid cooperative catalysis of the reaction of 2-aroylvinylcinnamaldehydes: a switch of the reaction pathway by Lewis acid activation. *Chemical Communications* **2016,** *52* (4), 788-791.

316. Fu, Z.; Xu, J.; Zhu, T.; Leong, W. W. Y.; Chi, Y. R., β-Carbon activation of saturated carboxylic esters through N-heterocyclic carbene organocatalysis. *Nat Chem* **2013,** *5* (10), 835-839.

317. Filloux, C. M.; Lathrop, S. P.; Rovis, T., Multicatalytic, asymmetric Michael/Stetter reaction of salicylaldehydes and activated alkynes. *Proceedings of the National Academy of Sciences* **2010,** *107* (48), 20666-20671.

318. White, N. A.; DiRocco, D. A.; Rovis, T., Asymmetric N-Heterocyclic Carbene Catalyzed Addition of Enals to Nitroalkenes: Controlling Stereochemistry via the Homoenolate Reactivity Pathway To Access δ-Lactams. *Journal of the American Chemical Society* **2013,** *135* (23), 8504-8507.

319. DiRocco, D. A.; Rovis, T., Catalytic Asymmetric Intermolecular Stetter Reaction of Enals with Nitroalkenes: Enhancement of Catalytic Efficiency through Bifunctional Additives. *Journal of the American Chemical Society* **2011,** *133* (27), 10402-10405.

320. White, N. A.; Rovis, T., Oxidatively Initiated NHC-Catalyzed Enantioselective Synthesis of 3,4-Disubstituted Cyclopentanones from Enals. *Journal of the American Chemical Society* **2015,** *137* (32), 10112-10115.

321. Reddi, Y.; Sunoj, R. B., Origin of Stereoselectivity in a Chiral N-Heterocyclic Carbene-Catalyzed Desymmetrization of Substituted Cyclohexyl 1,3-Diketones. *Organic Letters* **2012,** *14* (11), 2810-2813.

322. Reddi, Y.; Sunoj, R. B., Asymmetric Dual-Catalytic Cascade by Chiral N-Heterocyclic Carbene and Quinuclidine: Mechanism and Origin of Enantioselectivity in Benzofuranone Formation. *ACS Catalysis* **2015,** *5* (3), 1596-1603.

323. Kuniyil, R.; Sunoj, R. B., N-Heterocyclic Carbene Catalyzed Asymmetric Intermolecular Stetter Reaction: Origin of Enantioselectivity and Role of Counterions. *Org. Lett.* **2013,** *15* (19), 5040-5043.

324. Reddi, Y.; Sunoj, R. B., Mechanistic Studies on Stereoselective Organocatalytic Direct β-C–H Activation in an Aliphatic Chain by Chiral N-Heterocyclic Carbenes. *ACS Catalysis* **2015,** *5* (10), 5794-5802.

325. Wang, Y.; Wei, D.; Wang, Y.; Zhang, W.; Tang, M., N-Heterocyclic Carbene (NHC)-Catalyzed sp3 β-C–H Activation of Saturated Carbonyl Compounds: Mechanism, Role of NHC, and Origin of Stereoselectivity. *ACS Catalysis* **2016,** *6* (1), 279-289.

326. Wang, Y.; Tang, M.; Wang, Y.; Wei, D., Insights into Stereoselective Aminomethylation Reaction of α,β-Unsaturated Aldehyde with N,O-Acetal via N-Heterocyclic Carbene and Brønsted Acid/Base Cooperative Organocatalysis. *J. Org. Chem.* **2016,** *81* (13), 5370-5380.

327. Qiao, Y.; Wei, D.; Chang, J., Insights into the Unexpected Chemoselectivity for the N-Heterocyclic Carbene-Catalyzed Annulation Reaction of Allenals with Chalcones. *The Journal of Organic Chemistry* **2015,** *80* (17), 8619-8630.

328. Zhang, W.; Zhu, Y.; Wei, D.; Li, Y.; Tang, M., Theoretical Investigations toward the [4 + 2] Cycloaddition of Ketenes with N-Benzoyldiazenes Catalyzed by N-Heterocyclic Carbenes: Mechanism and Enantioselectivity. *The Journal of Organic Chemistry* **2012,** *77* (23), 10729-10737.

329. Pareek, M.; Sunoj, R. B., Cooperative Asymmetric Catalysis by N-Heterocyclic Carbenes and Brønsted Acid in γ-Lactam Formation: Insights into Mechanism and Stereoselectivity. *ACS Catalysis* **2016,** *6* (5), 3118-3126.

330. Wang, Y.; Wu, B.; Zheng, L.; Wei, D.; Tang, M., DFT perspective toward [3 + 2] annulation reaction of enals with [small alpha]-ketoamides through NHC and Bronsted acid cooperative catalysis: mechanism, stereoselectivity, and role of NHC. *Organic Chemistry Frontiers* **2016,** *3* (2), 190-203.

331. Zhang, M.; Wei, D.; Wang, Y.; Li, S.; Liu, J.; Zhu, Y.; Tang, M., DFT study on the reaction mechanisms and stereoselectivities of NHC-catalyzed [2 + 2] cycloaddition between arylalkylketenes and electron-deficient benzaldehydes. *Organic & Biomolecular Chemistry* **2014,** *12* (33), 6374-6383.

332. Um, J. M.; DiRocco, D. A.; Noey, E. L.; Rovis, T.; Houk, K. N., Quantum Mechanical Investigation of the Effect of Catalyst Fluorination in the Intermolecular Asymmetric Stetter Reaction. *Journal of the American Chemical Society* **2011,** *133* (29), 11249-11254.

333. Pareek, M.; Sunoj, R. B., Mechanism and Stereoselectivity in an Asymmetric N-Heterocyclic Carbene-Catalyzed Carbon–Carbon Bond Activation Reaction. *Organic Letters* **2016,** *18* (22), 5932-5935.

334. Reddi, Y.; Sunoj, R. B., Origin of Stereoselectivity in Cooperative Asymmetric Catalysis Involving N-Heterocyclic Carbenes and Lewis Acids toward the Synthesis of Spirooxindole Lactone. *ACS Catalysis* **2017,** *7* (1), 530-537.

335. Reddi, Y.; Sunoj, R. B., Origin of Stereoselectivity in Cooperative Asymmetric Catalysis Involving N-Heterocyclic Carbenes and Lewis Acids toward the Synthesis of Spirooxindole Lactone. *ACS Catal.* **2016,** *7*, 530-537.

336. Hovey, M. T.; Cohen, D. T.; Walden, D. M.; Cheong, P. H. Y.; Scheidt, K. A., A Carbene Catalysis Strategy for the Synthesis of Protoilludane Natural Products. *Angew. Chem. Int. Ed.* **2017,** *Just Accepted, DOI: 10.1002/anie.201705308*.

337. Kuwano, S.; Harada, S.; Kang, B.; Oriez, R.; Yamaoka, Y.; Takasu, K.; Yamada, K.-i., Enhanced Rate and Selectivity by Carboxylate Salt as a Basic Cocatalyst in Chiral N-Heterocyclic Carbene-Catalyzed Asymmetric Acylation of Secondary Alcohols. *Journal of the American Chemical Society* **2013,** *135* (31), 11485-11488.

338. Binanzer, M.; Hsieh, S.-Y.; Bode, J. W., Catalytic Kinetic Resolution of Cyclic Secondary Amines. *Journal of the American Chemical Society* **2011,** *133* (49), 19698-19701.

339. Kreituss, I.; Murakami, Y.; Binanzer, M.; Bode, J. W., Kinetic Resolution of Nitrogen Heterocycles with a Reusable Polymer-Supported Reagent. *Angewandte Chemie International Edition* **2012,** *51* (42), 10660-10663.

340. Hsieh, S.-Y.; Binanzer, M.; Kreituss, I.; Bode, J. W., Expanded substrate scope and catalyst optimization for the catalytic kinetic resolution of N-heterocycles. *Chemical Communications* **2012,** *48* (71), 8892-8894.

341. Lu, S.; Poh, S. B.; Zhao, Y., Kinetic Resolution of 1,1′-Biaryl-2,2′-Diols and Amino Alcohols through NHC-Catalyzed Atroposelective Acylation. *Angew. Chem. Int. Ed.* **2014,** *53* (41), 11041-11045.

342. Allen, S. E.; Hsieh, S.-Y.; Gutierrez, O.; Bode, J. W.; Kozlowski, M. C., Concerted Amidation of Activated Esters: Reaction Path and Origins of Selectivity in the Kinetic Resolution of Cyclic Amines via N-Heterocyclic Carbenes and Hydroxamic Acid Cocatalyzed Acyl Transfer. *Journal of the American Chemical Society* **2014,** *136* (33), 11783-11791.

343. Note that the stereoselectivity presented here for reaction I is opposite to that in Ref. 9.

344. The pure, dispersion-corrected GGA B97-D was used to optimize geometries for the reaction free energy profile for computational expediency.

345. This barrier is consistent with related work from Rovis et al. [see J. L. Moore, A. P. Silvestri, J. R. de Alaniz, D. A. DiRocco, T. Rovis, Org. Lett. 2011, 13, 1742-1745].

346. Cowan, J. A.; Clyburne, J. A. C.; Davidson, M. G.; Harris, R. L. W.; Howard, J. A. K.; Küpper, P.; Leech, M. A.; Richards, S. P., On the Interaction between N-Heterocyclic Carbenes and Organic Acids: Structural Authentication of the First N−H···C Hydrogen Bond and Remarkably Short C−H···O Interactions. *Angewandte Chemie International Edition* **2002,** *41* (8), 1432-1434.

347. Kozuch, S.; Shaik, S., How to Conceptualize Catalytic Cycles? The Energetic Span Model. *Accounts of Chemical Research* **2011,** *44* (2), 101-110.

348. Computationally, we replaced the Br leaving group with Cl and removed the nitro group from the catalyst. Neither change is expected to impact the energetics of the proton transfer under investigation.

349. The triazole-fused morpholine subunit of the NHC can adopt both cis and trans conformations, in which case we would need to consider 8 distinct conformations. However, previous work by Sunoj et al. has established that the trans conformation is rarely thermodynamically competitive, so only cis conformations were considered. See Refs. 7b and 7q, as well as SI, for more details.

350. Selectivity factors (S) were predicted based on a Boltzmann weighting of these relative free energy barriers computed within the quasi-RRHO approximation([see Grimme, S. Chem. Eur. J. 2012, 18, 9955-9964).

351. Similar results were obtained at the M06-2X/6-311G(d,p)//B97-D/TZV(2d,2p) level of theory.

352. Bader, R. F. W., A quantum theory of molecular structure and its applications. *Chemical Reviews* **1991,** *91* (5), 893-928.

353. Tognetti, V.; Joubert, L., Density functional theory and Bader's atoms-in-molecules theory: towards a vivid dialogue. *Physical Chemistry Chemical Physics* **2014,** *16* (28), 14539-14550.

354. TS structures for the cationic pathway have been computed at the M06-2X/6-311G(d,p)//B97-D/TZV(2d,2p) level of theory (see SI); the predicted stereoselectivity is not in agreement with experimental observations.

355. Nepal, B.; Scheiner, S., Anionic CH···X− Hydrogen Bonds: Origin of Their Strength, Geometry, and Other Properties. *Chemistry – A European Journal* **2015,** *21* (4), 1474-1481.

356. Nepal, B.; Scheiner, S., Effect of Ionic Charge on the CH···π Hydrogen Bond. *The Journal of Physical Chemistry A* **2014,** *118* (40), 9575-9587.

357. Yang, H.; Wong, M. W., Oxyanion Hole Stabilization by C–H···O Interaction in a Transition State—A Three-Point Interaction Model for Cinchona Alkaloid-Catalyzed Asymmetric Methanolysis of meso-Cyclic Anhydrides. *J. Am. Chem. Soc.* **2013,** *135* (15), 5808-5818.

358. Kochanek, S. E.; Clymer, T. M.; Pakkala, V. S.; Hebert, S. P.; Reeping, K.; Firestine, S. M.; Evanseck, J. D., Intramolecular Charge-Assisted Hydrogen Bond Strength in Pseudochair Carboxyphosphate. *The Journal of Physical Chemistry B* **2015,** *119* (3), 1184-1191.

359. Belding, L.; Taimoory, S. M.; Dudding, T., Mirroring Enzymes: The Role of Hydrogen Bonding in an Asymmetric Organocatalyzed Aza-Henry Reaction—a DFT Study. *ACS Catalysis* **2015,** *5* (1), 343-349.

360. Taimoory, S. M.; Dudding, T., An Evolving Insight into Chiral H-Bond Catalyzed Aza-Henry Reactions: A Cooperative Role for Noncovalent Attractive

Interactions Unveiled by Density Functional Theory. *The Journal of Organic Chemistry* **2016,** *81* (8), 3286-3295.

361. Reed, A. E.; Curtiss, L. A.; Weinhold, F., Intermolecular interactions from a natural bond orbital, donor-acceptor viewpoint. *Chemical Reviews* **1988,** *88* (6), 899-926.

362. Espinosa, E.; Molins, E.; Lecomte, C., Hydrogen bond strengths revealed by topological analyses of experimentally observed electron densities. *Chemical Physics Letters* **1998,** *285* (3–4), 170-173.

363. Pattawong, O.; Tan, D. Q.; Fettinger, J. C.; Shaw, J. T.; Cheong, P. H.-Y., Stereocontrol in Asymmetric γ-Lactam Syntheses from Imines and Cyanosuccinic Anhydrides. *Organic Letters* **2013,** *15* (19), 5130-5133.

364. Lyngvi, E.; Bode, J. W.; Schoenebeck, F., A computational study of the origin of stereoinduction in NHC-catalyzed annulation reactions of [small alpha],[small beta]-unsaturated acyl azoliums. *Chemical Science* **2012,** *3* (7), 2346-2350.

365. Samanta, R. C.; De Sarkar, S.; Frohlich, R.; Grimme, S.; Studer, A., N-Heterocyclic carbene (NHC) catalyzed chemoselective acylation of alcohols in the presence of amines with various acylating reagents. *Chemical Science* **2013,** *4* (5), 2177-2184.

366. Sarkar, S. D.; Grimme, S.; Studer, A., NHC Catalyzed Oxidations of Aldehydes to Esters: Chemoselective Acylation of Alcohols in Presence of Amines. *Journal of the American Chemical Society* **2010,** *132* (4), 1190-1191.

367. DiRocco, D. A.; Noey, E. L.; Houk, K. N.; Rovis, T., Catalytic Asymmetric Intermolecular Stetter Reactions of Enolizable Aldehydes with Nitrostyrenes: Computational Study Provides Insight into the Success of the Catalyst. *Angewandte Chemie International Edition* **2012,** *51* (10), 2391-2394.

368. Sorgenfrei, N.; Hioe, J.; Greindl, J.; Rothermel, K.; Morana, F.; Lokesh, N.; Gschwind, R. M., NMR Spectroscopic Characterization of Charge Assisted Strong Hydrogen Bonds in Brønsted Acid Catalysis. *J. Am. Chem. Soc.* **2016,** *138*, 16345-16354.

369. Lu, S.; Song, X.; Poh, S. B.; Yang, H.; Wong, M. W.; Zhao, Y., Access to Enantiopure Triarylmethanes and 1,1-Diarylalkanes by NHC-Catalyzed Acylative Desymmetrization. *Chem. Eur. J.* **2017,** *23*, 2275-2281.

370. Uyeda, C.; Jacobsen, E. N., Transition-State Charge Stabilization through Multiple Non-covalent Interactions in the Guanidinium-Catalyzed Enantioselective Claisen Rearrangement. *J. Am. Chem. Soc.* **2011,** *133*, 5062-5075.

371. Neel, A. J.; Hilton, M. J.; Sigman, M. S.; Toste, F. D., Exploiting non-covalent π interactions for catalyst design. *Nature* **2017,** *543* (7647), 637-646.

372. Warshel, A.; Sharma, P. K.; Kato, M.; Xiang, Y.; Liu, H.; Olsso, M. H. M., Electrostatic Basis for Enzyme Catalysis. *Chem. Rev.* **2006,** *106*, 3210-3235.

373. Fried, S. D.; Bagchi, S.; Boxer, S. G., Extreme electric fields power catalysis in the active site of ketosteroid isomerase. *Science* **2014,** *346* (6216), 1510-1514.

374. Wu, Y.; Boxer, S. G., A Critical Test of the Electrostatic Contribution to Catalysis with Noncanonical Amino Acids in Ketosteroid Isomerase. *Journal of the American Chemical Society* **2016,** *138* (36), 11890-11895.

375. Lu, T.; Zhu, R.; An, Y.; Wheeler, S. E., Origin of Enantioselectivity in the Propargylation of Aromatic Aldehydes Catalyzed by Helical N-Oxides. *Journal of the American Chemical Society* **2012,** *134* (6), 3095-3102.

376. Nguyen, Q. N. N.; Lodewyk, M. W.; Bezer, S.; Gagné, M. R.; Waters, M. L.; Tantillo, D. J., Effects of Helix Macrodipole and Local Interactions on Catalysis of Acyl Transfer by α-Helical Peptides. *ACS Catal.* **2015,** *5* (3), 1617-1622.

377. Lee, K.; Silverio, D. L.; Torker, S.; Robbins, D. W.; Haeffner, F.; van der Mei, F. W.; Hoveyda, A. H., Catalytic enantioselective addition of organoboron reagents to fluoroketones controlled by electrostatic interactions. *Nat Chem* **2016,** *8* (8), 768-777.

378. Pattawong, O.; Mustard, T. J. L.; Johnston, R. C.; Cheong, P. H.-Y., Mechanism and Stereocontrol: Enantioselective Addition of Pyrrole to Ketenes Using Planar-Chiral Organocatalysts. *Angewandte Chemie International Edition* **2013,** *52* (5), 1420-1423.

379. Corey, E. J., Enantioselective Catalysis Based on Cationic Oxazaborolidines. *Angewandte Chemie International Edition* **2009,** *48* (12), 2100-2117.

380. Seguin, T. J.; Wheeler, S. E., Stacking and Electrostatic Interactions Drive the Stereoselectivity of Silylium-Ion Asymmetric Counteranion-Directed Catalysis. *Angewandte Chemie International Edition* **2016,** *55* (51), 15889-15893.

381. Doney, A. C.; Rooks, B. J.; Lu, T.; Wheeler, S. E., Design of Organocatalysts for Asymmetric Propargylations through Computational Screening. *ACS Catalysis* **2016,** *6* (11), 7948-7955.

382. Kennedy, C. R.; Guidera, J. A.; Jacobsen, E. N., Synergistic Ion-Binding Catalysis Demonstrated via an Enantioselective, Catalytic [2,3]-Wittig Rearrangement. *ACS Central Science* **2016,** *2* (6), 416-423.

383. Yamada, S.; Iwaoka, A.; Fujita, Y.; Tsuzuki, S., Tetraalkylammonium-Templated Stereoselective Norrish–Yang Cyclization. *Organic Letters* **2013,** *15* (23), 5994-5997.

384. Xiao, G.; Cintron-Rosado, G. A.; Glazier, D. A.; Xi, B.-m.; Liu, C.; Liu, P.; Tang, W., Catalytic Site-Selective Acylation of Carbohydrates Directed by Cation–n Interaction. *Journal of the American Chemical Society* **2017,** *139* (12), 4346-4349.

385. Holland, M. C.; Metternich, J. B.; Muck-Lichtenfeld, C.; Gilmour, R., Cation-[small pi] interactions in iminium ion activation: correlating quadrupole moment & enantioselectivity. *Chemical Communications* **2015,** *51* (25), 5322-5325.

386. Krenske, E. H.; Houk, K. N.; Harmata, M., Origin of Stereoselectivity in the (4 + 3) Cycloadditions of Chiral Alkoxy Siloxyallyl Cations with Furan. *Organic Letters* **2010,** *12* (3), 444-447.

387. Bandar, J. S.; Sauer, G. S.; Wulff, W. D.; Lambert, T. H.; Vetticatt, M. J., Transition State Analysis of Enantioselective Brønsted Base Catalysis by Chiral Cyclopropenimines. *Journal of the American Chemical Society* **2014,** *136* (30), 10700-10707.

388. Hong, L.; Sun, W.; Yang, D.; Li, G.; Wang, R., Additive Effects on Asymmetric Catalysis. *Chemical Reviews* **2016,** *116* (6), 4006-4123.

389. Barone, V.; Cossi, M., QUantum calculation of molecular energies and energy gradients in solution by a conductor solvent model. *J. Phys. Chem. A* **1998,** *102*, 1995-2001.

390. Cossi, M.; Rega, N.; Scalmani, G.; Barone, V., Energies, structures, and electronic properties of molecules in solution with the C-PCM solvation model. *J. Comp. Chem.* **2003,** *24*, 669-681.

391. Grimme, S., Supramolecular Binding Thermodynamics by Dispersion-Corrected Density Functional Theory. *Chem. Eur. J.* **2012,** *18* (32), 9955-9964.

392. Ess, D. H.; Houk, K. N., Theory of 1,3-Dipolar Cycloadditions: Distortion/Interaction and Frontier Molecular Orbital Models. *Journal of the American Chemical Society* **2008,** *130* (31), 10187-10198.

393. van Zeist, W.-J.; Bickelhaupt, F. M., The activation strain model of chemical reactivity. *Organic & Biomolecular Chemistry* **2010,** *8* (14), 3118-3127.

394. Bickelhaupt, F. M., Understanding reactivity with Kohn–Sham molecular orbital theory: E2–SN2 mechanistic spectrum and other concepts. *Journal of Computational Chemistry* **1999,** *20* (1), 114-128.

395. Lu, T.; Wheeler, S. E., Quantifying the Role of Anion−π Interactions in Anion−π Catalysis. *Org. Lett.* **2014,** *16*, 3268-3271.

396. Legault, C. Y. *CYLview, 1.0b*, Université de Sherbrooke: 2009.

397. Hwang, J.; Li, P.; Carroll, W. R.; Smith, M. D.; Pellechia, P. J.; Shimizu, K. D., Additivity of Substituent Effects in Aromatic Stacking Interactions. *Journal of the American Chemical Society* **2014,** *136* (40), 14060-14067.

398. Diaz de Villegas, M. D.; Galvez, J. A.; Etayo, P.; Badorrey, R.; Lopez-Ram-de-Viu, P., Recent advances in enantioselective organocatalyzed anhydride desymmetrization and its application to the synthesis of valuable enantiopure compounds. *Chemical Society Reviews* **2011,** *40* (11), 5564-5587.

399. Bull, J. A.; Croft, R. A.; Davis, O. A.; Doran, R.; Morgan, K. F., Oxetanes: Recent Advances in Synthesis, Reactivity, and Medicinal Chemistry. *Chemical Reviews* **2016,** *116* (19), 12150-12233.

400. Yin, Q.; You, S.-L., Asymmetric Chlorination/Ring Expansion for the Synthesis of α-Quaternary Cycloalkanones. *Organic Letters* **2014,** *16* (6), 1810-1813.

401. Chen, Z.; Wang, Z.; Sun, J., Catalytic Enantioselective Synthesis of Tetrahydroisoquinolines and Their Analogues Bearing a C4 Stereocenter: Formal Synthesis of (+)-(8S,13R)-Cyclocelabenzine. *Chemistry – A European Journal* **2013,** *19* (26), 8426-8430.

402. Chen, Z.; Wang, B.; Wang, Z.; Zhu, G.; Sun, J., Complex Bioactive Alkaloid-Type Polycycles through Efficient Catalytic Asymmetric Multicomponent Aza-Diels–Alder Reaction of Indoles with Oxetane as Directing Group. *Angewandte Chemie International Edition* **2013,** *52* (7), 2027-2031.

403. Yadav, J. S.; Singh, V. K.; Srihari, P., Formation of Substituted Tetrahydropyrans through Oxetane Ring Opening: Application to the Synthesis of C1–C17 Fragment of Salinomycin. *Organic Letters* **2014,** *16* (3), 836-839.

404. Gronnier, C.; Kramer, S.; Odabachian, Y.; Gagosz, F., Cu(I)-Catalyzed Oxidative Cyclization of Alkynyl Oxiranes and Oxetanes. *Journal of the American Chemical Society* **2012,** *134* (2), 828-831.

405. Ruider, S. A.; Müller, S.; Carreira, E. M., Ring Expansion of 3-Oxetanone-Derived Spirocycles: Facile Synthesis of Saturated Nitrogen Heterocycles. *Angewandte Chemie International Edition* **2013,** *52* (45), 11908-11911.

406. Mizuno, M.; Kanai, M.; Iida, A.; Tomioka, K., An external chiral ligand controlled enantioselective opening of oxirane and oxetane by organolithiums. *Tetrahedron* **1997,** *53* (31), 10699-10708.

407. Straker, R. N.; Peng, Q.; Mekareeya, A.; Paton, R. S.; Anderson, E. A., Computational ligand design in enantio- and diastereoselective ynamide [lsqb]5+2[rsqb] cycloisomerization. *Nat Commun* **2016,** *7*.

408. Yamanaka, M.; Itoh, J.; Fuchibe, K.; Akiyama, T., Chiral Brønsted Acid Catalyzed Enantioselective Mannich-Type Reaction. *J. Am. Chem. Soc.* **2007,** *129*, 6756-6764.

409. Simón, L.; Goodman, J. M., Theoretical Study of the Mechanism of Hantzsch Ester Hydrogenation of Imines Catalyzed by Chiral BINOL-Phosphoric Acids. *J. Am. Chem. Soc.* **2008,** *130*, 8741-8747.

410. Yamanaka, M.; Hirata, T., DFT Study on Bifunctional Chiral Brønsted Acid-Catalyzed Asymmetric Hydrophosphonylation of Imines. *J. Org. Chem.* **2009,** *74*, 3266-3271.

411. Simón, L.; Goodman, J. M., Mechanism of BINOL−Phosphoric Acid-Catalyzed Strecker Reaction of Benzyl Imines. *J. Am. Chem. Soc.* **2009,** *131*, 4070-4077.

412. Overvoorde, L. M.; Grayson, M. N.; Luo, Y.; Goodman, J. M., Mechanistic Insights into a BINOL-Derived Phosphoric Acid-Catalyzed Asymmetric Pictet–Spengler Reaction. *The Journal of Organic Chemistry* **2015,** *80* (5), 2634-2640.

413. Greindl, J.; Hioe, J.; Sorgenfrei, N.; Morana, F.; Gschwind, R. M., Brønsted Acid Catalysis—Structural Preferences and Mobility in Imine/Phosphoric Acid Complexes. *Journal of the American Chemical Society* **2016**.

414. Sorgenfrei, N.; Hioe, J.; Greindl, J.; Rothermel, K.; Morana, F.; Lokesh, N.; Gschwind, R. M., NMR Spectroscopic Characterization of Charge Assisted Strong Hydrogen Bonds in Brønsted Acid Catalysis. *Journal of the American Chemical Society* **2016,** *138* (50), 16345-16354.

415. Fleischmann, M.; Drettwan, D.; Sugiono, E.; Rueping, M.; Gschwind, R. M., Brønsted Acid Catalysis: Hydrogen Bonding versus Ion Pairing in Imine Activation. *Angewandte Chemie International Edition* **2011,** *50* (28), 6364-6369.

416. Akiyama, T., Stronger Brønsted Acids. *Chemical Reviews* **2007,** *107* (12), 5744-5758.

417. Reid, J. P.; Goodman, J. M., Goldilocks Catalysts: Computational Insights Into The Role Of The 3, 3' Substituents On The Selectivity of BINOL-derived Phosphoric Acid Catalysts. *Journal of the American Chemical Society* **2016**.

418. Grayson, M. N.; Pellegrinet, S. C.; Goodman, J. M., Mechanistic Insights into the BINOL-Derived Phosphoric Acid-Catalyzed Asymmetric Allylboration of Aldehydes. *J. Am. Chem. Soc.* **2012,** *134*, 2716-2722.

419. Neel, A. J.; Hehn, J. P.; Tripet, P. F.; Toste, F. D., Asymmetric Cross-Dehydrogenative Coupling Enabled by the Design and Application of Chiral Triazole-Containing Phosphoric Acids. *J. Am. Chem. Soc.* **2013,** *135*, 14044-14047.

420. Grayson, M. N.; Goodman, J. M., Understanding the Mechanism of the Asymmetric Propargylation of Aldehydes Promoted by 1,1′-Bi-2-naphthol-Derived Catalysts. *J. Am. Chem. Soc.* **2013,** *135*, 6142-6148.

421. Jindal, G.; Sunoj, R. B., Axially Chiral Imidodiphosphoric Acid Catalyst for Asymmetric Sulfoxidation Reaction: Insights on Asymmetric Induction. *Angew. Chem., Int. Ed. Engl.* **2014,** *53*, 4432-4436.

422. Kanomata, K.; Toda, Y.; Shibata, Y.; Yamanaka, M.; Tsuzuki, S.; Gridnev, I. D.; Terada, M., Secondary stereocontrolling interactions in chiral Brønsted acid catalysis: study of a Petasis-Ferrier-type rearrangement catalyzed by chiral phosphoric acids. *Chem. Sci.* **2014,** *5*, 3515-3523.

423. Ajitha, M. J.; Huang, K.-W., Role of keto–enol tautomerization in a chiral phosphoric acid catalyzed asymmetric thiocarboxylysis of meso-epoxide: a DFT study. *Org. Biomol. Chem.* **2015,** *13*, 10981-10985.

424. Simon, L.; Paton, R. S., QM/MM study on the enantioselectivity of spiroacetalization catalysed by an imidodiphosphoric acid catalyst: how confinement works. *Organic & Biomolecular Chemistry* **2016,** *14* (11), 3031-3039.

425. Wang, Z.; Chen, Z.; Sun, J., Catalytic Enantioselective Intermolecular Desymmetrization of 3-Substituted Oxetanes. *Angew. Chem. Int. Ed.* **2013,** *52* (26), 6685-6688.

426. Yang, W.; Wang, Z.; Sun, J., Enantioselective Oxetane Ring Opening with Chloride: Unusual Use of Wet Molecular Sieves for the Controlled Release of HCl. *Angewandte Chemie International Edition* **2016,** *55* (24), 6954-6958.

427. Yang, W.; Sun, J., Organocatalytic Enantioselective Synthesis of 1,4-Dioxanes and Other Oxa-Heterocycles by Oxetane Desymmetrization. *Angewandte Chemie International Edition* **2016,** *55* (5), 1868-1871.

428. Rodríguez, E.; Grayson, M. N.; Asensio, A.; Barrio, P.; Houk, K. N.; Fustero, S., Chiral Brønsted Acid-Catalyzed Asymmetric Allyl(propargyl)boration Reaction of ortho-Alkynyl Benzaldehydes: Synthetic Applications and Factors Governing the Enantioselectivity. *ACS Catalysis* **2016**, 2506-2514.

429. Washington, I.; Houk, K. N., CH···O Hydrogen Bonding Influences π-Facial Stereoselective Epoxidations. *Angewandte Chemie International Edition* **2001,** *40* (23), 4485-4488.

430. Marenich, A. V.; Cramer, C. J.; Truhlar, D. G., Universal Solvation Model Based on Solute Electron Density and on a Continuum Model of the Solvent Defined by the

Bulk Dielectric Constant and Atomic Surface Tensions. *The Journal of Physical Chemistry B* **2009,** *113* (18), 6378-6396.

431. Grimme, S., Supramolecular Binding Thermodynamics by Dispersion-Corrected Density Functional Theory. *Chemistry- A European Journal* **2012,** *18* (32), 9955-9964.

432. Diphenylphosphoric acid as a model catalyst resulted in similar results concerning the relative energies of these three activation modes.

433. Gridnev, I.; Kouchi, M.; Sorimachi, K.; Terada, M., On the mechanism of stereoselection in direct Mannich reaction catalyzed by BINOL-derived phosphoric acids. *Tetrahedron Lett.* **2007,** *48*, 497-500.

434. Kim, H.; Sugiono, E.; Nagata, Y.; Wagner, M.; Bonn, M.; Rueping, M.; Hunger, J., Role of Ion-Pairs in Brønsted Acid Catalysis. *ACS Catalysis* **2015,** *5* (11), 6630-6633.

435. Merten, C.; Pollok, C. H.; Liao, S.; List, B., Stereochemical Communication within a Chiral Ion Pair Catalyst. *Angewandte Chemie International Edition* **2015,** *54* (30), 8841-8845.

436. Cook, T. C.; Andrus, M. B.; Ess, D. H., Quantum Mechanical Transition-State Analysis Reveals the Precise Origin of Stereoselectivity in Chiral Quaternary Cinchonidinium Phase-Transfer Catalyzed Enolate Allylation. *Organic Letters* **2012,** *14* (23), 5836-5839.

437. Paton, R. S., Dissecting non-covalent interactions in oxazaborolidinium catalyzed cycloadditions of maleimides. *Organic & Biomolecular Chemistry* **2014,** *12* (11), 1717-1720.

438. Knowles, R. R.; Jacobsen, E. N., Attractive noncovalent interactions in asymmetric catalysis: Links between enzymes and small molecule catalysts. *Proceedings of the National Academy of Sciences* **2010,** *107* (48), 20678-20685.

439. Uyeda, C.; Jacobsen, E. N., Transition-State Charge Stabilization through Multiple Non-covalent Interactions in the Guanidinium-Catalyzed Enantioselective Claisen Rearrangement. *Journal of the American Chemical Society* **2011,** *133* (13), 5062-5075.

440. Kennedy, C. R.; Lin, S.; Jacobsen, E. N., The Cation–π Interaction in Small-Molecule Catalysis. *Angewandte Chemie International Edition* **2016**, n/a-n/a.

441. Lau, V. M.; Gorin, C. F.; Kanan, M. W., Electrostatic control of regioselectivity via ion pairing in a Au(i)-catalyzed rearrangement. *Chem. Sci.* **2014,** *5*, 4975-4979.

442. Lau, V. M.; Pfalzgraff, W. C.; Markland, T. E.; Kanan, M. W., Electrostatic Control of Regioselectivity in Au(I)-Catalyzed Hydroarylation. *J. Am. Chem. Soc.* **2017,** *139*, 4035-4041.

443. Shinisha, C. B.; Sunoj, R. B., On the Origins of Kinetic Resolution of Cyclohexane-1,2-diols Through Stereoselective Acylation by Chiral Tetrapeptides. *Organic Letters* **2009,** *11* (15), 3242-3245.

444. Mesas-Sánchez, L.; Dinér, P., A Mechanistic Investigation of the Kinetic Resolution of Secondary Aromatic Alcohols Using a Ferrocene-Based Planar Chiral 4-(Dimethylamino)pyridine Catalyst. *Chemistry – A European Journal* **2015,** *21* (14), 5623-5631.

445. Vedejs, E.; Jure, M., Efficiency in Nonenzymatic Kinetic Resolution. *Angewandte Chemie International Edition* **2005,** *44* (26), 3974-4001.

446. Spivey, A. C.; Fekner, T.; Spey, S. E., Axially Chiral Analogues of 4-(Dimethylamino)pyridine: Novel Catalysts for Nonenzymatic Enantioselective Acylations. *The Journal of Organic Chemistry* **2000,** *65* (10), 3154-3159.

447. Maji, R.; Wheeler, S. E., Importance of Electrostatic Effects in the Stereoselectivity of NHC-Catalyzed Kinetic Resolutions. *Journal of the American Chemical Society* **2017,** *139* (36), 12441-12449.

448. Ma, G.; Deng, J.; Sibi, M. P., Fluxionally Chiral DMAP Catalysts: Kinetic Resolution of Axially Chiral Biaryl Compounds. *Angewandte Chemie* **2014,** *126* (44), 12012-12015.

449. Liu, P.; Yang, X.; Birman, V. B.; Houk, K. N., Origin of Enantioselectivity in Benzotetramisole-Catalyzed Dynamic Kinetic Resolution of Azlactones. *Organic Letters* **2012,** *14* (13), 3288-3291.

450. Liao, R.-Z.; Santoro, S.; Gotsev, M.; Marcelli, T.; Himo, F., Origins of Stereoselectivity in Peptide-Catalyzed Kinetic Resolution of Alcohols. *ACS Catalysis* **2016,** *6* (2), 1165-1171.

451. Pellissier, H., Organocatalyzed Dynamic Kinetic Resolution. *Advanced Synthesis & Catalysis* **2011,** *353* (5), 659-676.

452. Yang, X.; Liu, P.; Houk, K. N.; Birman, V. B., Manifestation of Felkin–Anh Control in Enantioselective Acyl Transfer Catalysis: Kinetic Resolution of Carboxylic Acids. *Angewandte Chemie* **2012,** *124* (38), 9776-9780.

453. Gaussian 09, Revision D.01, Frisch, M. J., et al. Gaussian, Inc., Wallingford CT, 2009

454. Kruse, H.; Goerigk, L.; Grimme, S., Why the Standard B3LYP/6-31G* Model Chemistry Should Not Be Used in DFT Calculations of Molecular Thermochemistry: Understanding and Correcting the Problem. *The Journal of Organic Chemistry* **2012,** *77* (23), 10824-10834.

455. We thank Prof. M.P.Sibi for sharing the crystal structure as well as for insightful discussions

456. Yamada, S.; Inoue, M., Regio- and Stereoselective Addition of Allylmetal Reagents to Pyridinium−π and Quinolinium−π Complexes. *Organic Letters* **2007,** *9* (8), 1477-1480.

457. Yamada, S., Intramolecular cation-[small pi] interaction in organic synthesis. *Organic & Biomolecular Chemistry* **2007,** *5* (18), 2903-2912.

458. Kennedy, C. R.; Lin, S.; Jacobsen, E. N., The Cation–π Interaction in Small-Molecule Catalysis. *Angewandte Chemie International Edition* **2016,** *55* (41), 12596-12624.

459. Gutierrez, O.; Aubé, J.; Tantillo, D. J., Mechanism of the Acid-Promoted Intramolecular Schmidt Reaction: Theoretical Assessment of the Importance of Lone Pair–Cation, Cation−π, and Steric Effects in Controlling Regioselectivity. *The Journal of Organic Chemistry* **2012,** *77* (1), 640-647.

460. Krenske, E. H., Origins of Aryl Substituent Effects on the Stereoselectivities of Additions of Silyl Enol Ethers to a Chiral Oxazolinium Ion. *Organic Letters* **2011,** *13* (24), 6572-6575.

461. Driver, R. W.; Claridge, T. D. W.; Scheiner, S.; Smith, M. D., Torsional and Electronic Factors Control the C−H···O Interaction. *Chemistry – A European Journal* **2016,** *22* (46), 16513-16521.

462. Xu, S.; Held, I.; Kempf, B.; Mayr, H.; Steglich, W.; Zipse, H., The DMAP-Catalyzed Acetylation of Alcohols—A Mechanistic Study (DMAP=4-(Dimethylamino)pyridine). *Chemistry – A European Journal* **2005,** *11* (16), 4751-4757.

463. Larionov, E.; Mahesh, M.; Spivey, A. C.; Wei, Y.; Zipse, H., Theoretical Prediction of Selectivity in Kinetic Resolution of Secondary Alcohols Catalyzed by Chiral DMAP Derivatives. *Journal of the American Chemical Society* **2012,** *134* (22), 9390-9399.

464. Bonduelle, C.; Martín-Vaca, B.; Cossío, F. P.; Bourissou, D., Monomer versus Alcohol Activation in the 4-Dimethylaminopyridine-Catalyzed Ring-Opening Polymerization of Lactide and Lactic O-Carboxylic Anhydride. *Chemistry – A European Journal* **2008,** *14* (17), 5304-5312.

465. During our initial study on fluxionality we not only observed the superior performance of B97D and MO6-2X functionals also noticed a close similarity between M06-2X method with M06-2X/6-311+G(d,p)//B97-D/TZV(2d,2p). Hence we decided to use the later method to determine the overall reaction energetics in order to have computational expediency.

466. Spivey, A. C.; Arseniyadis, S., Nucleophilic Catalysis by 4-(Dialkylamino)pyridines Revisited—The Search for Optimal Reactivity and Selectivity. *Angewandte Chemie International Edition* **2004,** *43* (41), 5436-5441.

467. We also used other methods and basis set to evaluate energy profile of the reaction and reached in similar conclusion.

468. Grabowski, S. J., A new measure of hydrogen bonding strength – ab initio and atoms in molecules studies. *Chemical Physics Letters* **2001,** *338* (4–6), 361-366.

469. Xue, X.-S.; Li, X.; Yu, A.; Yang, C.; Song, C.; Cheng, J.-P., Mechanism and Selectivity of Bioinspired Cinchona Alkaloid Derivatives Catalyzed Asymmetric Olefin Isomerization: A Computational Study. *Journal of the American Chemical Society* **2013,** *135* (20), 7462-7473.

470. Raju, R. K.; Bloom, J. W. G.; An, Y.; Wheeler, S. E., Substituent Effects on Non-Covalent Interactions with Aromatic Rings: Insights from Computational Chemistry. *ChemPhysChem* **2011,** *12* (17), 3116-3130.

471. Wheeler, S. E., Understanding Substituent Effects in Noncovalent Interactions Involving Aromatic Rings. *Accounts of Chemical Research* **2013,** *46* (4), 1029-1038.

472. Davies, D. L.; Macgregor, S. A.; McMullin, C. L., Computational Studies of Carboxylate-Assisted C–H Activation and Functionalization at Group 8–10 Transition Metal Centers. *Chemical Reviews* **2017,** *117* (13), 8649-8709.

APPENDIX A

Computational Details

Table A-1. Free energy corrections (hartrees), absolute energies (hartrees), total absolute free energies (hartrees), and relative free energies (kcal/mol) for the main configurations of **TS4**(zwitterionic pathway) for the KR of **4** catalyzed by **3** computed at five levels of theory (all using CPCM to model the solvent, DCM).

Configuration	Quasi-RRHO Free Energy Correction	Energy	Total Free Energy	Relative Free Energy (kcal/mol)
M06-2X/6-311+G(*d*,*p*)//B97-D/TZV(2*d*,2*p*)				
S(*si*)	0.643215	-2165.0206	-2164.377385	0
S(*re*)	0.641604	-2165.018027	-2164.376423	0.60
R(*si*)	0.642713	-2165.014681	-2164.371968	3.39
R(*re*)	0.643263	-2165.018687	-2164.375424	1.23
M06-2X/6-311+G(*d*,*p*)//B3LYP/6-31+G(*d*)				
S(*si*)	0.660928	-2165.015281	-2164.354353	0
S(*re*)	0.661384	-2165.014052	-2164.352668	1.05
R(*si*)	0.660792	-2165.005616	-2164.344824	5.97
R(*re*)	0.661886	-2165.012868	-2164.350982	2.11
M06-2X/6-311+G(*d*,*p*)//B3LYP-D3/6-31+G(*d*)				
S(*si*)	0.666331	-2165.022565	-2164.356234	0
S(*re*)	0.665738	-2165.019277	-2164.353539	1.69
R(*si*)	0.665382	-2165.016901	-2164.351519	2.95
R(*re*)	0.666477	-2165.02126	-2164.354783	0.91

M06-2X/6-311+G(*d*,*p*)//wB97X-D/6-31+G(*d*)				
S(*si*)	0.676567	-2165.025826	-2164.349259	0
S(*re*)	0.675567	-2165.022611	-2164.347044	1.38
R(*si*)	0.675554	-2165.01916	-2164.343606	3.54
R(*re*)	0.676561	-2165.024725	-2164.348164	0.86
M06-2X/6-311+G(*d*,*p*)//M06-2X/6-31+G(*d*)				
S(*si*)	0.673979	-2165.026055	-2164.352076	0
S(*re*)	0.674033	-2165.022432	-2164.348399	2.30
R(*si*)	0.673478	-2165.019839	-2164.346361	3.58
R(*re*)	0.675274	-2165.025207	-2164.349933	1.34

Table A-2. Relative free energies, Boltzmann-weighted free energy differences for formation of the major and minor stereoisomers, and theoretical S values in the KR of **4** catalyzed by **3** at five levels of theory.

Method	S(*si*)	S(*re*)	R(*si*)	R(*re*)	$\Delta\Delta G^{\ddagger}$	Theoretical S
M06-2X/6-311+G(*d*,*p*)//B97-D/TZV(2*d*,2*p*)	0	0.60	3.39	1.23	1.40	10.7
M06-2X/6-311+G(*d*,*p*)//B3LYP/6-31+G(*d*)	0	1.05	5.97	2.11	2.20	41.6
M06-2X/6-311+G(*d*,*p*)//B3LYP-D3/6-31+G(*d*)	0	1.69	2.95	0.91	0.92	4.8
M06-2X/6-311+G(*d*,*p*)//wB97xD/6-31+G(*d*)	0	1.38	3.54	0.86	0.91	4.7
M06-2X/6-311+G(*d*,*p*)//M06-2X/6-31+G(*d*)	0	2.30	3.58	1.34	1.34	9.7

Analyzing Steric environment around two key TS of Substrate 6

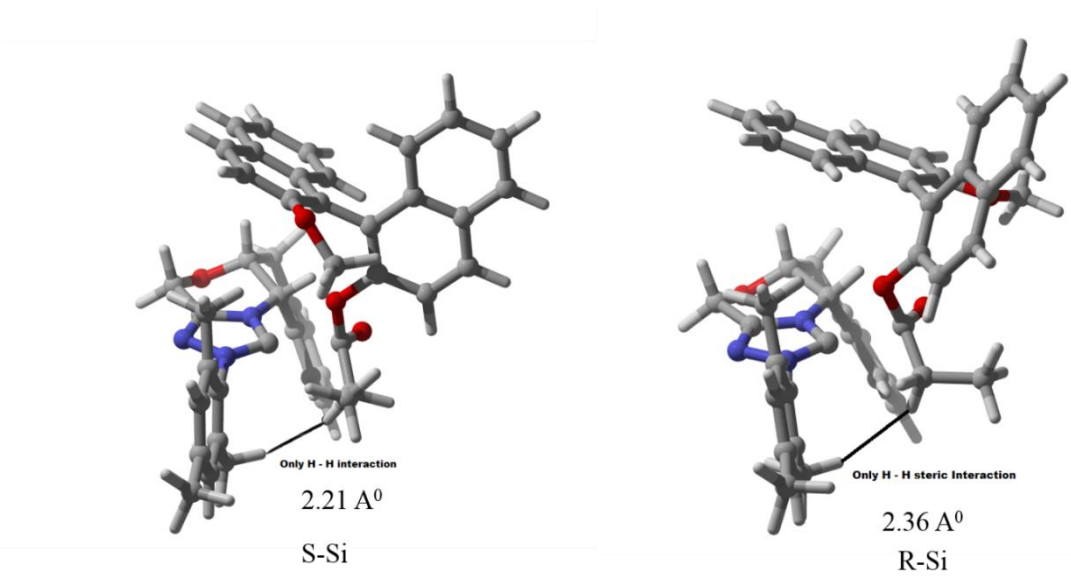

Figure A1**.** Analyzing Steric environment around two key TS of Substrate 6

Unfavorable steric interactions in the stereocontrolling TS structures for the KR of 6 catalyzed by 3 has shown in the figure above. It is clearly evident from this analysis that both TS have similar steric environment.

Identification of Non-Covalent Interactions using AIM for Substrate 5

The presence of a bond critical point between a pair of atoms is generally regarded as an indicator of interatomic non-covalent interaction in the AIM formalism and the value of electron densities (ρ) at such bond critical points correlates with the strength of interaction.

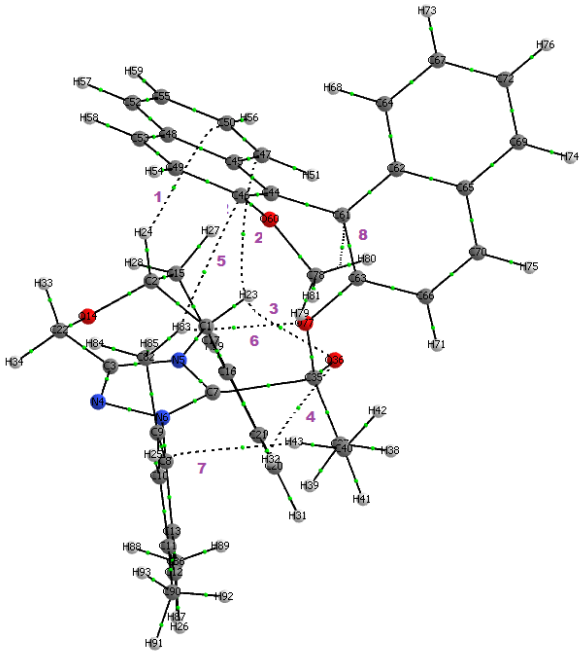

Table A-3. Electron densities at the bond critical points for the S(*si*) in the KR of 5.

BCP index	Non covalent Interactions S(*si*)	x 10^{-2} (a.u)			
		ρ	^{2}ρ	V	K
1	C-H(NHC cat) ···π (of OME_BINOL)	0.5101	1.326	-0.2298	-0.0509
2	C-H(NHC cat) ···π (of OME_BINOL)	0.2942	0.7725	-0.1258	-0.0337
3	(C=O) ···C-H(NHC cat)	1.4651	5.3378	-0.9941	-0.1702
4	(C=O) ···C-H(NHC cat)	0.732	2.5538	-0.4563	-0.0911
5	CH_3 of Mesityl···π (OME_BINOL)	0.5177	1.3874	-0.2419	-0.0525
6	CH_3 of Mesityl···O^- (OME_BINOL)	0.3946	1.3284	-0.2251	-0.0535
7	C-H(Ethyl) ···π (of Mesityl)	0.8431	2.3393	-0.4143	-0.0852
8	CH_3 (OME_BINOL) ···π (OME_BINOL)	1.1358	4.0054	-0.7069	-0.1472

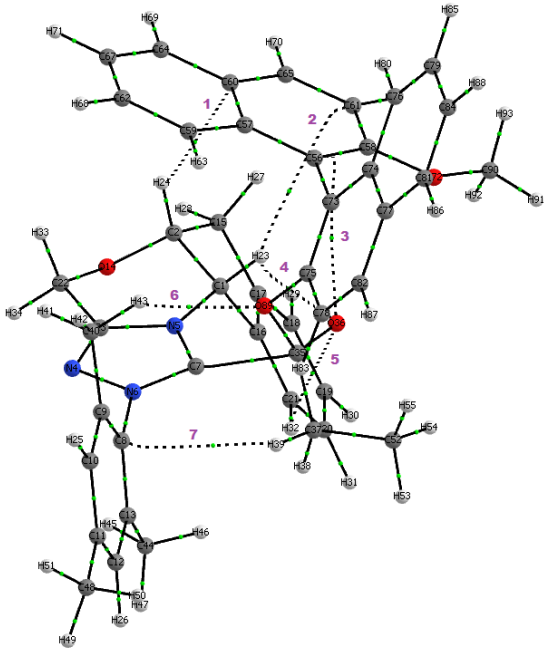

Table A-4. Electron densities at the bond critical points for the R(*si*) in the KR of **5.**

BCP index	Non covalent Interactions R(*si*)	x 10^{-2} (a.u)			
		ρ	^{2}ρ	V	K
1	C-H(NHC cat) ···π (of OME_BINOL)	0.2772	0.7642	-0.1266	-0.0322
2	C-H(NHC cat) ···π (of OME_BINOL)	0.2568	0.7106	-0.1213	-0.0282
3	lp (O) ···π (of OME_BINOL)	0.5666	1.7622	-0.3146	-0.063
4	(C=O) ···C-H(NHC cat)	1.3319	4.7195	-0.877	-0.1515
5	(C=O) ···C-H(NHC cat)	0.5389	1.8447	-0.3185	-0.0713
6	CH_3 of Mesityl···O^- (OME_BINOL)	0.9663	3.116	-0.5983	-0.0903
7	C-H(Ethyl) ···π (of Mesityl)	0.6288	1.7131	-0.3043	-0.062

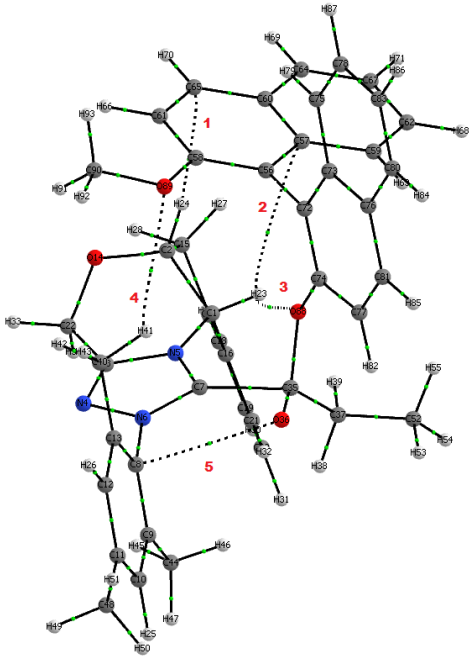

Table A-5. Electron densities at the bond critical points for the S(*re*) in the KR of 5.

BCP index	Non covalent Interactions S(*re*)	x 10^{-2} (a.u)			
		ρ	^{2}ρ	V	K
1	C-H(NHC cat) ···π (of OME_BINOL)	0.7378	2.0271	-0.3481	-0.0793
2	C-H(NHC cat) ···π (of OME_BINOL)	0.1641	0.5274	-0.0731	-0.0294
3	C-H(NHC cat) ···O^{-} (OME_BINOL)	0.5115	1.7897	-0.3279	-0.0598
4	CH_3 of Mesityl ···OMe of Substrate	0.4478	1.5224	-0.2699	-0.0553
5	(C=O) ···π (of Mesityl)	0.9684	3.1884	-0.6308	-0.0832

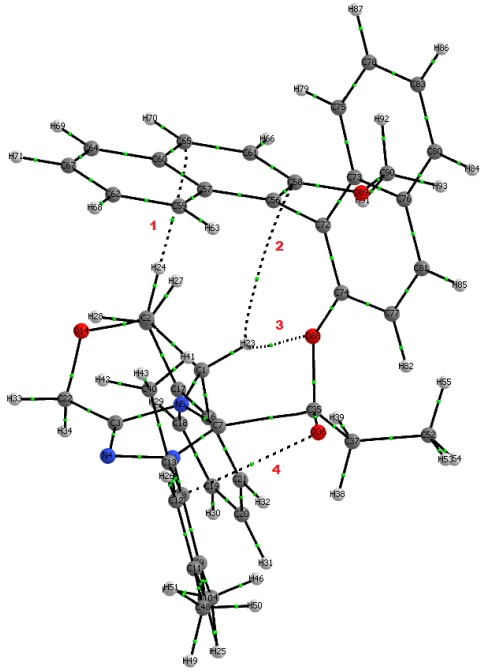

Table A-6. Electron densities at the bond critical points for the R(*re*) in the KR of 5.

BCP index	Non covalent Interactions R(*re*)	x 10^{-2} (a.u)			
		ρ	^{2}ρ	V	K
1	C-H(NHC cat) ···π (of OME_BINOL)	0.7657	2.0896	-0.3583	-0.082
2	C-H(NHC cat) ···π (of OME_BINOL)	0.1844	0.5585	-0.0819	-0.0289
3	C-H(NHC cat) ···O^{-} (OME_BINOL)	0.5307	1.8252	-0.3371	-0.0596
4	(C=O) ···π (of Mesityl)	0.9569	3.1482	-0.6214	-0.0828

Conformations

For all computations, special care has been taken to systematically search for all accessible conformations. In particular, we considered three main conformations generated by rotations about the bond to the α chiral center of the aldehyde. Denoted by A, B, and C. For each of these main conformations, additional conformers were considered arising from other rotations about single bonds; only the lowest conformation from each classis reported.

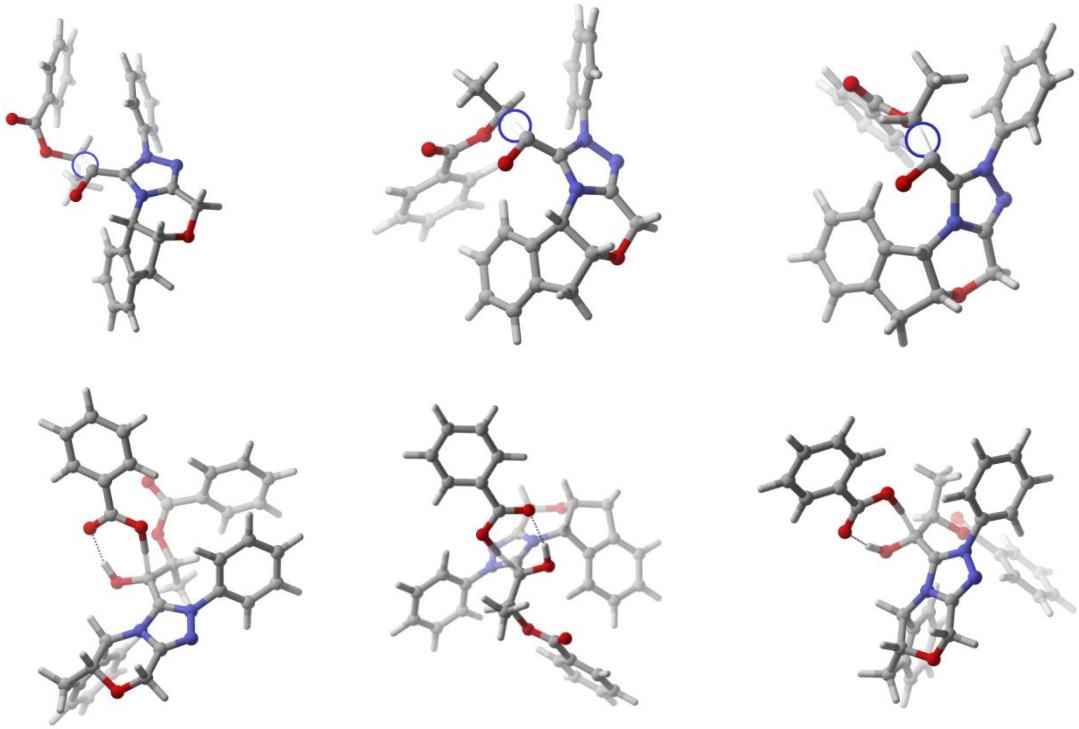

A B C

Major conformations of the activated catalyst both with (bottom row) and without (top row) BzOH (Ar = Ph).

APPENDIX B

Computational Details

Conformations

For all computations, special care has been taken to systematically search for all accessible conformations. In particular, we considered four main conformations generated by rotations about the bond of the Aryl side chain (pyrenyl groups) of the phosphoric acid moiety which is denoted by A, B, C and D.

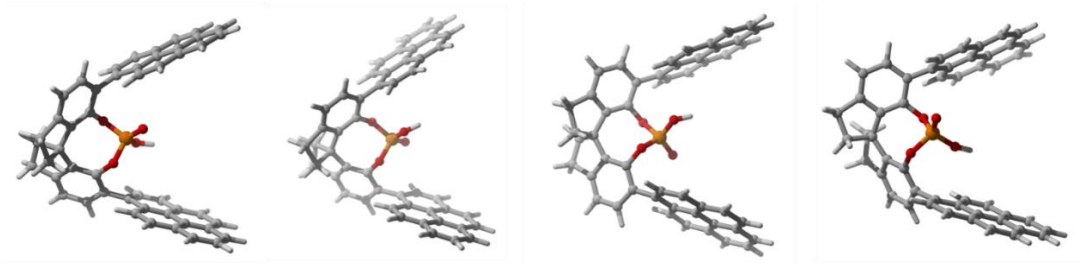

A B C D

Figure B1: Different Conformations (A-D) of prenyl groups considered in this study. Conformer A-D originates from rotation around the C-C bond between the SPINOL core and the Aryl side chain (pyrenyl). These are the four low lying conformers of the catalyst.

Table B-1. Comparison between BA and OA activation mode using different DFT methods

Method	**$\Delta\Delta E^{\ddagger}$ (Mode BA)**	**$\Delta\Delta E^{\ddagger}$ (Mode OA)**
Single point energy difference between two different activation mode using different levels of theory for Reaction 1 catalyzed by **PA-2**.*(Only Major isomer shown)*		
M06-2X/6-311+G(d,p)	3.3	0.0
wB97XD/6-311+G(d,p)	3.2	0.0
B3LYP-D3/6-311+G(d,p)	2.2	0.0
Single point energy difference between two different activation mode using different levels of theory for Reaction 1 catalyzed by **PA-3**.*(Only Major isomer shown)*		
M06-2X/6-311+G(d,p)	2.9	0.0
wB97XD/6-311+G(d,p)	3.1	0.0
B3LYP-D3/6-311+G(d,p)	1.7	0.0

Conclusion: For both PA-2 and PA-3, Mode-OA is favored over Mode-BA regardless of the DFT method employed.

Table B-2. Overall Energy Diagram for Substrate-1

		B97D-Quasi RRHO corrections to Gibbs Free Energy	M06-2X/6-311+G(d,p) single_pt (In solution)	Δ G(TS) Final	Relative Energy wrt. Free Reactant (kcal/mol)
Individual Fragment	Model PA catalyst (PA-1)	0.068638	-722.7243513	-722.6557133	
	SPINOL based PA (PA-2)	0.581969	-2528.079878	-2527.497909	
	BINOL based PA (PA-3)	0.575191	-2641.191211	-2640.61602	
	Oxetane 1	0.140746	-461.4259246	-461.2851786	
Uncatalyzed pathway					
Uncatalyzed Pathway	TS for desymmetrization for Oxetane 1	0.141473	-461.3511559	-461.2096829	47.3
Model PA catalyzed(PA-1) pathway					
Model PA catalyst(PA-1)	Most stable TS for desymmetrization for Oxetane 1 (corresponds to Mode OA)	0.235526	-1184.127599	-1183.892073	30.6
SPINOL based PA catalyzed(PA-2) pathway					
Reference Point	Reactant(Oxetane 1 + PA-2)	0.140746	-461.4259246	-461.2851786	0
	Product (Dioxane + PA-2)	0.144438	-461.4626791	-461.3182411	-20.74
Major Isomer	Rct. Complex for desymmetrization (PRC)	0.751693	-2989.536193	-2988.7845	-0.9
	TS desymmetrization for Oxetane 1(corresponds to Mode OA)	0.75416	-2989.500504	-2988.746344	23.0
	Pdt. Complex after desymmetrization (PC)	0.756655	-2989.529334	-2988.772679	-20.50

Representative Energy Diagram for PA-2 catalyzed transformation of Substrate 1

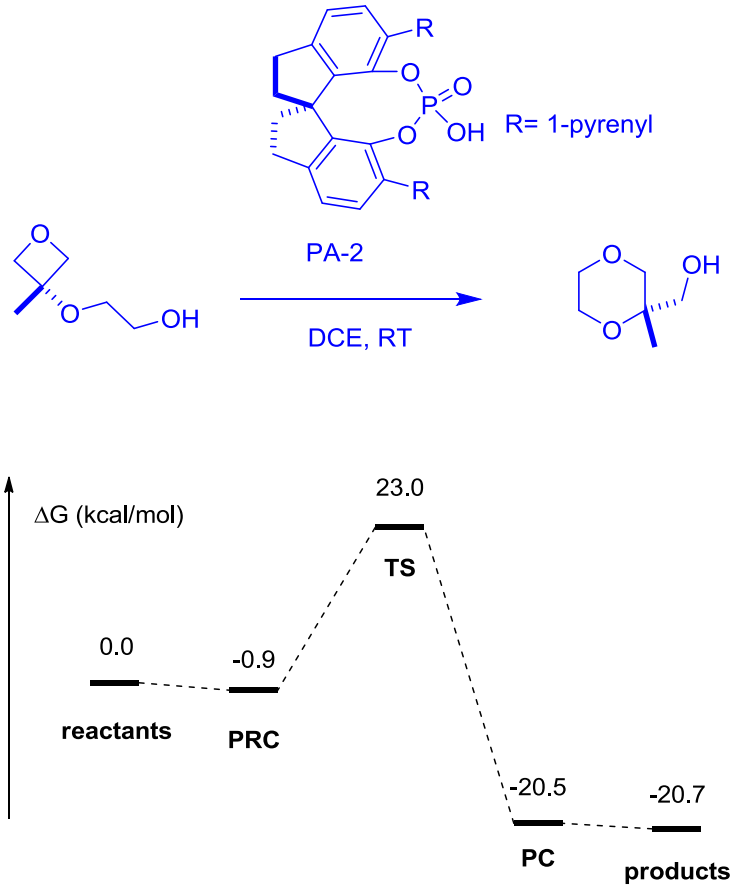

Figure B2. Relative Gibbs free energies (in kcal/mol) of different activation modes for PA-2 catalyzed ring opening of oxetane 1

Entry	**Major**	**Minor**
2	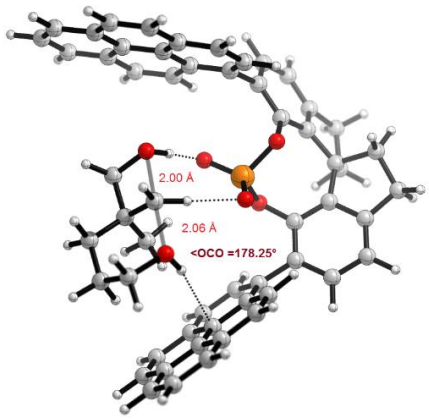	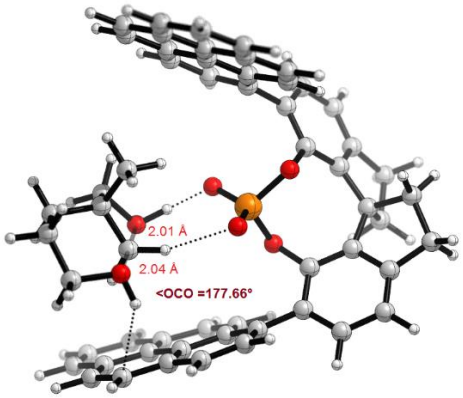
4	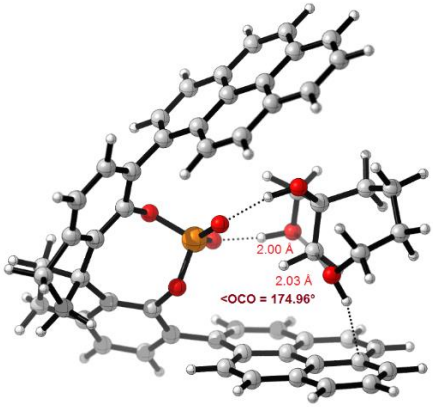	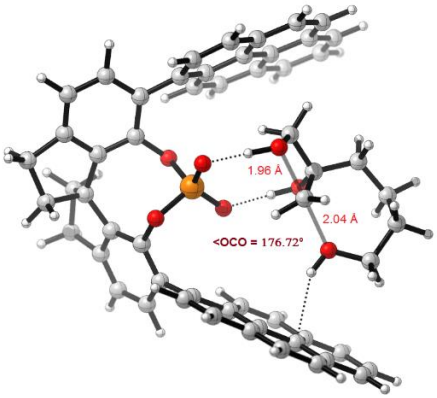

Figure B3. Conformational searches for lowest-lying transition states

APPENDIX C

Computational Details

Conformational searches for lowest-lying transition states

For each reaction/catalyst combination, we considered all reasonable conformations in order to identify the lowest-lying (R,R) and (S,S) transition states. Similarly, the 5-OMe substituent of the nucleophile in equation 3.1 can exist in two conformations, both of which were considered for each transition state for each catalyst. Finally, there are a number of ways of orientating the nucleophile and electrophile within the binding site of the catalyst. That is, in addition to the most favorable orientation depicted in Figure III-2 of Chapter III, additional TS(S,S) configurations were considered in which the substrates were rotated 90 degrees to take advantage of the same electrostatic stabilization discussed in the paper. However, these orientations were always less favorable.

Comparison of predicted er values from different DFT methods

Data presented in Chapter III were computed at the B97-D3/def2-TZVP//PCM-B97-D/def2-TZVP level of theory using quasi-RRHO free energy corrections. However, for comparisons, we also predicted er values for the reaction/catalyst combinations for which experimental data are available using wB97X-D/6-311+G(d,p)//wB97X-D/6-31G(d) and M06-2X/6-311+G(d,p)//M06-2X/6-31G(d) using both RRHO and quasi-RRHO free energy corrections. The corresponding data is listed below, where "B97D" denotes B97-D3/def2-TZVP//PCM-B97-D/def2-TZVP, "wB97XD" denotes wB97X-D/6-311+G(d,p)//wB97X-D/6-31G(d), and "M06-2X" denotes M06-2X/6-

311+G(d,p)//M06-2X/6-31G(d). All computations used PCM to account for solvent effects.

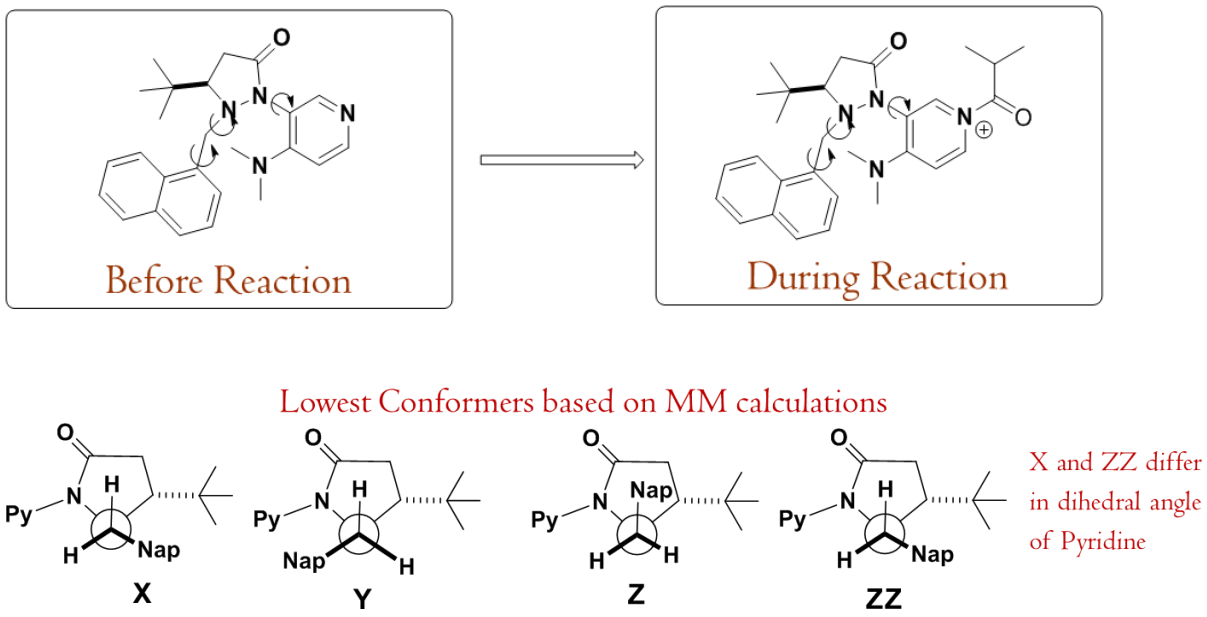

Figure C1. Key Lowest lying catalyst conformers obtained after MM search.

Table C-1**.** Energetic Ordering of key conformers using DFT methods.

Method	Conformers (Before Acylation)			Relative Population X :Y: ZZ	Conformers (After Acylation)			Relative Population X′ :Y′: ZZ′
	X	Y	ZZ		X′	Y′	ZZ′	
M06-2X	0.0	3.0	0.68	82 :0: 18	3.37	6.05	0.0	0 :0: 100
MO6-2X/B97D	0.0	3.34	0.79	86: 0: 14	3.64	6.93	0.0	0 :0: 100
wB97XD	1.47	2.25	0.0	3:1: 96	2.95	3.72	0.0	0 :0: 100
B3LYP-D3	0.2	1.42	0.0	38: 2: 60	2.26	4.59	0.0	1 :0: 99
B3LYP	0.38	3.85	0.0	30: 0: 70	0.0	2.25	3.07	99 : 1 : 0

Table C-2. AIM details of Trans(*Re*) and Cis(*Si*) Transition States

BCP index	Non covalent Interactions Trans(*Re*)	x 10^{-2} (a.u)			
		ρ	$\Delta^2\rho$	V	K
1	C-H(N-Methyl) ···O (cat.)	1.2426	4.2712	-0.7878	-0.14
2	α C-H(Substrate)···O (cat.)	0.7019	2.3177	-0.4227	-0.0784
3	β C-H(Napthayl Substrate) ···O (cat)	0.3589	1.3504	-0.2068	-0.0654
4	lp (N-Methyl) ··· π Napthyl (cat.)	0.9611	2.7555	-0.5449	-0.072
5	C-H(N-Methyl) ··· π Napthyl (cat)	0.721	2.1175	-0.3613	-0.084
6	π (of Substrate) ···π^+ (of cat.)	0.5631	1.5904	-0.2761	-0.0608
7	π (of Substrate) ···π^+ (of cat.)	0.807	2.3726	-0.387	-0.1031
8	CH_3 of Methyl··· π Napthyl (cat.)	0.7543	2.1948	-0.3486	-0.1001
9	α C-H (cat.) ···O (acetate)	1.0229	3.4251	-0.5949	-0.1307

10	OH (alcohol Substrate)$^{\cdots}$ O (acetate)	4.5735	14.548	-4.5494	0.4562
11	C-H(Methyl)$^{\cdots}$O (acetate)	0.937	2.8014	-0.5628	-0.0688
12	C-H(Napthyl Substrate)$^{\cdots}$O (acetate)	0.6223	2.0847	-0.3621	-0.0795

BCP index	Non covalent Interactions Cis(*Si*)	x 10^{-2} (a.u)			
		ρ	$\Delta^2\rho$	V	K
1	π (of Substrate)$^{\cdots}\pi^+$(of cat.)	0.6696	1.9291	-0.3039	-0.0892
2	π (of Substrate)$^{\cdots}\pi^+$(of cat.)	0.3903	0.9645	-0.1745	-0.0333
3	lp (N-Methyl)- π Napthyl (catalyst)	0.967	2.7903	-0.5496	-0.074
4	C-H(N-Methyl)- π Napthyl (substrate)	0.8276	2.4954	-0.4244	-0.0997
5	C-H(CH3 of acetate)- π Napthyl (catalyst)	0.7613	2.3031	-0.3674	-0.1042
6	α C-H(Catalyst)-O (acetate)	0.8456	2.9023	-0.5138	-0.1059
7	CH3 of isopropyl-O (acetate)	0.9174	2.7213	-0.5439	-0.0682
8	OH (alcohol)- O (acetate)	4.725	14.6557	-4.7364	0.5362

Table C-3**.** Quantification of individual non-covalent interactions (kcal/mol) in key conformations of A and A′ based on SAPT0 and M06-2X computations.

Conf.	Int.	Elec.	Exch.	Ind.	Disp	E(SAPT)	M06-2X
X	CH$^{\cdots}\pi$	-2.1	6.6	-0.70	-5.8	-1.9	-2.4
Y	$\pi^{\cdots}\pi$	-6.0	19.8	-2.2	-15.8	-4.2	-4.8
X'	CH$^{\cdots}\pi$	-1.2	3.4	-0.3	-4.1	-2.3	-2.5
Y'	$\pi^{\cdots}\pi^+$	-12.9	25.5	-4.8	-20.0	-12.2	-13.1